Lung measurement and quantification of lung heterogeneity using the Inspired Sinewave Test



Minh Cong Tran
Christ Church College
University of Oxford

A thesis submitted for the degree of
Doctor of Philosophy
Trinity 2021

I, Minh Cong Tran, declare that my thesis entitled "Lung measurement and quantification of lung heterogeneity using Inspired Sinewave Test" was my work. The development and analysis were carried out by myself for the degree of Doctor of Philosophy in Engineering Science under the guidance and supervision of Professor Stephen J. Payne, Professor Andrew D. Farmery and Professor Phi Anh Phan.

Acknowledgements

I would like to thank my supervisor, Professor Stephen J. Payne, for his excellent advice and encouragement during my time in Oxford. I would like to give considerable acknowledgments to my co-supervisors Professor Andrew D. Farmery and Professor Phi Anh Phan. They have provided valuable advice and clinical perspectives to my works. Thanks for always being open to teaching, guidance and inspiration. The work would not have been possible without the help of Professor Federico Formenti, Doctor Huy Phan, Doctor Vu Nguyen, Doctor Lam Pham and Doctor Son C. Chu. I have been grateful for the collaboration that I have been involved in during my PhD, especially my colleague and my friend, Doctor Douglas C. Crockett. I wish you all the bests.

I would like to thank my parents, Doctor Chung Van Tran (M.D., Ph.D.) and Doctor Hien Thi Nguyen (M.D.) who gave me a chance to be in Oxford. Many thanks to my brother, Thang C. Tran for his supports. Most importantly, I would like to thank the most special one, my wife, Lam Thanh Doan and my son, Vinh Cong Tran.

Thanks, are also due to my friends in Oxford, Stephen Payne's group, Selena Milanovic and Yun-Kai Lee. Thanks to my friends, VOX members and Kyle Pattinson's group. Thank you for your support!

Abstract

The lung is a complex organ. The most familiar and significant lung disease, chronic obstructive pulmonary disease (COPD), can be severely debilitating. Additionally, acute lung injury in the critically ill can be life-threatening. Lung diseases are known to be correlated with the heterogeneity of the lung (ventilation mismatch and perfusion mismatch). Currently, there is no "standard" method for assessing lung heterogeneity. Many lung function tests and computational methods have been proposed to diagnose and monitor lung heterogeneity. The Inspired Sinewave Test (IST) is a non-invasive and practical test to investigate lung pathophysiology.

To investigate the usability of the IST, we compare the IST results to similar lung function tests (current "standard" tests). A mathematical lung simulation is developed to enable the IST to quantify lung heterogeneity. This simulation is proved to work with the IST by testing with simulated data and sensitivity analysis. The resulting validated process is implemented in thirteen pigs (pre-injury and post-injury) and 104 human volunteers (healthy and COPD patients, including different phenotypes). The IST lung heterogeneity measurement is compared to CT scan results.

The IST results show that it is potentially a suitable device for bedside monitoring in mechanically ventilated patients. Additionally, by using the lung simulation, lung heterogeneity can be quantified by the IST using 60 s and 180 s period tracer gas. The ventilation and perfusion heterogeneity in injured animals are found to be higher than in non-injured animals. There is no clear distinction between healthy subjects and patients with COPD in the COPD human data set. The multiple alveolar compartments lung simulation is proposed to boost the COPD prediction accuracy using only IST data.

The results in this thesis suggest the translation of the IST into human medicine as a tool for detection and prevention of lung injury. Future investigations are proposed, which could potentially improve the works in this thesis.

Contents

1 Introduction **1**
- 1.1 Clinical motivations . . . 1
- 1.2 Aims of this Thesis . . . 5
- 1.3 Thesis Outline . . . 7

2 Literature review **9**
- 2.1 Human respiratory system and lung physiology . . . 10
- 2.2 Lung Heterogeneity . . . 14
- 2.3 Functional lung volume measurement . . . 17
  - 2.3.1 Medical imaging . . . 18
  - 2.3.2 Gas-based tests . . . 23
    - 2.3.2.1 Multiple Inert Gas Elimination Technique (MIGET) 23
    - 2.3.2.2 Multiple breath Nitrogen washout . . . 24
    - 2.3.2.3 Sulphur hexafluoride (SF_6) washout . . . 26
    - 2.3.2.4 Spirometry . . . 27
    - 2.3.2.5 Plethysmography . . . 29
    - 2.3.2.6 Inspired Sinewave Test (Device and system) . . . 31
- 2.4 Lung modelling and lung simulation . . . 33
  - 2.4.1 Model verification and validation . . . 37
  - 2.4.2 Sensitivity analysis . . . 38
  - 2.4.3 Parameter estimation . . . 40
- 2.5 Conclusion . . . 45

3 Materials and Methods **47**
- 3.1 Introduction . . . 48
- 3.2 Available data sets . . . 48
  - 3.2.1 Simulated data . . . 49
  - 3.2.2 Animal data (Control vs ARDS model) . . . 51
    - 3.2.2.1 General protocol . . . 51
    - 3.2.2.2 Animal preparation . . . 52
    - 3.2.2.3 Saline lavage lung injury model of ARDS . . . 53
  - 3.2.3 Human data (Healthy vs COPD subjects) . . . 54
- 3.3 Breath-by-breath analysis (IST analysis) . . . 56
- 3.4 Lung simulations . . . 60
  - 3.4.1 Compartmental model of the lung simulation . . . 60

3.4.2 Parameters for the lung simulation . . . 65
3.4.3 Heterogeneity lung simulation . . . 67
3.4.3.1 Two alveolar compartments model . . . 68
3.4.3.2 Multiple alveolar compartments model . . . 69
3.4.4 Model verification and model validation . . . 70
3.4.4.1 Model sensitivity analysis . . . 70
3.4.4.2 Healthy, Emphysema and Pulmonary Embolism . . . 71
3.4.5 Parameter estimation . . . 73
3.5 Lung heterogeneity measured by the CT scanning . . . 74
3.6 Classification model and statistics . . . 77
3.7 Conclusion . . . 78

4 Investigating lung parameters measured by the IST in comparison with SF_6 & thermodilution 79
4.1 Study details . . . 80
4.2 Results . . . 81
4.2.1 Deadspace volume, a comparison of IST to SF_6 . . . 81
4.2.2 Effective Lung Volume, a comparison of IST to SF_6 . . . 82
4.2.3 Pulmonary blood flow, a comparison to thermodilution . . . 86
4.3 Discussion . . . 86
4.4 Key findings and conclusion . . . 90

5 A simple lung simulation to detect lung heterogeneity with Inspired Sinewave Test 92
5.1 Methodology . . . 95
5.1.1 Two alveolar compartments simulation . . . 95
5.1.2 Parameter estimation . . . 97
5.1.3 Validation in animal and human data . . . 100
5.1.4 Sensitivity analysis and Statistical test . . . 100
5.2 Results . . . 101
5.2.1 The model sensitivity analysis results . . . 101
5.2.2 Feasibility of using the IST to quantify lung heterogeneity . . . 104
5.2.3 The validation of the IST heterogeneity ratios in simulated data 106
5.2.4 IST heterogeneity ratios in animal data . . . 107
5.2.5 IST heterogeneity ratios in human data . . . 109
5.2.6 Comparison of the IST heterogeneity ratios vs CT images . . . 110
5.3 Discussion . . . 112
5.4 Key findings and conclusion . . . 115

6 Multiple compartment simulation-based optimisation for Inspired Sinewave Test 117
6.1 Methodology . . . 118
6.1.1 Lung heterogeneity presented in a lognormal distribution . . . 121
6.1.2 Multinomial logistic regression . . . 124
6.1.3 Statistical analysis . . . 124

6.2 Results . . . 125
6.2.1 Verification of the lung simulation model with simulated patients 125
6.2.2 IST heterogeneity indices in animal data . . . 127
6.2.3 IST heterogeneity indices in healthy . . . 128
6.2.4 Classification of COPD types using the IST heterogeneity indices 132
6.2.5 Comparison of the IST heterogeneity ratios vs CT scan . . . 134
6.2.6 Optimisation PEEP setting for mechanical ventilator . . . 137
6.2.7 Optimisation performance . . . 140
6.3 Discussion . . . 141
6.3.1 Ventilation and perfusion heterogeneity measured by lung simulation . . . 141
6.3.2 Validation of the lung heterogeneity to CT imaging . . . 143
6.3.3 Lung heterogeneity to classify COPD patients . . . 143
6.3.4 Optimal PEEP prediction . . . 144
6.3.5 Strengths and limitations of this model . . . 145
6.4 Key findings and Conclusion . . . 146

7 Conclusion **148**
7.1 General summary . . . 148
7.2 Strengths and limitations of this study . . . 151
7.3 Future directions . . . 154
7.3.1 Translation of the IST in human medicine . . . 154
7.3.2 Integrated new hardware and testing technique for the IST . . . 155
7.3.3 Development of more advanced lung simulations . . . 156

List of Figures

2.1 Human airway structure [1]. 11
2.2 Lung volume distribution in a healthy lung [1]. 13
2.3 The ventilation-perfusion ratio differences in a lung unit (from left to right: a poorly ventilated zone, a normal zone and a poorly perfused zone) [1]. 14
2.4 A lognormal distribution of the lung heterogeneity and a schematic diagram of the ventilation-perfusion heterogeneity of the lung in three lung compartments (from left to right: the poorly ventilated zone, the normal zone and the poorly perfused zone) [2]. 15
2.5 Example of the quantitative specific ventilation (SV) in proton MRI. Panel a shows the quantitative SV. Panel b shows the histogram of the SV distribution of the lung slice shown in panel a [3]. 19
2.6 Example CT images of the one-dynamic slice used in this study [4]. Panel a shows the range of Hounsfield Unit. Panel b and c show results of segmentation. 21
2.7 Example of the lung heterogeneity in CT images in ARDS patients at PEEP $5cmH_2O$ [5]. Colour coded to present the lung heterogeneity scores. Light blue = stress raisers, 1.61; orange = stress raisers between 1.61 and 3; red = stress raisers > 3. 22
2.8 A presentation of the lognormal distribution of ventilation - perfusion ratio measured by MIGET [6]. 24
2.9 Schematic of Nitrogen washout technique [7]. 25
2.10 Schematic diagram of a sulphur hexafluoride (SF_6) multiple breaths inert gas washout test. Panel a and b are the washin and washout phase. The red trace in panel c shows the decay in the SF_6 concentration during the washout [8]. 27
2.11 Flow – volume spirometry loop of a healthy subject [9]. 28
2.12 Measurement of FRC with a body plethysmograph [1]. 30
2.13 Collected signals from the Inspired Sinewave Test in one example animal. Inhaled and exhaled signals are shown (blue line and crosses are inhaled signal, red line and dots are exhaled signal and the green line is the measured signal from N_2O gas sensor). 31
2.14 A schematic diagram of the Inspired Sinewave Test device. MFC: mass flow controller, FM: flow meter and GS: gas sensor. 33
2.15 3D model of the lung according to the lung airway tree structure [10]. 34

2.16 Continuous (panel a) and tidal (panel b) lung compartment models [11]. Panels c to e show three type of deadspace simulation model [12]. Panel c shows a "balloon and a straw" model, a simple tidal lung simulation. Panel d shows one mixing deadspace compartment connected with a tidal lung compartment. Panel e shows two mixing deadspace compartments. 36
2.17 Lognormal distributions of thee different lung conditions [13]. 37
2.18 Simplified explanation of the model verification and validation [14, 15]. 39
2.19 Bayesian optimisation coding example and a demonstration graph. Left: Algorithm for Bayesian optimisation using Gaussian process (GP) as a surrogate model to make a query for evaluation. Right: Example of Gaussian process and Bayesian optimization procedure over three iterations (three red points) [16]. The top plot shows the mean and variance estimated with a GP of the objective function. The lower plot also shows the acquisition function. 45

3.1 Block diagram of the tidal lung simulation in the IST system. The top diagram is the IST device and the bottom diagram is the IST simulated system developed in Matlab. 50
3.2 Timeline for the animal experimental protocol. 52
3.3 Signal processing block diagram of the inspired sinewave test analysis. 56
3.4 One lung compartment model of the IST analysis. 58
3.5 Schematic diagram of the tidal lung simulation with three alveolar compartments. 62
3.6 Simulated vs measured signals from the IST. 68
3.7 Schematic diagram of the lung compartment models in three different modular design. 69
3.8 Example of the simulated healthy and COPD lognormal distributions. 70
3.9 Cressoni's method to calculate lung heterogeneity from CT images. . 76
3.10 Examples of lung heterogeneity measured by the CT images at PEEP 5 cmH_2O in a pig. 77

4.1 Overall comparison of the paired deadspace volume measurements made by the SF_6 and IST techniques in the control (pre-injured) and injured lungs (ARDS model). 82
4.2 Linear regression of absolute deadspace volume measured by IST and SF_6. The red lines represent the regression lines and the black dashed lines the reference lines. Panel c and d are Bland-Altman plots, the bias lines are the red dashed line and the black dashed lines are the limits of agreement ($\pm$1.96SD). 83
4.3 General trend of the effective lung volume measured by IST and SF_6 as a function of the PEEP level. 84
4.4 Linear regression and Bland-Altman plots of the effective lung volume measured by both the IST and the SF_6. 85

4.5 Pulmonary blood flow measured by the IST and the thermodilution methods. Paired measurements between IST and thermodilution at incremental values of PEEP in control (panel a) and injured lungs (panel b). Panels c and d show Bland-Altman plots for absolute pulmonary blood flow measurements made by IST and thermodilution. 87
4.6 Thermodilution (white diamonds) vs IST (blue dots) in changes of pulmonary blood flow (L/min) of two pigs [17]. 90

5.1 Flow diagram to experiment the IST heterogeneity ratios using the lung simulation. 96
5.2 A schematic of the two-compartment tidal lung simulation. 98
5.3 Morris analysis results in the IST lung simulation model outputs. Panel a, b and c subsequently show the effects of the input parameters to the IST recovered outputs: deadspace volume (V_D), effective lung volume (ELV) and pulmonary blood flow ($\dot{Q}_P$). The greater the value of μ^* , the more the i^{th} factor affects the model output, while the greater the σ value, the more the factor is non-linear or involved with interactions with other factors; a low σ, however, indicates a linear, additive factor. 102
5.4 Partial correlation coefficient and linear regression results of the IST lung simulation model. Panels a, c and e present the correlation ranking of the input parameters to the outputs (VD_{IST}, ELV_{IST}, $\dot{Q}_{p\ IST}$). Panels b, d and f show the linear relationship between model input to the relative output of the IST. The Gaussian white noise was added (red dots). 103
5.5 The divergence of ELV values (from reality, and from each other) with increasing ventilation heterogeneity in simulated lungs. Panels a and b show the IST values in different variations in ventilation heterogeneity. In panel b, increasing heterogeneity (i.e. increasing f_{v1}) results in increasing heterogeneity index. 104
5.6 The divergences of the $\dot{Q}_P$ values and IST perfusion heterogeneity in simulated heterogeneous lungs. 105
5.7 Mean and standard deviations of the IST ventilation and perfusion heterogeneity ratios in three simulated lung conditions. The results are analysed by the Kruskal-Wallis test for multiple comparisons in non-parametric data. $**** = p < 0.0001$. 106
5.8 IST heterogeneity ratios in control and ARDS animals at different PEEP levels. Student's t-tests were performed. $*** = p < 0.001$, $** = p < 0.01$ and $* = p < 0.05$ 108
5.9 ROC curve analysis of the classification between control and ARDS animals at PEEP 10 cmH_2O. 109

5.10 Comparison of the IST ratios in healthy vs COPD groups. Panel a shows the IST ratio of ventilation heterogeneity and panel b is the perfusion heterogeneity ratio. The Student t-test was applied to each pair comparisons with ns: non-significant, $**: p < 0.01$, $***: p < 0.001$. 110
5.11 The overall influences of PEEP levels to lung heterogeneity. Panel a shows the lung heterogeneity measured by CT images changed with PEEP. Panels b shows the lung heterogeneity measured by the IST. . 111
5.12 Colour coded animal in the comparisons of the lung heterogeneity measured by the CT scan and IST ratios. 111
5.13 Four quadrant plots showing the changes of lung heterogeneity measured by the IST versus CT scan with changes in PEEP level. The exclusion zone (black rectangle) is 15 % of the maximum values. R^2 and r values are calculated from linear regressions. The agreement is the percentage of data points that lie in the I$(+;+)$ and III$(-;-)$ quadrants, excluding the exclusion zone. 113

6.1 Schematic diagram of the lung simulation-based optimisation and an example of the simulated ventilation and perfusion lognormal distributions. 119
6.2 The verification of lung simulation. Linear regressions present the relationship between set-input and recovered output calculated by the Bayesian optimisation lung simulation. Black dash lines are reference lines and red lines are regression lines. The simulation contains Gaussian random noise in the tidal volume to represent the real patient breathing pattern. 126
6.3 Example of healthy, emphysema and pulmonary embolism patients shown in lognormal distribution recovered from the simulation. . . . 127
6.4 The IST lung heterogeneity indices (σ_v - the standard deviation of the lognormal distribution graphs) in animal data. Panels a and b show the distribution of the IST ventilation heterogeneity (σ_v), and c and d show the IST perfusion heterogeneity (σ_P). Panels a and c show the mean and standard deviation of the IST heterogeneity indices vs PEEP. Panels b and d present the paired t-test comparison with ns: non-significant and $****: p < 0.0001$. 129
6.5 The IST heterogeneity indices in human data. Panels a and b show unpaired Student's t-test of the IST ventilation (σ_V) and perfusion heterogeneity (σ_P) indices. $**: p < 0.01, ***: p < 0.001$. 130
6.6 Linear regression of the IST heterogeneity indices vs age in healthy subjects. $*: p < 0.05, ****: p < 0.0001$. 131
6.7 The ROC curve of the COPD classification (Healthy vs COPD) using only IST heterogeneity indices. 131

6.8 The IST heterogeneity results in the human data. Panel a and b show the distribution of the IST heterogeneity indices in different lung conditions. Statistical test was applied for multiple groups comparison $* : p < 0.05$. 132
6.9 The IST heterogeneity results in the human data normalised for the effect of age. COPD patients were grouped into four GOLD groups. Panel a and b show the distribution of the IST heterogeneity indices in different lung conditions. Statistical test was applied for multiple groups comparison $* : p < 0.05$. 133
6.10 Confusion matrix for the logistic regression analysis in percentage values. This analysis grouped patients by the IST heterogeneity indices compared with the classification results using Spirometry (GOLD standard method). 134
6.11 Colour coded animals in the comparisons of the lung heterogeneity measured by the CT scan and IST. 135
6.12 Four quadrant plots showing the changes of lung heterogeneity measured by the IST ($\Delta\sigma_V$ and $\Delta\sigma_P$) versus CT scan with changes in PEEP level. The exclusion zone (black rectangle) is 15% of the maximum values. The agreement is the percentage of data points that lie in the I(+;+) and III(-;-) quadrants, excluding the exclusion zone. . 136
6.13 The overall influences of PEEP levels to lung parameters. Panel a shows lung heterogeneity measured by CT scan changed with PEEP. Panels d and e show the changes of $PaO2/FiO2$ and V_D/V_T vs PEEP. Mean and standard deviation of are plotted. 137
6.14 Optimal PEEP level according to lung heterogeneity measured by IST (black vertical line) and physiological and CT indices (red vertical line) in six individual animal. The physiological indices included $PaO2/FiO2$, V_D/V_T and H_{CT}. The second-degree polynomial functions were fit to normalised data. The optimal PEEP value (vertical lines) were calculated according to the minimum point of the second-degree polynomial functions. 139
6.15 Comparison of the performance in the loss function (panel a), computational time (panel b) and success rate (panel c) of three methods in one example data. 140

List of Tables

2.1 Classification of airflow limitation severity in COPD [18]. 29

3.1 Animal baseline characteristics for $n = 13$ animals pre-(control) and post-lung injury. Mean (SD) are shown. p-values show results of paired Student's t-test. ns = non-significant. 54
3.2 Mean (standard deviation) of participant characteristics (Healthy and COPD GOLD phenotypes). BMI: body mass index. 55
3.3 Body compartments data of a $70kg$ standard man. 66
3.4 Lung simulation parameters in healthy condition. Mean and standard deviation are shown. 67
3.5 Lung simulation parameters for emphysema and pulmonary embolism conditions. Mean values and (standard deviations) are shown. c_i is the alveolar compartment i. $* = 1 - c_1 - c_2$, $** = 1 - c_1$ 72
3.6 Initial prior distribution for the optimisation process. 74
3.7 Mean (standard deviation) characteristics of $n = 6$ pigs. FIO_2: fraction of inspired O_2, Hb: haemoglobin, SaO_2: oxygen saturation. . . . 75

5.1 Fraction for volume, ventilation and perfusion of the two alveolar compartments. 97
5.2 Linear regression results of the comparison between IST heterogeneity ratios and CT scans in six pigs. 113

6.1 Characteristic summary of the animal and human data measured by the IST. Mean (standard deviation) values are shown. Statistical t-test was applied, ns: non-significant. 120
6.2 The participant characteristics and Inspired Sinewave Test results ($n =$ 48 :26 men and 22 women) [19]. 122
6.3 Linear regression results of the comparison between IST lung heterogeneity indices and CT scans in six pigs. 136

Nomenclature

$ARDS$ Acute respiratory distress syndrome

$C_{\bar{a}}$ Mixed-arterial concentration

$C_{\bar{v}}$ Mix venous gas concentrations

C_a Pulmonary end-capillary gas concentrations

$COPD$ Chronic obstructive pulmonary disease

EE_i The elementary effect of the element i

ELV_{60s} Effective lung volume measured by the IST 60s period tracer gas (L)

ELV_{IST} Effective lung volume measured by the IST

$F_{\bar{E}}$ The expired average tracer gas concentration

$F_{\bar{V}}(t)$ The mixed venous fraction concentration

$F_A(t)$ The fractional concentrations coming back from the lung compartment to the deaspace compartment (The alveolar fraction concentration)

$F_a(t)$ The arterial fraction concentration

$F_E(t)$ The exhaled fraction concentration

$F_{I,n}$ The inspired concentration of breath n

$F_{IA}(t)$ The fraction concentration coming out from the deadspace compartment to the lung compartment

$F_I(t)$ The inspired tracer gas fraction concentration

F_I^o The inspired sinewave concentration fraction at steady state

$F_{M,i}(t)$ The fractional concentrations of the tracer gas coming into the i deadspace compartment

FEV_1 Forced expiratory volume measured by the spirometry (L)

FRC Functional residual capacity (L)

FRC	Functional residual capacity
FVC	Forced vital capacity measured by the spirometry (L)
$f_{p,i}$	Perfusion fraction to compartment i
$f_{v,i}$	Fraction of ventilation to compartment i
H_{Perf}	Perfusion heterogeneity index measured by the IST
H_{Ven}	Ventilation heterogeneity index measured by the IST
ICU	Intensive care unit
LoA	Limit of agreement
$\dot{Q}_p$ or Qp	Perfuison (L/min)
$\dot{Q}_S$	Shunt
$\dot{Q}_T$	Total blood flow (L/min)
QP_{IST}	Blood flow measured by the IST
Qp_T	Pulmonary blood flow measured by the thermodilution (L)
$\bar{V}_A$	End-expired lung volume (L)
$\dot{V}_A$	Ventilation (L/min)
$\dot{V}_A/\dot{Q}_p$	Ventilation-perfusion heterogeneity ratio
V_A	Alveolar volume (mL)
$V_{b,i}$	Blood volume of compartment i
V_D	Deadspace volume (mL)
V_i	Fraction of lung volume of compartment i
$V_{M,i}$	The deadspace volume of a compartment i
$V_{t,i}$	Volume tissue of compartment i
$V_{T,n}$	The tidal volume of breath n
V_T	Tidal volume (L/min)
σ_p	Standard deviation of the perfusion heterogeneity in lognormal format
σ_v	Standard deviation of the ventilation heterogeneity in lognormal format
Δt_n	The duration of breath n
λ	Solubility of N_2O
$\lambda_{t,i}$	Ostwald coefficient of compartment i

List of Publications

1. **Tran, M.C.**, Crockett, D.C., Formenti, F., Phan, P.A., Hedenstierna, G., Larsson, A., Payne, S.J. and Farmery, A.D., (2020). Lung heterogeneity and deadspace volume in acute respiratory distress syndrome animals using the inspired sinewave test. *Physiological Measurement*, 41(11).

2. **Tran, M.C.**, Nguyen, V., Bruce, R., Crockett, D.C., Formenti, F., Phan, P.A., Payne, S.J. and Farmery, A.D., (2021). Simulation-based optimisation to quantify heterogeneity of specific ventilation and perfusion in the lung by the Inspired Sinewave Test. *Scientific Report,* 11.

3. **Tran, M.C.**, Crockett, D.C., Phan, P.A., Payne, S.J. and Farmery, A.D., (2020), July. A tidal lung simulation to quantify lung heterogeneity with the Inspired Sinewave Test. *2020 42nd Annual International Conference of the IEEE Engineering in Medicine & Biology Society (EMBC)* (pp. 2438-2441).

4. **Tran, M.C.**, Crockett, D.C., Phan, P.A., Payne, S.J. and Farmery, A.D., (2021), July. Lung simulation to support non-invasive pulmonary blood flow measurement, Inspired Sinewave Test. *2021 43rd Annual International Conference of the IEEE Engineering in Medicine & Biology Society (EMBC)* (**In Press**).

5. **Tran, M.C.**, Crockett, D.C., Cronin, J.N., Borges, J.B., Hedenstierna, G., Larsson, A., Farmery, A., Formenti, F. (2021). Bedside monitoring of lung volume available for gas exchange. *Intensive Care Medicine Experimental*, 9(1).

6. **Tran, M.C.**, Phan, P.A., Crockett, D.C., Formenti, F., Cronin, J.N., Payne, S.J., Farmery, A.D., (2021). Validating the inspired sinewave technique to measure lung heterogeneity compared to atelectasis & over-distended volume in computed tomography images. *The international Conference on Acoustics, Speech, & Signal Processing (ICASSP) 2021.*

7. Crockett, D.C., **Tran, M.C.**, Formenti, F., Cronin, J.N., Hedenstierna, G., Larsson, A., Phan, P.A. and Farmery, A.D., (2020). Validating the inspired sinewave technique to measure the volume of the 'baby lung' in a porcine lung-injury model. *British journal of anaesthesia*, 124(3), pp.345-353.

8. Bruce, R. M., Phan, P. A., Rigolli, M., **Tran, M. C.**, Pacpaco, E., Rahman, N. M., & Farmery, A. D. (2021). Assessment of Ventilatory Heterogeneity

in Chronic Obstructive Pulmonary Disease Using the Inspired Sinewave Test. *International Journal of Chronic Obstructive Pulmonary Disease*, 16, 401.

9. Bruce, R.M., Crockett, D.C., Morgan, A., **Tran, M.C.**, Formenti, F., Phan, P.A. and Farmery, A.D., (2019). Noninvasive cardiac output monitoring in a porcine model using the inspired sinewave technique: a proof-of-concept study. *British journal of anaesthesia*, 123(2), pp.126-134.

Chapter 1

Introduction

1.1 Clinical motivations

The lung is an essential organ, responsible for the exchange of oxygen and carbon dioxide between blood and air. Lung diseases disrupt normal lung physiology and cause impaired ventilatory function and/or gas exchange. Lung diseases are broadly categorised as "obstructive diseases" such as asthma and chronic obstructive pulmonary disease (COPD), acute lung injury, such as acute respiratory distress syndrome (ARDS), and respiratory infections. Smoking, pollution, infection and genetic factors are responsible for most lung diseases.

COPD is now considered a significant public health problem. According to the World Bank/World Health Organisation, COPD will be ranked as the fifth most common cause of death in 2020 [20, 21]. COPD is the third most common cause of death in the European Union [22]. It affects 3 million people in the UK and over 2 million people are undiagnosed [23]. In developing countries, COPD caused

3.17 million deaths in 2015 [24]. The symptoms develop slowly and tend to become apparent after 40 or 50 years of age [24]. Therefore, early diagnosis plays a vital role in COPD prevention.

Unlike COPD, which is widely prevalent in the community, acute lung injury and Acute Respiratory Distress Syndrome (ARDS) are typically seen in critically-ill patients being treated with mechanical ventilation in Intensive Care Units (ICU). ARDS has a high mortality rate, brings higher hospital costs and survivors are associated with a low health-related quality of life [25]. In $2019-2020$, Coronavirus disease 2019 (COVID-19) became an emerging infectious disease that put the world into a pandemic [26, 27]. In a study of 201 COVID-19 patients, 41.8% patients developed ARDS and 52.4% died [27]. The ICU community must prepare for the challenges of this and future pandemics [26]. Mechanical ventilation is a life-saving therapy required by nearly half of patients in the ICU. However, it also causes damage to the lung through two main mechanisms: *atelectotrauma*, the opening/collapsing of lung units, and *volutrauma*, the repetitive over-inflating of the lung [28, 29].

The mechanical ventilator has been developed for over a century. It was transformed from negative-pressure ventilation, which first appeared in the early 1800s to positive-pressure devices around 1900 [30]. However, the first mechanical ventilator-induced pulmonary complication was in "iron lungs" used in the fight against polio [31]. The term ventilator-induced lung injury (VILI) was coined [28]. Simultaneously, researchers and doctors have been proposing new interventions and studies to prevent VILI. Gattinoni et al. discovered the relationship between lung "stress" and "strain" in the lung and proposed a method to calculate dynamic strain and static strain for the

lung to prevent VILI [32, 33]. To minimise VILI and optimise the ventilator for the patient's lung, several lung parameters are investigated, such as tidal volume, breathing rate, inspiration/expiration ratio, and PEEP level (positive end-expiratory pressure). PEEP is a mode of therapy used in conjunction with mechanical ventilation to prevent lung damage and collapse of pulmonary units by providing an end-expiratory pressure to keep the lung open throughout the respiratory cycle [34]. Furthermore, the risk of developing VILI is increased considerably in patients with ARDS, because of the "baby lung" concept [35]. According to Gattinoni et al., the "baby lung" refers to the reduced volume of the lung which remains aerated at end-expiration in patients with ARDS. There would be a potential benefit in measuring the size of the baby lung at the bedside to prevent VILI. Future versions of mechanical ventilators will have advanced technology to benefit patients, such as integrated bedside monitoring, smart system and close-loop control [30].

Currently, monitoring the lung accurately at the bedside to prevent the risk of VILI is challenging. Therefore, when setting up mechanical ventilation, anaesthesiologists may over-ventilate (and hence over-stress) or under-ventilate the patient's lung (leaving the lung prone to regional collapse) or way even do both at the same time. These actions increase the risk of ARDS [36]. Opportunities to measure key lung parameters such as end-expiratory lung volume in these patients are scarce. Whereas spirometry and plethysmography can be used in ambulatory patients [22], these methods require co-operation from the patient and do not show an abnormal lung in terms of its heterogeneity (defined below). Lung parameters of patients who are under mechanical ventilation or who are unconscious cannot be measured by these

tests. Thus, there is a clear need for a bedside lung monitor. Based on the physiological lung parameters monitored at the bedside, clinicians can understand more about the patient's lung condition and provide optimal ventilator setting.

Lung measurement techniques have been developed and improved to measure the lung at the bedside. Mechanical ventilators incorporated with lung function tests have been introduced to doctors and clinicians. Although the accuracy and repeatability of the bedside lung measurement are questionable, these tests play a vital role in guiding ventilator setup. For example, Spirometry is a compact device that can be attached to many different types of ventilator, and it can provide some lung function parameters in couple of minutes [9]. However, the spirometry can not fully provide in details the pulmonary gas-exchange and the 'baby lung' volume. Imaging technique such as computed tomography scan can provide details information of the lung under the image format. But, this technique induces risks to patients. Additionally, electrical impedance tomography (EIT) shown a potential application in guiding ventilator setting. In the research of Becher, et al., the EIT-based protocol shown a significant improvement of the oxygenation and reducing the global over-distension volume inside the lung of 20 subjects [37]. The EIT also can provide information on re-tractability, over-distension, and alveolar cycling to adjust the mechanical ventilation. In depth review of lung function tests will be covered in the literature review chapter.

One novel key parameter is the lung heterogeneity index. This index quantifies the unequal distribution of the airflow (ventilation heterogeneity) relative to the size of the lung regions to which it is distributed or to the gas exchange to the bloodstream (perfusion heterogeneity) [1]. Lung injury can cause ventilation or/and perfusion

heterogeneity. The ratio of ventilation to perfusion ($\dot{V}_A/\dot{Q}_P$) throughout the lung is commonly used to summarise the lung heterogeneity. If lung disease has occurred, changes can be observed in the lung heterogeneity index. Scientific studies have shown that the lung heterogeneity indices including ventilation, perfusion and ventilation-perfusion heterogeneities are potential indicators to detect lung diseases and to guide ventilator setting [38, 5, 39, 13].

Measurements of lung parameters are not easily made in intubated and ventilated critical care patients [40]. Recently, the Inspired Sinewave Test (IST) was introduced as a non-invasive, non-ionising lung function test that does not require the patient's cooperation [41]. The advantage of the IST is usability. This method can measure lung function parameters after a 10 minutes testing time with a straightforward setup [19]. Several lung parameters measured by the IST have been validated in animal testing and clinical trials [19, 12, 42, 43]. Thus, the IST has been proposed to be used in the intensive care unit as a bedside lung monitor. However, there has yet been no clinical evidence of the use of IST in ventilated subjects.

1.2 Aims of this Thesis

The ultimate focus of this thesis is to provide a better lung monitor for all patients during both conscious and unconscious conditions. The IST was selected because of its usability. Instead of using multiple lung functions tests, the IST can provide similar results within 10 minutes test. In previous studies, lung parameters estimated by the IST were compared with the plethysmography and thermodilution [19, 17, 12].

However, these comparisons contained limitations, such as comparing values were not quite appropriate. Furthermore, a pilot study of the combination results of IST and plethysmography could show the ventilation heterogeneity of the lung. But, the IST results alone could not show any significant difference between healthy and COPD subjects [19].

The novelty of this thesis is a comprehensive study of the lung parameters measured by the IST, especially the lung heterogeneity indices, in different lung pathology. These parameters include deadspace volume, effective lung volume, pulmonary blood flow and lung heterogeneity. Additionally, this thesis concentrates in particular on determining the lung heterogeneity indices using only the IST results. There are three primary aims in this thesis:

1. To assess the accuracy of the IST in measuring functional lung parameters, deadspace volume, effective lung volume, and pulmonary blood flow in comparison with SF_6 washin-washout and thermodilution in ventilated subjects.

2. To investigate the ability of the IST in measuring lung ventilation and perfusion heterogeneity using two periods tracer gas (at 180s and 60s).

3. To develop and use a lung simulation to establish an accurate method for detecting lung heterogeneity from the IST results only (not being reliant on additional measurement techniques).

By pursuing these goals, it is hypothesised that:

- COPD can be diagnosed and characterised by the IST heterogeneity results.
- The IST heterogeneity results can provide suggestions to set up optimal ventilator settings. Thus, the development of ARDS in mechanically ventilated patients and ventilation-induced lung injury can be reduced by a better understanding of lung heterogeneity.

1.3 Thesis Outline

This Thesis is structured as follows:

- Chapter 2 includes a literature review of lung physiology, lung heterogeneity and state-of-the-art lung function tests.
- Chapter 3 provides details of the materials, details of protocols and techniques in this thesis. This chapter introduces the collection of animal and clinical data, lung simulation development and the estimation of lung heterogeneity using the inspired sinewave test.
- Chapter 4 compares the IST results to the values measured by similar "gold standard" lung function tests (SF6 washout and thermodilution). This experiment confirms the repeatability and reliability of the IST test for further investigations.
- Chapter 5 shows the development of the lung simulation model. This model can be used with the IST to explain how lung heterogeneity can be quantified using IST 60 s and 180 s tracer gas periods. In this chapter, animal and patient

data are both used to validate this simulation model. The IST heterogeneity is compared with heterogeneity values measured by CT scan.

- Chapter 6 investigates further lung heterogeneity by lung modelling. A complex lung simulation is introduced to work with the Bayesian optimisation (named simulation-based optimisation). The results of this method are validated and analysed in both animal (with and without ARDS) and clinical human (healthy vs COPD) data. The comparison with the lung heterogeneity measured by CT scan also is performed.

- In the final chapter, Chapter 7 summarises and concludes this thesis. The limitations and advantages of this thesis are mentioned. It also provides several possible avenues for future research in the future based on the work presented in this thesis.

Chapter 2

Literature review

This chapter aims to provide the fundamental background of this thesis. To start with, the physiology of lung and lung heterogeneity are introduced. The terminology and definitions of different lung physiologies and lung parameters are explained here. Next, current standard lung function tests and lung simulations are described. Techniques to develop lung models are explained with relevant examples, including model verification, validation, and sensitivity analysis. Subsequently, lung simulation and the uses of lung simulations in conjunction with lung function tests to determine lung physiological parameters are discussed. Last but not least, an in-depth review of the inspired sinewave test is included.

2.1 Human respiratory system and lung physiology

The lung is an essential organ of the human body responsible for the exchange of oxygen with the blood and elimination of carbon dioxide [1]. The air coming in from the mouth or nose travels down the trachea. In this section, the air is divided into two primary bronchi, left and right. The main primary bronchi continue dividing to up to sixteen generations, similar to a tree structure. In most of this branching structure, gas molecules travel predominantly by bulk flow or convection. With each division of the airway, the total cross-sectional area of the airways increases exponentially. So the convection velocity reduces exponentially until by the 17^{th} generation the flux of gas molecules to the terminal alveoli is due solely to diffusion.

From here, diffusion through the alveolar wall transfers gas to and from the alveolar-capillary blood. Figure 2.1 illustrates the complex anatomical airway structure of the human lung. Travelling down alongside the tree structure, the structure of the tissues gradually changes from a thick tube supported by cartilage to a less solid wall until the cartilage disappears entirely. There are three lobes in the right lung: the superior, middle, and inferior lobes. The left lung consists of two lobes: the superior and inferior lobes. A healthy lung contains about 300 million alveoli and the lung volume is approximately $3L$, but the whole surface area is about $85m^2$ [44].

Not all of this amount of volume is involved in the gas-exchange process. The lung volume contains a deadspace volume. The term deadspace refers to the portion of each breath, which is not involved in gas exchange and its normal value is about

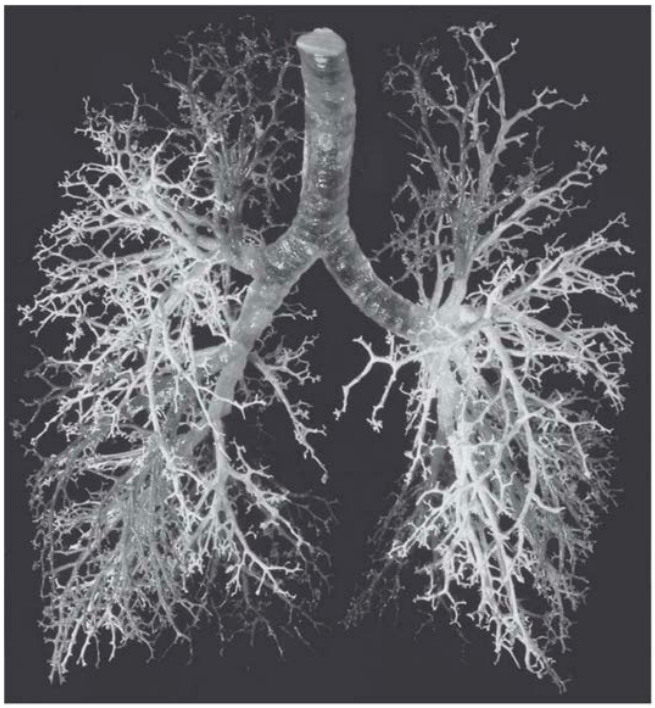


Figure 2.1: Human airway structure [1].

$150mL$ [1]. This volume also determines the efficiency of the ventilation [41] since any part of the tidal breath which remains in the conducting airways, or which enters any alveoli which receive no blood supply, is not available for gas exchange in the perfused alveoli.

Like the deadspace, the shunt refers to that portion of the pulmonary blood flow, leaving the right heart, which does not pass through ventilated areas [1]. No-perfusion regions comprise the deadspace and no-ventilation regions comprise the shunt. In a healthy lung, the shunt is less than 2% of total pulmonary blood flow; therefore, it can be treated as negligible in healthy lungs [1].

The main function of the lungs is to perform oxygen and carbon dioxide exchange, which requires blood from the pulmonary circulation. The pulmonary artery carries

deoxygenated blood from the right heart to the lungs. The pulmonary artery branches multiple times as it follows the bronchi, terminating in a network of capillaries which meet the alveolar wall and create the respiratory membrane to oxygenate the blood. Each red blood cell spends about 0.75 seconds in the capillary network [1]. Diffusion is sufficiently efficient for the red cell to become equilibrated with the alveolar gas within $< 0.5s$.

The breathing cycle is mainly supported by the action of the diaphragm by creating a differential pressure between the lung and the external environment. The diaphragm consists of a thin, dome-shaped sheet of muscle that is inserted into the lower ribs [1]. In normal tidal breathing, the level of the diaphragm moves about $1cm$ or so, but on forced inspiration and expiration, a total excursion of up to 10 cm may occur. After being expanded, the lung and the chest wall tend to return to their equilibrium positions. Expiration is passive during quiet breathing. Breathing rate can be calculated easily by the number of breaths per minute [44].

Figure 2.2 describes the lung volume components. Total lung capacity (TLC) is the amount of air contained in the lung after maximum inhalation. Residual volume (RV) is the amount of air contained in the lung after maximal exhalation. Tidal volume (VT) is the amount of air inhaled or exhaled with a regular breath. Functional residual capacity (FRC) is the volume of air in the lung at the average end-expiratory level. After reaching FRC, the lung can be forced to exhale additional air of about $1500mL$, this is ERV or expiratory reserve volume.

The lung is a complicated structure with many physical processes occurring, and

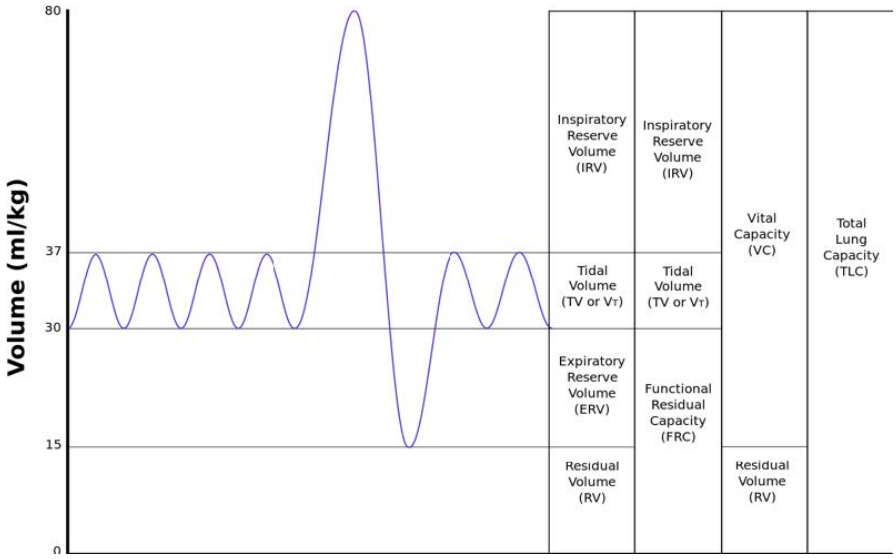


Figure 2.2: Lung volume distribution in a healthy lung [1].

three processes transfer oxygen from the outside to the blood through the lungs, which are ventilation, diffusion and perfusion. Ventilation moves the air to the lungs. Diffusion is a gas exchange process that occurs spontaneously in alveoli across the alveolar membranes. Perfusion requires the cardiovascular system to pump blood throughout the lungs. If any one of these processes goes wrong, problems will occur.

There are regional differences in ventilation and blood flow. Because of the unequal distribution of air sacs and blood vessels, the lung can be divided into three different regions, a poorly ventilated zone, a middle zone (a normal zone) and a poorly perfused zone. These zones can be modelled as in Figure 2.3. The ventilation-perfusion ratio can be obtained by infusing into a peripheral vein a mixture of dissolved inert gases having a range of solubilities and then measuring the concentrations of the gases in both the arterial blood and the expired gas (multiple inert gas elimination technique) [6, 1].

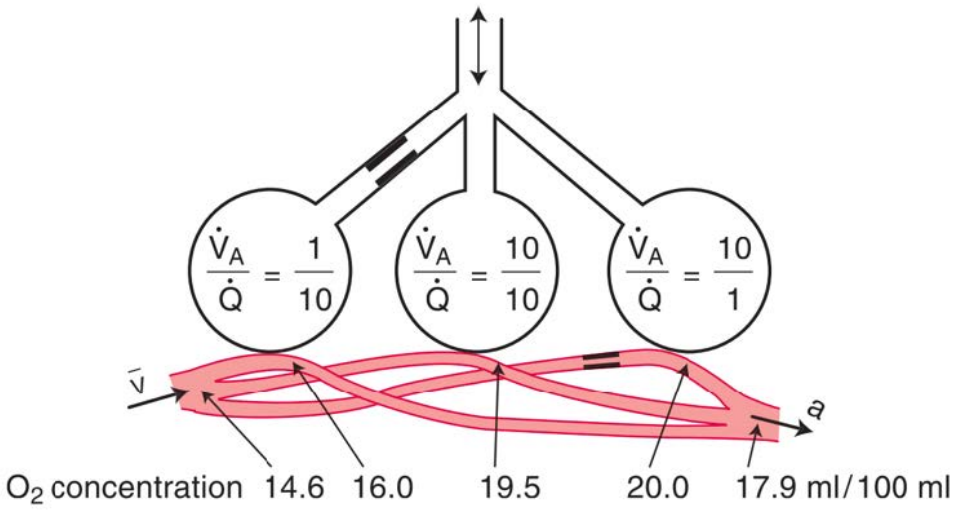


Figure 2.3: The ventilation-perfusion ratio differences in a lung unit (from left to right: a poorly ventilated zone, a normal zone and a poorly perfused zone) [1].

2.2 Lung Heterogeneity

In health, heterogeneity is principally due to the effect of gravity producing different effects on alveoli and capillaries depending on whether they are at the top of the lung or at the bottom of the lung, bearing the weight of the lung tissue above. Lung heterogeneity respects to the relative balance of ventilation and perfusion ratio ($\dot{V}_A/\dot{Q}_P$). In Figure 2.4a, the spectrum of lung ventilation and perfusion is presented in a lognormal distribution. In summary, there are three type of heterogeneity in the lung: ventilation heterogeneity, perfusion heterogeneity and ventilation-perfusion ratio heterogeneity.

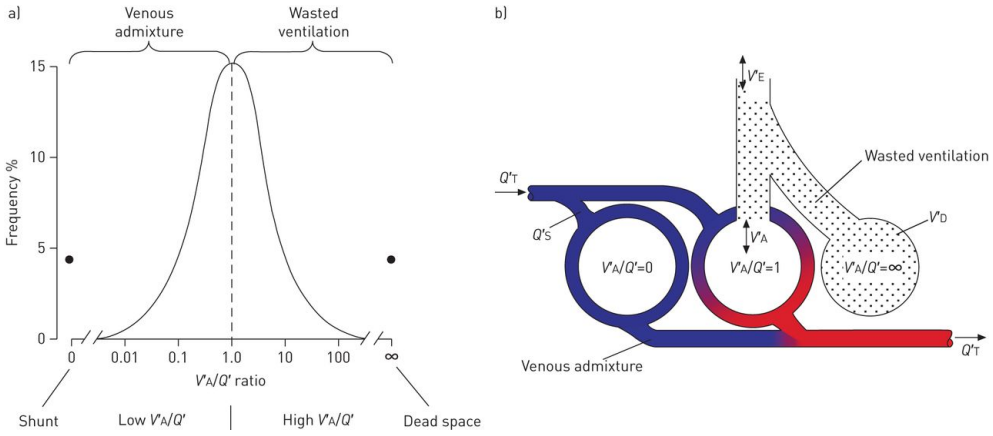


Figure 2.4: A lognormal distribution of the lung heterogeneity and a schematic diagram of the ventilation-perfusion heterogeneity of the lung in three lung compartments (from left to right: the poorly ventilated zone, the normal zone and the poorly perfused zone) [2].

For example, in Figure 2.4b, the lung can be divided into three regions, a poorly ventilated zone (wasted ventilation), a normal zone and a poorly perfused zone (venous admixture). However, in a healthy lung, the distribution of the ventilation-perfusion heterogeneity might be considered to be negligible [11, 1]. Thus, the lung could be easily presented as one single well-mixed compartment.

Not only can $\dot{V}_A/\dot{Q}_p$ ratios be heterogeneously distributed, but also ventilation itself can be heterogeneously distributed with respect to the volume of the region ventilated. The term *specific ventilation* refers to the ratio of the ventilation of a region to its volume $\dot{V}_A/V_A$. Such distributions in the normal lung are well represented by a lognormal distribution [6, 45, 13]. An example of the lognormal distribution of a healthy lung is shown in Figure 2.8.

Since the lung heterogeneity can describe the mismatch between ventilation, alveolar volume and pulmonary blood flow, it is a useful index to detect abnormal

lung conditions. In a study of ARDS and lung inhomogeneity, Cressoni et al. described how the lung heterogeneity index (measured by computed tomography scan) increased with the severity of ARDS [5]. The lung heterogeneity can tell the effectiveness of the lung and also the *baby lung*, so doctors can evaluate patients with ARDS more accurately and quickly. Emphysema and chronic bronchitis are the two main components of COPD. In patients with emphysema, the walls of the air sacs (alveoli) in the lungs are damaged. The sacs break apart and merge into each other, so the effectiveness of the gas exchanged is reduced [18]. Clinically, patients are diagnosed by chest imaging (chest x-ray or CT scan).

Emphysema causes the mismatch in ventilation related to the volume (air coming into the air sacs) leading to the increase in ventilation heterogeneity of the lung. When symptomatic, patients may complain of chronic cough, wheezing, chest pain secondary to mediastinal shift, haemoptysis and bronchorrhea [46]. Pulmonary embolism is a blockage in one of the pulmonary vessels in the lungs, it can be life-threatening if not treated quickly [47]. For example, pulmonary embolism is the result of blood clots that travel to the lungs from veins in other parts of the body (thrombosis) [48]. The blockage of the pulmonary blood vessel leads to the relative changes in perfusion heterogeneity of the lung. These lung conditions are related directly to lung heterogeneity. Yem et al. studied and parameterised both emphysema and pulmonary embolism patients for the compartment lung model [45].

Furthermore, COPD represents a wide variety of pathology and severity, and further still, the GOLD categories (from class I to class IV) were based on spirometry (FEV_1 and FVC values) and reported symptoms that themselves have a poor correl-

ation with pathological severity. There is, therefore, a need for a reliable biomarker of disease severity and progression particularly in the early 'pre-symptomatic' stages. Age is currently known to be an essential factor in COPD disease prediction [19]. Recent research indicated that in COPD, the clinical grade of severity correlates with lung heterogeneity [13].

In summary, there was no standard definition, direct measurement and benchmark for the lung heterogeneity index, each method has its assumptions and calculations to refer to lung heterogeneity index in a different format.

2.3 Functional lung volume measurement

"Lung volume" can be explained in many ways in different contexts. In the lung function test, lung volume could be referred to as FRC or the effective lung volume (ELV). In this thesis, the term lung volume will be used to imply the aerated volume inside the lung. Knowledge of the absolute value of the lung volume would be of use in preventing VILI, especially patients with ARDS. Since tidal volume could be selected as a fraction of this values rather than as a % of body weight. This would allow personalised titration of the tidal volume to minimise the stress to the healthy lung. Secondly, optimised PEEP level can limit the atelectasis (closured region) and over-distension regions in the lung [49]. To measure the lung volume, in this section, there are two main methods: medical imaging tests and gas-based tests.

2.3.1 Medical imaging

Lung function has been investigated using medical imaging technologies, such as hyper-polarised gas magnetic resonance imaging, computational tomography and positron emission tomography (PET).

MRI uses a strong magnetic field to cause precession of hydrogen atoms of water to generate images of the organs in the body [50]. Although conventional MRI does not image airspaces of the lung, adding hyper-polarised gas such as ^{129}Xe and ^{3}He can detect changes in ventilation, perfusion, and lung microstructure that appear to be associated with both normal lung development and disease progression [51, 52]. A contrast agent in proton MRI can assess regional ventilation in the human lung, mostly in qualitative applications [3]. An example image of this technique is included in Figure 2.5. Further advanced analyses allow scientists to capture more data from a single slice of the lung image.

An emerging technology using the combination of non-invasive and non-ionising method, Electrical impedance tomography (EIT) allows bedside assessment of regional changes in lung impedance. This method can be used to identify small changes inside the lung, and provide clinicians with an tomographic image of the lung [37]. It has a great potential in clinical application. However, further research should be carried on to confirm it usability and repeatability.

Positron emission tomography is able to measure the lung heterogeneity [53]. Despite the promising results from medical imaging techniques to quantify inhomogeneity,

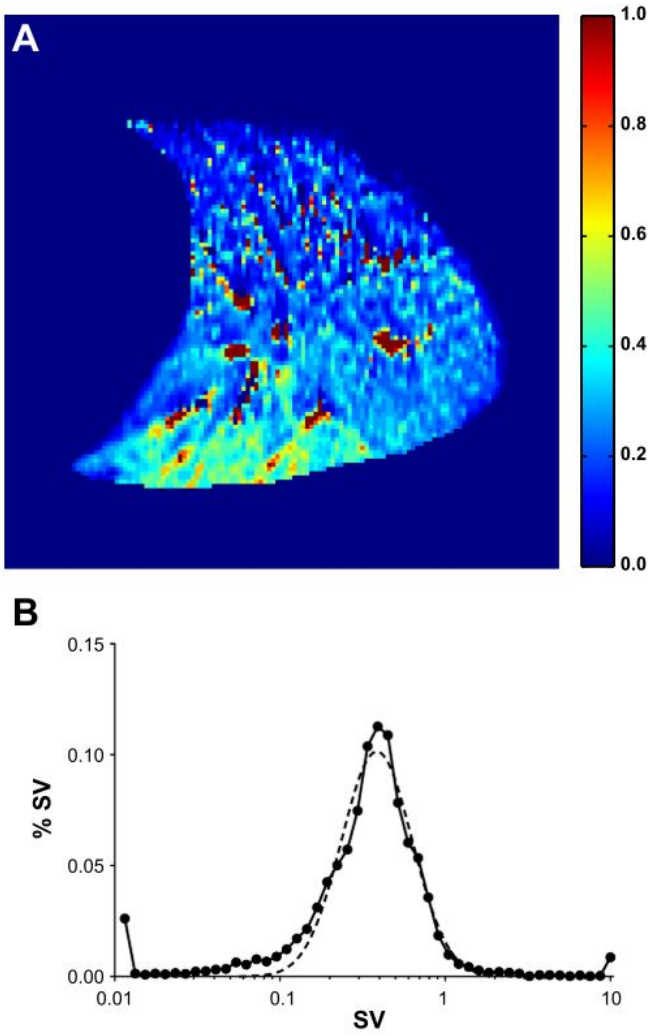


Figure 2.5: Example of the quantitative specific ventilation (SV) in proton MRI. Panel a shows the quantitative SV. Panel b shows the histogram of the SV distribution of the lung slice shown in panel a [3].

MRI and PET are significantly more expensive and challenging to acquire than other methods.

Computed tomography (CT) images have been widely used to detect lung disease. The most common way to quantify moderate to severe lung damage is to measure the percentage of voxels below a certain Hounsfield unit (HU) threshold [54]. In a CT image, a voxel is a unit that defines a point in three-dimensional space. All images are sub-segmented according to the voxel density. Aerated lung volume is calculated according to mean HU density within the segmented lung volume. An example of lung segmentation and classification according to HU are shown in Figure 2.6. The HU boundaries are water with a density of 1 gcm^{-3} (0 HU) and air with a density of 1 gcm^{-3} (-1000 HU). There are four sub-segments including [55]:

- Over-distended lung: -1000 to -901 HU.
- Normally aerated lung: -900 to -501 HU.
- Poorly aerated lung: -101 to -500 HU.
- Collapse lung (or atelectasis): -100 to +100 HU.

Additionally, CT images have been processed to detect lung heterogeneity. ARDS patients could be identified, according to lung heterogeneity [5]. In the CT image processing method, the tissue/gas ratio of one voxel (a three-dimensional unit of the CT images) can be compared with the surrounding voxels to compute the lung heterogeneity. A spherical crust filter was applied to all voxels.

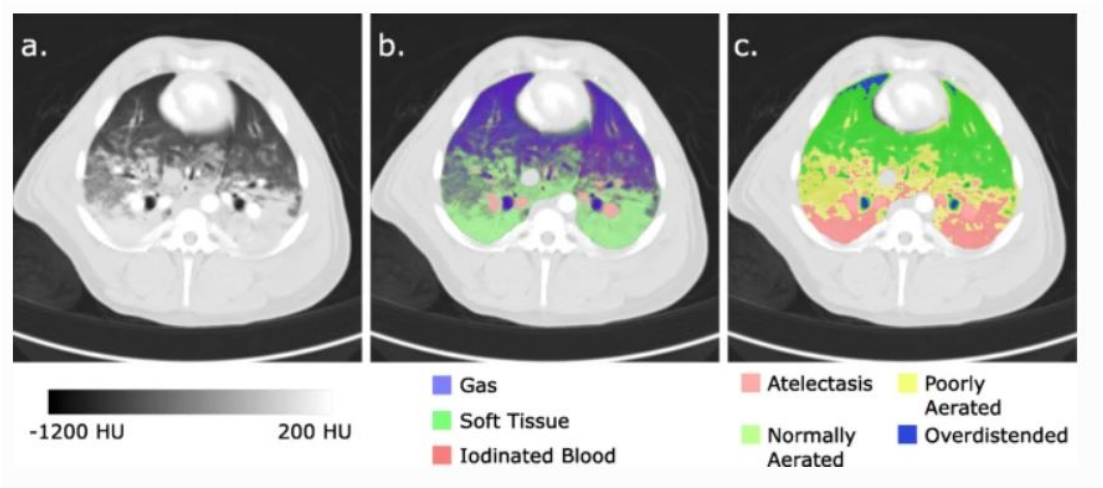


Figure 2.6: Example CT images of the one-dynamic slice used in this study [4]. Panel a shows the range of Hounsfield Unit. Panel b and c show results of segmentation.

Depending on the values calculated by this technique, the lung can be divided into three parts: *average lung heterogeneity*, *the extent of lung heterogeneity* and *intensity of lung heterogeneity*. This research illustrated that a significant difference in ARDS patients versus healthy subjects as found in *the extent of lung heterogeneity* (the heterogeneity score should be greater than 1.61) [5]. An example of processed image by Cressoni's method is shown in Figure 2.7.

However, CT has several limitations in its use to detect lung heterogeneity: the ionising radiation and inherent risks associated with critically unwell patients, and the practical problem of transporting critically ill, ventilated patients to the scanner is not trivial. A single slice CT could reduce the ionisation risk but still retain provide important results [56].

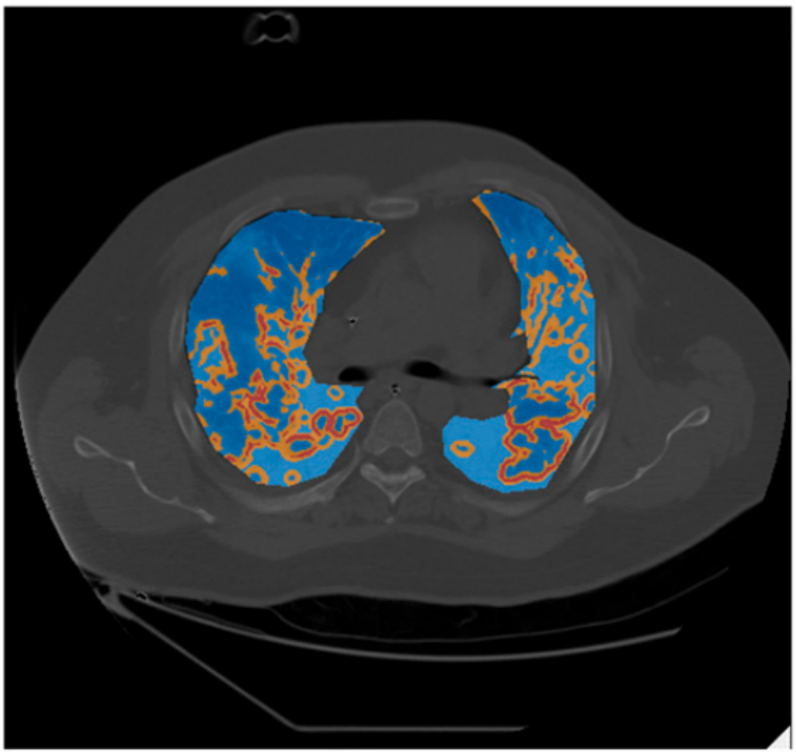


Figure 2.7: Example of the lung heterogeneity in CT images in ARDS patients at PEEP $5cmH_2O$ [5]. Colour coded to present the lung heterogeneity scores. Light blue = stress raisers, 1.61; orange = stress raisers between 1.61 and 3; red = stress raisers > 3.

2.3.2 Gas-based tests

2.3.2.1 Multiple Inert Gas Elimination Technique (MIGET)

MIGET was developed in the 1970s. This test measures the elimination/retention of a set of six different inert gases dissolved together in saline (or dextrose) and infused intravenously (varying solubility from 0.005 to 300) into the bloodstream [1, 6]. The solubility could be defined as the ratio of concentration to partial pressure expressed in mL of gas dissolved per dL of blood per mmHg of the gas in the blood.

MIGET can measure the distribution of ventilation-perfusion ratios, true shunt and physiological dead space ventilation. These values are calculated by mass conservation principles. Gases of different solubility have different retentions for any given $\dot{V}_A/\dot{Q}_p$ ratio. From these retention and partition coefficients, the corresponding distribution of ventilation-blood flow is calculated (as shown in Figure 2.8). The mathematical technique is mentioned elsewhere [6].

MIGET describes the heterogeneity of $\dot{V}_A/\dot{Q}_p$ in the form of the width of a lognormal distribution. Healthy subjects appear to have narrow lognormal distributions, older subjects have broader lognormal distributions, and COPD subjects may show multi-modal lognormal distributions [6]. Using MIGET, the lung heterogeneity was suggested to indicate the abnormality earlier than using spirometry in mild COPD patients [57]. The idea of using the lognormal distribution to present the lung heterogeneity was relatively easy to understand by clinicians. The lognormal presentation was adapted by other techniques to show the lung heterogeneity [13].

The limitations of this technique are the technical complexity, invasiveness and

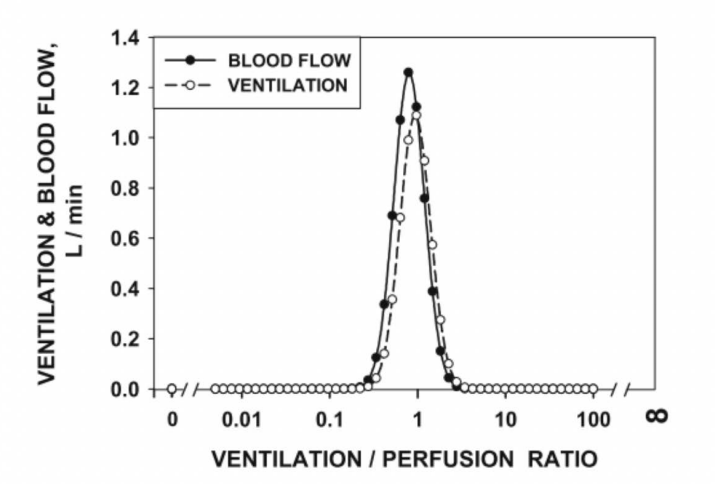


Figure 2.8: A presentation of the lognormal distribution of ventilation - perfusion ratio measured by MIGET [6].

random experiment errors. As a result, these measurements are highly sensitive to measurement error [58, 6]. Since this technique has proven to be difficult to implement outside one or two specialist centres, it has not been adopted widely by the clinical community.

2.3.2.2 Multiple breath Nitrogen washout

The washout method may use one of several different tracer gases such as sulphur hexafluoride (SF_6), nitrogen(N_2) and nitrous oxide (N_2O) to estimate lung parameters. There are both single-breath and multiple-breath washout methods. Single breath washout can define the anatomic dead space using one tracer gas by calculating this gas concentration in an individual's exhalation. It was first established by Fowler's experiment in 1948 [59].

Multiple breath Nitrogen washout (MBNW) has been used to determine total lung

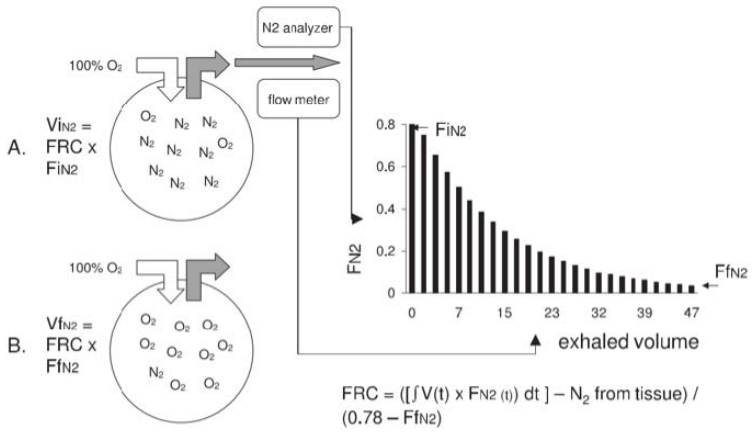


Figure 2.9: Schematic of Nitrogen washout technique [7].

volume and the heterogeneity of ventilation. The expired concentration of nitrogen is monitored during washout. Assuming that the N_2 fraction at $t = 0$ is uniform everywhere in the lungs, the test starts by delivering 100% oxygen into the patient's inspired gas. The expired gas concentration of the N_2 is recorded as the N_2 is "washed out" of the respiratory system. The FRC can be calculated, as shown in Figure 2.9.

MBNW can produce a Lung Clearance Index (LCI), which reflects ventilation heterogeneity and obstructive lung disease. This technique is performed during tidal breathing and does not require co-operation; therefore, it can be used in children and ventilated patients. The LCI is defined as:

$$LCI = \frac{Litres\,of\,ventilation\,required\,for\,N_2\,concentration\,to\,fall\,to\,\frac{1}{40}}{FRC} \tag{2.1}$$

The analysis method of the MBNW assumes that the lung is a single compartment model and so N_2 decay should be a simple exponential. If it deviates from this, then it must not be homogeneous. The LCI really presents a "breakdown" of a simple model. For example, the LCI of cystic fibrosis patient is higher and almost double the LCI of healthy patients [60]. Owens et al. showed a similar result to diagnose cystic fibrosis in comparison between the LCI and the high resolution computed tomography [61]. Lum et al. provided promising results when using LCI to diagnose cystic fibrosis in children [62].

2.3.2.3 Sulphur hexafluoride (SF_6) washout

Although this technique is not very popular in clinical applications, it can provide accuracy in repeated measurements. This technique was first introduced and developed by Larsson, et al. [63]. The SF_6 washout was introduced into the inspired gases via a catheter. As described in Figure 2.10, during the washin washout process, a flow analyser and a gas analyser were used to record the SF_6 concentration data. The estimation of the effective lung volume (ELV) is obtained by:

$$ELV = \frac{V_{SF6}}{[Alveolar]_{SF6}} \times k - V_{app} \tag{2.2}$$

where: V_{SF6} is the total volume of SF_6 washout, k is the conversion factor (1.09), $[Alveolar]_{SF6}$ is the alveolar concentration of SF_6 at the end of washin, and V_{app} is the apparatus deadspace volume.

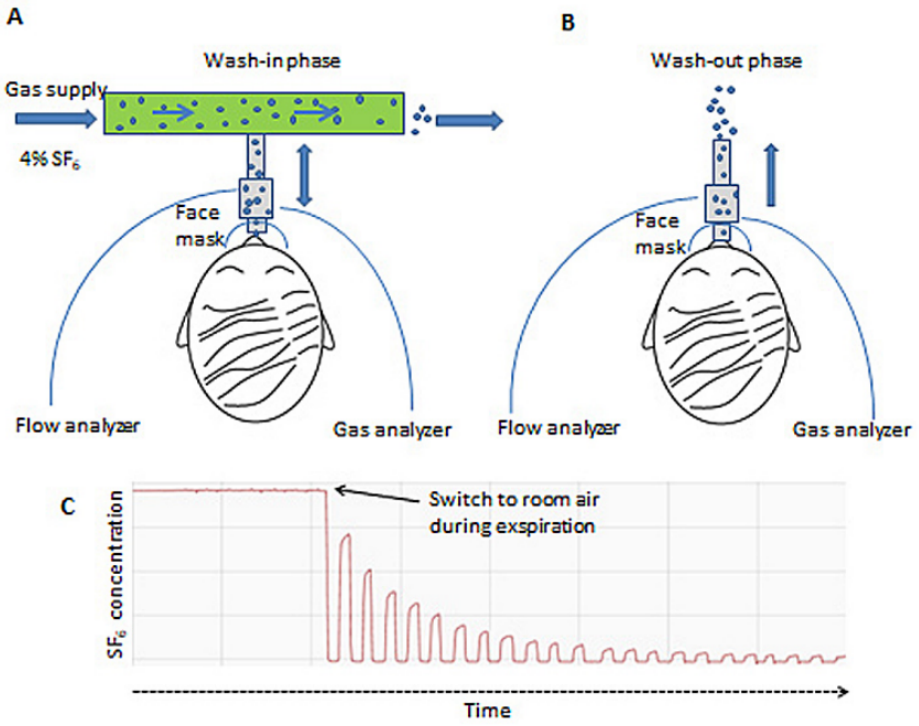


Figure 2.10: Schematic diagram of a sulphur hexafluoride (SF_6) multiple breaths inert gas washout test. Panel a and b are the washin and washout phase. The red trace in panel c shows the decay in the SF_6 concentration during the washout [8].

2.3.2.4 Spirometry

Spirometry is the most common technique used to help to diagnose and to monitor certain lung conditions by measuring how much inhaled and exhaled air is found in one forced breath. The patients breathe through a device, which has flow sensors so that the flow and integrated volume are captured as functions of time. The most vital aspects of spirometry are the forced vital capacity (FVC) and the forced expiratory volume (FEV_1) in one second [9]. FVC is the exhaled volume when exhaled as forcefully and completely as possible starting from full inspiration. FEV is the volume

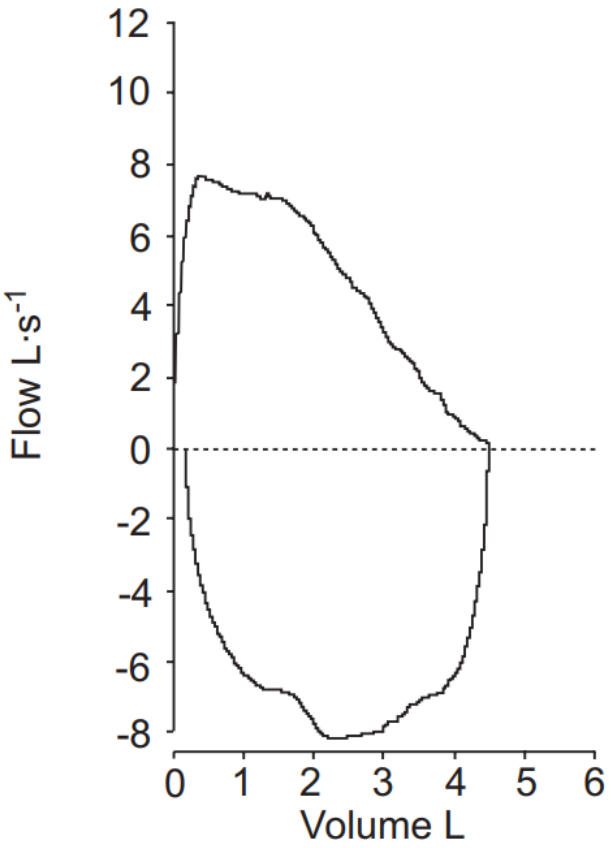


Figure 2.11: Flow – volume spirometry loop of a healthy subject [9].

in the first second of an FVC manoeuvre. An example of a spirometry flow-volume loop is shown in Figure 2.11. Spirometry is a compact device that can be attached to different types of equipment. A full description and technical standard of this device can be found in [9].

The conditions that can be picked up and monitored using spirometry include asthma, COPD, cystic fibrosis and pulmonary fibrosis. Spirometry is a standard screening test for these conditions and to assess response to medical treatment. According to the Pocket Guide to COPD diagnosis 2020, spirometry in conjunction with

Table 2.1: Classification of airflow limitation severity in COPD [18].

GOLD Classification	Type	Spirometry result
GOLD 1	Mild	$FEV_1 > 80\%$ predicted
GOLD 2	Moderate	50% predicted
GOLD 3	Severe	$30\% \leq$ predicted
GOLD 24	Very Severe	$FEV_1 < 30\%$ predicted

patient history and symptoms are vital roles for diagnosing, prognosticating and considering other important therapeutic approaches for COPD [18]. They also created a classification of airflow limitation severity in COPD according to spirometry results (Table 2.1).

Additionally, spirometry is a straightforward test and is considered very safe, but it has limitations. This test is easy and convenient, but it has low sensitivity. Spirometry only shows abnormal results in advanced diseases states, which is a limitation of this test. Furthermore, this test require patient's co-operation, which is not suitable to quantify the lung at the bedside.

2.3.2.5 Plethysmography

Plethysmography can estimate a patient's FRC and then compare it with standard values for the patient's age, gender, height, and weight. Plethysmography uses the ideal gas law, which relates pressure to volume [64]. Boyle's law is used to calculate

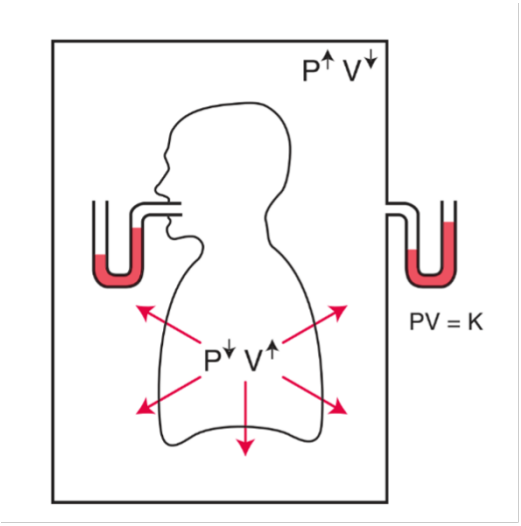


Figure 2.12: Measurement of FRC with a body plethysmograph [1].

the unknown volume within the lungs. Boyle's law derivation for plethysmography is:

$$P_1 \times V_1 = P_2 \times V_2 \tag{2.3}$$

In Figure 2.12, when the subject makes an inspiratory effort against a closed airway, they slightly increase the volume of their lung (V_1), airway pressure (P_1) decreases, and box pressure (P_2) increases. Since (V_2) is measured, from Boyle's law, lung volume (V_1) can be calculated.

However, plethysmography might overestimate the value of FRC compared to other techniques such as helium dilution, CT scan and IST [19, 65], since plethysmography contains the volume of the poorly ventilated lung units. According to O'Donnell,

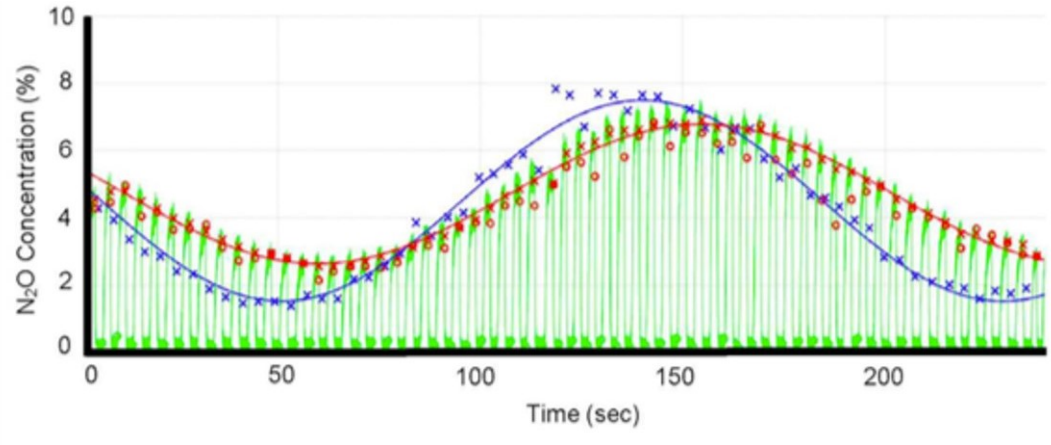


Figure 2.13: Collected signals from the Inspired Sinewave Test in one example animal. Inhaled and exhaled signals are shown (blue line and crosses are inhaled signal, red line and dots are exhaled signal and the green line is the measured signal from N_2O gas sensor).

et al., since plethysmography overestimates FRC of the patients, they did not recommend plethysmography in COPD diagnosis [66].

2.3.2.6 Inspired Sinewave Test (Device and system)

IST is a simple and non-invasive method to measure cardiopulmonary indices by using oscillating concentrations of gas. The principles of IST were introduced by Zwart et al. [67] and modified by Hahn et al. [68, 69]. Hahn et al. improved this method by using non-toxic gases such as nitrous oxide (N_2O) instead of halothane [68]. Tracer gas N_2O is injected into the patient's airflow during IST. This tracer gas passes through the deadspace into the lung and diffuses into the alveolar-capillary blood, which later joins all capillaries to become arterial blood. After being distributed to different parts of the body, this tracer gas returns to the lung in the mixed venous or

'venous recirculation'. After that, the N_2O is exhaled. By using a one-compartment lung model, the dead space volume (V_D), effective lung volume (ELV) and blood flow rate ($\dot{Q}_P$) can be calculated after the test.

IST applies a forced oscillation of a low dose N_2O tracer gas with a sinusoidal period which can be determined by the user. Figure 2.13 shows an example of IST patient signals. The blue line is inspired signal, $F_I(t)$ and red line is expired signal $F_E(t)$. The input signal is forced into the lung, the output signal is recorded. Then the IST analysis is performed in the recorded signals to provide the IST results. The whole process lasts approximately 10 minutes.

Figure 2.14 shows the schematic diagram of the IST. The tracer gas is generated by a computer-controlled mass flow controller (Alicat Scientific, USA). A flow sensor (VenThor-22/2A, Hungary) and infrared sensor gas sensor (SquareOne, USA) capture the exhaled air flow and N_2O concentration which also has a sinusoidal breath-by-breath waveform. The breath-by-breath analysis was introduced by Farmery [70]. The technique analyses each breath of the patients and integrates the information to find the average results. This method produces a high accuracy for deadspace recovery. Phan, et al. determined that IST has a 10% error in recovered deadspace volume compared with the 50% error of the traditional Bohr method [65].

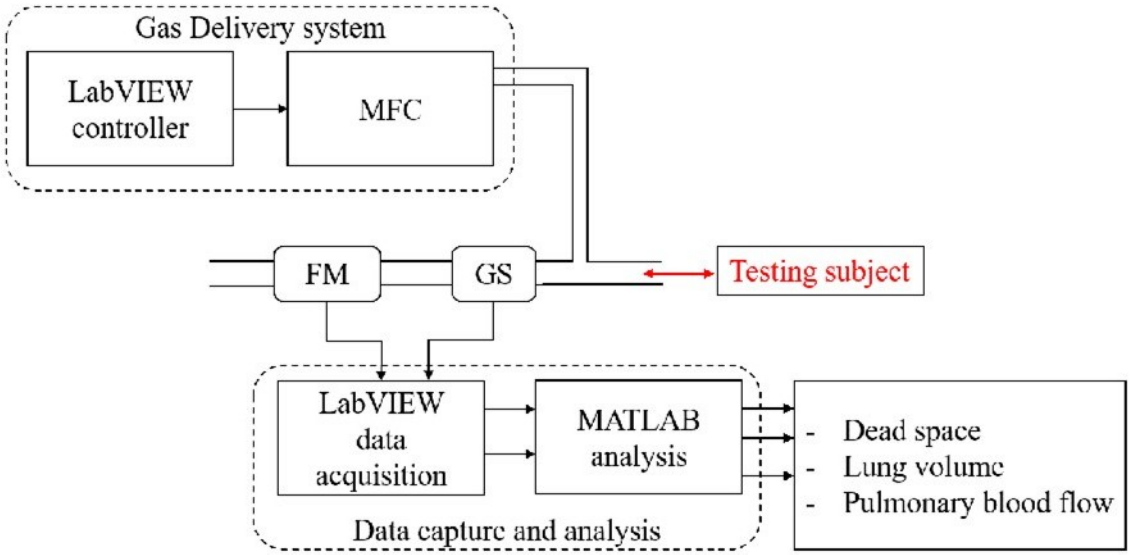


Figure 2.14: A schematic diagram of the Inspired Sinewave Test device. MFC: mass flow controller, FM: flow meter and GS: gas sensor.

2.4 Lung modelling and lung simulation

Lung simulation or lung modelling is a well-established method to support lung measurement techniques. Lung simulations can be developed and refined to solve wide applications. Modelling, in general, is needed to reduce the time, cost and risk associated with full-scale testing of products, materials and systems.

A particular simulation is designed to test a particular aspect of a lung model, and so such a simulation cannot be universally applied to any or all aspects of lung behaviour. For nearly two decades, several prototypes of lung simulation from simple to advanced have been introduced and developed. There are simple techniques: continuous compartment [13] and tidal volume [71, 45] simulations; and advanced techniques: imaging-model combinations [72], mechanical and fluid dynamic models. For example, Figure 2.15 shows a simulation of the lung created by using mathematical

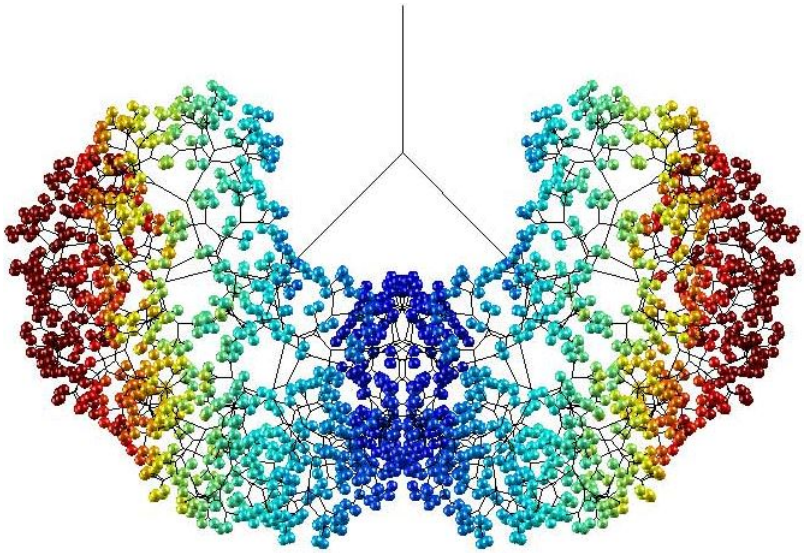


Figure 2.15: 3D model of the lung according to the lung airway tree structure [10].

equations and a real lung airway tree in a study on surfactant replacement therapy. The Multiple Breath Nitrogen Washout technique has been incorporated with lung simulation in the past to investigate the ventilation–volume heterogeneity distribution [73, 74, 75].

In this thesis, the primary focus of using lung simulation is to justify the measurement of lung heterogeneity using the IST. These lung simulations use the mathematical equations of the gas exchange and distribution inside the lung and these models should work with the IST. Thus, the lung simulation models were built up to describe the function of the lung [76, 11, 77]. These lung models normally contain different compartments linked together in parallel or in series to represent the physiological function of the lung. A lung simulation may have deadspace compartments, alveolar compartments and body compartments [43]. These compartments can be developed

and evaluated individually. To simulate the alveolar compartment, there are two well-established methods: continuous compartment and tidal compartment. Although continuous models are simple to implement, the tidal lung simulations provide more realistic lung behaviour. Figure 2.16 shows the differences between continuous and tidal lung simulations (panels a and b). The tidal model considers both inspired and expired phases discretely, while the continuous model assumes a continuous and constant flow of air traversing the lung unidirectionally. The continuous simulation assumes that a constant flow enters the lung, passes through all compartments, and vents out downstream, while the tidal simulation uses a “balloon and straw" model to simulate breath pattern.

In the development of the IST, several lung simulations have been applied. Whiteley and colleagues used a tidal ventilation simulation with multiple compartments to generate data sets to understand the influence of forcing different period signals in the IST [78]. Gavaghan and Hahn used the tidal lung simulation to prove that the IST was reliable and robust for cardiopulmonary parameter recovery [76]. In recent years, Harrison developed a serial deadspace compartment simulation to help predict accurately the alveolar volume using the IST [12]. This serial deadspace model proved that it could reduce the mean limits of agreement of the lung volume measured by IST vs the whole body plethysmography by up to 41% [12]. Figure 2.16 c-e show the diagram of three methods to simulate the deadspace compartment. However, Harrison's model only uses one lung compartment, so his model did not investigate lung heterogeneity.

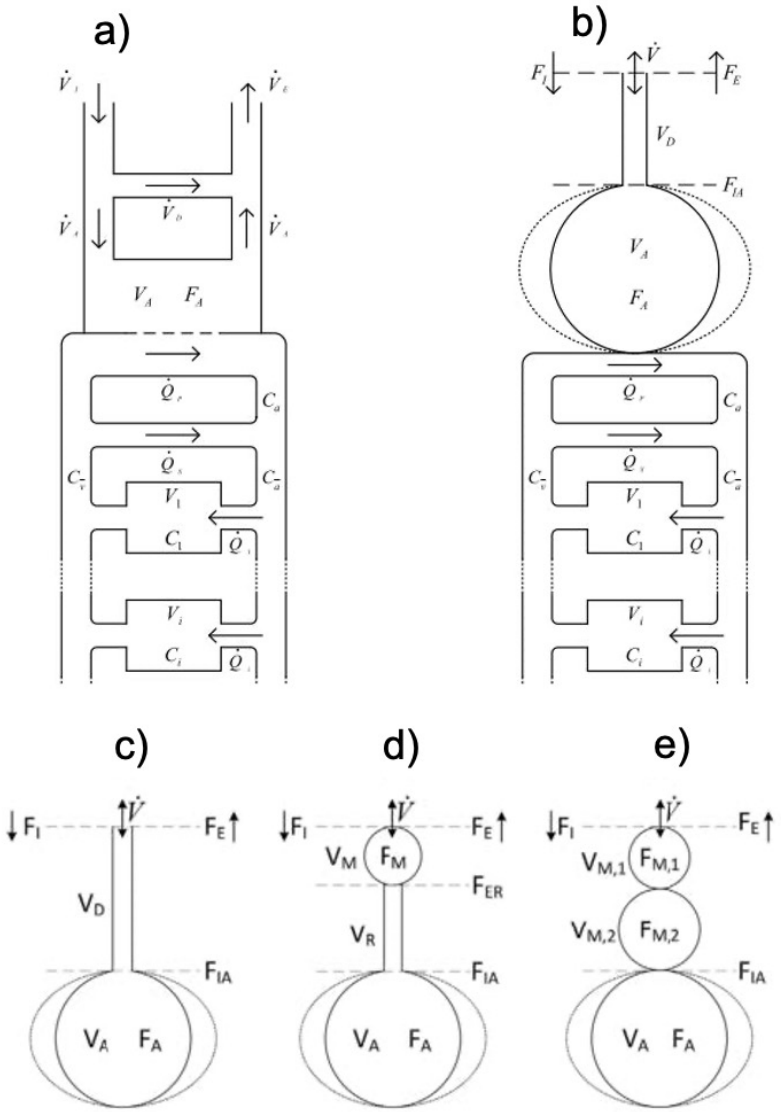


Figure 2.16: Continuous (panel a) and tidal (panel b) lung compartment models [11]. Panels c to e show three type of deadspace simulation model [12]. Panel c shows a "balloon and a straw" model, a simple tidal lung simulation. Panel d shows one mixing deadspace compartment connected with a tidal lung compartment. Panel e shows two mixing deadspace compartments.

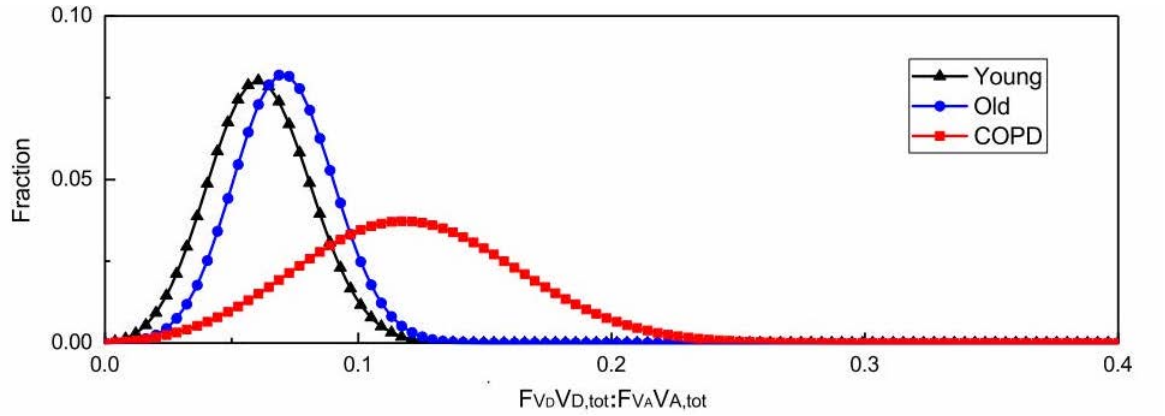


Figure 2.17: Lognormal distributions of thee different lung conditions [13].

Recently, in 2018, Mountain et al. implemented his sophisticated multiple lung compartment model on top of the modified washout test to show a potential prediction of COPD patients [13]. The model was built to perform further analysis on top of a lung function test could enhance the test results. In Mountain's model, instead of one lung compartment, 125 lung compartments were used. The fraction of ventilation, perfusion and volume for each compartment was calculated from a lognormal distribution. This method matched the measured to simulated signals using optimiser tool running on a super-cluster. Figure 2.17 shows the output of the lognormal distributions of young, old and COPD subjects in Mountain's work.

2.4.1 Model verification and validation

A number of studies have developed guidelines and procedures for conducting model verification and validation programs to ensure the quality and accuracy of model calculations [15]. Model verification and validation according to the 1998 AIAA

Guide, could be explained [79]:

- Verification is the process of determining that a model implementation accurately represents the developer's conceptual description of the model.
- Validation is the process of determining the degree to which a model is an accurate representation of the real world from the perspective of the intended uses of the model.

By following the model verification and validation protocol, errors and mistakes can be eliminated to provide accurate and reliable solutions. According to Schlesinger, the simple version of the model verification and validation process could be presented in Figure 2.18 [14].

In Figure 2.18, the computer model presents the implementation of the mathematical model in the form of solution algorithms in a computer program (software implementation or code). The important parameters could be selected as the outcomes of the simulation. To develop a fully completed model, there are further steps that were not included in Figure 2.18; such as, model design, quantification of uncertainties, objective mechanism for improvement, etc.

2.4.2 Sensitivity analysis

Sensitivity analysis is essential to the development of a simulation. It can be defined as a measure of how much uncertainty in a model's output can be apportioned to

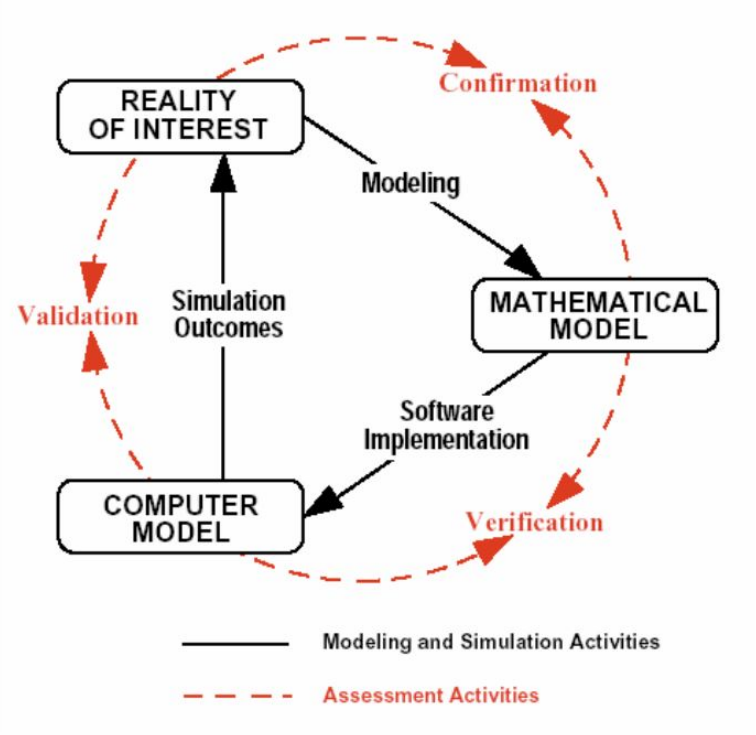


Figure 2.18: Simplified explanation of the model verification and validation [14, 15].

different sources of uncertainty in the model input. According to Qian et al. [80], there are three aims of the sensitivity analysis:

- *Ranking:* involves ordering the inputs in terms of their effect on the variability of model output.
- *Screening*: by identifying important parameters, the model can be reduced the complexity by setting non-important parameters to fixed values.
- *Mapping*: quantify the relationship between the model input and the output.

There are many sensitivity analysis methods, but this work will just focus on two methods: particle rank correlation coefficient (PRCC) and the Morris method. PRCC provides a measure of monotonicity after the removal of the linear effects of all but one

variable. In other words, the PRCC can characterize the linear relationship between the inputs and outputs of the model, after the remaining linear effect of the inputs to the outputs is excluded. PRCC can rank the input parameters according to the linear correlation between these input parameters and the output. This method provides a ranking value between -1 and 1 [81, 82].

Additionally, the Morris method is an efficient method to evaluate multiple changing inputs at the same time. This method defines the elementary effect (EE_i) [83, 84, 80]:

$$EE_i = \frac{f(X_1, X_2, ..., X_i + \Delta, ..., X_n) - f(X_1, X_2, ..., X_i, ..., X_n)}{\Delta} \tag{2.4}$$

where f is the output parameter. X_1 to X_n are input parameters of the simulation, Δ is a very small change of the input and n is the number of input parameters. Each input parameter, the mean μ and standard deviation σ can be calculated. μ reflects the magnitude of influence of this parameter to the model output. In addition, the standard deviation σ shows the non-linearity or interaction with other input factors [80].

2.4.3 Parameter estimation

Parameter estimation is a common technique of interest to scientists, engineers, and medics. This technique deals with estimating the values of parameters based on measured empirical data or experimental data. The estimation process can be performed in two main ways: the probabilistic approach and the set-membership approach [85].

While the first way assumes that the measured data are randomly distributed with a probability distribution, the other assumes that the measured data would belong to a set of known parameters. One simple well-known parameter estimation method is a minimum mean square error (MMSE), which optimises the difference between estimated values ($\hat{\theta}$) and actual values (θ):

$$min(f) = min(|\hat{\theta} - \theta|) \tag{2.5}$$

In theory, parameter estimation is a straightforward process to perform. However, the optimisation process (finding the minimum or maximum values) might practically cost a lot of time and computing power. Optimisation arises in all quantitative disciplines from computer science, engineering to sciences and economics. The optimisation problem includes finding "best" values of some objective function given a defined region (or domain input) [86]. Optimisation usually requires repeating the evaluation function many times to find optimal values. This process can involve a huge computational effort. In some cases, the computational complexity and running time for the optimisation problem may be excessively high. Thus, different computation programs and algorithms have been proposed to find the balance between resources and performance. Some optimisation algorithms might require complex analysis with a super-high-speed computer to obtain highly accurate results, but other techniques can be performed using desktop computers for lower accuracy. Therefore, choosing the right parameter estimation method and an optimiser might be a vital process for

model development.

The least-squares method was developed as a standard approach for parameter estimation. This method is by far the most widely used for solving linear optimisation problems, especially in the field of identification [87]. Finding the maximum-likelihood of the squared residuals, this technique can be done analytically [88]. On the other hand, non-linear least-squares optimisation methods rely on minimising the sum of squared residuals. This can be done analytically in simple cases; however, in some complex non-linear problems, the solution requires different approaches. These approaches can be divided into derivative-based methods and other methods.

When the lung simulation becomes more sophisticated and attempts to fully represent the lung physiology and pathology, the patient's data can be fit into the model and perform parameter estimation. According to the literature on lung measurements, the constraints for parameters of the lung model can be set. The optimisation can be performed in these constraints. The whole method is named simulation-based optimisation. Simulation-based optimisation takes advantages of simulations, model phenomena and systems [89]. During the optimisation process, the same input signal is fitted to both patient and the lung simulation. The difference between the output signal and the simulated signal is optimised by changing the parameters of the lung simulation. Final results might confirm the match of both lung simulation and the patient's lung. Therefore, in this context, the lung simulation could be described as a 'black-box' function.

Bayesian optimisation

Bayesian optimisation (BO) has a potential to speed up the experimental pro-

cess by using machine learning to guide the search [90]. This method provides a principled technique based on Bayes' Theorem (probability and statistics theory) to direct a search of a global optimisation problem that is efficient and effective [91]. BO views an experiment as the black-box function $y = f(x)$ which takes an input x (design choice) and produces an outcome y (target measurement) to be optimised (Figure 2.19). Fundamentally, Bayesian optimisation is a sequential model-based approach that aims to optimise the black-box function. In one example, the Bayesian optimisation prescribes a prior belief over the possible objective functions using a Gaussian process regression model [92] and then sequentially refine this model as data are observed via Bayesian posterior updating.

Formally, let $f : X \to R$ be a well-behaved function defined on a subset $X \subseteq R^d$. Our goal is to solve the following global optimisation problem $x^* = argmax f(x)$ where $(x \in X)$. In the context of the lung simulation, a well-behaved function is that a single set of lung parameters should provide an only one value of the output signals. As a black-box function, the closed-form expression for f is not required, and this expression is expensive to evaluate. In Figure 2.19, the left panel shows the algorithm for BO. The right panel shows an example of BO in an application to suggests the next point (star point) depending on three previous observations (red points). BO builds and sequentially updates a surrogate model, typically through a Gaussian process (GP) [93]. Then, given the GP posterior update, BO defines a decision function - known as the acquisition function - to select a next experimental setting.

Gaussian process

Bayesian optimisation reasons about f by building a GP through evaluations [93]. GP is a nonparametric model that is fully characterized by its prior mean function [91]. This flexible distribution allows the model to associate a normally distributed random variable at every point in the continuous input space. The predictive distribution is acquired for a new observation x' that also follows a Gaussian distribution, where the predictive mean $\mu(x)$ (indicating the expected function value) can be estimated and predictive variance $\sigma(x)$ (indicating the uncertainty).

Acquisition functions

The acquisition function $\alpha(x)$ was constructed from the GP surrogate model above, to determine a next point to evaluate. The acquisition functions are carefully designed to optimise the trade-off between expanding the search space, and exploring current promising regions. A simple example of the acquisition function is the upper confidence bound: $\alpha(x) = \mu(x) + \kappa\sigma(x)$ where κ is the parameter controlling the exploration. Another common acquisition function is the expected improvement [94, 95], where we consider the expectation of improving (E) over a certain threshold y^+ as $E[max(0, f(x) - y^+)]$. Using the analytical form of the Gaussian distribution, the closed-form computation of the expected improvement can be derive [96]. After that, maximise the acquisition function can select the next point $x_{t+1} = \underset{x \in \mathscr{X}}{argmax}\,[\alpha_t(x)]$. In this auxiliary maximisation problem, the acquisition function form is known and can be easily optimized by standard numerical techniques.

Few studies have sought to estimate parameters via the lung simulation. However, researchers from other fields have developed parameter estimation methods for many

Algorithm 1 Bayesian Optimisation

initial data $\mathscr{D}_0$, #iter T

1: **for** $t = 1$ to T **do**
2: Fit a surrogate model as a GP from $\mathscr{D}_t$
3: Build an acquisition function from this GP
4: Select a next query $\mathbf{x}_t = \arg\max \alpha(\mathbf{x})$
5: Evaluate $y_t = f(\mathbf{x}_t)$
6: Augment $\mathscr{D}_t = \mathscr{D}_{t-1} \cup (\mathbf{x}_t, y_t)$
7: **end for**

Output: $\mathbf{x}_{\max}, y_{\max}$

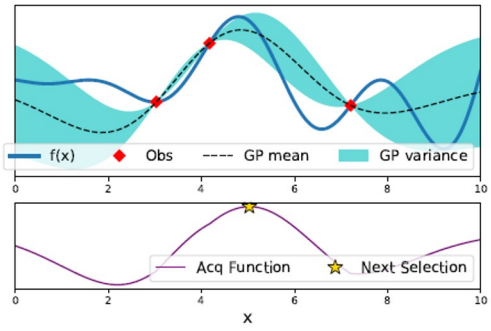


Figure 2.19: Bayesian optimisation coding example and a demonstration graph. Left: Algorithm for Bayesian optimisation using Gaussian process (GP) as a surrogate model to make a query for evaluation. Right: Example of Gaussian process and Bayesian optimization procedure over three iterations (three red points) [16]. The top plot shows the mean and variance estimated with a GP of the objective function. The lower plot also shows the acquisition function.

similar cases and problems. The parameter estimation for the multiple compartment lung is a challenging question. Harrison applied an approximation Bayesian computation method to match simulation to measurement [97]. Recently, Mountain developed his method using Nelder–Mead optimisation to use in the super-high-speed cluster [98]. The problems with this approach are that it is time and computational resource consuming. Although the results might be useful for research purposes, practically speaking for ventilated patients, the lung function tests might require a real-time analysis algorithm.

2.5 Conclusion

In conclusion, lung heterogeneity appears in the literature review to have a strong connection with lung disease. Therefore, lung function tests have been developed to calculate this parameter and also other related lung parameters. The Inspired

Sinewave Test stands out as being a non-invasive technique that is easy to set up and requires no active collaboration from patients. IST has the potential to measure and monitor the lung parameters at the bedside. However, there is a gap in the use of the IST to capture lung heterogeneity. There was no direct comparison or any comprehensive study of the IST heterogeneity previously. Thus, firstly, the lung simulations can be used to provide a fundamental understanding of how IST can measure lung heterogeneity. After that, a comparison of the IST heterogeneity vs recently available measurements could be performed. Further understanding the IST heterogeneity may improve the performance of the IST to help people with lung conditions. The lung simulation plays a vital role in testing the IST heterogeneity. To verify a lung simulation, several methods and techniques have been developed to assess it, including sensitivity analysis and computational tests. A good lung simulation combining with a non-invasive lung function test could be potentially beneficial for patients.

Chapter 3

Materials and Methods

3.1 Introduction

To evaluate the reliability and practicality of the Inspired Sinewave Test, several experiments were developed and implemented in both animal and human subjects. This chapter describes fully the methodology for all experimental data used in this thesis, including animal data collection, human data collection, pre-analysis, lung model development and also parameter estimation. Firstly, the methods to collect three sources of data (simulation, animal and human datasets) are presented. These data are available later for analysis. Secondly, the methods used to compare the measured results from the IST to 'gold standard' tests (the SF_6 washout and thermodilution) is described. The IST analysis (breath-by-breathy analysis) is mentioned here. Thirdly, two settings of the comprehensive lung simulations, one with two alveolar compartments and another with multiple alveolar compartments are presented. These simulations help to understand how the heterogeneity of the lung can be captured by the IST. Finally, based on this simulation, a simulation-based optimisation is developed to measure the lung heterogeneity directly by optimally matching simulated signals to measured signals.

3.2 Available data sets

The up-to-date available data will be presented here. In all three data sets, the inputs were the lung conditions, and the outputs were the IST results from these conditions. There are three main sources of data used in this study:

- Simulated data – these data were generated from a lung simulation with known conditions and lung heterogeneity. Parameters of these simulated lungs were recorded from the literatures. The aim of using this dataset is to verify the IST by comparing known input parameters of the simulation to the same parameters recovered by the IST.

- Animal data – these data were collected from anaesthetised pigs (pre-injury and post-injury). Outputs of these data were the IST results of different input conditions (ARDS or control). The primary purpose of this dataset is to compare the performance of the IST with the current 'gold-standard method' and to validate the method to calculate lung heterogeneity from the lung simulation model. This animal data allow us to test the device before lung injury (ARDS model in animal) and after lung injury.

- Human data – these data were collected from human subjects (healthy and COPD patients). Similarly to the animal data, the outputs of the human data were the IST estimated lung parameters. This data set is used to confirm and validate the method to calculate lung heterogeneity from the lung simulation model in human subjects. This dataset is more extensive than the animal dataset and it included subjects with a variety of lung conditions.

3.2.1 Simulated data

Parameters of patients with healthy or damaged lungs were taken from Yem, et al. [45]. This data set include ($n = 90$, healthy, emphysema and pulmonary embolism).

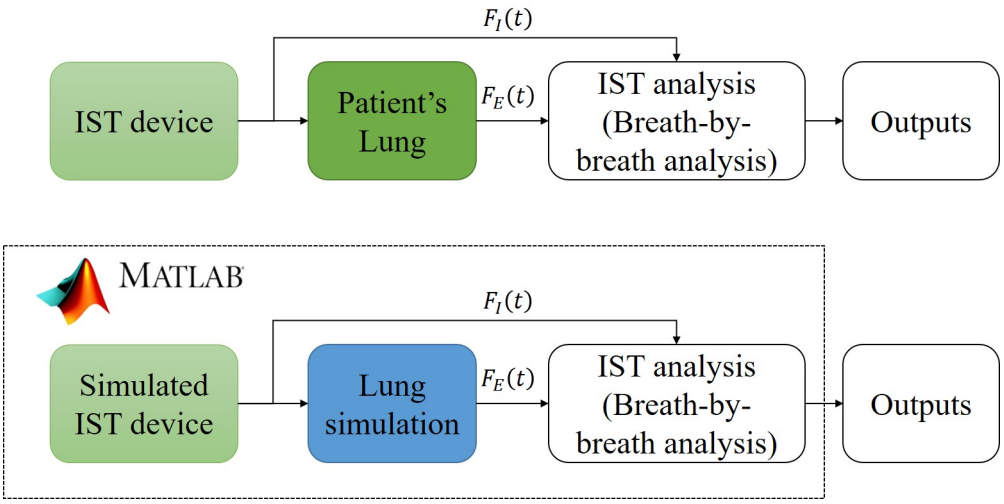


Figure 3.1: Block diagram of the tidal lung simulation in the IST system. The top diagram is the IST device and the bottom diagram is the IST simulated system developed in Matlab.

This set has two main purposes, which are to test the lung simulation and to examine the lung heterogeneity using only the IST results.

In the first part, the lung simulation should be verified with data from the literature (healthy human data from other studies). Secondly, after the lung simulation has been proven to work as a tool to represent the lung, a heterogeneity parameter will be added to the simulation. A tidal lung simulation was created to test the IST heterogeneity ratios among healthy, emphysema (patients with ventilation mismatch) and pulmonary embolism (patients with perfusion mismatch).

To fully simulate a lung to be tested by the IST, there are three main parts, the simulation of the device (IST), the simulation of the lung and the IST analysis. Thus, the novelty in this work is the development of the simulated IST device and the tidal lung simulation. The IST device can be simulated easily by simulating the input

equation (F_I):

$$F_I(t) = A + B \times sin(\frac{2\pi}{T} \times t) \tag{3.1}$$

where A is the mean, B is the amplitude and T is the time period of the sinewave at time t. In the second part, a tidal lung simulation is developed to simulate the behaviour of the lung. The lung simulation takes $F_I(t)$ as the input signal and provides exhaled signal $F_E(t)$ as the output signal. Figure 3.1 shows a systematic block diagram of the tidal lung simulation (bottom diagram) in conjunction with the IST system (on top diagram). The lung simulation output signal can be changed by the lung parameters, which present the lung condition. The tidal lung simulation and the IST breath-by-breath analysis combine to form a complete loop of the IST lung model. The inputs of this model are the lung parameters and the outputs are there recovered lung parameters calculated by the IST. The IST analysis is described in Section 3.3 and the tidal lung simulation in Section 3.4.

3.2.2 Animal data (Control vs ARDS model)

3.2.2.1 General protocol

Thirteen anaesthetised pigs were studied using the IST method both before lung injury (control) and after lung injury (injured). Lachmann's method (using saline lavage) was applied to induce lung injury to model the ARDS [99]. Figure 3.2 shows the timeline of the experiment in the animals. The rectangular blocks at the bottom

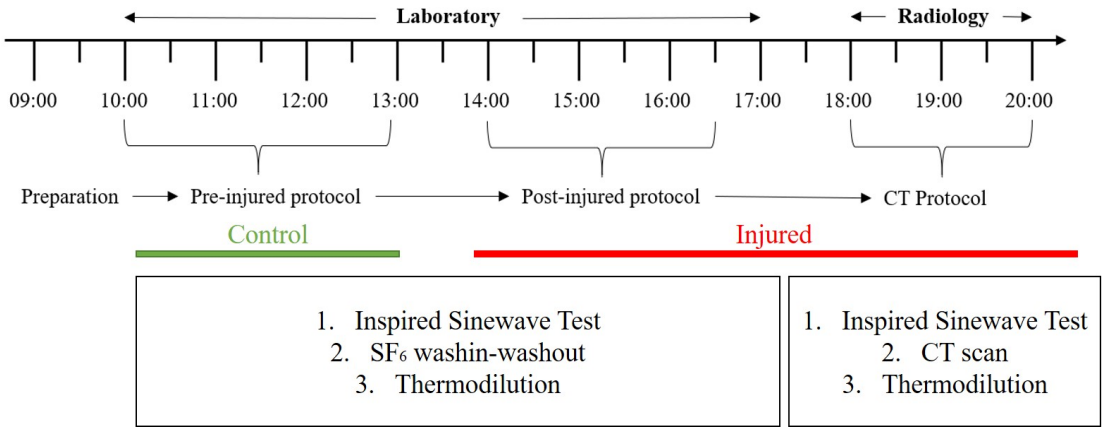


Figure 3.2: Timeline for the animal experimental protocol.

show the available tests. The studies were approved by the regional animal welfare ethics committee ($Ref : C98/16$) and adhered to the Animal Research: Reporting of in vivo Experiments guidelines [100]. Pigs were chosen as the species of investigation for several physiological and pragmatic reasons. In the laboratory, IST, SF_6 washin-washout and thermodilution were available. After that, in the CT scanning room, the SF_6 washin-washout was replaced by the CT scanner. Physiological parameters were recorded on LabChart via a PowerLab AD board (AD Instruments, NZ). At the end of the protocol, animals were humanely euthanised under anaesthesia with an overdose of pentobarbital.

3.2.2.2 Animal preparation

The study was performed in a total of 13 domestic pigs (mean weight $(SD) = 30(2)$ kg) as part of different experiments at the Hedenstierna Laboratory, Uppsala University, Sweden. Animals were prepared and the summary baseline characteristics of

these animals are given in Table 3.1. Before the experiment, the pigs were weighed, cleaned and prepared for general anaesthesia. Animals received intramuscular sedation and were anaesthetised with total intravenous anaesthesia as described elsewhere [101]. Mechanical ventilation was delivered at $20-25$ breaths per minute with a tidal volume (V_T) of $10mL/kg$ and an inspiratory: expiratory ratio (I:E) of $1:2$ (Servo-I, Maquet Critical Care, Solna, Sweden). Lack of spontaneous movements, absence of reaction to painful stimulation between the front hooves and absence of cardiovascular signs of sympathetic stimulation (increases in heart rate or arterial blood pressure) confirmed the depth of anaesthesia. Once anaesthesia was ascertained, rocuronium was administered for muscle relaxation. Continuous infusion of Ringerfundin^{TM} solution (Braun Melsungen Ag, Melsungen, Germany) was used for fluid replacement at 10 $mL/(kg \times h)$ during the preparation and at 7 $mL/(kg \times h)$ thereafter. Cardiac output was monitored intermittently by pulmonary artery catheter thermodilution [102].

3.2.2.3 Saline lavage lung injury model of ARDS

Saline lavage was used to induce lung injury (ARDS model in animal). In this method, the mechanical ventilation was disconnected and 0.9% saline solution (37^oC) was transferred to the lung via the endotracheal tube. This saline was drained out of the lungs after 30 s. The protocol was repeated until a PaO_2/F_IO_2 value of less than 300 mmHg was achieved.

Table 3.1: Animal baseline characteristics for $n = 13$ animals pre-(control) and post-lung injury. Mean (SD) are shown. p-values show results of paired Student's t-test. ns = non-significant.

Parameter	**Control**	**ARDS**	**p**
Weight (Kg)	29(2)	-	-
HR (bpm)	86(12)	85(11)	ns
CO (L/min)	3.4(0.8)	3.2(0.4)	ns
pH	7.38(0.07)	7.25(0.08)	0.0004
PaO_2(mmHg)	144(20)	96(40)	ns
F_IO_2	0.4(0.1)	0.8(0.1)	0.0002
PFR	377(30)	128(50)	0.0002

CO = cardiac output calculated by thermodilution, PaO_2 = arterial O_2 partial pressure, F_IO_2= fraction of inspired O_2, $PFR = PaO_2/F_IO_2$ ratio.

3.2.3 Human data (Healthy vs COPD subjects)

The characteristics of the human data set (healthy vs COPD) are shown in Table 3.2. 104 volunteers with different lung conditions and ages were recruited and tested by the IST at 60 s and 180 s period tracer gases. The ages of the participating subjects ranged between 20 and 86 years and subjects were defined as healthy through clinical screening with the following criteria: no childhood/past medical history of respiratory diseases.

All procedures for each participant were performed at the same sitting within the Respiratory Medicine Department of the Churchill Hospital, Oxford University Hospitals, NHS Foundation Trust and King's College London. The protocol for the

Table 3.2: Mean (standard deviation) of participant characteristics (Healthy and COPD GOLD phenotypes). BMI: body mass index.

	Healthy	**Type 1**	**Type 2**	**Type 3**	**Type 4**
n	32	12	31	19	10
Male/Female	18/14	3/9	20/11	13/6	9/11
Age(years)	70(9)	64(8)	67(10)	71(9)	66(9)
Height(m)	1.68(0.1)	1.66(0.1)	1.70(0.1)	1.68(0.1)	1.75(0.1)
Weight (Kg)	77(10)	79(19)	80(16)	78(19)	79(14)
BMI (kg/m^2)	27(4)	28(5)	28(5)	28(6)	26(3)

study was approved by an NHS ethical committee ($16/SC/0057$, ethics protocol 1.0) and conformed to the Declaration of Helsinki, 2013.

The medical history and anthropometric data were recorded before testing. Body plethysmography (FRC_{Pleth}) [103], spirometry (FEV_1 and FVC) [9] and the IST at two time periods (ELV_{180} and ELV_{60}) were measured. COPD volunteers were classified into GOLD standard (from type 1 to type 4) using the first two questions of the CAT questionnaire. An additional symptom score was produced specifically to assess the frequency of cough and presence of phlegm/mucus (Cough + Mucus score) [104]. COPD patients met the inclusion criteria if they were aged > 40 years, had a 10-pack year smoking history, and a $FEV_1/FVC < 0.7$. Patients were classified into the four 'GOLD' categories (1-4) based upon $FEV_1\%$ [105, 21, 106]. The classification was done by doctors working in the Lung function laboratory, Respiratory Medicine, Oxford University Hospitals.

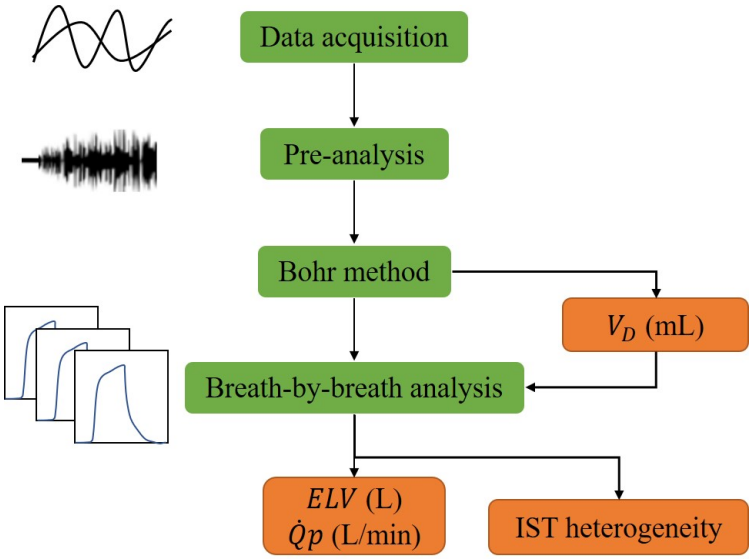


Figure 3.3: Signal processing block diagram of the inspired sinewave test analysis.

3.3 Breath-by-breath analysis (IST analysis)

The IST device including history, hardware and system was described in the literature review chapter. In this section, the IST analysis is presented. This is the process to calculate cardiopulmonary parameters from collected IST signals. Figure 3.3 shows a block diagram of the signal processing performed in the IST analysis (a specially developed algorithm). In this program, the measured signals are filtered, pre-processed and the breath-by-breath is performed [41].

A one-compartment lung is assumed to represent the whole lung in the breath-by-breath IST analysis. Figure 3.4 shows the working flow of the tracer gas from the lung to inside the body as a one-compartment model. This simple model is easy to use to derive the relation of the tracer gas inside the body. In this analysis, the lung consists of one dead space compartment V_D and one alveolar lung compartment

$V_A(t)$. During the inspired sinewave test, $F_I(t)$ follows the input sinewave patterns. The alveolar concentration, $F_A(t)$, the arterial concentration $F_a(t)$ and the mixed venous concentration, $F_{\overline{V}}(t)$, are therefore all forced to follow sinusoidal patterns. The mass balance of the tracer gas can thus be generated.

VD_{IST} was measured using the modified Bohr method [65]. ELV_{IST} and QP_{IST} were calculated from a model assuming one well-mixed lung compartment model, called the IST analysis [19]. To begin, the deadspace volume is calculated using this equation:

$$VD = V_T \frac{F_E - F_{\bar{E}}}{F_E - F_I} \tag{3.2}$$

where $F_{\bar{E}}$ is the expired average or "mixed" tracer gas concentration. Mass balance equations of the tracer gas breath-by-breath can then be generated from this model:

$$F_{E,n-1}V_A + F_{\bar{I},n}(V_{T,n} - V_D) + F_{E,n-1}V_D - \lambda \dot{Q}_P(F_{E,n} - F_{\bar{v}}\Delta t_n) = V_A F_{E,n} + V_{T,n}F_{E,n} \tag{3.3}$$

so that:

$$V_A(F_{E,n} - F_{E,n-1}) + \lambda \dot{Q}_P(F_{E,n} - F_I^0)\Delta t_n = V_D(F_{E,n-1} - F_{\bar{I},n}) + V_{T,n}(F_{\bar{I},n} - F_{E,n}) \tag{3.4}$$

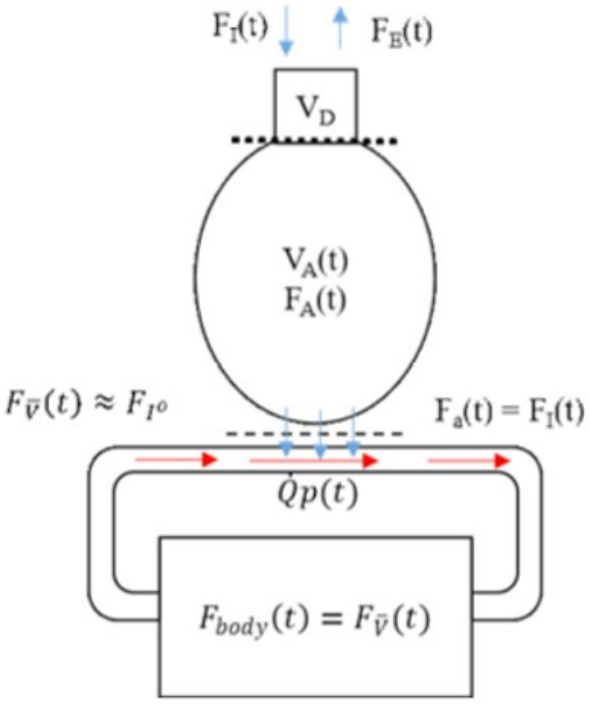


Figure 3.4: One lung compartment model of the IST analysis.

where $F_{I,n}$ is the inspired concentration of breath n. $F_{E,n}$ and $F_{E,n-1}$ are the expired concentration of breath n and $n-1$. λ is the solubility of N_2O, 0.47 [41]. $F_{\bar{V}}$ is the mixed venous concentration assumed to equal to the mean of the inspired sinewave concentration at steady state F_I^o, Δt_n is the duration of breath n and $V_{T,n}$ is the tidal volume of breath n. The IST analysis uses breath-by-breath analysis; therefore, each breath provides one dataset. V_A and $\dot{Q}_p$ are estimated by solving a set of these equations.

In term of lung heterogeneity, in a completely homogeneously ventilated and perfused lung, the values of ELV and $\dot{Q}p$ recovered from the IST are assumed to be

independent of the tracer gas period used. As the degree of heterogeneity increases, the ELV and $\dot{Q}p$ values (based on the assumption of perfect homogeneity, i.e., a well-mixed single compartment) begin to diverge from true values, and those values recovered from periods of the 60 s and 180 s also diverge from each other. Consequently, the ratio of these latter values seems to provide an index of the degree of heterogeneity. The IST ventilatory and perfusion heterogeneity indices of the lung are given by the following ratios:

$$H_{Vent} = \frac{ELV_{180}}{ELV_{60}} \tag{3.5}$$

$$H_{Perf} = \frac{\dot{Q}_{P60}}{\dot{Q}_{P180}} \tag{3.6}$$

where ELV_{60s} is the estimated of effective lung volume at a forced tracer gas period of $60s$ and similar in the ELV_{180s}; and similarly for $\dot{Q}_{P60}$ (for pulmonary blood flow). Just like the Lung Clearance Index of the Multiple Breath Nitrogen Washout, the simplest of the IST heterogeneity indices exploits the fact that a single compartment model will breakdown when supplied by data from a multi-compartment lungs, whereas ELV_{60s} should be identical to ELV_{180s} if the ventilation is homogeneously distributed. Mean and amplitude of the input signal was fixed at 10% and $\pm$5% of N_2O concentration.

The ratio of $60s$ and $180s$ were chosen because previous studies used the same setting with $60s$ and $180s$. The basic principle is that for perfectly homogeneous

lungs, theoretically, the recovered lung parameters would be the same regardless of the period used. In lungs with heterogeneously distributed ventilation, the recovered parameters will be incorrect (if a single compartment model is used to recover them). Moreover, the error will be greater as the period gets smaller. We exploit this 'model breakdown' to infer something about the degree of heterogeneity. In its simplest application, if the parameters recovered at 180s are the same as those recovered at 60s, we can infer that the ventilatory distribution is homogeneous. The greater discrepancy between the two datasets, the greater must be the heterogeneity.

1. Clearly, we would like periods which are sufficiently different (choosing 180 and 170s, for example, would not give sufficient separation).

2. Periods much shorter than 60s would give a very heavily attenuated alveolar sinewave, which would be difficult to measure.

3. Periods much greater than 180s would give an alveolar sinewave that was hardly be attenuated at all (so no useful info), and we would also risk the problem of failure to attenuate the mixed-venous signal (which we assume to be heavily attenuated by the tissues, and to behave as a quasi-constant)

3.4 Lung simulations

3.4.1 Compartmental model of the lung simulation

This lung simulation was built from a previously validated model, including deadspace compartments [97], tidal alveolar lung compartments, five body compartments for a

standard 70 kg patient and a shunt compartment [107]. A schematic of this simulation is shown in Figure 3.5. The lung simulation was developed and validated in Matlab (MathWorks, USA, www.mathworks.com). The novelty of this model is adding two more alveolar compartments to create the multiple alveolar compartments (three compartments in Figure 3.5), which can be set to represent the lung heterogeneity. The *ode45* solver and *Simulink-Matlab* were chosen for simulation. Compartments can be added or modified easily in the *Simulink* environment.

The compartmental model was chosen to present the lung because it can fully represent the gas-exchange process inside the lung and it is easy to modify and improve in the future with the presence of lung heterogeneity. This model consists of deadspace compartments, alveolar compartments (or tidal lung compartments) and body compartments. The equation of each deadspace compartment during inspiration is:

$$V_{M,i}\frac{dF_{M,i}}{dt} = \dot{V}_A(t)(F_{M,i-1}(t) - F_{M,i}(t)) \tag{3.7}$$

where i is the number of deadspace compartments (from 1 to 3); and $F_{(M,1)}(t) = F_I(t)$ and $F_{M,3}(t) = F_{IA}(t)$. $V_{M,i}$ is the deadspace volume of a compartment i and $\dot{V}_A(t)$ is the air flow at time t (or ventilation). The equivalent equation during expiration is:

$$V_{M,i}\frac{dF_{M,i}}{dt} = \dot{V}_A(t)(F_{M,i}(t) - F_{M,i+1}(t)) \tag{3.8}$$

where $F_{M,1}(t) = F_E(t)$ and $F_{M,3}(t) = F_A(t)$. F_I, F_{IA}, F_A and F_E are the fractional concentrations of the tracer gas coming into the deadspace compartment; coming out

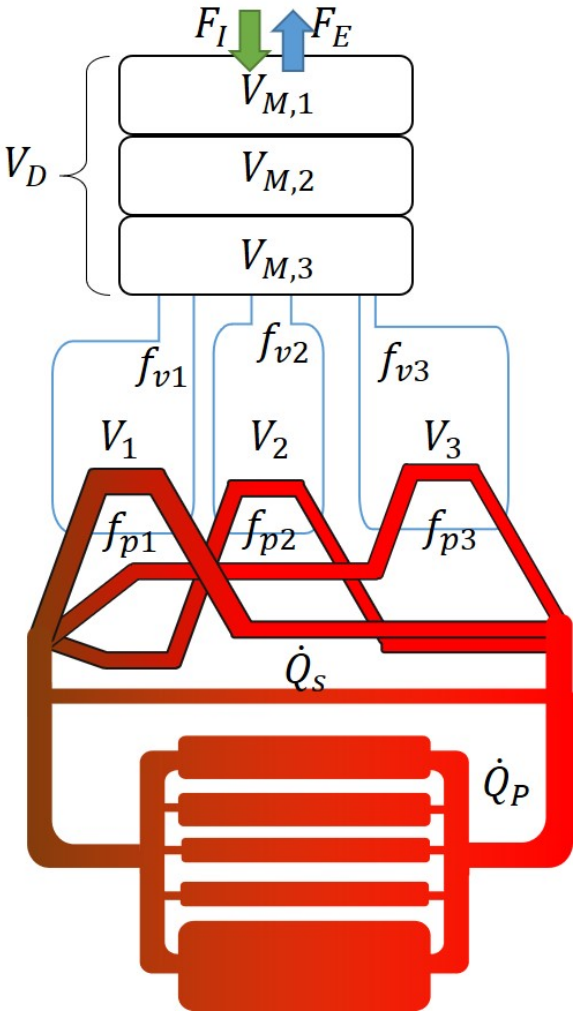


Figure 3.5: Schematic diagram of the tidal lung simulation with three alveolar compartments.

from the deadspace compartment to the lung compartment; coming back from the lung compartment to the deadspace compartment and exhaling from the deadspace to the environment, respectively. Multiple deadspace compartments present the true deadspace better than one compartment [12]. Three deadspace compartments were chosen because there was no more significant improvement with more than three compartments [42].

The deadspace compartments are serially connected with three parallel lung blocks. These lung blocks are generated from physiological equations of the tidal lung [11]. The tidal lung equation during inspiration:

$$V_A(t) = \bar{V}_A + \frac{V_T \times t}{t_I} \tag{3.9}$$

and during expiration:

$$V_A(t) = \bar{V}_A + V_T \times exp(-\gamma(t - t_I)) \tag{3.10}$$

where γ is the rate-constant of expiratory flow, $V_A(t)$ is the alveolar volume at time t, V_T is the tidal volume and t_I is the inspiration starting time. $\bar{V}_A$ is end-expired alveolar volume. Alveolar volume (V_A) was assumed as a constant value, in this model defined as $\bar{V}_A$. In order to create the tidal flow breathing pattern, it is assumed the subject is ventilated. The breathing pattern proposed by Gavaghan and then Harrison is thus used a linear increase during inspiration and then following by an exponential decay during expiration [76, 97].

The whole set of compartments is linked together by governing equations which

represent the equilibrium of the mass concentration of the tracer gas. $C_{\bar{v}}$ and C_a are the mixed venous and pulmonary end-capillary gas concentrations, respectively. Inspiration:

$$\frac{d}{dt}(V_A(t) \times F_A(t)) = f_{v,i} \times \dot{V}_{A,i}(t) \times F_{IA}(t) + f_{p,i} \times \dot{Q}_{p,i}(C_{\bar{v}} - C_a) \tag{3.11}$$

Expiration:

$$\frac{d}{dt}(V_A(t) \times F_A(t)) = f_{v,i} \times \dot{V}_{A,i}(t) \times F_A(t) + f_{p,i} \times \dot{Q}_{p,i}(C_{\bar{v}} - C_a) \tag{3.12}$$

where i is the number of the tidal compartment, each compartment has their own fraction of ventilation $f_{v,i}$ and fraction of perfusion $f_{p,i}$. The sum of ventilation fraction was equal to 1, similarly with perfusion fraction and volume fraction.

The body compartments of a standard human consist of five different tissues inside the human body with different values of tissue-gas coefficient [68, 107, 70].

$$V_i^* \frac{dC_i(t)}{dt} = \dot{Q}_i(C_{\bar{a}}(t) - C_i(t)) \tag{3.13}$$

where V_i^*, C_i and $\dot{Q}_i$ are the equivalent blood volume, concentration of the tracer gas and blood flow rate of i compartment. V_i is given by the following equation where $V_{(b,i)}$ and $V_{(t,i)}$ are the blood and tissue volumes of each body compartments and $\lambda_{(t,i)}$ is the Ostwald tissue-gas coefficient of each compartment. The values of $V_{(b,i)}$, $V_{(t,i)}$ and $\lambda_{(t,i)}$ are given in Table 3.3. [70].

$$V_i^* = V_{b,i} + \frac{\lambda_{t,i}}{\lambda} V_{t,i} \tag{3.14}$$

The Ostwald coefficient is a relation between the concentrations of the tracer gas in the blood and the fractional concentration in the lung. λ is the blood-gas partition coefficient. The body temperature is assumed to be constant (37^oC), so the Ostwald coefficient can be assumed to be stable.

$$C_a = \lambda \times F_A \tag{3.15}$$

The mixed-arterial concentration $C_{\bar{a}}$ is given below with $\dot{Q}_S$ being the shunt flow rate, $\dot{Q}_P$ pulmonary blood flow rate and $\dot{Q}_T$ total blood flow:

$$C_{\bar{a}}(t) = \frac{\dot{Q}_S}{\dot{Q}_T} C_{\bar{v}}(t) + \frac{\dot{Q}_p}{\dot{Q}_T} C_a(t) \tag{3.16}$$

Since $\dot{Q}_S = \dot{Q}_T - \dot{Q}_P$, the shunt equation becomes:

$$\frac{\dot{Q}_S}{\dot{Q}_T} = \frac{C_a(t) - C_{\bar{a}}(t)}{C_a(t) - C_{\bar{v}}(t)} \tag{3.17}$$

3.4.2 Parameters for the lung simulation

To make this simulation run, recorded parameters from the literature were taken and put into the model. These parameters are given in Table 3.3 and Table 3.4 [108, 45, 68]. Table 3.3 shows parameters for a body compartment of a healthy man

Table 3.3: Body compartments data of a $70kg$ standard man.

Compartment	Blood volume (L)	Tissue volume (L)	Blood flow (L/min)	Ostwald coefficient
Lung	0.37	0.55	5.34	0.47
Viscera Fast	0.87	0.35	1.39	0.40
Viscera Liver	0.98	3.73	1.48	0.43
Viscera Rest	0.62	1.89	1.09	0.51
Lean	0.53	37.4	1.13	0.40
Fat	0.16	12.8	0.25	1.40

70 kg. These parameters were assumed to be unchanged, however, further research could be done to understand the influence of changes of these body parameters on the model output. The initial condition for the differential equations was fixed from the beginning of the simulation. It was assumed that the lung is going to achieve the equilibrium, so the inspired and expired concentrations are constant.

In Table 3.4, other parameters for the lung model are included. Mean and standard deviation values in the Table 3.4 are used for the sensitivity analysis.

An example of the simulated signals from the lung model is plotted in Figure 3.6. This figure shows a comparison of a simulated signal vs the measured N_2O signal from an anaesthetic pig. Pig's lung was assumed to fully represent the healthy lung.

Table 3.4: Lung simulation parameters in healthy condition. Mean and standard deviation are shown.

Parameter	**Symbol**	**Healthy**
Deadspace volume (L)	V_D	0.15(0.025)
Alveolar volume (L)	V_A	2.5(0.75)
Tidal volume (L)	V_T	0.7(0.3)
Inhaled time (s)	t_I	2(0.5)
Respiration rate (Breath/min)	RR	12(5)
Expiratory flow coefficient (L/s)	γ	1(0.3)
Pulmonary blood flow (L/min)	$\dot{Q}_P$	5.0(2.0)
Shunt (L/min)	$\dot{Q}_{Shunt}$	0.3(0.1)

The simulated and measured signal in this figure are not perfectly in alignment with each other. However, this could be caused by lung heterogeneity.

3.4.3 Heterogeneity lung simulation

According to Figure 3.6, the simulation data cannot fit perfectly to the measured data. By introducing heterogeneity into the lung simulation, it should be possible to significantly improve the alignment between simulated and measured signals. In this thesis, three lung simulations were created (the summary graph is included in Figure 3.7). Because of the lung simulation setting, the deadspace and body compartments were kept unchanged, while the alveolar compartment was varied in three different modules (2a, 2b and 2c). In Figure 3.7, Module 2a (in the Figure) represents a healthy lung (single compartment only). This simulation was used for the model

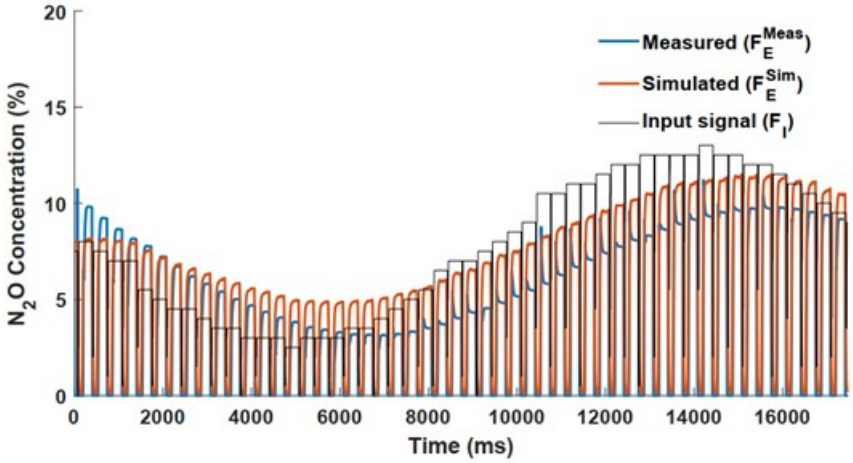


Figure 3.6: Simulated vs measured signals from the IST.

verification process. Module 2b (two alveolar compartments) and model 2c (multiple alveolar compartments) were assumed to represent lung heterogeneity. Module 2b was used to study how IST could capture the lung heterogeneity. Next, module 2c was developed to be used as a tool to measure the lung heterogeneity from the model directly. The design of module 2b will be presented in Chapter 5 and module 2c will be in Chapter 6.

3.4.3.1 Two alveolar compartments model

This simulation contained two alveolar compartments to simulate lung heterogeneity. The heterogeneity of both ventilation and perfusion (relative to compartment volume) could be controlled by fraction parameters. To simplify the lung heterogeneity, the volume fractions of the two tidal lung compartments were fixed at 0.1 and 0.9 ratio, meaning that each comprised 10 % and 90 % of the total lung volume. The ventilation

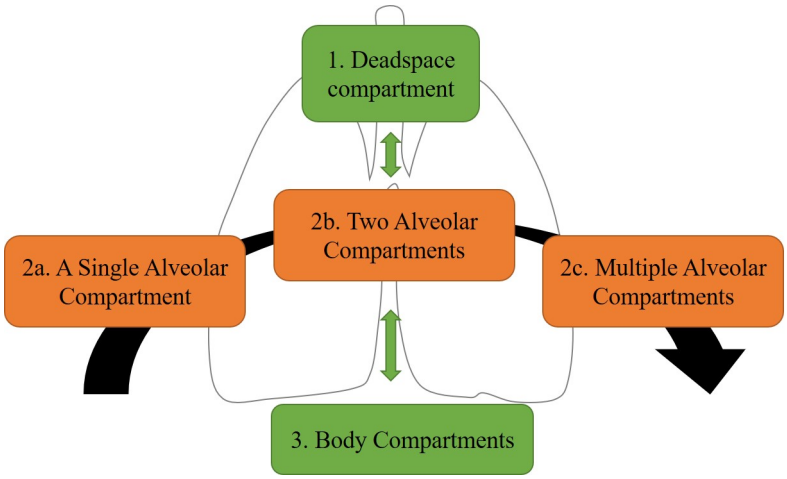


Figure 3.7: Schematic diagram of the lung compartment models in three different modular design.

and perfusion fractions for the first lung compartment are f_v and f_p respectively. The ventilation and perfusion fractions to the second compartment are by definition $(1-f_v)$ and $(1-f_p)$. By these conventions, the lung was homogeneous when $f_{v1} = 0.1$ and $f_{p1} = 0.1$. An increase in value of f_{v1} causes the mismatch of the ventilation and higher lung ventilation heterogeneity. Similarly, when f_{p1} increases, the lung perfusion heterogeneity also increases.

3.4.3.2 Multiple alveolar compartments model

Similar to the two alveolar compartments model, this simulation contained a higher number of 125 alveolar compartments. Each compartment had its volume, ventilation and perfusion fractions. These fractions were controlled by the lognormal distribution (Figure 3.8) [13]. The fraction was sampled from the distribution equation:

$$y = f(x|\mu,\sigma) = \frac{1}{x\sigma\sqrt{2\pi}} exp\left\{\frac{-(logx-\mu)^2}{2\sigma^2}\right\}, x > 0 \tag{3.18}$$

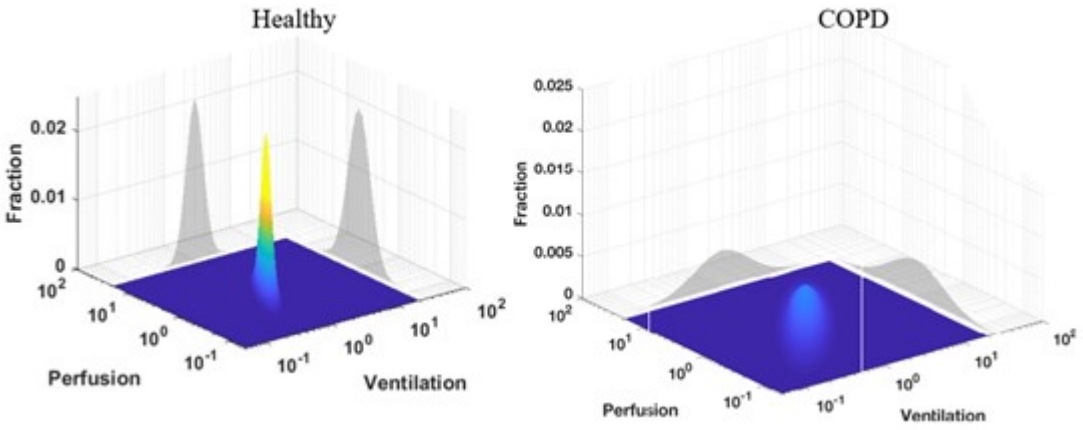


Figure 3.8: Example of the simulated healthy and COPD lognormal distributions.

where μ is mean of logarithmic values and σ is standard deviation of logarithmic values. In Figure 3.8, a COPD patient had a spread-out distribution compared to a tighter distribution in a healthy volunteer. These data were simulated from literature parameters [13]. With the lung simulation has more than two compartments, reverser calculation using breath-by-breath analysis is challenging. Therefore, in the multiple compartment simulations, heterogeneity values can be estimated basing on finding the best fit of a simulation to the measured values.

3.4.4 Model verification and model validation

3.4.4.1 Model sensitivity analysis

Sensitivity analysis is used to verify that the model is working correctly with the IST. Key parameters and model robustness of the model to noise also is revealed. One hundred patients with a healthy lung are simulated with the parameters set in

Table 3.4. Gaussian white noise was introduced to the tidal volume of the simulation. The particle rank correlation coefficient (PRCC) and Morris method are used for the sensitivity analysis. After that, linear regression analysis between set parameters and recovered parameters is performed with and without noise.

3.4.4.2 Healthy, Emphysema and Pulmonary Embolism

Furthermore, simulated patients with emphysema and pulmonary embolism were created to test the recovered lung heterogeneity parameters (Table 3.5) [45]. In Table 3.5, the mean values and (standard deviations) of two abnormal lung conditions (emphysema and embolism) are presented. These parameters were obtained from the paper of Yem, et al. [45]. Lung heterogeneity values were recorded and compared to see if it could detect the difference between emphysema, pulmonary embolism, and healthy simulated lungs. This process is the first step, *in silico* validation of the lung simulation, before moving on to the animal and human testing.

Next, animal and human data are used to validate the model. Recovered parameters of the lung heterogeneity are reported in both animal (non-injured vs injured) and human (healthy vs COPD) data. After that, the IST lung heterogeneity results are compared with the heterogeneity values measured by CT scan. Statistical tests are performed to justify the reliability and accuracy of the lung model. The animal data and human data sets were described in the previous sections of this chapter.

Table 3.5: Lung simulation parameters for emphysema and pulmonary embolism conditions. Mean values and (standard deviations) are shown. c_i is the alveolar compartment i. $* = 1 - c_1 - c_2$, $** = 1 - c_1$

Parameter	**Emphysema**	**P. Embolism**
Deadspace volume (L)	0.33(0.05)	0.157(0.12)
Alveolar volume (L)	4.5(0.75)	2.82(0.75)
Tidal volume (L)	0.45(0.3)	0.46(0.3)
Inhaled time (s)	1(0.5)	0.75(0.5)
Respiration rate (Breath/min)	22(5)	29(5)
Expiratory flow coefficient (1/s)	1(0.3)	1(0.3)
Shunt(L/min)	0.015(0.01)	0.74(0.05)
Alveolar compartment number	3	2
Ventilation fraction (c_1)	0.102(0.30)	0.334(0.08)
Ventilation fraction (c_2)	0.065(0.06)	0.666(**)
Ventilation fraction (c_3)	0.833(*)	-
Volume fraction (c_1)	0.196(0.02)	0.333(0.07)
Volume fraction (c_2)	0.577(0.02)	0.667(**)
Volume fraction (c_3)	0.277(*)	-
Blood flow fraction (c_1)	0.889(0.02)	0.507(0.02)
Blood flow fraction (c_2)	0.072(0.01)	0.493(**)
Blood flow fraction (c_3)	0.039(*)	-

3.4.5 Parameter estimation

For the single alveolar compartment model, the IST breathy-by-breath analysis could straightforwardly provide estimated parameters for the model. Similarly, with two alveolar compartments simulation, the IST breath-by-breath combined with two tracer gases (60 s and 180 s) could recover the parameters.

For the multiple alveolar compartment model, on optimisation method was applied to match simulated to measured signals. To recover the parameter values, Bayesian optimisation was applied to match simulated to measured data [16]. Vu et al. modified Bayesian optimisation to approach specified search space for hyper-parameter tuning [16]. This method was implemented in Python to recover the parameters for the lung simulation. According to recorded data and data from the literature, ranges for individual parameters were set. Next, Bayesian optimisation can statistically provide guessed values for the simulation to minimise the lost function effectively. The optimisation algorithm searched in these ranges only. Minimising the loss function $f(\theta)$ estimated the lung simulation input parameters θ:

$$f(\theta) = argmin(|\frac{Simulated(\theta) - Measured}{Measured}|) \tag{3.19}$$

This method aims to provide a suggestion to minimise the loss function between simulated and measured outputs. The optimal value of the loss function is obtained when the simulated and the measured outputs match perfectly. Thus, the lung heterogeneity value in the simulated lung should be the same as that in the measured

Table 3.6: Initial prior distribution for the optimisation process.

Parameter	**Initial prior**	**Minimum value**	**Maximum value**
Deadspace volume (mL)	150	50	350
Alveolar volume (L)	2.0	0.5	4.0
Cardiac output (L/min)	5	2	10
Mean of ventilation	0	-1.0	1.0
Mean of perfusion	0	-1.0	1.0
Standard deviation of ventilation	0.5	0.2	2.0
Standard deviation of perfusion	0.5	0.2	2.0

patient. The initial prior distribution was presented in 3.6. The distribution of the prior was assumed to be the uniform distribution from the minimum to maximum values.

3.5 Lung heterogeneity measured by the CT scanning

This aims to compare measurements of lung heterogeneity made by the IST method with those measured from CT images in animals with ARDS. Six anaesthetised pigs were measured and analysed by both CT scan and the IST. Thirteen animals were

Table 3.7: Mean (standard deviation) characteristics of $n = 6$ pigs. FIO_2: fraction of inspired O_2, Hb: haemoglobin, SaO_2: oxygen saturation.

Parameter	**Mean(SD)**
Weight (kg)	30.3(1.64)
Heart rate (bpm)	99.5(20.5)
Cardiac output (L/min)	3.35(0.38)
Hb (g/L)	88.5(12.0)
FIO_2	0.78(0.02)
SaO_2 (%)	98.3(0.85)

studied with the IST. Six animals had both IST results and CT images to compare. The summary of the animals' baseline characteristics is shown in Table 3.7.

In our research, CT images were acquired during imposed breath-holds by closing both the expiratory and inspiratory airway valves of the ventilator at end-expiration. The whole lung was scanned by a Somatom Denition Flash or Somatom Denition Edge (Siemens, Munich, Germany). A tube voltage of 80 kV, 364 mA current and 64×60 mm collimation was used. Collected images have a resolution of $0.5 \times 0.5 \times 5$ mm. The CT images were segmented using 3D Slicer by hand (https://www.slicer.org) [109]. Exclusion of intrapulmonary vessels within regions of increased voxel density was not possible as they were not distinguishable from lung tissue, and these, along with the conducting airways up to the level of the clavicles. Human error should be mentioned in the segmentation process.

According to Cressoni, et al., the lung inhomogeneity index of one voxel can

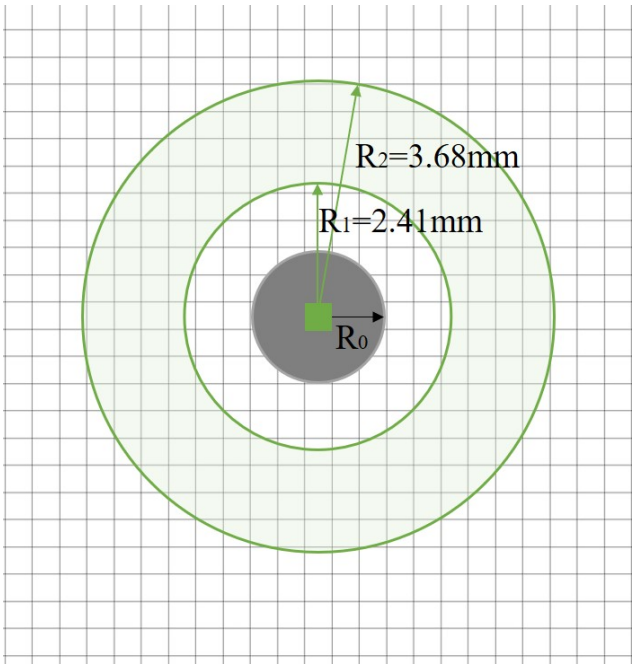


Figure 3.9: Cressoni's method to calculate lung heterogeneity from CT images.

be calculated from the difference of the HU in one voxel to its surrounding voxels. The term "Extent of lung inhomogeneities" refers to the fraction of lung volume that presents a lung inhomogeneity index greater than 1.61 [5]. This method is applied to calculate the lung heterogeneity for the collected data (Figure 3.9). The heterogeneity score was calculated by comparing the HU of the centre voxel (black voxel) to surrounding voxels (from R_1 to R_2). The volume inside R_1 is not included.

The heterogeneity index calculated by the Cresoni's score is:

$$H_{CT} = \frac{N_{\text{Extent of lung inhomogeneity}}}{N_{Total}} \tag{3.20}$$

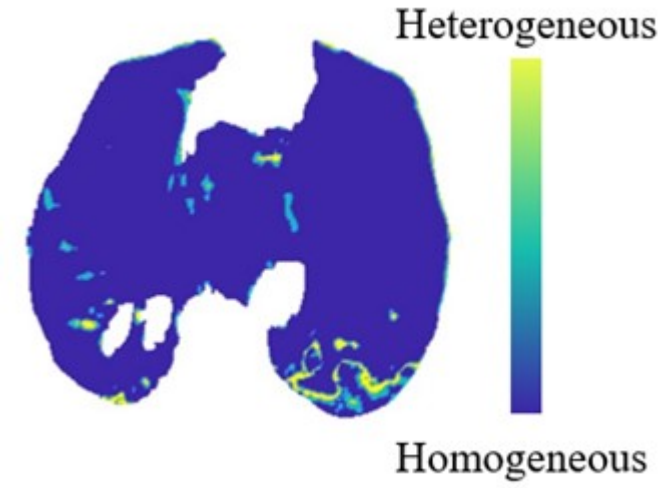


Figure 3.10: Examples of lung heterogeneity measured by the CT images at PEEP 5 cmH_2O in a pig.

where, $N_{\text{Extent of lung inhomogeneity}}$ is the number of voxels that have the lung inhomogeneity index greater than 1.61. N_{Total} the total number of voxels. Figure 3.10 shows examples of the lung heterogeneity analysed by Cressoni's method in a pig's lung.

3.6 Classification model and statistics

With the development of machine learning algorithms and advanced computing power, classification problems can be solved in a couple of coding lines. Machine learning algorithms such as decision trees or support vector machines can take advantage of an extensive dataset with multiple features. Furthermore, the classification of lung diseases is not a new problem in the machine learning field. This method is learning a set of rules from a training set, or in other words, creating a classifier that can be

used to generalize from new instances [110]. However, machine learning models are not the focus of this thesis.

Therefore, a simple classification method and basic statistics are used. Logistic regression and Student's t-test are applied to compare two groups. Receiver operating characteristics (ROC) curve and area under the curve (AuC) were used to show the classification between two groups [111]. Linear regressions are used to compare the agreement and relationship between two pair of measurements.

3.7 Conclusion

In this chapter, the main material and methods of this thesis were presented. The available data sets in this thesis (simulated, animal and human data) were presented. The detailed simulation of the lung and method to quantify the lung parameters using the IST were described. Verification and validation methods of the lung simulation model are included. Further analysis such as statistical analysis and additional interpolation of the data will be described in detail in each subsequent chapter.

Chapter 4

Investigating lung parameters measured by the IST in comparison with SF_6 & thermodilution

In this chapter, the IST results were compared with those from current 'gold-standard' tests, SF_6 washin-washout and thermodilution. This comparison study was performed in pigs both pre-injury (control) and post-injury (ARDS model) under anaesthesia. The working principles of the IST and the animal experiments have been described in the method chapter previously.

Results in this chapter indicated good agreements between the IST and other tests. Firstly, the absolute deadspace volumes measured by the IST and SF_6 washin-washout were found to exhibit a strong relationship (in control subjects, $r = 0.87, R^2 = 0.5$). Secondly, the absolute effective lung volume measured by the IST was compared with

the measured values of SF_6 ($r = 1.0, R^2 = 0.77$). Finally, the relationship between the IST pulmonary blood flow and the thermodilution technique is investigated. This too shown good agreement with a bias of 0.2 L/min .

This chapter confirmed that the IST can measure lung parameters directly from mechanically ventilated subjects. Its results were found to exhibit strong correlations and agreements with results from similar gas transfer lung function tests. Using the IST alone can provide the similar results to both SF_6 and thermodilution.

4.1 Study details

In the animal protocol, thirteen anaesthetised pigs (weight of 29 ± 2 kg) were studied using the IST, both before lung injury (control) and after lung injury (injured). Lachmann's method was applied to induce lung injury to model the ARDS. The experiments were performed in the Uppsala University Hospital. Each animal was studied over the course of one day from 9 am to 7 pm. This protocol abided by the animal welfare laws and regulations. The animal model was used because its results have a direct translation to human medicine. Using human subjects will be not suitable for this ARDS study. There is difficulty in finding a patient with the conditions of both before and after ARDS.

During the experiment, the measurements were repeated twice using the IST, the SF_6 washin-washout and thermodilution at each PEEP level. While other parameters of the ventilator setting were kept unchanged, the PEEP levels were incrementally increased from 5 to 10, 15 and 20 cmH_2O and then reduced back to 5 cmH_2O. The

changes in PEEP level induce changes in lung volume capacity. The results of the IST from the 180 s forced period tracer gas were used. After the measurements in the control group, lung injury was induced, and the same measurements were repeated. For the statistical analysis, linear regression and Bland-Altman analysis were applied to understand the statistical relationship and agreement between paired measurements [112].

4.2 Results

A total of 140 paired measurements in thirteen animals at four different PEEP levels were recorded. The values of repeated measurements were averaged due to the negligible variations shown (less than 3% in SF_6 and less than 5% in IST). The deadspace volume and effective lung volume estimated by the IST are reliable than pulmonary blood flow in comparison with the SF_6 and thermodilution tests.

4.2.1 Deadspace volume, a comparison of IST to SF_6

Figure 4.1 shows the relationship and correlation between deadspace volume measured by the IST and the SF_6. In general, deadspace volume increased when the PEEP was raised, and the injured (ARDS) group had larger deadspace volumes than the control group, Figure 4.1 panels a and b. The standard deviation value of injured lung measurement was 137% larger than the noninjured values on average.

In Figure 4.2, linear regression and Bland-Altman plots illustrated the good relationships between IST and SF_6 deadspace volume measurement. Specifically, the SF_6

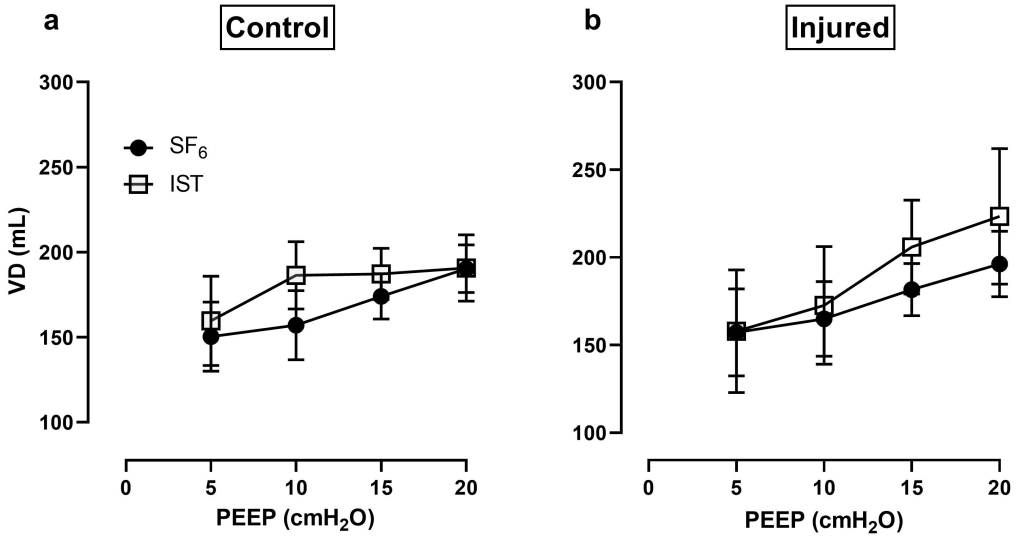


Figure 4.1: Overall comparison of the paired deadspace volume measurements made by the SF_6 and IST techniques in the control (pre-injured) and injured lungs (ARDS model).

deadspace volume measurements are shown to exhibit smaller variations compared to the IST. There is a robust relationship between V_DIST and V_DSF_6: the linear regression slope was found to be 0.87 with a $R^2 = 0.51$, in the control group, panel a. The volume bias was 9 mL (limits of agreement -79 mL to 57 mL) in control and similarly, 10 mL (limits of agreement -51 mL to 32 mL) in ARDS lungs (panels c and d).

4.2.2 Effective Lung Volume, a comparison of IST to SF_6

The effective lung volumes measured in control and injured animals were presented in Figure 4.3. Overall, strong agreements were found between IST and SF_6 in both control and injured groups. When PEEP increased, ELV_{IST} and ELV_{SF6} also increased.

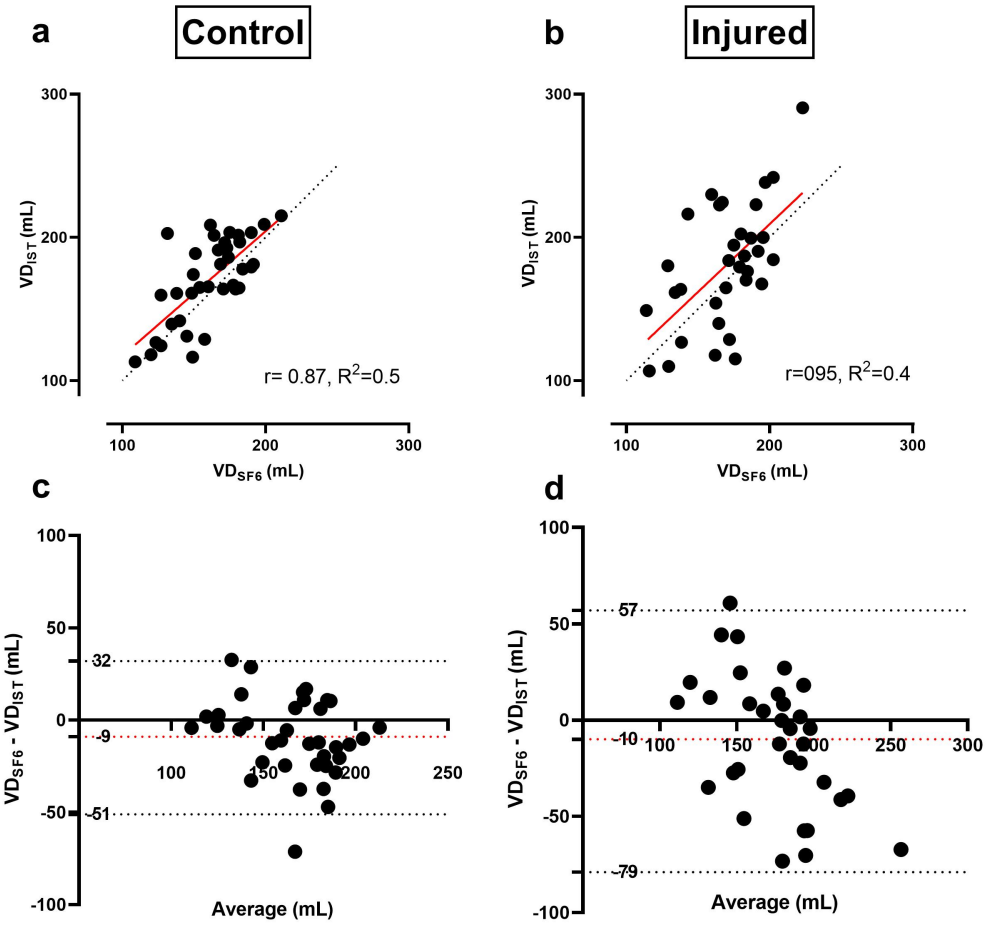


Figure 4.2: Linear regression of absolute deadspace volume measured by IST and SF_6. The red lines represent the regression lines and the black dashed lines the reference lines. Panel c and d are Bland-Altman plots, the bias lines are the red dashed line and the black dashed lines are the limits of agreement (± 1.96SD).

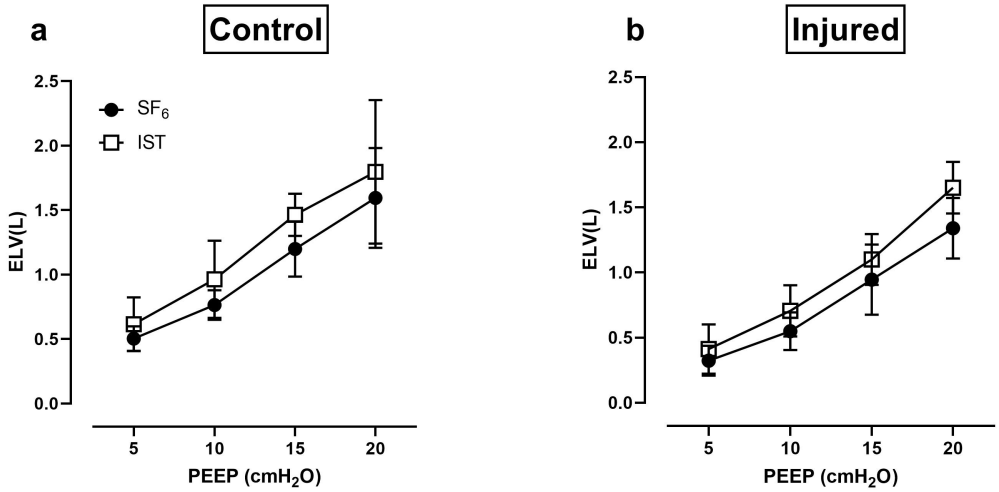


Figure 4.3: General trend of the effective lung volume measured by IST and SF_6 as a function of the PEEP level.

In panel a, the variance of the IST at PEEP 20 cmH_2O was found to be double that of the variation in the previous PEEP level.

Linear regression and Bland-Altman plots, shown in Figure 4.4, were used to investigate further the relationship between paired ELV measurements. A strong relationship in both control and injured lungs was observed using linear regression, (slope =1.0, $R^2 = 0.77$ in the control and slope =1.1, $R^2 = 0.85$ in the injured group), panels c and d. The correlation biases between IST and SF_6 were found to be 0.15 L (LoA was from -0.22 to 0.52) in control and 0.19 L (LoA was from -0.33 to 0.70) in injured animals, panels a and b.

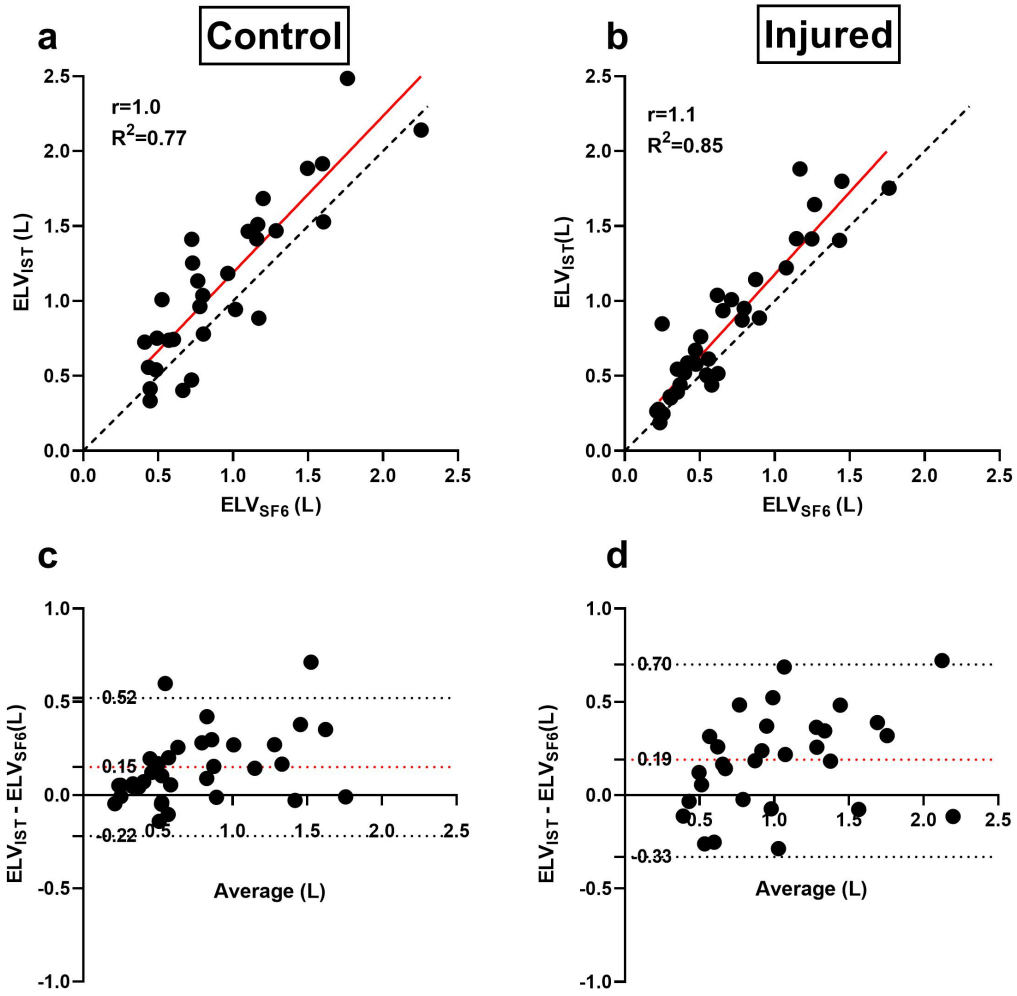


Figure 4.4: Linear regression and Bland-Altman plots of the effective lung volume measured by both the IST and the SF_6.

4.2.3 Pulmonary blood flow, a comparison to thermodilution

The pulmonary blood flow measured by thermodilution was compared with the IST results in Figure 4.5. In the control group, the standard deviation of $\dot{Q}_P$ calculated at each value of PEEP was found to be smaller than in the injured group. IST blood flow values were overestimated by $0.2L/min$ (limit of agreement was from -2.4 to $2L/min$) compared to the thermodilution values in the control group. In Figure 4.5 c and d, the limit of agreement in the control was narrower than in the injured group by $0.4L/min$.

4.3 Discussion

This study examines the ability of IST to measure absolute values of lung parameters in comparison with the SF_6 washout and the thermodilution techniques. The results presented here have shown that in both uninjured lungs and injured lungs (ARDS model), IST can reliably measure values of deadspace volume, effective lung volume and pulmonary blood flow. The repeatability of ELV_{IST} under the same conditions in the same subject is within the reported international acceptable limits of coefficient of variation (< 10 %) [113]. These results are consistent with the previous study in which Bruce et al. illustrated that IST underestimated the functional residual capacity (FRC) by 32% (1.08 L) compared to body plethysmography in humans where the mean FRC was 3.4 L [19]. But, the body plethysmography over estimated FRC by adding the amount of air inside the body. So, it was not a suitable comparison.

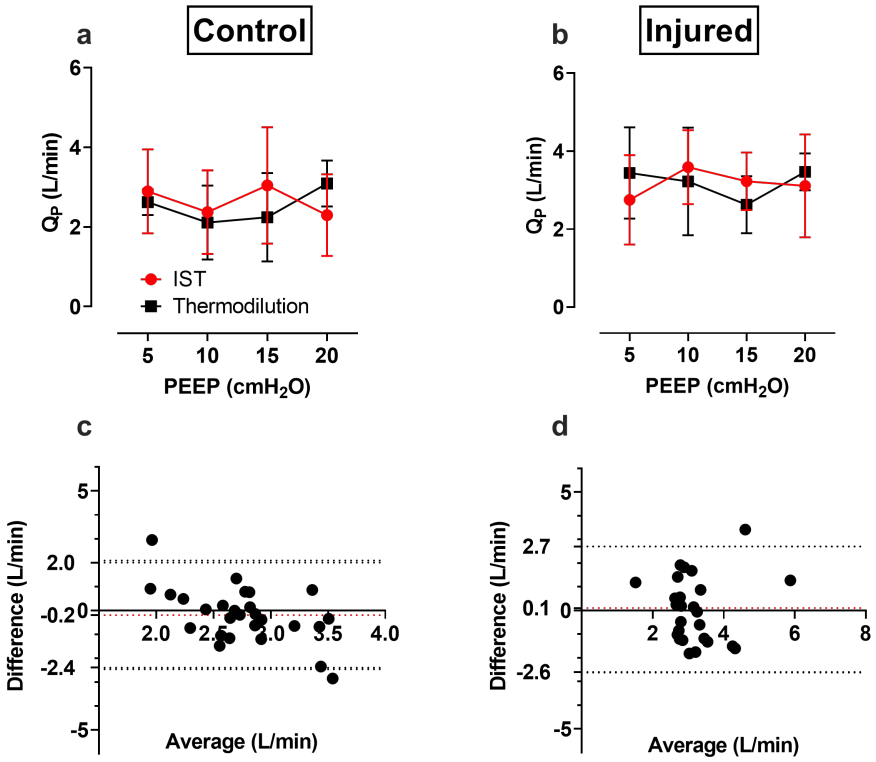


Figure 4.5: Pulmonary blood flow measured by the IST and the thermodilution methods. Paired measurements between IST and thermodilution at incremental values of PEEP in control (panel a) and injured lungs (panel b). Panels c and d show Bland-Altman plots for absolute pulmonary blood flow measurements made by IST and thermodilution.

SF_6 washout was chosen as a comparison method for validation of the IST deadspace and effective lung volume measurement, because of its accuracy and repeatability in ventilated subjects. Both IST and SF_6 working principles are based on a similar gas-exchange method. Therefore, the agreement between IST and SF_6 values may be stronger than that between body plethysmography and also the CT scanner [19, 101]. Furthermore, during the experiment in Hedenstierna Laboratory, Sweden, technical support for SF_6 was available.

Besides, this study reveals the ability of the IST to measure the absolute deadspace volume which compares well to the SF_6 washout method. The correlation between the two methods had a slope of $0.87, R^2 = 0.51$ and the limits of agreements were found to be -51 mL to 32 mL in control lungs. Clinically, deadspace volume has a strong association with mortality risk in patients with ARDS, wherein the risk of death increased by 22% for every 0.05 increase in the VD:VT ratio [114].

The IST calculates the effective lung volume involved in gas exchange; therefore, SF_6 washout with the same mechanism is a suitable method with which to compare it. Each lung measurement has its techniques and assumptions; therefore, the two tests are unlikely to have 100% agreement. The ELV could be a crucial parameter to monitor in patients undergoing mechanical ventilation. The comparison between ELV_{IST} with volumes derived from CT scanning is not made here, but has been made elsewhere [101]. Here it was found that CT scanning easily overestimates ELV since it reports all aerated volume regardless of whether it is ventilated or not. The difference between the ELV values measured by IST and the SF_6 might be related to the non-solubility of the N_2O. This might cause the rise of the mix venous concentration of

the N_2O, which was assumed to be constant in the analysis.

Additionally, the IST can measure absolute values and changes of pulmonary blood flow in comparison with thermodilution within a reasonable range. However, in this study, the blood flow was largely unchanged during the experiments on all 13 pigs, except for the small reduction which resulted from increasing PEEP. Hence, the results in Figure 4.5 only show the comparison measurements between IST and thermodilution techniques in the absolute values. In another proof-of-concept study in eight pigs, where cardiac output was successively depressed and elevated by infusions of stimulant or depressant drugs, it was demonstrated that IST and thermodilution show good agreement and trending ability [17]. Example time series for two pigs are shown in Figure 4.6. There is still room for further development of the blood flow measurement by the IST.

The estimation of the pulmonary blood flow by the IST contains limitations. Firstly, the IST is not designed to measure the absolute values of the pulmonary blood flow. The IST is based on the gas exchanged working principles, so the IST blood flow value might be the blood flow that is only involved in the gas exchange process. Secondly, the IST estimation algorithm assumed that the mixed venous concentration of N_2O was unchanged. However, fixing the mixed venous concentration might introduce error to the estimation. Further researches should be carried on the estimation of the IST pulmonary blood flow.

The inspired sinewave test is a potentially translatable research tool. The IST is easy to use at the bedside and does not rely on patient nor operator input. This study

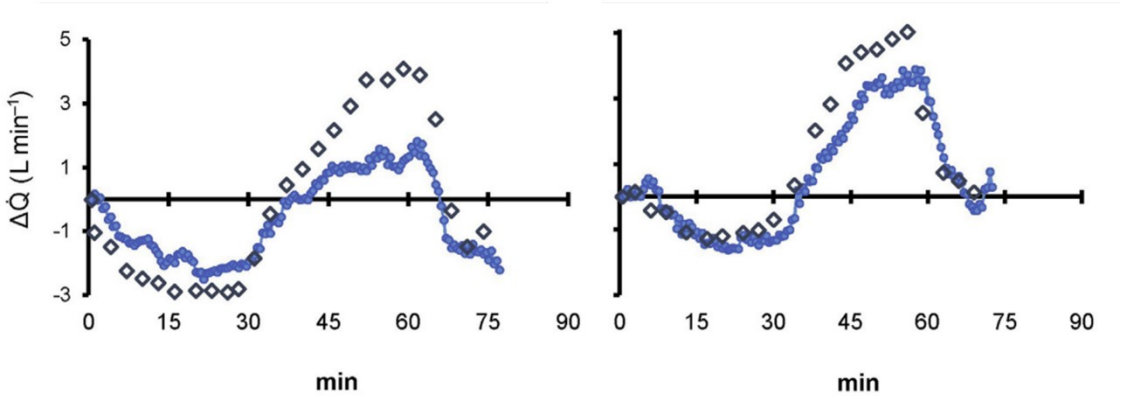


Figure 4.6: Thermodilution (white diamonds) vs IST (blue dots) in changes of pulmonary blood flow (L/min) of two pigs [17].

examined the utility of the IST in measuring effective lung volume, deadspace volume and pulmonary blood flow in ventilated lungs at the bedside. Accurate deadspace volume and lung volume measurements could help in the prognostication of acute lung injury/ARDS. This technique also does not rely on a fixed inspiratory flow, so it can be used in spontaneously ventilating patients.

Furthermore, measurement of the heterogeneity of the lung could be used to quantify the extent of lung injury and hence to inform ventilatory therapy. Our results support further development of these IST heterogeneity indices and their translation to human medicine.

4.4 Key findings and conclusion

In this chapter, it has been shown that the IST is a potential lung function test for mechanically ventilated subjects. The IST can measure accurate effective lung volume, deadspace volume and pulmonary blood flow with small biases compared

to the SF_6 washin-washout and thermodilution in both healthy and ARDS lungs. Instead of using two to three different techniques spontaneously, the IST can offer similar results in one set measurement in less than ten minutes.

The inspired sinewave technique offers several strengths, including commercial availability, translation to human medicine and ease of use at the bedside. As IST does not rely on a fixed inspiratory flow, it can be used in spontaneously ventilating patients. Further research should be carried out to understand the relationship between IST parameters and the optimal setting of mechanical ventilators.

Chapter 5

A simple lung simulation to detect lung heterogeneity with Inspired Sinewave Test

In this chapter, the ratio method of using the IST at the 60s and 180s tracer gas periods to measure the specific ventilation and perfusion heterogeneity of the lung are investigated in detail using both lung simulation and experiments. In the previous chapter, the IST method has shown that it can measure lung function parameters accurately and reliably compared to other current tests. In 2018, Bruce et al. used IST combined with another lung measurement technique (the whole-body plethysmography) to detect ventilation heterogeneity [19]. This method exploits the fact that the "single lung compartment model" calculations of the IST analysis break down as the lung becomes more heterogeneous, and so the recovered values for parameters

such as ELV increasingly deviate from reality. Bruce, et al. exploited this concept by assessing the degree of discrepancy of ELV_{IST} and an independent method of measuring lung volume (i.e. plethysmography). In the same study, ELV values recovered at different periods (e.g ELV_{60} and ELV_{180}) also become increasingly divergent from each other. Bruce, et al. proposed that the IST can capture a ventilation heterogeneity in the format of the IST results ratio at 180s and 60s tracer gas periods.

A two alveolar compartment lung simulation was developed and implemented here. It can illustrate how IST capture the lung heterogeneity using ratio of 180s and 60s results. Using this lung simulation, simulated patients are created. These patients have lung conditions such as emphysema (ventilatory heterogeneity) and pulmonary embolism (perfusion heterogeneity), can be use for *in silico* testing. After verifying the 180s-60s ratio method to calculate lung heterogeneity in simulated patients, this method is applied to estimate lung heterogeneity in animals and human volunteers.

The results in this chapter illustrated that the IST can detect lung heterogeneity. To study the concept of lung heterogeneity, animal and clinical tests are costly to run. Lung simulation is a suitable additional method for investigation. The lung can be simulated with different heterogeneity conditions for the IST to test. There are different methods to simulate the lung; however, the compartmental model is used more often due to its ease to use and effectiveness.

Hypothesis and aims

Therefore, in this chapter, a lung simulation model (simulating the lung and lung heterogeneity fully) was developed to understand how the 60 s and 180 s tracer gas can capture the lung heterogeneity. A practical method to quantify lung heterogeneity is proposed by using the ratio of different IST results (e.g. H_{Vent} and H_{Perf}). The proposed method is then verified by simulated data and validated in both animal and human experimental data.

The hypothesis is that the IST can capture the lung heterogeneity using results from 60 s and 180 s tracer gas. To answer this hypothesis, several objectives were set:

- A lung simulation that can present the lung heterogeneity is required to test the IST. This lung simulation should be reliable and usable to explain how IST can capture lung heterogeneity.
- The heterogeneity calculation method using the ratio of different IST results should be assessed in animal data (control vs ARDS injured) and human data (healthy vs COPD).
- The results of IST heterogeneity should be compared with the heterogeneity values captured by CT scan.

5.1 Methodology

A heterogeneous lung simulation was developed with two alveolar compartments. This simulation was built from previously validated models and simulations, including a serial deadspace compartment, tidal lung compartments, and five body compartments of a standard 70 kg patient and a shunt compartment.

The developed model was verified by sensitivity analysis (Morris's method and particle rank correlation coefficient). After the model was confirmed to work, it was applied to experimental data and validation process. The validation process was performed in animal lungs (including pre- and post-injury) and human data (healthy vs COPD). Additionally, the absolute values and changes of the lung heterogeneity measured by the IST and values measured by the CT scan were compared. Four data sets were included in this chapter:

1. Simulated data ($n = 90$, healthy, emphysema and pulmonary embolism).
2. Animal data ($n = 13$, pre- and post-injury).
3. Human data ($n = 94$, healthy and COPD).
4. Animal data ($n = 6$, injured lung with CT scan).

5.1.1 Two alveolar compartments simulation

As a simple means of creating lung heterogeneity, a lung simulation model was developed and contained only two lung compartments, as shown in Figure 5.2. This simulation can work with the IST and provides a theoretical framework to understand

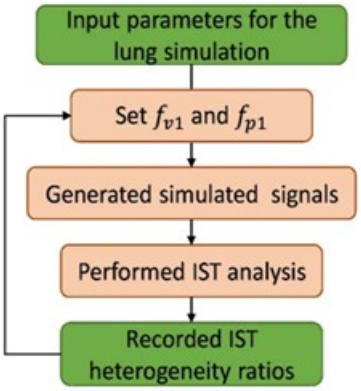


Figure 5.1: Flow diagram to experiment the IST heterogeneity ratios using the lung simulation.

lung heterogeneity. The ventilation and perfusion heterogeneity values can be varied or fixed within this model. Figure 5.1 shows a flow diagram of the method to identify lung heterogeneity using the lung simulation model.

The lung simulation in this chapter contains 3 serial deadspace compartments, 2 alveolar compartments (tidal behaviour) and 5 compartments to represent the whole body (lung, viscera fast, viscera liver, lean and fat), as shown in Figure 5.2. All compartments were linked together by conservation of mass equations. The main purpose of this simulation was to provide suitable simulated tests for the IST with the presence of lung heterogeneity. The simulated patient is assumed to weigh 70 kg and to have 2.5 L of lung volume and 5.0 L/min of pulmonary blood flow.

This technique assumed the heterogeneity of the lung could be fully simulated by two alveolar compartments with a fixed volume. The fraction was added in the parameters to make sure that the sum of the alveolar volume was the same, similarly

Table 5.1: Fraction for volume, ventilation and perfusion of the two alveolar compartments.

Parameter	**Fraction (Compartment 1)**	**Fraction (Compartment 2)**
Alveolar Volume	0.1	0.9
Ventilation	f_v	$1 - f_v$
Perfusion	f_p	$1 - f_p$

with the fractions for ventilation and perfusion. These fractions are summarised in Table 5.1.

For example, the alveolar volume for compartment 1 will be $0.1 \times V_A$ and compartment 2 will be $0.9 \times V_A$. Similarly, in compartment 1, the ventilation is now $(\dot{V}_A) \times f_v$ and perfusion is $(\dot{Q}_P) \times f_p$. By following this setup, the ventilation can be controlled by f_v and perfusion is controlled by f_p. The ratio of 0.1 and 0.9 of the volume was set to amplify the recovery of the lung heterogeneity. For further improvement, the number of alveolar compartments could be increased to more than two. However, generating fractions for each compartment might be time-consuming.

5.1.2 Parameter estimation

In this chapter, the breath-by-breath analysis was applied to estimate parameters (V_D,ELV and Q_p) for the simulation. The breath-by-breath analysis of the IST was mentioned in the Method Chapter previously. This method divided the output signal into different breaths sections and performed the fitting algorithm through

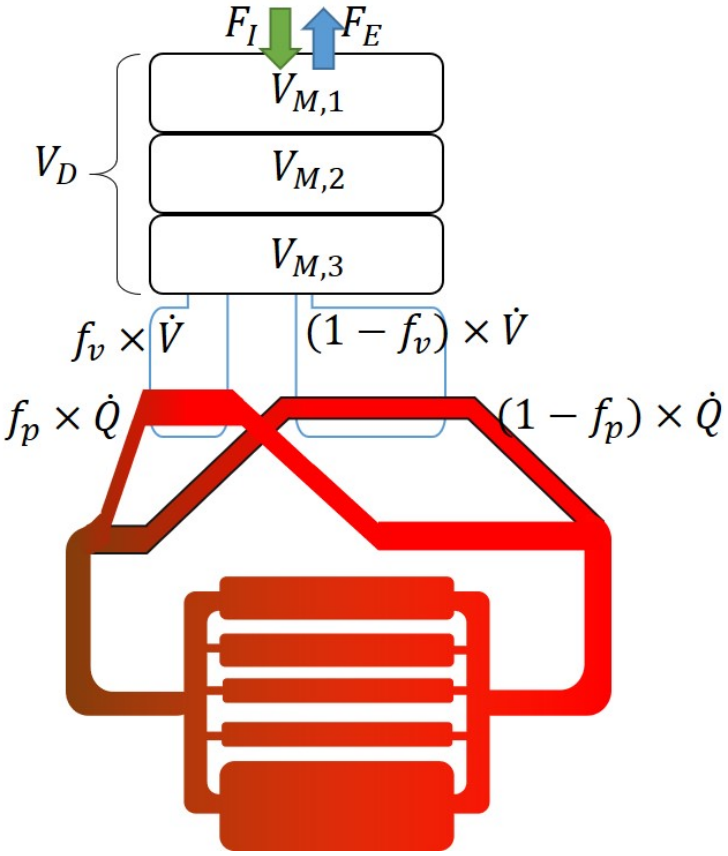


Figure 5.2: A schematic of the two-compartment tidal lung simulation.

these breaths. If the lung is homogeneous, the recovered outputs will not depend on the tracer gas periods. However, if the lung is heterogeneous, the calculated outputs at different tracer gas periods will be different. The difference between the results calculated of two tracer gas periods was assumed to represent the lung heterogeneity.

According to the previous works in Bruce, et al., the IST heterogeneity ratios can be calculated from the results of two tracer gas signals (60 s and 180 s) [19]. The calculation of ratios and the uses of 180s/60s tracer gas signals were explained previously in the method chapter. Ventilation heterogeneity (H_{Vent}):

$$H_{Vent} = \frac{ELV_{180}}{ELV_{60}} \tag{5.1}$$

Perfusion heterogeneity (H_{Perf}):

$$H_{Perf} = \frac{Qp_{60}}{Qp_{180}} \tag{5.2}$$

Because this method involves calculating the ratio between IST results, this calculation is now called the IST heterogeneity ratio. This name is used to distinguish it from the next method, which will be introduced in the next chapter.

5.1.3 Validation in animal and human data

I assessed the usability of the IST heterogeneity ratios (H_{Vent} and H_{Perf}) using data from different lung conditions in both animal and human experiments. I used the animal dataset including 13 anaesthetised pigs that were reported in the method chapter. The animal data thus contain both pre-injured (control) and post-injured (ARDS model) data. A comparison of IST heterogeneity to the CT scan was performed in a subset of 6 animals.

The human data include healthy and COPD patients. The ages of participating subjects ranged between 20 and 86 years and were defined as healthy through clinical screening with the following criteria: no childhood/past medical history of respiratory diseases.

5.1.4 Sensitivity analysis and Statistical test

In a healthy lung simulation, Morris method and partial correlation coefficient (PRCC) were performed for the sensitivity analysis. The Student's t-test was applied to verify the significant identification of control versus injured using IST lung heterogeneity ratios at different PEEP levels. The changes in lung heterogeneity between IST vs CT were reported using the four-quadrant plot. Receiver operating characteristics (ROC) curve and area under the curve (AuC) were used to quantify the classification of control versus injured lungs using the IST heterogeneity parameters.

5.2 Results

5.2.1 The model sensitivity analysis results

Figure 5.3 shows the results of the Morris analysis of the IST lung simulation model. The greater the value of μ^* , the more the i^{th} factor affects the model output, while the greater the σ value, the more the factor is non-linear or involved with interactions with other factors; a low σ, however, indicates a linear, additive part [80]. In Figure 5.3, overall, tidal volume and deadspace produce random errors to the IST results. In panel b, the input of the alveolar volume related linearly to the IST measurement of the ELV. Similarly, in panel c, the simulation input $\dot{Q}_P$ had a strong linear relationship with the IST measured $\dot{Q}_P$ output.

There is a relationship between output ELV and $\dot{Q}_P$ values. This relationship was shown by both Morris analysis and PRCC, Figure 5.4c and e. The highest rank parameters in Figure 5.4c and e were alveolar volume and pulmonary blood flow. In 5.4b, d and f, linear relationships between input and recovered output of the IST were observed ($R^2 = 0.99$). In panel d, when the noise was added, the recovered ELV_{IST} values were slightly smaller than the true alveolar volume input (5 %). In panel f, the IST recovered values of blood flow were underestimated at high input values (input $\dot{Q}_P > 7L/min$).

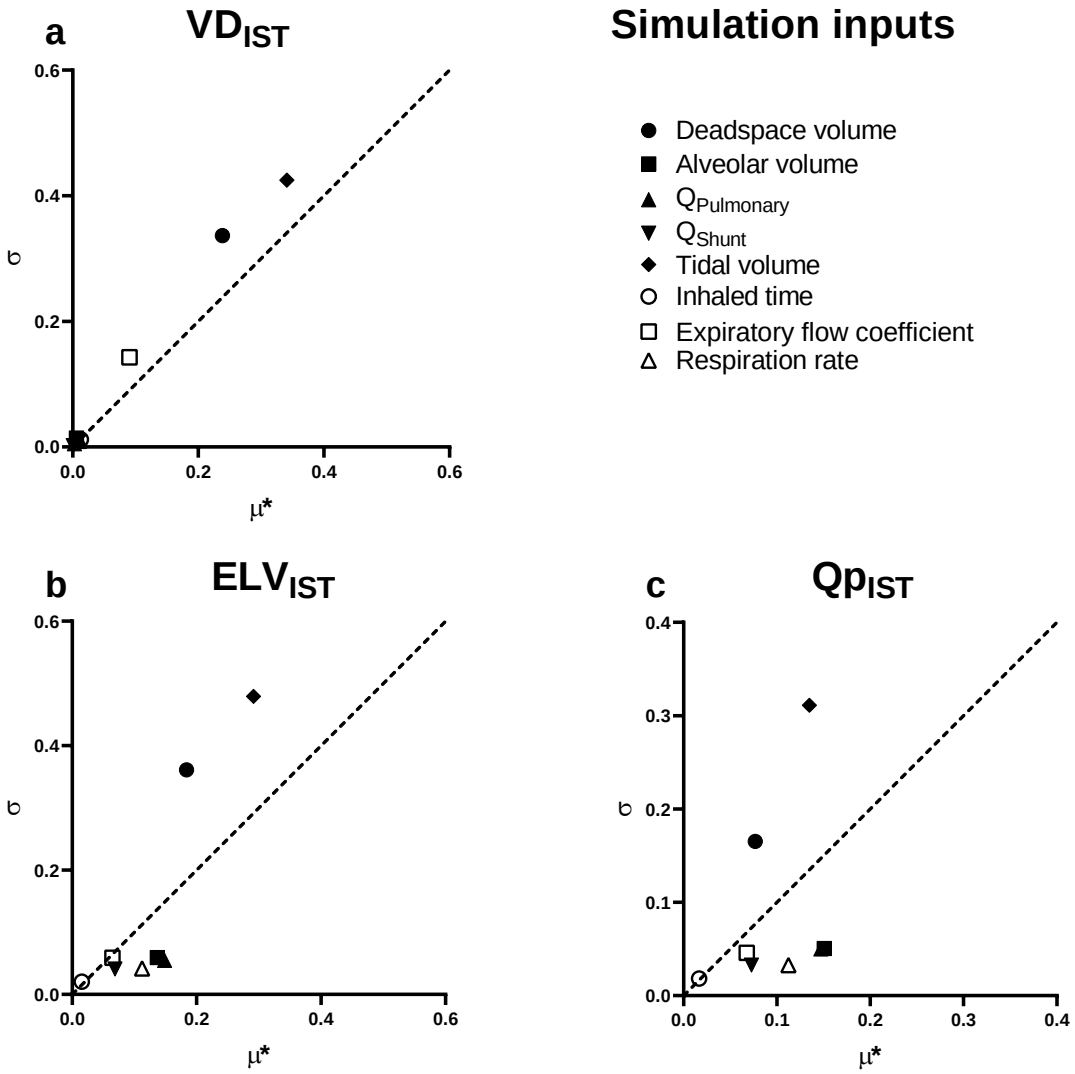


Figure 5.3: Morris analysis results in the IST lung simulation model outputs. Panel a, b and c subsequently show the effects of the input parameters to the IST recovered outputs: deadspace volume (V_D), effective lung volume (ELV) and pulmonary blood flow ($\dot{Q}_P$). The greater the value of μ^* , the more the i^{th} factor affects the model output, while the greater the σ value, the more the factor is non-linear or involved with interactions with other factors; a low σ, however, indicates a linear, additive factor.

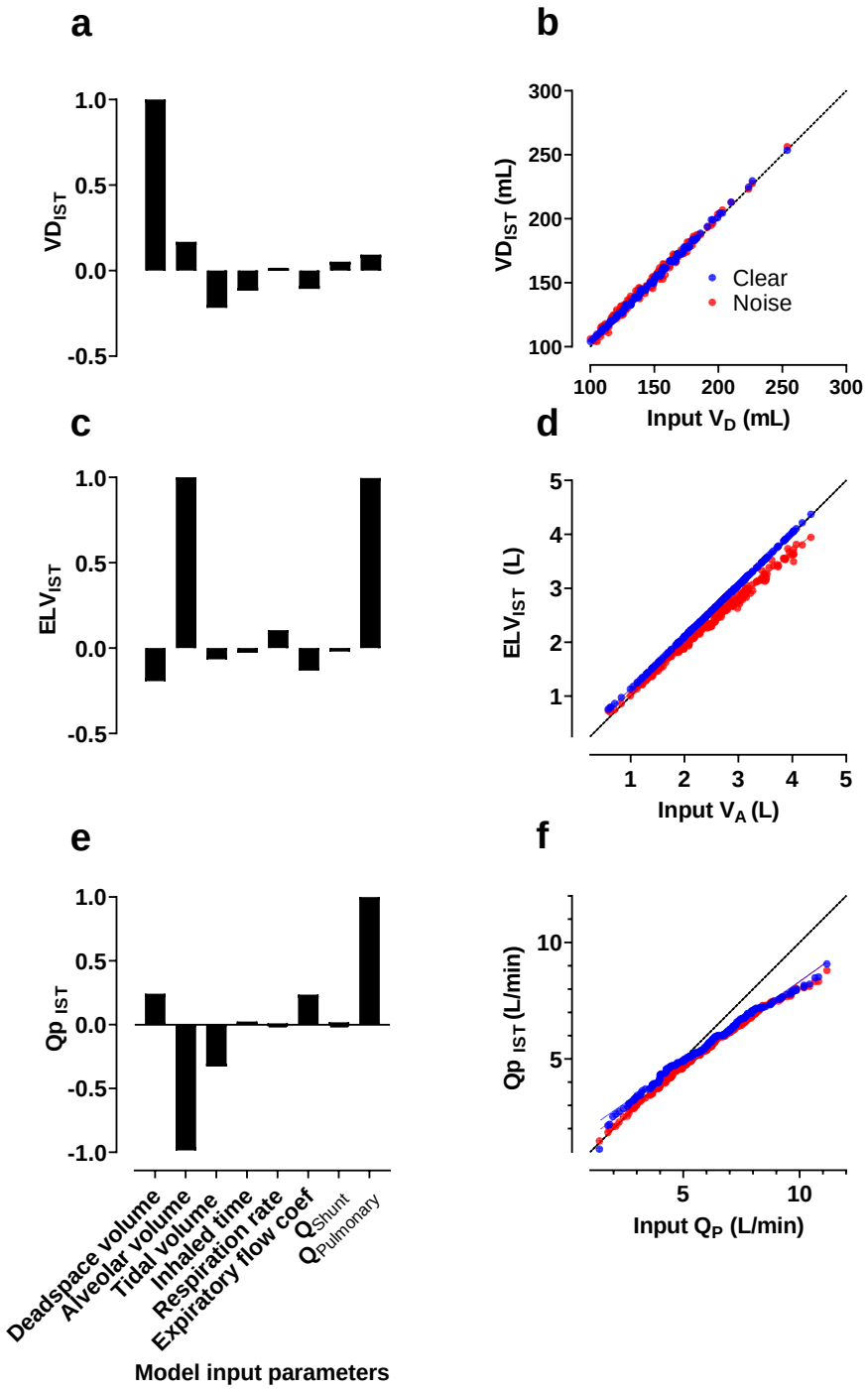


Figure 5.4: Partial correlation coefficient and linear regression results of the IST lung simulation model. Panels a, c and e present the correlation ranking of the input parameters to the outputs (VD_{IST}, ELV_{IST}, $\dot{Q}_{p\ IST}$). Panels b, d and f show the linear relationship between model input to the relative output of the IST. The Gaussian white noise was added (red dots).

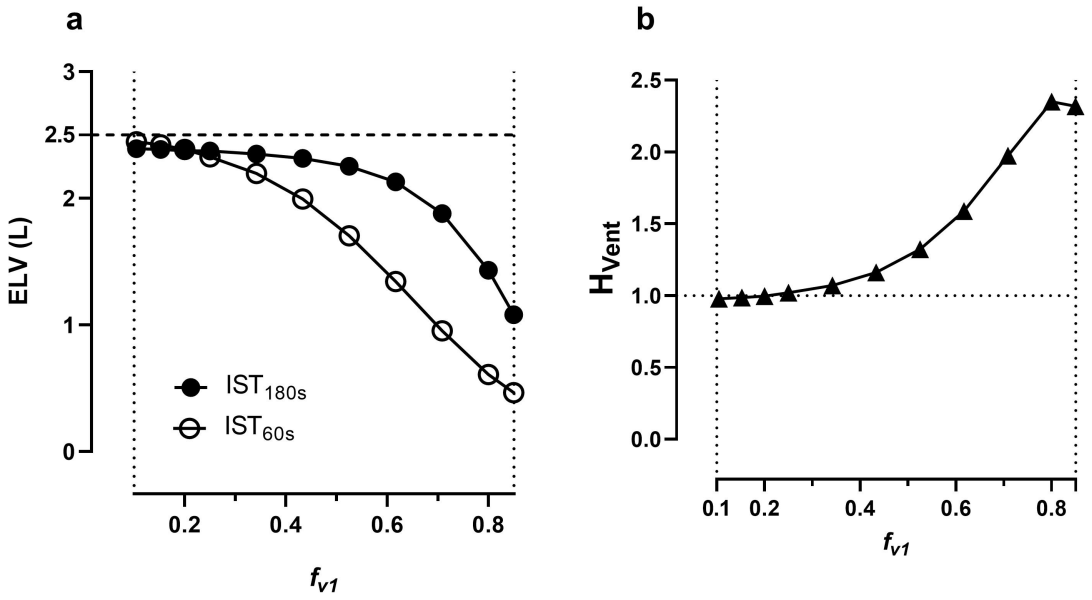


Figure 5.5: The divergence of ELV values (from reality, and from each other) with increasing ventilation heterogeneity in simulated lungs. Panels a and b show the IST values in different variations in ventilation heterogeneity. In panel b, increasing heterogeneity (i.e. increasing f_{v1}) results in increasing heterogeneity index.

5.2.2 Feasibility of using the IST to quantify lung heterogeneity

Figure 5.5 and Figure 5.6 show the IST results in the simulated heterogeneous lungs. As the heterogeneity value increases, the ELV and $\dot{Q}_P$ values of the 60 s and 180 s sinewave periods start diverging, as shown in Figure 5.5 a. Tracking the degree of divergence could provide a measure of lung heterogeneity, as shown in panel b. A simple exponential fitting was apply (red line in panel b).

When the ventilatory fraction assigned to compartment 1 (which comprises 10 % of the lung volume) is 0.1 ($f_{v1} = 0.1$), the lung is assumed to be entirely homogeneous.

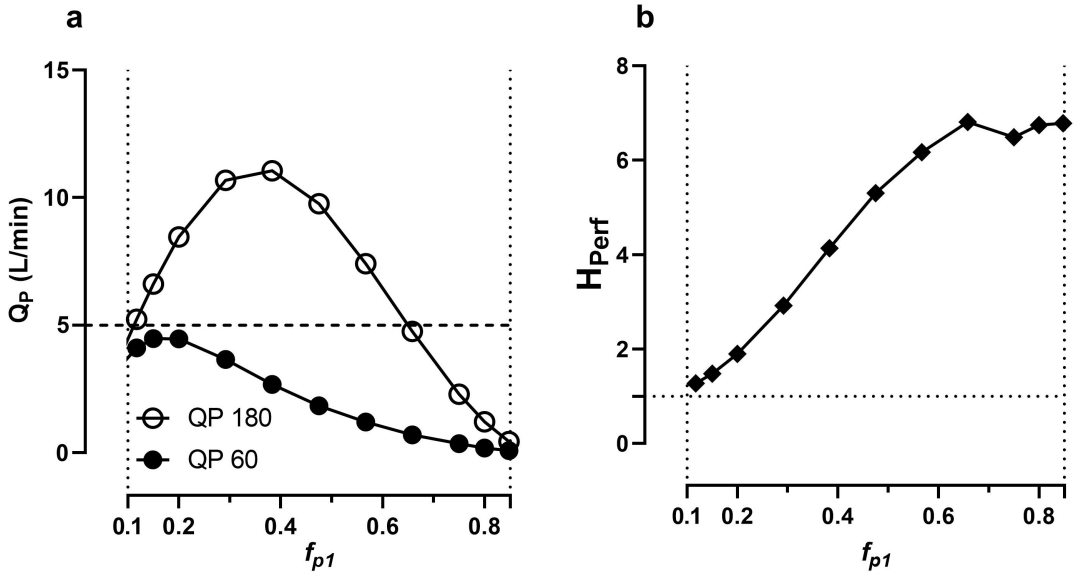


Figure 5.6: The divergences of the $\dot{Q}_P$ values and IST perfusion heterogeneity in simulated heterogeneous lungs.

Thus, ELV values at both 60 s and 180 s were found to be equal, with a value of approximately 2.46 L (98 % of the set value of 2.5 L) in Figure 5.5 a. As f_{v1} increased from 0.1 to 0.85, the heterogeneity of the lung progressively increased. As a result, the ELV values declined for both time periods (panel a) and the decrease in ELV at the 60 s was greater than in ELV at 180 s. This divergence, represented as a ratio of H_{Vent}, is shown in panel b.

In Figure 5.6 , similar to the ventilation, when the perfusion fraction to compartment 1 is 0.1 ($f_{p1} = 0.1$, perfect perfusion homogeneity), the ratio of the recovered $\dot{Q}_P$ values predicts the degree of perfusion heterogeneity (H_{Perf} in panel a). A healthy lung would typically have a heterogeneity ratio of about 1.

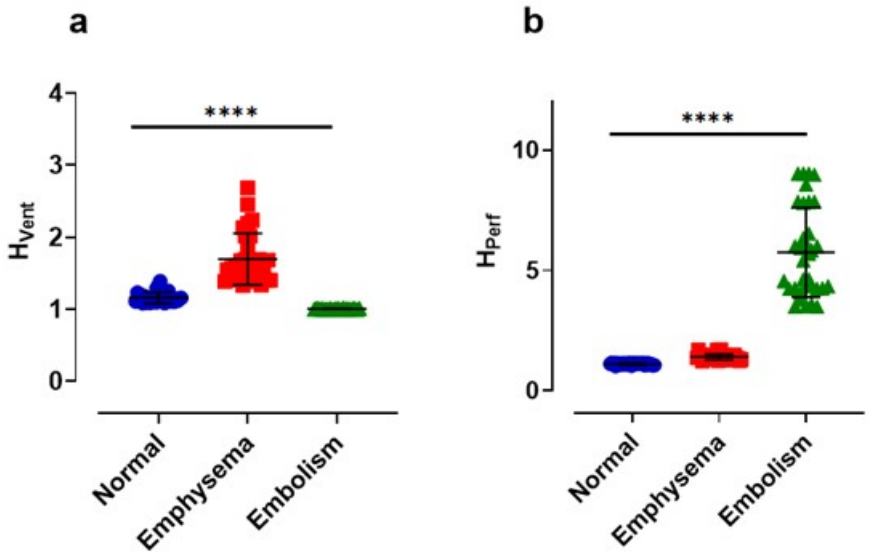


Figure 5.7: Mean and standard deviations of the IST ventilation and perfusion heterogeneity ratios in three simulated lung conditions. The results are analysed by the Kruskal-Wallis test for multiple comparisons in non-parametric data. **** $= p < 0.0001$.

5.2.3 The validation of the IST heterogeneity ratios in simulated data

Diseased and healthy simulated patients could be distinguished easily using the different IST ratios, Figure 5.7, panel a and b ($p < 0.0001$). In emphysema, the ratio of H_{Vent} identified the ventilation heterogeneity of the lung (about 1.58). However, the opposite was observed in the embolism patients. The ratio of H_{Perf} was 5.8, much higher than the values in the healthy and emphysema conditions.

Diseased and healthy simulated patients are distinguished using the different IST ratios, as shown in Figure 5.7 panel a and b ($p < 0.0001$). In emphysema, the mean value of H_{Vent} is seen to be higher than control, indicating increased ventilation

heterogeneity of the lung (about 1.58) which is a feature of this disease. However, in the case of embolism, no increase in ventilatory heterogeneity was seen, which is also consistent with this pathology. Conversely, perfusion heterogeneity was near normal in emphysema, and markedly elevated (mean $H_{Perf} = 5.8$) in the case of embolism. These results are again as expected for these pathologies.

5.2.4 IST heterogeneity ratios in animal data

The IST heterogeneity ratios in control and injured groups at different levels of applied PEEP are shown in Figure 5.8 a and b. At low PEEP levels (5 and 10 cmH_2O) the mean heterogeneity indices in the injured lungs were higher than in the control group (3.4 vs 2.2 at the PEEP of 5, and 2.9 vs 2.1 at PEEP 10 cmH_2O, $p < 0.05$ for both), as shown in Figure 5.8 both panels a and b. The injured group also shows a greater scatter of the IST heterogeneity values at low values of PEEP. The increase of PEEP from 5 through 15 cmH_2O reduced mean heterogeneity within the injured group and also reduced data scatter, indicating a stabilising effect of PEEP.

In Figure 5.8b, the IST perfusion heterogeneity ratio shows significant differences between the two groups in both PEEP 10 ($p < 0.05$) and 15 cmH_2O ($p < 0.001$). Additionally, the ROC curve was applied to classify control vs ARDS at PEEP 10 cmH_2O (Figure 5.9). The area under the curve was 0.85 ($p < 0.001$) with a 95 % confidence interval from 0.69 to 0.99.

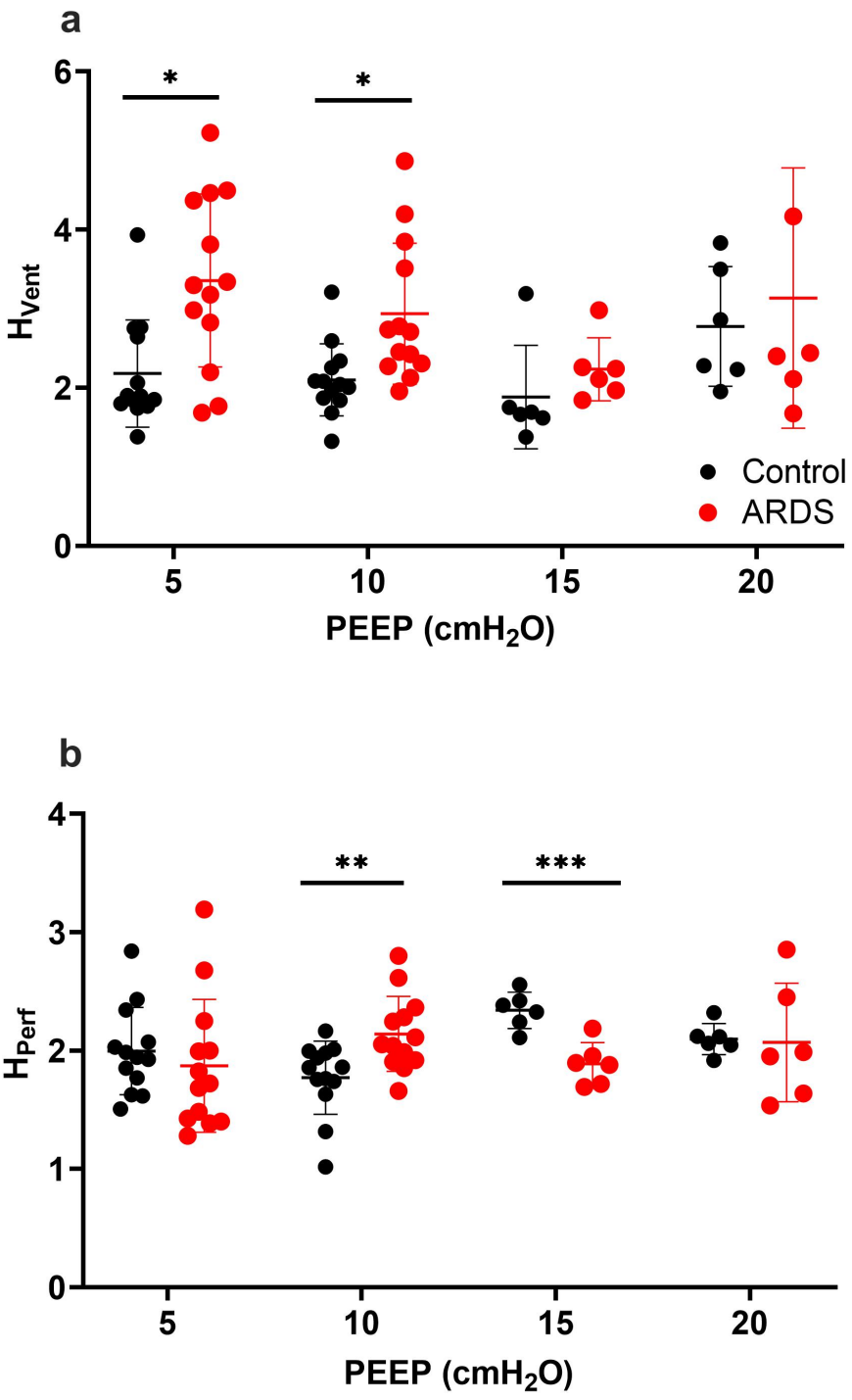


Figure 5.8: IST heterogeneity ratios in control and ARDS animals at different PEEP levels. Student's t-tests were performed. $*** = p < 0.001$, $** = p < 0.01$ and $* = p < 0.05$

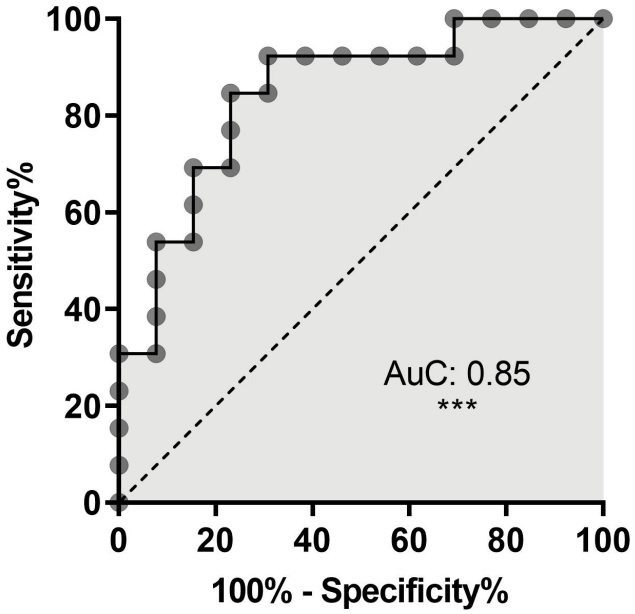


Figure 5.9: ROC curve analysis of the classification between control and ARDS animals at PEEP 10 cmH_2O.

5.2.5 IST heterogeneity ratios in human data

Figure 5.10 shows the IST heterogeneity ratios in healthy and COPD patients. For perfusion heterogeneity (panel b) there is no statistically significant discrimination among COPD groups or between healthy patients. For ventilation, IST ratios could classify the patients in COPD type 4 relative to others. However, there is no clear separation between the different COPD phenotypes. Because COPD is a mix of a wide range of complex lung conditions, the lung heterogeneity might not identify correct COPD phenotypes.

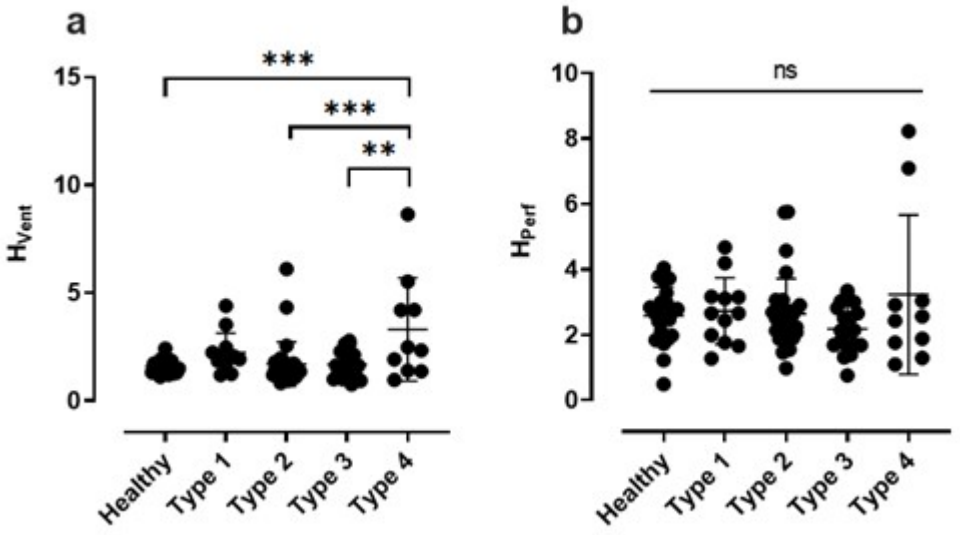


Figure 5.10: Comparison of the IST ratios in healthy vs COPD groups. Panel a shows the IST ratio of ventilation heterogeneity and panel b is the perfusion heterogeneity ratio. The Student t-test was applied to each pair comparisons with ns: non-significant, $** : p < 0.01$, $*** : p < 0.001$.

5.2.6 Comparison of the IST heterogeneity ratios vs CT images

Figure 5.11 shows the overall influence of the PEEP level on lung heterogeneity measured by both CT and IST. I observed that the difference between incremental and decremental PEEPs are negligible (continuous lines versus dashed lines in Figure 5.11, were <10% of the mean values). In terms of lung heterogeneity, when PEEP increased, the lung became more homogeneous. This could be seen in CT results (panels a). In panel b, the IST ventilation heterogeneity followed this trend, but the perfusion heterogeneity did not.

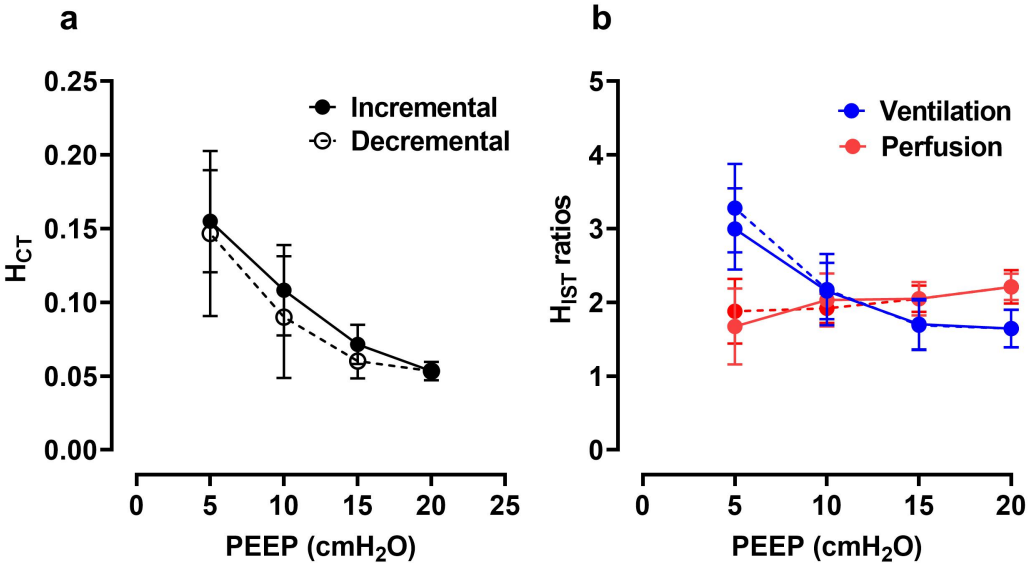


Figure 5.11: The overall influences of PEEP levels to lung heterogeneity. Panel a shows the lung heterogeneity measured by CT images changed with PEEP. Panels b shows the lung heterogeneity measured by the IST.

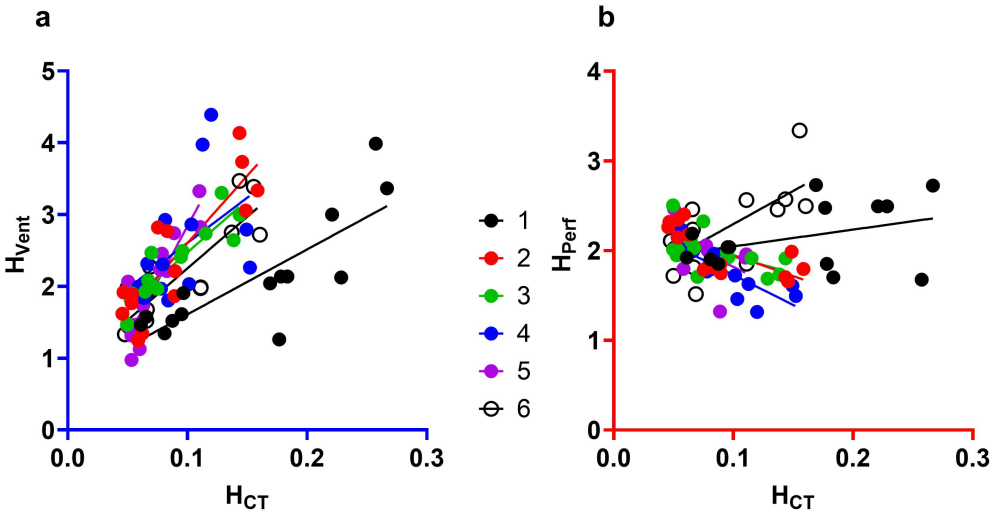


Figure 5.12: Colour coded animal in the comparisons of the lung heterogeneity measured by the CT scan and IST ratios.

Figure 5.12 shows scatter plots and linear regression comparison of the lung heterogeneity between IST and CT images in six animals. The full report of the linear regression in individual pigs is presented in Table 5.2. The mixed regression results were not as good as the regression results in individual animals. In individual animals, there was a strong correlation of the H_{Vent} and H_{CT}. The highest correlation was at $R^2 = 0.82$ and the lowest was $R^2 = 0.24$. However, the correlation between H_{Perf} and H_{CT} were not quite as good with the highest was $R^2 = 0.67$ and lowest was $R^2 = 0.14$.

Figure 5.13 shows the four-quadrant plots that demonstrate the relationship between the changes in heterogeneity measured by CT and IST. The concordance rate and correlation between ΔH_{CT} and ΔH_{Vent} were higher than between ΔH_{CT} and ΔH_{Perf}.

5.3 Discussion

This analysis shows the ability of the IST to measure lung heterogeneity in both uninjured lungs and an ARDS model of lung injury. The heterogeneity indices derived from the ratios ELV_{180}/ELV_{60} have the potential to identify ARDS vs control subjects with reasonable diagnostic accuracy; the area under the ROC curve $= 0.85 (p < 0.001)$ at a value of PEEP of $10 cmH_2O$.

Lung simulations can be used to validate lung measurement techniques such as

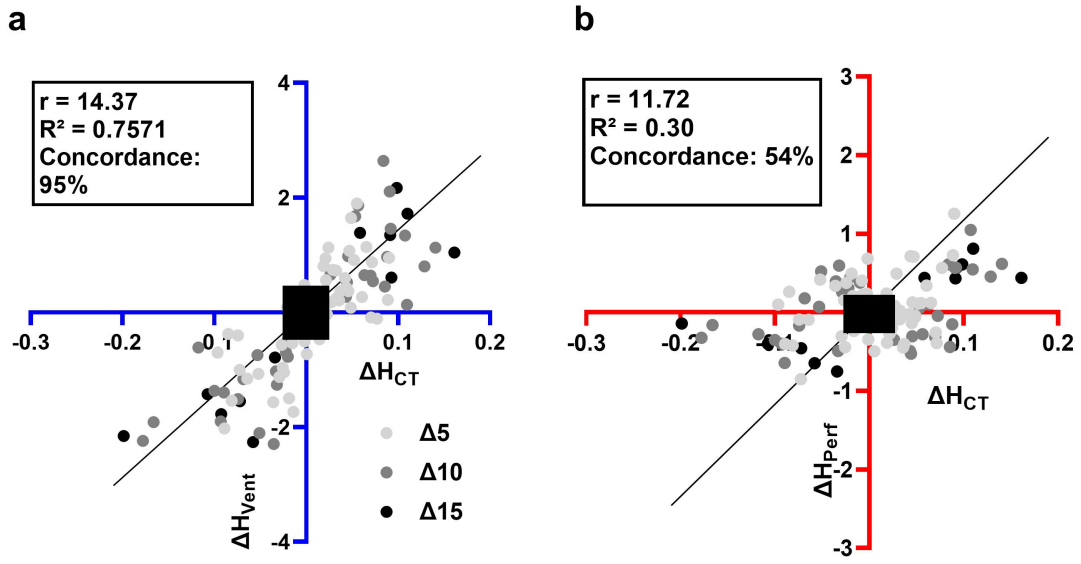


Figure 5.13: Four quadrant plots showing the changes of lung heterogeneity measured by the IST versus CT scan with changes in PEEP level. The exclusion zone (black rectangle) is 15 % of the maximum values. R^2 and r values are calculated from linear regressions. The agreement is the percentage of data points that lie in the I$(+;+)$ and III$(-;-)$ quadrants, excluding the exclusion zone.

Table 5.2: Linear regression results of the comparison between IST heterogeneity ratios and CT scans in six pigs.

Pig number	H_{Vent}		H_{Perf}	
	Gradient	R^2	Gradient	R^2
1	1.89	0.66	1.88	0.14
2	3.17	0.74	-4.68	0.54
3	2.00	0.82	-3.67	0.31
4	6.50	0.24	-6.67	0.67
5	4.45	0.80	-6.62	0.26
6	2.34	0.76	7.39	0.47

the IST and to provide information to improve performance. This work has combined a validated lung simulation using parameters taken from the literature to undertake error analysis and evaluation of the accuracy and precision of the IST. I empirically demonstrated that the IST ratio of two frequencies applied to two discrete compartments is a useful method to quantify lung heterogeneity using only the IST.

A previous study [19] of lung heterogeneity measured by the IST in human patients did not achieve any significant outcome because of the wide variability in the severity of conditions in the study population. However, in this chapter, for the first time, the IST was proved to measure the lung heterogeneity without the need of another test. The simulation was implemented to understand the IST heterogeneity indices and their ranges. A healthy simulated lung would have IST heterogeneity ratios of 1, although even a healthy human subject would not quite achieve this due to the system and equipment errors.

This simple heterogeneity index, based on the breakdown of the one compartment assumption may not be sensitive enough to detect moderate disease severity in COPD, although it was able to detect abnormalities in severe (type 4) patients. More sophisticated modelling, aiming to characterise the ventilation and perfusion distributions in more detail may be more successful in COPD.

Furthermore, the absolute values and changes of the lung heterogeneity measured by IST with that measured using CT scan images were compared. A clear influence of lung heterogeneity on the PEEP level was captured. Furthermore, the changes of the ventilation heterogeneity (H_{Vent}) have better concordance with the CT scan (95 %) than the perfusion heterogeneity (H_{Vent}). The limitations of this comparison

were mainly the use of the porcine model to describe ARDS in humans. There was no comparison with healthy lungs. Due to the experimental setup, the animal's lung was damaged before moving into the CT scanner.

I implemented a lung simulation to study how the IST can capture lung heterogeneity. However, this contains limitations. The discretisation or dichotomisation into two alveolar compartments may be insufficient to represent the complexity of real-life lung heterogeneity, a continuous distribution. Lung volume fractions were restricted at 0.1 and 0.9 of the total volume. Modelling this lung as two homogeneous compartments with 10% and 90% of the volume would likely be inaccurate. For example, suppose 25% of a lung volume is diseased or damaged, and the remaining 75% is healthy. Depending on the severity of the 25% damaged volume, the IST might not detect this volume. However, it is a challenge to see the collapsed region of the lung only using the IST.

5.4 Key findings and conclusion

IST has the potential to measure the ventilation and perfusion heterogeneity non-invasive using different IST tracer gas periods (180s and 60s). In this chapter, the method to quantify lung heterogeneity was introduced and applied to the IST results in simulation, animal and human data. In the animal study, the IST heterogeneity results were shown to be able to identify control vs injured lungs at the specific PEEP level (PEEP 10 cmH_2O). However, in the human data set, the IST failed to classify patients with COPD diseases vs healthy. Further research is required to determine

how this technique might be used in practice. The IST ventilation heterogeneity ratios has a better agreement with the heterogeneity values measured by CT, comparing to the IST perfusion heterogeneity ratios.

There was no relationship between the PEEP level and the lung heterogeneity estimated by the IST. However, a better understanding of the lung heterogeneity might provide suggestions for the optimal PEEP setting. The heterogeneity parameters can inform and optimise mechanical ventilation strategies at the bedside in real-time for patients with ARDS. This work provides a foundation for the study of lung heterogeneity in clinical trials.

Chapter 6

Multiple compartment simulation-based optimisation for Inspired Sinewave Test

To prevent COPD, early detection and strict monitoring can help to reduce the risks of further complications. In this chapter, a simulation-based optimisation for the IST to estimate the lung heterogeneity parameters (specific ventilation and perfusion heterogeneities) is proposed. The simulation included 125 alveolar compartments (each compartment contains ventilation, perfusion and volume fractions). This method combines the advantages of the multi-compartment lung simulation and the Bayesian optimisation to improve performance. Simulation data are fitted to measured data using the Bayesian optimisation.

The new method is tested in large datasets including 13 anaesthetised pigs (pre-

and post-lung injury - ARDS model) and 104 human subjects (32 healthy and 72 COPD subjects). 72 COPD subjects were classified into four COPD phenotypes 'GOLD' standard groups). An additional method to calculate the optimal PEEP according to the lung heterogeneity is introduced in the chapter. CT scan to calculate the lung heterogeneity is used to compare with the Bayesian optimisation method.

The results in this chapter show the potential to use Bayesian optimisation to calculate the lung heterogeneity for the IST. In contrast to the simpler model in Chapter 5, the IST heterogeneity calculated using Bayesian optimisation method could distinguish different phenotypes of COPD with 73 % agreement with the spirometry classification. This is the first study to evaluate the changes in lung heterogeneity using the non-invasive IST in a variety of lung conditions.

6.1 Methodology

A sophisticated lung simulation was developed here to work with the IST. Bayesian optimisation was then applied to match simulated and measured data, creating a simulation-based optimisation model. At first, the model was verified by simulated patient data from the literature (healthy vs emphysema and pulmonary embolism) [45]. Then, this model was applied to analyse the results of IST in animal and human data. A schematic diagram of the model and results of simulated heterogeneous lungs are shown in Figure 6.1.

When the model was completed and verified, it can calculate lung heterogeneity

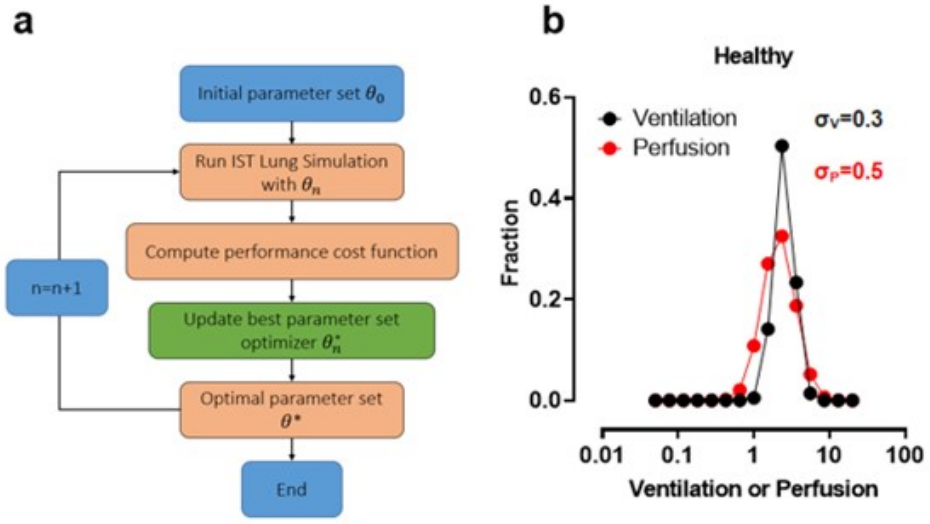


Figure 6.1: Schematic diagram of the lung simulation-based optimisation and an example of the simulated ventilation and perfusion lognormal distributions.

indices from data collected from IST patient and animal studies. The summary information for these data is presented in Table 6 1. In each patient or animal, the IST measurements were performed at two tracer gas oscillation frequencies (periods 180 s and 60 s).

Details of the animal preparation can be found in the Chapter 3. Animal data were obtained from 13 anaesthetised pigs which were studied by the IST both before lung injury (non-injured) and after lung injury (injured). Lachmann's method was applied to induce lung injury to model the ARDS [99].

The human clinical data used here comprise two datasets taken from a previous research study [19]. The data were collected from 104 participants (32 healthy and 72 COPD). More details of the data collection and protocol of this COPD data set were mentioned in the method chapter.

Table 6.1: Characteristic summary of the animal and human data measured by the IST. Mean (standard deviation) values are shown. Statistical t-test was applied, ns: non-significant.

Animal	**Parameter**	**Non-injured**	**Injured**	**p**
	Number	13	-	-
	Weight (kg)	29(2)	-	-
	Heart rate (bpm)	86(12)	85(11)	ns
	pH	7.42(0.03)	7.28(0.09)	ns
	FIO2	0.4(0.1)	0.8(0.1)	$<$0.0001
	Cardiac output (L/min)	3.4(0.8)	3.2(0.4)	ns
Human	**Parameter**	**Healthy**	**COPD**	**p**
	Number	32	72	-
	Age	53(22)	67(10)	$<$0.01
	Height (m)	1.7(0.1)	1.70(0.1)	ns
	Weight (kg)	72(12)	79(18)	ns
	IBM	25(4)	28(5)	ns

6.1.1 Lung heterogeneity presented in a lognormal distribution

The lung simulation used in this Chapter is a modified version of the previous lung simulation in Chapter 5. The model was developed in a Matlab-Simulink environment with an integrated *ode45* solver. Similar to the previous model, serial deadspace compartments are linked to lung compartments and 5 body compartments. The difference in this model is the lung compartment contains 125 alveolar compartments with different ventilation, volume and perfusion fractions. The distributions of these fractions are described by a lognormal function, with a mean, mode and standard deviation, which can be set and varied. Figure 6.1 shows a schematic diagram of the IST and the lung simulation.

Figure 6.1a presents a schematic diagram of the lung simulation-based optimisation model. This model contains two parts, which are lung simulation and Bayesian optimisation. The lung was simulated by 10 dead-space compartments and 5 body compartments [12].

If the model were to have too few compartments, it would not be possible to reliably fit a lognormal distribution. On the other hand, too many compartments would require excessive computational effort [98, 97]. 125 compartments is a workable trade-off. The fraction of ventilation and perfusion for an individual compartment are sampled by the lognormal distribution:

$$y = f(x|\mu,\sigma) = \frac{1}{x\sigma\sqrt{2\pi}} exp\left\{\frac{-(logx-\mu)^2}{2\sigma^2}\right\}, x > 0 \tag{6.1}$$

Table 6.2: The participant characteristics and Inspired Sinewave Test results (n = 48 :26 men and 22 women) [19].

Parameter	**Mean(SD)**
Age (years)	53.5(22)
Height (m)	1.7(0.1)
Weight (kg)	71.5(12)
BMI (kgm^{-2})	24.9(4..2)
$ELV_{180}(L)$	2.3(0.8)
$ELV_{60}(L)$	1.5(0.5)
$Qp(L/min)$	4.9(1.7)

BMI, body mass index; ELV_{180} and ELV_{60}, inspired sine-wave technique estimate of end-expired lung volume measure during a sine-wave with a 180 or a 60s period, respectively; and Qp inspired sine-wave technique estimate of pulmonary blood flow.

where μ is mean of logarithmic values and σ is standard deviation of logarithmic values. According to clinical results [6, 45], the more damaged lung, the greater the width of the distribution (larger σ or μ is further away from 1). The shapes of the distributions are controlled by σ_V and μ_V in the ventilation heterogeneity and σ_Q and μ_Q in the perfusion heterogeneity, Figure 6.1b.

This lung simulation can work directly with the IST to produce IST simulated results. The known parameters of this lung simulation are taken directly from the patient's record, such as tidal volume, respiration rate, inspiration time and IST input setup values.

The unknown parameters in this model are alveolar volume, pulmonary blood flow, the shape of the heterogeneity lognormal distribution, which are thus included in the optimisation. Bayesian optimisation is used to match the lung simulated data to measured data. The best match can reveal these unknown parameters [90, 115]. Bayesian optimisation reasons about f by building a Gaussian process (GP) [116] through evaluations. This flexible distribution allows us to associate a normally distributed random variable at every point in the continuous input space. A loss function is introduced as a gap between simulated and measured values. This is a completed 'black-box' model.

Minimising the loss function $f(\theta)$ can estimate input parameters θ, including $(V_A, Q_P, \sigma_V, \mu_V, \sigma_P, \mu_P)$, with V_A is alveolar volume and Q_P is pulmonary blood flow

$$\begin{aligned} \arg\min_{\theta} f(\theta) \quad &= \quad \arg\min_{\theta} \left\{ \left| \frac{ELV_{180}^{Sim}(\theta) - ELV_{180}^{M}}{ELV_{180}^{M}} \right| + \left| \frac{ELV_{60}^{Sim}(\theta) - ELV_{60}^{M}}{ELV_{60}^{M}} \right| \right\} \\ &+ \quad \left\{ \left| \frac{Q_{P,180}^{Sim}(\theta) - Q_{P,180}^{M}}{Q_{P,180}^{M}} \right| + \left| \frac{Q_{P,60}^{Sim}(\theta) - Q_{P,60}^{M}}{Q_{P,60}^{M}} \right| \right\} \end{aligned} \tag{6.2}$$

where $ELV_{180}^{Sim}(\theta)$ is the simulated values of the set parameter θ and ELV_{180}^{M} was the measured IST values from the patients, similarly with $Q_{P,180}^{Sim}(\theta)$ and $Q_{P,180}^{M}$. $180s$ and $60s$ are the periods of the IST tracer gas oscillation.

6.1.2 Multinomial logistic regression

Logistic regression is a statistical model that uses a logistic function to model a binary dependent variable [117]. This method is widely applied for binary classification [118]. This model has traditionally been solved via maximum likelihood estimation or stochastic gradient descent. This model well classifies two classes. However, in three or more classes, the multi-class logistic regression model was introduced. This method generalises logistic regression to multi-class problems.

A maximum likelihood estimation of the logistic regression model using only IST outputs was created to classify participants as healthy or into the 1-4 GOLD categories [117, 119]. This classification model was developed and validated in Matlab by Vu, et al. [119]. This classification aims to compare the classification results between IST parameters and ground truth (here taken to be the spirometry measurement).

6.1.3 Statistical analysis

Statistical analyses were conducted using GraphPad Prism (GraphPad Software inc.) and Matlab v2018b (Mathworks, Natick, MA, USA). To compare differences between healthy participants and patients in the 1-4 GOLD classifications, the Kruskal–Wallis test was used [120]. To compare two groups, an unpaired t-test was used. The Area Under The Curve (AuC) of the Receiver Operating Characteristics (ROC) curve was used to measure the ability of our test to distinguish between healthy and COPD.

6.2 Results

Overall, the standard deviations of the lognormal distributions (σ_V and σ_P) show potential for lung condition identification. Noticeably, the results of σ_V (standard deviation of the ventilation lognormal distribution) show significant differences in all datasets ($p < 0.0001$ in the animal set, $p < 0.01$ and $p < 0.05$ in COPD sets). Further investigation is thus carried out on these parameters.

6.2.1 Verification of the lung simulation model with simulated patients

In Figure 6.2, the verification results of the model shows that it can work accurately with the IST. The linear regression analysis of the model output with the simulated true input indicated strong agreements and correlations. In panel a and b, according to simulated data results, our model can calculate values for alveolar volume and pulmonary blood flow ($R^2 = 0.99$). Furthermore, in the heterogeneity results (the shape of the lognormal distribution) in panel c and d, strong relationships were found between input and output. The confidence with which σ_V and σ_P are recovered ($R^2 = 0.7$ and $R^2 = 0.9$) is not as great as V_A and $\dot{Q}p$. Nevertheless, this model can determine the heterogeneity of the lung in simulated data and present in the format of σ_V and σ_P.

Repeated calculations in the same data were undertaken. The repeated results had a variation of less than 5 %. An example of the simulated lognormal lung for

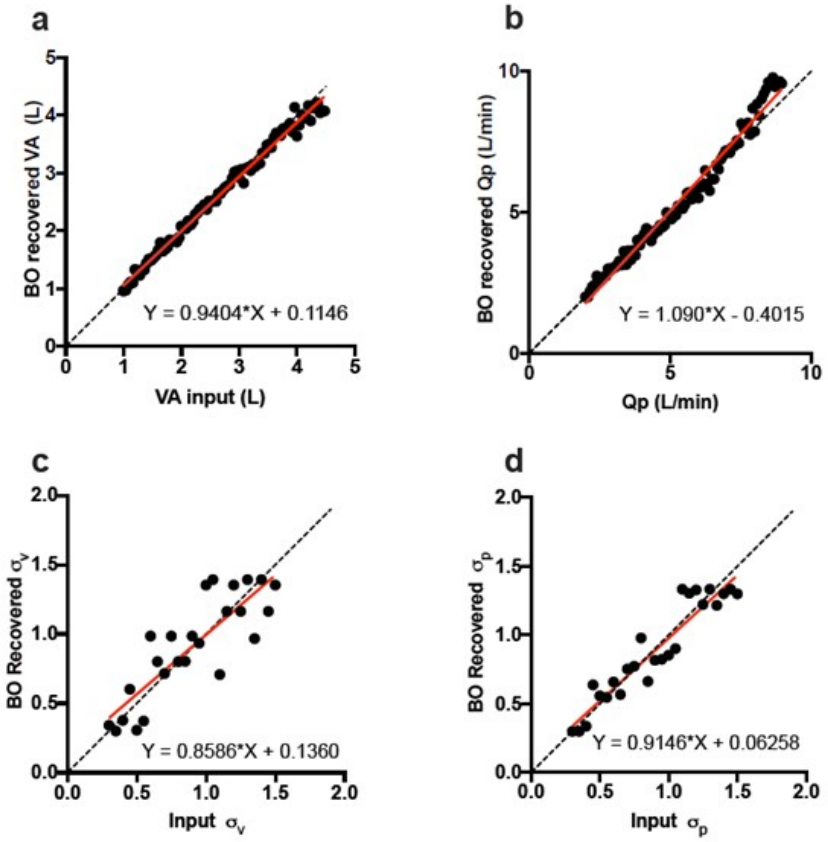


Figure 6.2: The verification of lung simulation. Linear regressions present the relationship between set-input and recovered output calculated by the Bayesian optimisation lung simulation. Black dash lines are reference lines and red lines are regression lines. The simulation contains Gaussian random noise in the tidal volume to represent the real patient breathing pattern.

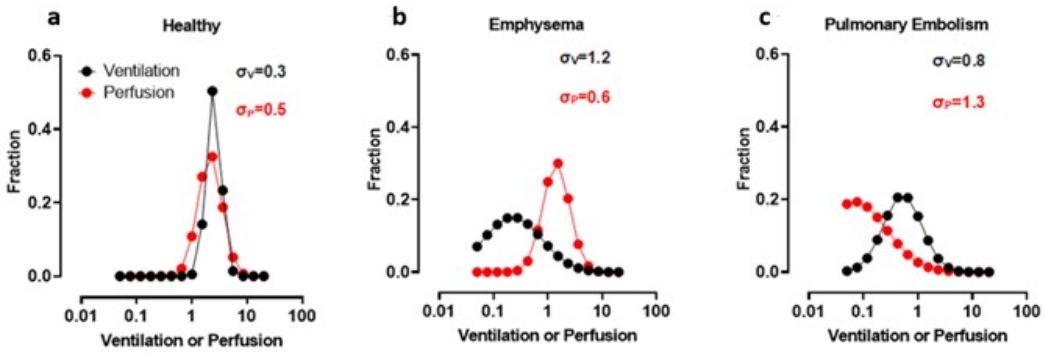


Figure 6.3: Example of healthy, emphysema and pulmonary embolism patients shown in lognormal distribution recovered from the simulation.

both emphysema and pulmonary embolism is shown in Figure 6.3. In this Figure, the emphysema patient has a wider distribution of ventilation (greater heterogeneity) than the healthy one ($\sigma_v = 1.2$ compared with $\sigma_v = 0.3$ in healthy). In pulmonary embolism, the patient has a wider distribution of both ventilation and perfusion than the healthy case ($\sigma_v = 0.8$ and $\sigma_p = 1.3$).

6.2.2 IST heterogeneity indices in animal data

Figure 6.4 shows the IST heterogeneity results in non-injured vs injured animal data. The measurements were performed at different levels of PEEP. In panel a, the IST ventilation heterogeneity was not significantly influenced by the PEEP level in non-injured animals. Figure 6.4 b shows pooled data separated into non-injured and injured data in all PEEP levels. A significant difference was observed in the IST ventilation heterogeneity (σ_v), $p < 0.0001$, however, no significance was seen in the IST perfusion heterogeneity (σ_p), Figure 6.4 d. At PEEP 15 cmH_2O, there was a

wide separation between non-injured and injured data.

6.2.3 IST heterogeneity indices in healthy

Healthy vs COPD: In the human data, Figure 6.5, the IST heterogeneity indices show potential to classify healthy vs COPD groups. In panels a and b, the results of the unpaired t-test illustrate the ability to identify healthy vs COPD subjects ($p < 0.01$ in ventilation and $p < 0.001$ in perfusion indices). Interestingly, in panel a, two distinct sub-populations of COPD phenotype can be observed in the distribution of σ_v, indicating the wide range of disease severities within the diagnostic label of COPD.

Furthermore, in healthy subjects, Figure 6.6 shows the relationship between IST heterogeneity indices and age. A linear relationship between age and ventilation heterogeneity was found($R^2 = 0.42, p < 0.0001$).

Based on this relationship, IST heterogeneity was normalised to account for the influences of normal ageing in further analysis. The equations are reported below (age in years):

$$\sigma_V = 0.0043 * age + 0.46 \tag{6.3}$$

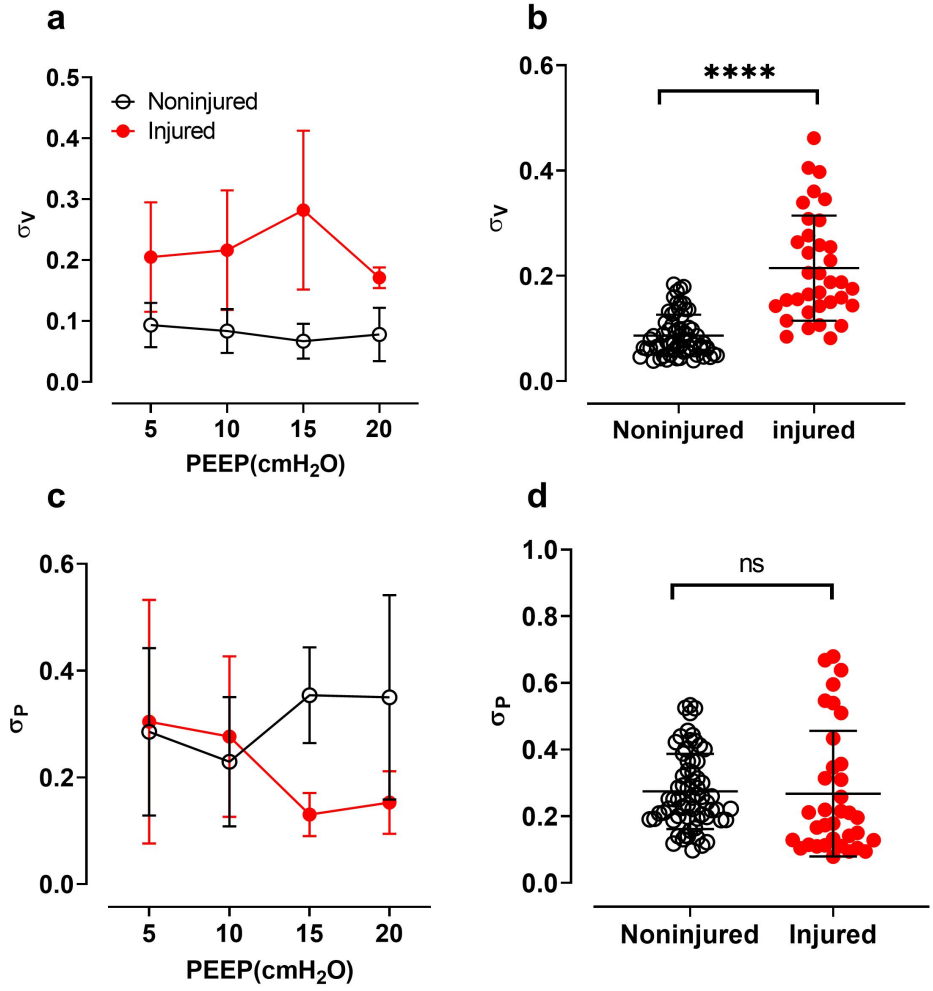


Figure 6.4: The IST lung heterogeneity indices (σ_v - the standard deviation of the lognormal distribution graphs) in animal data. Panels a and b show the distribution of the IST ventilation heterogeneity (σ_v), and c and d show the IST perfusion heterogeneity (σ_P). Panels a and c show the mean and standard deviation of the IST heterogeneity indices vs PEEP. Panels b and d present the paired t-test comparison with ns: non-significant and $****: p < 0.0001$.

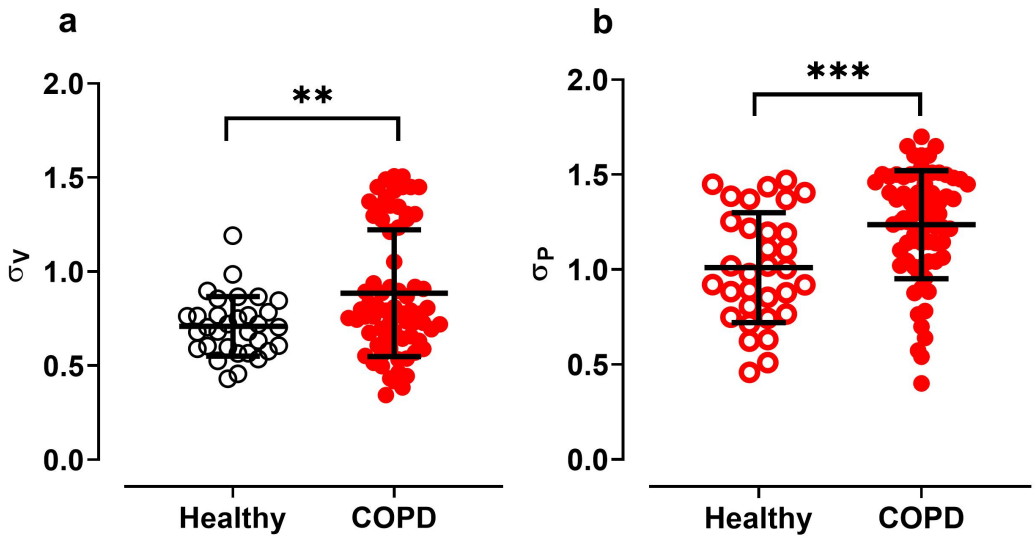


Figure 6.5: The IST heterogeneity indices in human data. Panels a and b show unpaired Student's t-test of the IST ventilation (σ_V) and perfusion heterogeneity (σ_P) indices. $** : p < 0.01, *** : p < 0.001$.

$$\sigma_P = 0.0045 * age + 0.75 \tag{6.4}$$

The ROC curve, shown in Figure 6.7, gave a value of AuC of 0.76 ($p < 0.0001$). This result indicates that the COPD classification method only using the heterogeneity indices was better than the previous method (IST ratios in Chapter 5). In the IST ratios, there was no significant difference between healthy and injured.

Healthy vs four COPD types. The IST heterogeneity indices illustrated differences between healthy and COPD phenotypes according to the GOLD classification in Figure 6.8. The significant differences might not be visible by eye, but the Kruskal-

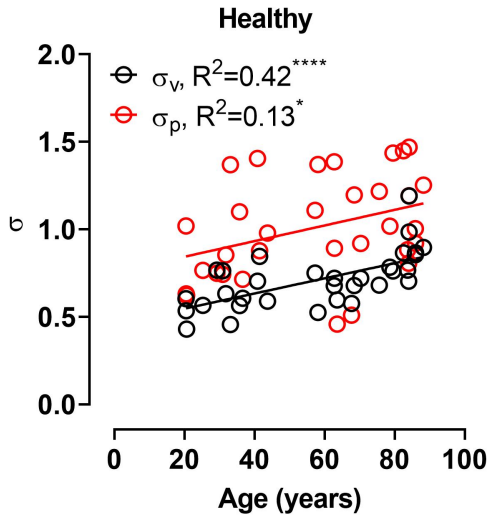


Figure 6.6: Linear regression of the IST heterogeneity indices vs age in healthy subjects. $* : p < 0.05, **** : p < 0.0001$.

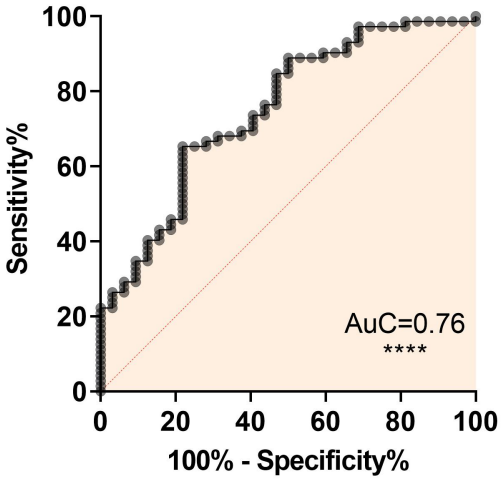


Figure 6.7: The ROC curve of the COPD classification (Healthy vs COPD) using only IST heterogeneity indices.

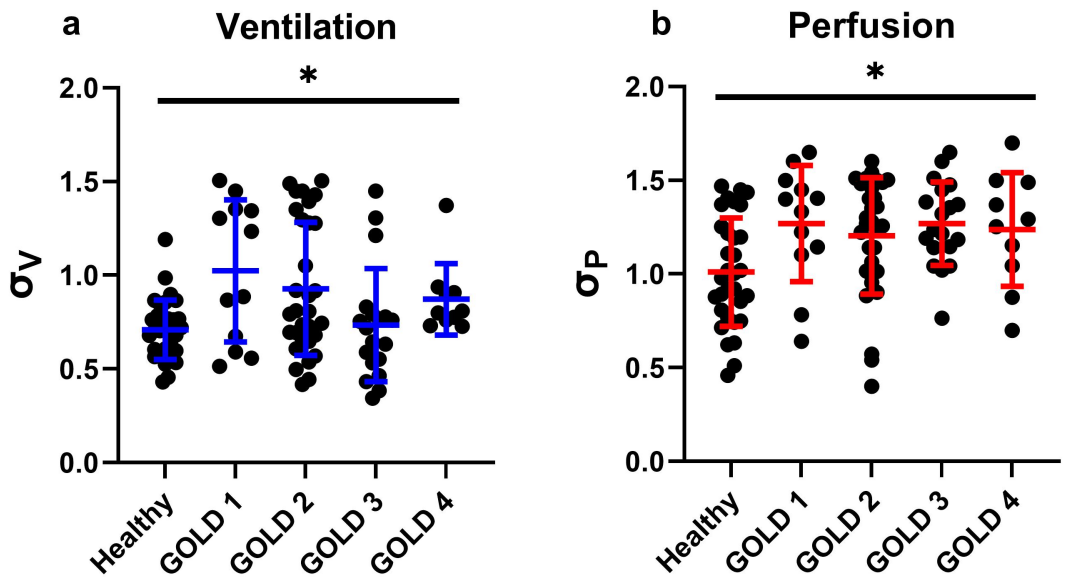


Figure 6.8: The IST heterogeneity results in the human data. Panel a and b show the distribution of the IST heterogeneity indices in different lung conditions. Statistical test was applied for multiple groups comparison $* : p < 0.05$.

Wallis test results (multiple comparison for non-parametric distributed data) showed that $p < 0.05$ in both ventilation and perfusion heterogeneity indices.

6.2.4 Classification of COPD types using the IST heterogeneity indices

In Figure 6.9, further understanding of the IST lung heterogeneity in different COPD phenotype is revealed. In this figure, % of predicted values for age were calculated according to Equations 6.3 and Equation 6.4, thereby eliminating the influence of normal ageing and there by eliminating variance unrelated to disease severity. The IST heterogeneity indices (both ventilation and perfusion) for healthy and COPD pa-

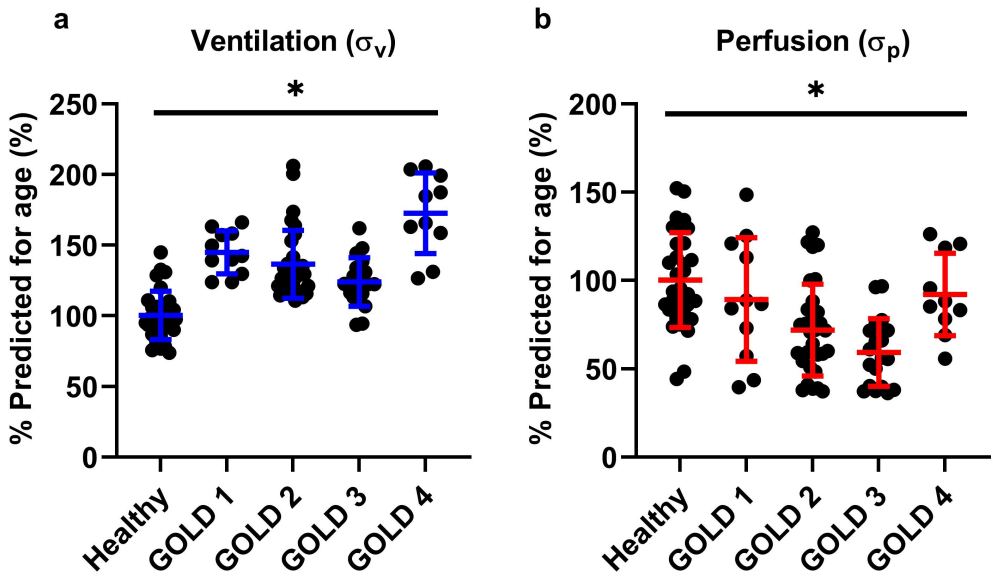


Figure 6.9: The IST heterogeneity results in the human data normalised for the effect of age. COPD patients were grouped into four GOLD groups. Panel a and b show the distribution of the IST heterogeneity indices in different lung conditions. Statistical test was applied for multiple groups comparison $* : p < 0.05$.

tients ($p < 0.05$) are now clearly distinct. However, there was still no clear distinction found among the COPD groups.

Additionally, Figure 6.10 shows a confusion matrix for patient classification results using only IST heterogeneity indices. The 'GOLD' classification was assumed to present the ground truth. This matrix shows the misclassification in percentage values compared to the clinical scale of COPD phenotype classification. These classification results achieved an overall accuracy of 73% based on GOLD classification. The highest predicted accuracy was the healthy group (100% accuracy) and the lowest was between COPD phenotype 1 and 4 (57%).

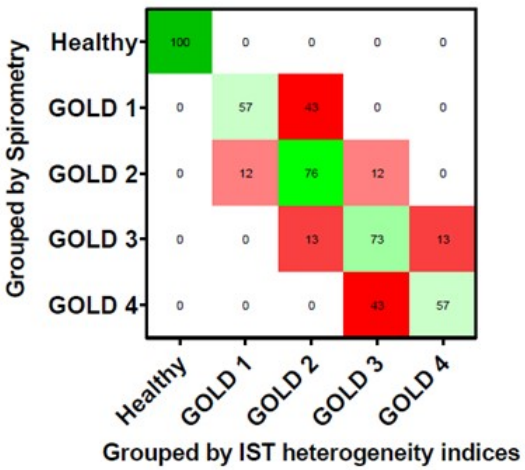


Figure 6.10: Confusion matrix for the logistic regression analysis in percentage values. This analysis grouped patients by the IST heterogeneity indices compared with the classification results using Spirometry (GOLD standard method).

6.2.5 Comparison of the IST heterogeneity ratios vs CT scan

There are $n = 105$ paired measurements in total including both IST and CT scans at four different PEEP levels. This comparison shows a slightly better agreement between the IST heterogeneity indices and CT heterogeneity values than in the previous method (mentioned in Chapter 5).

Figure 6.11 shows the scatter plots and linear regression comparison of the lung heterogeneity between IST and CT images in six animals. The full report of the linear regression in individual pigs is presented in Table 6.3. Better agreements were observed between IST vs CT compared to previous method of IST ratios. Furthermore, in the previous chapter, the perfusion heterogeneity comparison (Figure 5.12), the results of H_{Perf} had no correlation with the H_{CT}, while in this method, there was

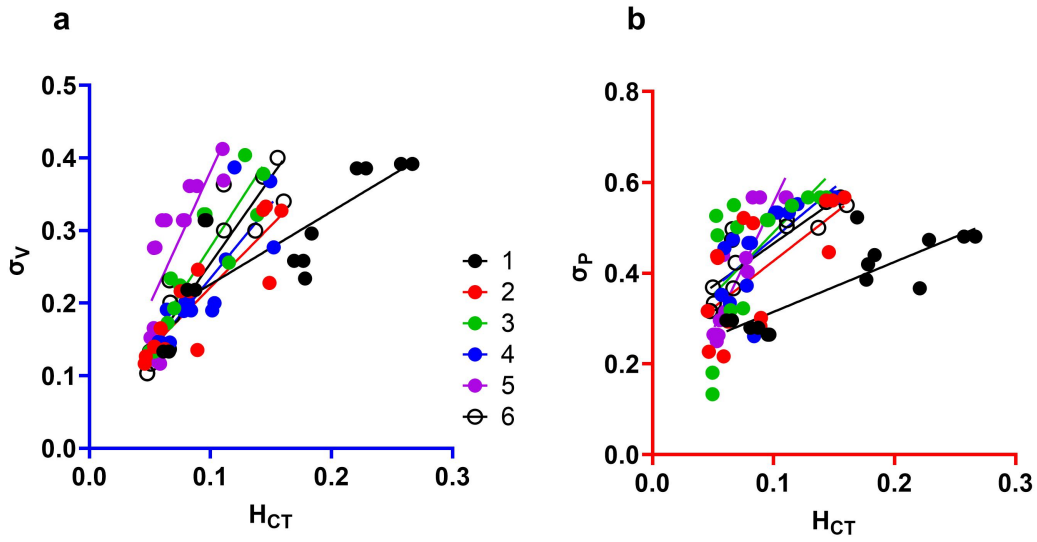


Figure 6.11: Colour coded animals in the comparisons of the lung heterogeneity measured by the CT scan and IST.

a weak correlation between σ_P and H_{CT}. Highest correlation values between σ_P and H_{CT} was $R^2 = 0.81$ and lowest was $R^2 = 0.40$.

Figure 6.12 shows the four-quadrant plots that demonstrate the relationship between the changes in heterogeneity measured by CT and IST. Strong correlation and concordance rates were observed. The agreement between $\Delta\sigma_V$ and ΔH_{CT} was found to be 98% in ventilation and 89% in perfusion. Additionally, in perfusion, the agreement between $\Delta\sigma_P$ and ΔH_{CT} of 54% ($R^2 = 0.30$) in the previous method (Figure 5.13 panel b) was improved to 89% ($R^2 = 0.60$).

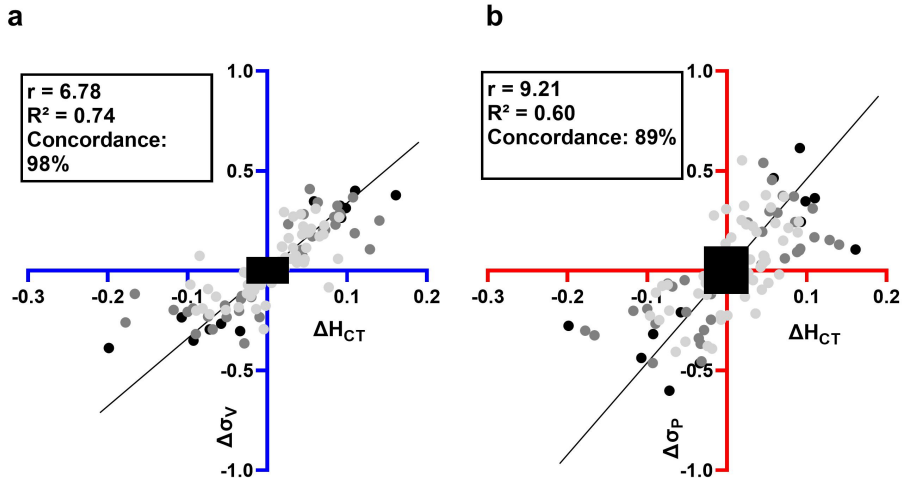


Figure 6.12: Four quadrant plots showing the changes of lung heterogeneity measured by the IST ($\Delta\sigma_V$ and $\Delta\sigma_P$) versus CT scan with changes in PEEP level. The exclusion zone (black rectangle) is 15% of the maximum values. The agreement is the percentage of data points that lie in the I(+;+) and III(-;-) quadrants, excluding the exclusion zone.

Table 6.3: Linear regression results of the comparison between IST lung heterogeneity indices and CT scans in six pigs.

Pig number	σ_v		σ_p	
	Gradient	R^2	Gradient	R^2
1	0.61	0.67	0.59	0.72
2	0.76	0.79	1.98	0.45
3	1.00	0.83	2.94	0.40
4	1.18	0.69	1.90	0.51
5	2.62	0.59	2.38	0.81
6	0.79	0.87	0.90	0.77

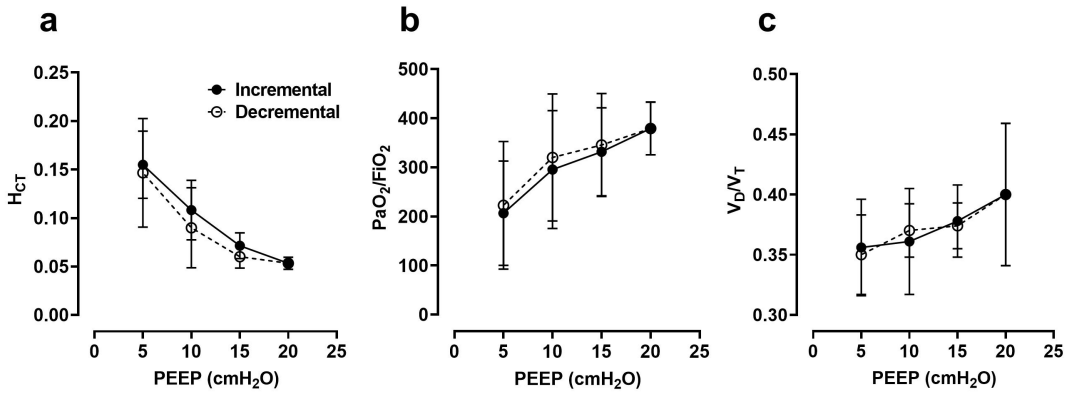


Figure 6.13: The overall influences of PEEP levels to lung parameters. Panel a shows lung heterogeneity measured by CT scan changed with PEEP. Panels d and e show the changes of $PaO2/FiO2$ and V_D/V_T vs PEEP. Mean and standard deviation of are plotted.

6.2.6 Optimisation PEEP setting for mechanical ventilator

In Figure 6.13 b and c, when PEEP level raised, $PaO2 : FiO2$ ratio and V_D/V_T also increased with negligible variation between incremental and decremental PEEP levels. For this initial proof-of-concept study, two separated models were proposed to predict the optimal PEEP for individual pigs. The first model uses IST heterogeneity ventilation and perfusion parameters. A second-degree polynomial function ($f(x)$) was fitted to the normalised IST heterogeneity values:

$$\widehat{\sigma_V} + \widehat{\sigma_P} = f_1(x) \tag{6.5}$$

where, $\widehat{\sigma_V}$ and $\widehat{\sigma_P}$ are the normalised IST heterogeneity index of ventilation and

perfusion. x is the PEEP level. Optimal PEEP is obtained when $f(x)$ is minimum. The decremented and incremented PEEP measurements were assumed to be similar, due to negligible variation.

Similarly, the second model to optimise PEEP consists of physiological parameters and CT heterogeneity index.

$$\widehat{H_{CT}} - \widehat{PFR} + \widehat{V_D/V_T} = f_2(x) \tag{6.6}$$

where, $\widehat{H_{CT}}$ is the normalised CT heterogeneity index, $\widehat{PFR}$ is the normalised $PaO2 : FiO2$ ratio, $\widehat{V_D/V_T}$ is the normalised V_D/V_T ratio and x is the PEEP level. Optimal PEEP is obtained when $f_2(x)$ is minimum.

Figure 6.14 shows preliminary results of the detection of optimal PEEP values in individual animals. The calculations were compared between the method based on the heterogeneity indices (black lines and dots) and the method based on physiological parameters (red lines and dots). According to the results of the lung heterogeneity, the average optimal PEEP level of all 6 pigs is 15 ± 1 cmH_2O. In comparison, the lung physiological parameters suggested the optimal PEEP level is 16 ± 2 cmH_2O. The difference of optimal PEEP using two methods is smaller than 2 cmH_2O in the pig number 1, 4 and 6. Pig 5 has the largest variation of the calculated optimal PEEPs (5 cmH_2O).

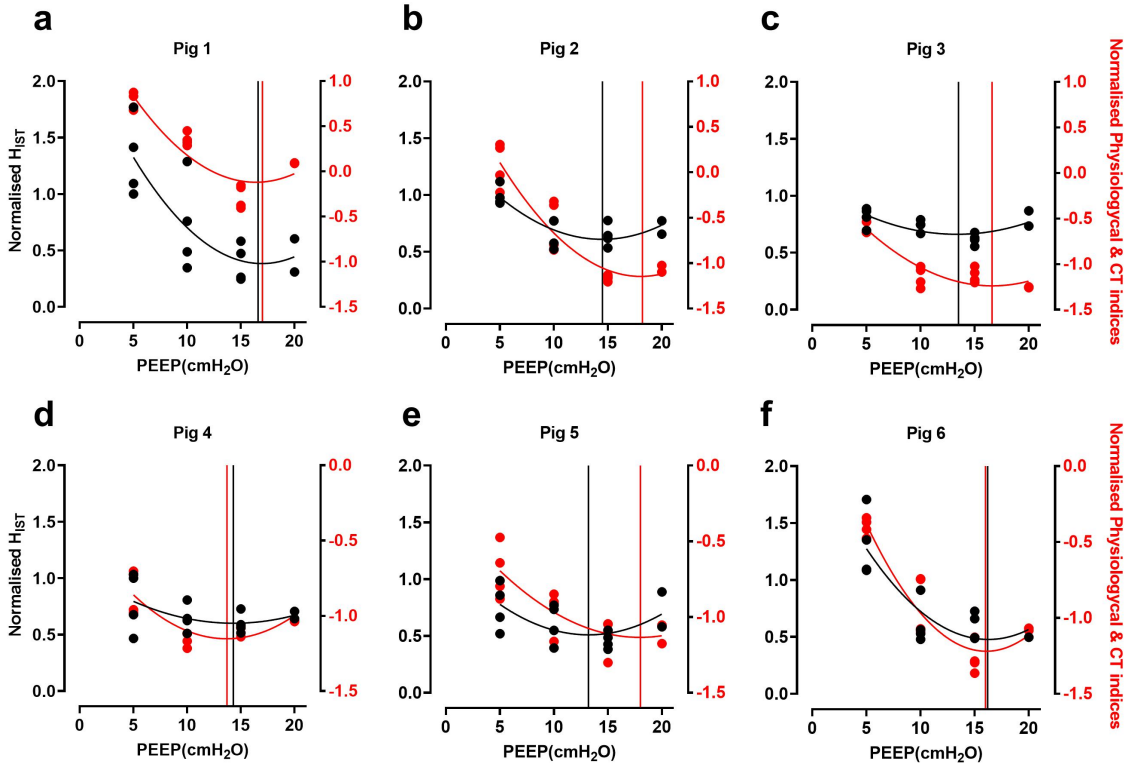


Figure 6.14: Optimal PEEP level according to lung heterogeneity measured by IST (black vertical line) and physiological and CT indices (red vertical line) in six individual animal. The physiological indices included $PaO2/FiO2$, V_D/V_T and H_{CT}. The second-degree polynomial functions were fit to normalised data. The optimal PEEP value (vertical lines) were calculated according to the minimum point of the second-degree polynomial functions.

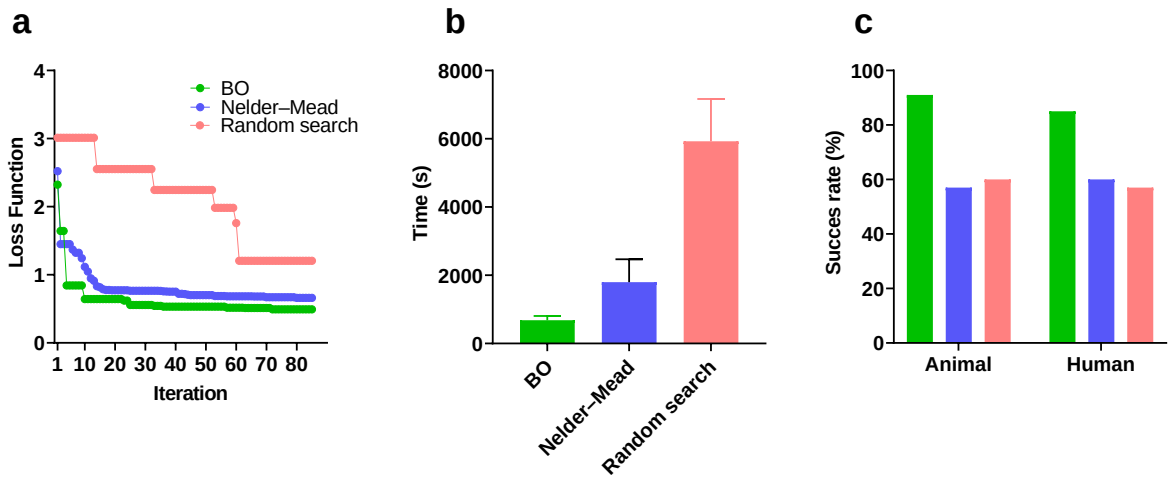


Figure 6.15: Comparison of the performance in the loss function (panel a), computational time (panel b) and success rate (panel c) of three methods in one example data.

6.2.7 Optimisation performance

Figure 6.15 compares the efficiency among different optimisation methods (Bayesian optimisation, Neider-Mead and random search). This figure shows one example of the loss function vs iterations in one example data. Bayesian optimisation illustrates a clear advantage in finding the optimal minimum loss variable within the first ten iterations.

Figure 6.15b and c show the computational time and success rate of the three optimisation algorithms. The Bayesian optimisation can provide more accurate approximations in less than 15 minutes compared to others. These data in panel a show the mean and standard deviations of the time consumption in both animal and human data.

Since the optimisation may not return results within acceptable ranges, I initiated a scale named 'success rate'. The success rate is the percentage of meaningful results reached after the average running time. According to panel c, the percentage in Bayesian optimisation was the highest when compared to other methods (92% in animal data, 83% in COPD data).

6.3 Discussion

Overall, this study has quantified lung heterogeneity using a non-invasive lung function test, the Inspired Sinewave Test, combined with advanced computational methods. Heterogeneity values were captured and demonstrated in both animal and human studies, in both health and disease. In this section, I discuss in detail the method to calculate the lung heterogeneity non-invasively, and consider the use of these indices as a tool to classify lung conditions.

6.3.1 Ventilation and perfusion heterogeneity measured by lung simulation

Ventilatory heterogeneity is the mismatch in the distribution of the ventilation relative to compartment size. The latter is sometimes referred to as 'specific ventilation' and represents the reciprocal of the time-constant of a compartment. Perfusion heterogeneity is the mismatch of perfusion relative to compartment size. Both of these forms of heterogeneity are related to, but distinct from, V/Q heterogeneity which is the non-uniform distribution of V/Q ratios (with respect to perfusion or ventilation),

which will be discussed in the future work.

In this work, the standard deviation of the lognormal distributions of ventilation and perfusion (σ_V and σ_P) was shown to adequately represent and usefully quantify heterogeneity of both ventilation and perfusion (both relative to compartment size). Such heterogeneity has previously been shown to be represented by a lognormal distribution. An example of this is the Multibreath Nitrogen Washout technique; a relatively technically complex technique that assumes this distribution [121, 74]. Ventilatory heterogeneity could be usefully presented to clinicians in both numerical formats (standard deviation) and visually, in the form of a lognormal plot. The lognormal distribution is straightforward to understand and relatively easily recognised by clinicians. Thirdly, this distribution could be upgraded easily in the future to allow for bi-modal or multimodal distributions.

Our results for the ventilation and perfusion lognormal distributions agreed with previous studies. Other research using different lung measurement techniques has shown similar standard deviations of ventilation and perfusion of 0.53 and 0.55 in healthy people, albeit in a much smaller sample ($n = 6$) [13, 98]. In our study, in Figure 6.5, healthy people had mean values of $\sigma_v = 0.71$ and $\sigma_p = 1.0$. Because age is an important factor in COPD, in Figure 6.6, this effect could be compensate in the analyses. The outlying results in the confusion matrix for the GOLD phenotypes were never greater than ± 1 indicating generally good agreement. Heterogeneity indices (expressed as % predicted for age) were significantly different between healthy and COPD cohorts. Overall, % predicted values of σ_v was 100 ± 17 (healthy) vs $\sigma_v = 140 \pm 26$ (pooled COPD).

6.3.2 Validation of the lung heterogeneity to CT imaging

Agreement in both absolute and changes of heterogeneity values were observed. The influence of PEEP level on the lung heterogeneity was also calculated. The degree of lung heterogeneity shows a wider scatter, but it is decreased with increasing PEEP. The changes in the ventilation heterogeneity have a good concordance rate with the CT scan (more than 95 %). Calculation of the IST ratio (as shown in the previous chapter) does not require optimisation or significant computational effort, but IST σ (the focus of this chapter) shows stronger agreement with the CT heterogeneity results. Therefore, depending on the method, the purpose of use, both IST methods could fit well to different applications. Due to strong agreement with CT scan results, the IST σ value can potentially reflect the condition of the lung in the same way as does the CT scan.

6.3.3 Lung heterogeneity to classify COPD patients

The ability to measure lung heterogeneity could improve the impact of the IST when used as a diagnostic tool. For example, in Figure 6.10, a simple multi-class logistic classification was implemented. The GOLD classification (based on the spirometry values and reported symptoms) was assumed to be a ground truth for the classification comparison [106]. The comparison result using the IST heterogeneity values could predict 73 % similarly to the ground truth. The classification results also mentioned a full agreement 100% of predicting healthy patients in both methods. Furthermore, the IST could also classify ARDS lungs (injured) versus control (non-injured), with a

value of $AuC = 0.76$ ($p < 0.0001$) of the ROC curve (in Figure 6.7). This investigation could benefit patients with lung diseases under mechanical ventilation.

In the human data (classified according to 'GOLD'), the results were not accurately classified by the IST heterogeneity indices. This is likely because a COPD diagnosis covers a wide variety of pathology and severity, and the GOLD classification is based on spirometry and reported symptoms which themselves have an unknown relationship to pathological severity. Age is also known to be an essential factor in COPD disease prediction [19]. This work shown similar results. The correlation between ventilatory and perfusion heterogeneity versus age in healthy participants were stated. Thus, although lung heterogeneity was normalised to account for the effect of age, other factors such as genetic factors, tobacco smoke and outdoor air pollutants also play essential roles in a patient's lung heterogeneity [122] which could not be controlled for in this study. In contrast, however, in the animal experiments, there was greater uniformity in experimental conditions both before and after lung injury, which allowed the specific effects of injury to be more evidently displayed.

6.3.4 Optimal PEEP prediction

A potential PEEP detection method according to the lung heterogeneity was presented. There are different protocols to detect optimal PEEP and different anaesthetists have their own protocol to determine the best PEEP level. In this work, a relatively simple mathematical model was applied to quantify PEEP values using available lung physiology parameters including lung heterogeneity. The results show similar

optimal PEEP results between the method acquired by physiological parameters and the method acquired by lung heterogeneity. The difference of optimal PEEP values calculated by both methods were smaller than 5 cmH_2O in all 6 pigs.

This is a foundation for other uses of lung heterogeneity and a pilot study for research in the future. In this way, lung heterogeneity measured by the IST could be used to detect optimal PEEP level for individual subjects.

6.3.5 Strengths and limitations of this model

In this work, the ability to use the IST was emphasised, a relatively simple to implement lung function test, as a diagnostic tool. The IST results themselves are reliable and clinically meaningful [17, 101].

This study has several strengths. This study included many animals and patient data from IST studies (13 animals and 104 participants). This is the first study to provide detailed lung heterogeneity data in both ARDS and COPD patients using the IST. However, several limitations were acknowledged. The experiments in this study were undertaken in parallel with data collection for other studies. Moreover, because the IST is a gas exchange technique, and N_2O has only modest blood solubility, the influence of perfusion is weaker than that of ventilation. This is likely to yield less reliable parameter recovery values for this parameter than for ventilation. Furthermore, our lung simulation and its lognormal assumptions might not fit the measured data to a high degree of accuracy. Therefore, future work will aim to loosen the prior assumptions of the distribution and to accommodate alternative possibilities. More

sophisticated lung simulations or advanced optimisation methods could also be introduced in the future. However, the required time and computer power consumption might then be prohibitive.

Although the optimisation process was time-consuming, Bayesian optimisation boosted the performance of the lung simulation-based optimisation model. Previous work required a supercomputer to optimise the lung heterogeneity indices. However, in this work, by modifying the lung simulation and applying Bayesian optimisation, computing power was reduced to about ten minutes using a standard desktop computer.

6.4 Key findings and Conclusion

A new approach to quantify lung heterogeneity using Bayesian optimisation combined with a non-invasive lung function test (the inspired sinewave technique) has been presented. This method substantially reduced the computing time and power for the optimisation process. The IST heterogeneity values illustrated strong agreements with CT values in both absolute values and changes. The analysis also revealed the relationship between ventilation heterogeneity vs age in human data ($R^2 = 0.42$). According to the age relationship with lung heterogeneity, the % prediction values can classify healthy vs COPD phenotypes ($p < 0.05$).

The ventilation heterogeneity can well classify ARDS lung vs control in the animal model ($p < 0.0001$). A simple method to optimise the PEEP level using the lung heterogeneity values was proposed and tested against optimal values obtained from

physiological parameters. The difference was found to be less than $\pm 5\ cmH_2O$ in all 6 pigs.

Chapter 7

Conclusion

7.1 General summary

This thesis contributes to the development of the respiratory medical device known as the Inspired Sinewave Test. Experiments and studies in this thesis show the comparisons of the IST to current standard devices. Experimental results confirmed the accuracy, reliability and repeatability of the IST. After that, a method to measure the lung heterogeneity was proposed and implemented using only the IST results. The lung simulation and experimental data assessed this simple method to measure heterogeneity using two-period tracer gases. The results concluded that, using a single compartment model and two $180s$ and $60s$ period tracer gases, the IST could determine the heterogeneity of the lung. However, the accuracy and reliability were found to be relatively low in the human dataset. Therefore, a more sophisticated method (lung simulation-based optimisation) was introduced and validated to improve the lung heterogeneity calculation. Finally, the heterogeneity results using this advanced

method were found to be strongly correlated with the values measured by CT images. According to these heterogeneity results, the IST can detect COPD and potentially provide optimal PEEP values for ventilated subjects.

This thesis started with the hypothesis that using the IST lung heterogeneity can predict COPD, and the heterogeneity results can also suggest setting up optimal ventilator settings. The results in this work supported the hypotheses. In the COPD prediction results, the IST heterogeneity had 73% agreement to the spirometry only using a simple classification method (logistic regression in this work). There is more room to develop the classification model to achieve a better agreement with spirometry in the future. On the other hand, to provide optimal PEEP values, a study in 6 pigs indicated a good correlation between optimal PEEP suggested by physiological parameters (CT scan, of $PaO2/FiO2$ and V_D/V_T) and the one indicated by the IST heterogeneity. The difference was about 2 cmH_2O.

Chapter 4 answered the questions of the reliability of the IST results. The IST could provide similar results to several lung function tests after 10 minutes. The comparisons with current standard methods illustrated the ability to accurately measure the lung parameters (deadspace volume, effective lung volume and pulmonary blood flow rate) of the IST. In both injured and non-injured animals, the effective lung volume, and deadspace volume had good agreement with the SF_6 washin washout method. Estimated values of the blood flow by the IST contained limitations. Further research should be carried on to study the pulmonary blood flow estimated by the IST. Furthermore, the setup in this study also confirmed the ability to measure lung parameters at the bedside for ventilated subjects of the IST.

Chapter 5 tested the hypothesis that IST can measure lung heterogeneity using two different periods of tracer gas ($180s$ and $60s$). The lung simulation with heterogeneous ventilation and perfusion was created. This lung simulation was used to examine the hypothesis. The simulated results confirmed the hypothesis and illustrated that the IST can calculate the heterogeneity of the lung. In the data from 13 animals, at PEEP values of 10 cmH_2O, the IST was found to be able to well distinguish control lungs from ARDS lungs ($AUC = 0.85$). Ventilation heterogeneity is a relatively strong indicator to classify lung conditions. However, this analysis could not distinguish the different levels of COPD.

Chapter 6 describes an analysis by which the IST can measure lung heterogeneity accurately by using more advanced lung simulations. Lung simulations with multiple complex compartments were generated. The parameters of these compartments were controlled by the lognormal distribution, assumed to represent the lung more realistically. An advanced optimisation method was applied. The results shown the lung heterogeneity measured by the IST to be more accurate and reliable. Again, the ventilation heterogeneity can distinguish between the control and ARDS groups in 13 animals ($p < 0.0001$). This method also can distinguish different COPD phenotypes with 73% agreement with the spirometry classification. According to the IST heterogeneity, optimal PEEP levels were suggested. These values were compared with the values indicated by physiological parameters. The difference was about 2 cmH_2O indicating very good agreement.

7.2 Strengths and limitations of this study

This study has contributed to the development of the IST. The strengths of this study are the usability of the IST in clinical environments (ventilated subjects and human clinical testing). This work included big data sets collected for the IST (13 animals in Uppsala, Sweden and 104 human volunteers in the UK). These data included various lung conditions in humans (healthy and COPD, including phenotypes) and animal data (ARDS model in animals and control animals). The whole datasets were collected in three years in between the United Kingdom and Sweden. These data have been stored and readied to reuse in the future.

One of the advantages of the IST is usability. The IST running protocol is straightforward. Additionally, this non-invasive, non-ionising lung function test has been studied for a number of years. The setup for the IST experiment may be executed quickly. The lung parameters can be seen after a short testing time (about 10 minutes). Due to the IST setup a detachable sensor can be plugged immediately into the airway tube of any ventilated subjects.

The studies in this thesis confirmed that the IST could measure accurately lung parameters and lung heterogeneity. The works in this thesis strengthened the foundation for using the IST as a diagnostic tool. The calculation of lung heterogeneity using the IST is the next step to expand the application of the IST. Furthermore, in animal studies, the changes in lung heterogeneity at different PEEP levels were recorded. According to these values, optimal PEEP level could be suggested and personalised for the individual subject. So, ventilated subjects with damaged lung

(ARDS and VILI) can gain potential benefit from the IST measurement. The IST lung heterogeneity could potentially be an suggestion to guide mechanical ventilator settings together with other lung indices.

In terms of lung simulation, this work provided the fundamentals of using lung simulation to quantify lung heterogeneity using a non-invasive lung function test. Several types of lung simulations were mentioned in the literature review, such as imaging model, dynamic flow model and mixed models. The tidal compartment lung simulations were used in this because of their usability and ease of modification. Simulink-Matlab was used to develop the model. The list first order differential equations were transformed and solved in frequency domain rather than in time domain. This action could save time and computing power. Furthermore, this simulation can work with other lung function tests with similar working principles to the IST (tracer gas exchange).

However, this study has its limitations. Firstly, the lung simulation and optimisation methods contain disadvantages. The lung simulation cannot perfectly match the real lung behaviour. The two alveolar compartments with fixed 0.1 and 0.9 fractions of the volume may be insufficient to represent the complexity of real-life lung heterogeneity, a continuous distribution. These constrained volume fractions will introduce some inaccuracies into the estimation. For example, the volume fractions of 0.2 and 0.8 might not be recovered precisely. Additionally, collapsed volumes of the lung might not be detected using this simulation. In the works using the 125 alveolar compartments simulation, to create an optimisation algorithm, details tuning and dealing with hyper-parameters might require time and expertise to set up. Better

lung simulations could solve this problem. In theory, optimisation to match simulated data to measured data is a well-established method. However, practically, the integration of the optimisation inside a lung function test is not a good combination. For example, the users have to wait for a long time for the results in just one analysis.

Secondly, during animal and human testing, the IST measurements were performed in parallel with other studies. Therefore, the data quality might be slightly influenced by the design of these other studies. However, I followed the experimental protocol strictly and human errors were minimised during the experiments.

Thirdly, the pig lung can not illustrate all conditions of the human lung, but it might be the closest animal lung to simulate the human lung *in-vivo*. Using animal data to model the human lung was another limitation of this thesis. The human data have many variations (which can not be controlled, such as weight, height, age, lifestyle and many other physiological parameters), so the results might not reveal the significant points. The animal data, instead, can be controlled and ensured the same standard is applied.

Fourthly, while other studies focus on the ventilation heterogeneity in conjunction with the perfusion, this work measure separately the specific ventilation heterogeneity and perfusion heterogeneity. This work pointed out the specific ventilation heterogeneity can be measured accurately by the IST and it has shown clinical impacts on lung diseases detection. On the other hand, the perfusion heterogeneity does not show any statistical significance in terms of lung condition detection. Perfusion values could be the limitation of the IST because this test is more related to the gas exchanged

process. Therefore, merged these values might provide more confusion to the results.

Last but not least, the IST contains limitations itself. The calculation of the IST might come from the non-solubility of the N_2O. This can introduce the higher value of the mixed venous concentration of N_2O. Additionally, IST applies the gas-exchanged principle; therefore, it is difficult to detect a collapsed region inside the lung, which does not involve in the gas-exchanged process.

7.3 Future directions

7.3.1 Translation of the IST in human medicine

The potential method to measure lung heterogeneity using the Inspired Sinewave Test was illustrated. In this work, one of the use of IST was as a diagnostic tool; however, there are more potential applications. In the next studies, the investigation of the IST in humans under anaesthesia might be an interesting topic, as well as the personalised optimisation of mechanical ventilator. Further experiments could be done with the mechanical ventilated patients (patients in the Intensive Care Unit) to test the usability of the IST in the ICU. The investigation could be done with damaged lung and healthy lung in the ICU. This test can confirm the feasibility of using IST in the ICU environment, which contains different types of ventilator machines.

Furthermore, using the IST for COVID-19 patients may be a potential project. Researchers can collect IST data at a certain time point during the recovery of COVID-19

patients. The track record of the lung function results in days, weeks or months might be useful to suggest suitable rehabilitation and treatments.

The IST was approved to be tested in clinical testing with COPD patients in King's College London, London, UK. The main priority aim of this project is to compare the lung heterogeneity measured by the IST with the lung clearance index (measured by the multiple breath nitrogen washout). The paired measurements will be performed in the same subject within a variety of ageing group including both healthy and COPD patients.

7.3.2 Integrated new hardware and testing technique for the IST

The IST has been developed with new accurate infrared sensors to detect flow and gas concentrations more accurately. The new sensor would provide a better alignment of the flow and concentration signals which are very likely to improve the results acquired. This new sensor has both integrated signal processing and noise filter, thus it can respond quickly to the changes in flow and concentration. On the other hand, a calibration method may be integrated into the system. So, it can be more effective and more accurate. Further research to compare the new sensor with the old sensor should be developed, before using the new sensing units. For instance, two sensors can be connected to measure the data from the same subject.

Furthermore, it could be possible to improve the performance of the IST by using mixed periods N_2O. This novel testing technique might reduce the testing time for

an individual patient and benefit the optimisation process of the IST analysis. In theory, mixed tracer gas periods or random tracer gas periods can provide an unique output. This special output signal will be beneficial for the optimisation process since the proposed method matches simulated output to the measured output. In this research, suitable mix periods should be carefully chosen, such as a mixed-signal of 60 s and 100 s periods. The time for each IST measurement will be shortened. Currently, the IST takes about 5 minutes for one measurement in one-period tracer gas. Using the mixed-signal, instead of doing twice times 5 minutes test, the IST will only need half of the time.

7.3.3 Development of more advanced lung simulations

Future development of the simulation can be performed to improve the lung simulation and the optimisation process. This work illustrated that simulation-based optimisation could be a potential method to obtain lung parameters accurately. In the future, the IST optimisation process could benefit from machine learning and advanced computing power. There are currently advanced lung simulations such as graphical based lung simulation, multiple dimensional lung simulation. In this work, only compartmental lung simulations were used. It can well represent lung behaviour, but it might not perfectly match lung physiology and pathology. Additionally, with the development of computational technology and advanced algorithms, the optimisation process may be less time consuming and work more efficiently so that the optimisation can be done during the IST. The results can be seen in real-time.

The work in this thesis can be developed in another way. An advanced classification model could be developed to classify patients with lung diseases. This model could be a data-driven model, which means that the model is developed based on collected data. A machine learning algorithm and, furthermore, deep learning can be applied here. In such a model, more signals and parameters can be added, such as lung sound, patient's living habit, smoking story, etc.

References

[1] J. B. West, *Respiratory Physiology-The Essentials*, 2012, vol. Ninth Edit.

[2] J. Petersson and R. W. Glenny, "Gas exchange and ventilation-perfusion relationships in the lung," *European Respiratory Journal*, vol. 44, no. 4, pp. 1023–1041, 2014.

[3] R. C. Sá, A. K. Asadi, R. J. Theilmann, S. R. Hopkins, G. K. Prisk, and C. Darquenne, "Validating the distribution of specific ventilation in healthy humans measured using proton MR imaging," *Journal of Applied Physiology*, vol. 116, no. 8, pp. 1048–1056, 2014.

[4] J. N. Cronin, J. B. Borges, D. C. Crockett, A. D. Farmery, G. Hedenstierna, A. Larsson, M. C. Tran, L. Camporota, and F. Formenti, "Dynamic single-slice CT estimates whole-lung dual-energy CT variables in pigs with and without experimental lung injury," *Intensive Care Medicine Experimental*, vol. 7, no. 1, dec 2019.

[5] M. Cressoni, P. Cadringher, C. Chiurazzi, M. Amini, E. Gallazzi, A. Marino, M. Brioni, E. Carlesso, D. Chiumello, M. Quintel, G. Bugedo, and L. Gattinoni,

"Lung inhomogeneity in patients with acute respiratory distress syndrome," *American Journal of Respiratory and Critical Care Medicine*, vol. 189, no. 2, pp. 149–158, 2014.

[6] P. D. Wagner, "The multiple inert gas elimination technique (MIGET)," *Applied Physiology in Intensive Care Medicine 1: Physiological Notes - Technical Notes - Seminal Studies in Intensive Care, Third Edition*, pp. 35–42, 2012.

[7] D. Y. Sue, "Measurement of Lung Volumes in Patients with Obstructive Lung Disease. A Matter of Time (Constants)," *Annals of the American Thoracic Society*, vol. 10, no. 5, pp. 525–530, 2013.

[8] J. Usemann, S. Yammine, F. Singer, and P. Latzin, "Inert gas washout: background and application in various lung diseases," *Swiss Medical Weekly*, vol. 147, no. August, pp. 1–13, 2017.

[9] M. R. Miller, J. Hankinson, V. Brusasco, F. Burgos, R. Casaburi, A. Coates, R. Crapo, P. Enright, C. P. M. van der Grinten, P. Gustafsson, R. Jensen, D. C. Johnson, N. MacIntrye, R. McKay, D. Navajas, O. F. Pedersen, R. Pellegrino, G. Viegi, and J. Wagner, "Standardisation of spirometry," *European Respiratory Journal*, vol. 26, no. 2, pp. 319–338, 2005.

[10] M. Filoche, C. F. Tai, and J. B. Grotberg, "Three-dimensional model of surfactant replacement therapy," *Proceedings of the National Academy of Sciences of the United States of America*, vol. 112, no. 30, pp. 9287–9292, 2015.

[11] C. E. Hahn and A. D. Farmery, "Gas exchange modelling: No more gills, please," *British Journal of Anaesthesia*, vol. 91, no. 1, pp. 2–15, 2003.

[12] C. Harrison, P. A. Phan, C. Zhang, D. Geer, A. Farmery, and S. Payne, "Modelling mixing within the dead space of the lung improves predictions of functional residual capacity," *Respiratory Physiology and Neurobiology*, vol. 242, pp. 12–18, 2017.

[13] J. E. Mountain, P. Santer, D. P. O'Neill, N. M. Smith, L. Ciaffoni, J. H. Couper, G. A. Ritchie, G. Hancock, J. P. Whiteley, and P. A. Robbins, "Potential for noninvasive assessment of lung inhomogeneity using highly precise, highly time-resolved measurements of gas exchange," *Journal of Applied Physiology*, vol. 124, no. 3, pp. 615–631, 2018.

[14] S. Schlesinger, *Terminology for model credibility*, 1979, vol. 32, no. 3.

[15] B. H. Thacker, S. W. Doebling, F. M. Hemez, M. C. Anderson, J. E. Pepin, and E. a. Rodriguez, "Concepts of Model Verification and Validation," *Concepts of Model Verification and Validation*, p. 41, 2004.

[16] V. Nguyen, "Bayesian Optimization for Accelerating Hyper-Parameter Tuning," in *2019 IEEE Second International Conference on Artificial Intelligence and Knowledge Engineering (AIKE)*. IEEE, 2019, pp. 302–305.

[17] R. R. Bruce, D. Crockett, A. Morgan, M. C. M. Tran, F. Formenti, P. A. P. Phan, and A. D. Farmery, "Noninvasive cardiac output monitoring in a porcine

model using the inspired sinewave technique: a proof-of-concept study," *British Journal of Anaesthesia*, vol. 123, no. 2, pp. 126–134, 2019.

[18] B. et al Agustí, A. Beasley, R. Celli, "Pocket guide to COPD diagnosis, management, and prevention: A guide for health care professionals," *Global Initiative for Chronic Obstructive Lung Disease, Inc.*, pp. 1–43, 2019.

[19] R. M. Bruce, P. A. Phan, E. Pacpaco, N. M. Rahman, and A. D. Farmery, "The inspired sine-wave technique: A novel method to measure lung volume and ventilatory heterogeneity," *Experimental Physiology*, vol. 103, no. 5, pp. 738–747, 2018.

[20] M. Hussain, P. Madl, and A. Khan, "Lung deposition predictions of airborne particles and the emergence of contemporary diseases, Part-I," *The Health*, vol. 2, no. 2, pp. 51–59, 2011.

[21] R. A. Pauwels, A. S. Buist, P. M. A. Calverley, C. R. Jenkins, and S. S. Hurd, "Global Strategy for the Diagnosis , Management , and Prevention of Chronic Obstructive Pulmonary Disease NHLBI / WHO Global Initiative for Chronic Obstructive Lung Disease (GOLD) Workshop Summary," vol. 163, pp. 1256–1276, 2001.

[22] N. M. Siafakas, P. Vermeire, N. B. Pride, P. Paoletti, J. Gibson, P. Howard, J. C. Yernault, M. Decramer, T. Higenbottam, D. S. Postma, and J. Rees, "Optimal assessment and management of chronic obstructive pulmonary disease (COPD)," *European Respiratory Journal*, vol. 8, no. 8, pp. 1398–1420, 1995.

[23] NICE, "Chronic obstructive pulmonary disease in adults," 2016.

[24] WHO, "Chronic obstructive pulmonary disease (COPD)," 2017. [Online]. Available: https://www.who.int/news-room/fact-sheets/detail/chronic-obstructive-pulmonary-disease-(copd)

[25] J. Marti, P. Hall, P. Hamilton, S. Lamb, C. McCabe, R. Lall, J. Darbyshire, D. Young, and C. Hulme, "One-year resource utilisation, costs and quality of life in patients with acute respiratory distress syndrome (ARDS): Secondary analysis of a randomised controlled trial," *Journal of Intensive Care*, vol. 4, no. 1, pp. 1–11, 2016.

[26] J. Phua, L. Weng, L. Ling, M. Egi, C.-M. Lim, J. V. Divatia, B. R. Shrestha, Y. M. Arabi, J. Ng, C. D. Gomersall, M. Nishimura, Y. Koh, and B. Du, "Intensive care management of coronavirus disease 2019 (COVID-19): challenges and recommendations," *The Lancet Respiratory Medicine*, vol. 2019, no. 20, pp. 1–12, 2020.

[27] C. Wu, X. Chen, Y. Cai, J. Xia, X. Zhou, S. Xu, H. Huang, L. Zhang, X. Zhou, C. Du, Y. Zhang, J. Song, S. Wang, Y. Chao, Z. Yang, J. Xu, X. Zhou, D. Chen, W. Xiong, L. Xu, F. Zhou, J. Jiang, C. Bai, J. Zheng, and Y. Song, "Risk Factors Associated with Acute Respiratory Distress Syndrome and Death in Patients with Coronavirus Disease 2019 Pneumonia in Wuhan, China," *JAMA Internal Medicine*, vol. 180, no. 7, pp. 934–943, 2020.

[28] A. S. Slutsky and V. M. Ranieri, "Ventilator-Induced Lung Injury," *New England Journal of Medicine*, vol. 369, no. 22, pp. 2126–2136, 2013.

[29] N. de Prost, J.-D. Ricard, G. Saumon, and D. Dreyfuss, "Ventilator-induced lung injury: historical perspectives and clinical implications," *Annals of Intensive Care*, vol. 1, no. 1, p. 28, 2011.

[30] R. M. Kacmarek, "The mechanical ventilator: Past, present, and future," *Respiratory Care*, vol. 56, no. 8, pp. 1170–1180, 2011.

[31] P. D'Avignon, G. Hedenström, and C. Hedman, "XIII. Pulmonary Complications in Respirator Patients," *Acta Medica Scandinavica*, vol. 154, no. 316 S, pp. 86–90, 1956.

[32] L. Gattinoni, D. Mascheroni, A. Torresin, R. Marcolin, R. Fumagalli, S. Vesconi, G. P. Rossi, F. Rossi, S. Baglioni, F. Bassi, G. Nastri, and A. Pesenti, "Morphological response to positive end expiratory pressure in acute respiratory failure. Computerized tomography study," *Intensive Care Medicine*, vol. 12, no. 3, pp. 137–142, 1986.

[33] L. Gattinoni, J. J. Marini, A. Pesenti, M. Quintel, J. Mancebo, and L. Brochard, "The "baby lung" became an adult," *Intensive Care Medicine*, vol. 42, no. 5, pp. 663–673, 2016.

[34] L. Gattinoni, E. Carlesso, L. Brazzi, and P. Caironi, "Positive end-expiratory pressure," *Current Opinion in Critical Care*, vol. 16, no. 1, pp. 39–44, 2010.

[35] L. Gattinoni, A. Pesenti, and L. Gattinoni, "The concept of "baby lung"," *Intensive Care Med*, vol. 31, pp. 776–784, 2005.

[36] C. Summers, N. R. Singh, L. Worpole, R. Simmonds, J. Babar, A. M. Condliffe, K. E. Gunning, A. J. Johnston, and E. R. Chilvers, "Incidence and recognition of acute respiratory distress syndrome in a UK intensive care unit," *Thorax*, vol. 71, no. 11, pp. 1050–1051, 2016.

[37] T. Becher, V. Buchholz, D. Hassel, T. Meinel, D. Schädler, I. Frerichs, and N. Weiler, "Individualization of PEEP and tidal volume in ARDS patients with electrical impedance tomography: a pilot feasibility study," *Annals of Intensive Care*, vol. 11, no. 1, 2021.

[38] A. Aliverti, F. Pennati, C. Salito, and J. C. Woods, "Regional lung function and heterogeneity of specific gas volume in healthy and emphysematous subjects," *European Respiratory Journal*, vol. 41, no. 5, pp. 1179–1188, 2013.

[39] J. K. Lui and K. R. Lutchen, "The role of heterogeneity in asthma: a structure-to-function perspective," *Clinical and Translational Medicine*, vol. 6, no. 1, p. 29, 2017.

[40] G. Hedenstierna, "The recording of FRC - is it of importance and can it be made simple?" *Intensive Care Medicine*, vol. 19, no. 7, pp. 365–366, 1993.

[41] P. A. Phan, A. Farmery, and C. Hahn, "Method and apparatus for measurement of cardiopulmonary function," apr 2015.

[42] M. C. Tran, D. C. Crockett, F. Formenti, P. A. Phan, G. Hedenstierna, A. Larsson, S. J. Payne, and A. D. Farmery, "Lung heterogeneity and dead-space volume in animals with acute respiratory distress syndrome using the inspired sinewave test," *Physiological Measurement*, vol. 41, no. 11, pp. 1–10, 2020.

[43] M. C. Tran, D. C. Crockett, P. A. Phan, S. J. Payne, and A. D. Farmery, "A tidal lung simulation to quantify lung heterogeneity with the Inspired Sinewave Test," in *Proceedings of the Annual International Conference of the IEEE Engineering in Medicine and Biology Society, EMBS*, vol. 2020-July, 2020, pp. 2438–2441.

[44] S. Payne and M. Chappell, *Physiology for Engineers: Applying Engineering Methods to Physiological Systems*, 2015.

[45] J. S. Yem, M. J. Turner, A. B. Baker, I. H. Young, and A. B. H. Crawford, "A tidally breathing model of ventilation, perfusion and volume in normal and diseased lungs," *British Journal of Anaesthesia*, vol. 97, no. 5, pp. 718–731, 2006.

[46] I. Petrache and K. Serban, *Pathobiology of Human Disease*, 2014.

[47] S. I. Cha, K. M. Shin, J. Lee, Y. Hwangbo, S. S. Yoo, J. Lee, S. Y. Lee, C. H. Kim, J. Y. Park, and T. H. Jung, "Clinical relevance of pulmonary infarction in patients with pulmonary embolism," *Thrombosis Research*, vol. 130, no. 3, pp. e1–e5, 2012.

[48] NHS, "Pulmonary embolism," 2020. [Online]. Available: https://www.nhs.uk/conditions/pulmonary-embolism/

[49] L. Gattinoni, F. Collino, G. Maiolo, F. Rapetti, F. Romitti, T. Tonetti, F. Vasques, and M. Quintel, "Positive end-expiratory pressure: How to set it at the individual level," *Annals of Translational Medicine*, vol. 5, no. 14, pp. 1–10, 2017.

[50] L. Minati, M. Grisoli, and M. G. Bruzzone, "MR spectroscopy, functional MRI, and diffusion-tensor imaging in the aging brain: A conceptual review," *Journal of Geriatric Psychiatry and Neurology*, vol. 20, no. 1, pp. 3–21, 2007.

[51] S. B. Fain, F. R. Korosec, J. H. Holmes, R. O'Halloran, R. L. Sorkness, and T. M. Grist, "Functional lung imaging using hyperpolarized gas MRI," *Journal of Magnetic Resonance Imaging*, vol. 25, no. 5, pp. 910–923, 2007.

[52] J. P. Mugler and T. A. Altes, "Hyperpolarized 129Xe MRI of the human lung," *Journal of Magnetic Resonance Imaging*, vol. 37, no. 2, pp. 313–331, 2013.

[53] S. Treppo, S. M. Mijailovich, and J. G. Venegas, "Contributions of pulmonary perfusion and ventilation to heterogeneity in VA/Q measured by PET," *Journal of Applied Physiology*, vol. 82, no. 4, pp. 1163–1176, 1997.

[54] R. E. Jacob and J. P. Carson, "Automated measurement of heterogeneity in CT images of healthy and diseased rat lungs using variogram analysis of an octree decomposition," *BMC Medical Imaging*, vol. 14, no. 1, pp. 1–11, 2014.

[55] L. Gattinoni, A. Pesenti, M. Bombino, S. Baglioni, M. Rivolta, F. Rossi, G. Rossi, R. Fumagalli, R. Marcolin, D. Mascheroni, and A. Torresin, "Relationships between lung computed tomographic density, gas exchange, and PEEP in acute respiratory failure," *Anesthesiology*, vol. 69, no. 6, pp. 824–832, 1988.

[56] J. N. Cronin, D. C. Crockett, A. D. Farmery, G. D. Hedenstierna, A. Larsson, L. Camporota, and F. Formenti, "Mechanical Ventilation Redistributes Blood to Poorly Ventilated Areas in Experimental Lung Injury," *Critical Care Medicine*, p. 1, dec 2019.

[57] R. Rodríguez-Roisin, M. Drakulovic, D. A. Rodríguez, J. Roca, J. A. Barberà, and P. D. Wagner, "Ventilation-perfusion imbalance and chronic obstructive pulmonary disease staging severity," *Journal of Applied Physiology*, vol. 106, no. 6, pp. 1902–1908, 2009.

[58] J. W. Evans and P. D. Wagner, "Limits on VA/Q distributions from analysis of experimental inert gas elimination," *Journal of Applied Physiology*, vol. 42, pp. 889–898, 1977.

[59] W. S. Fowler, "Lung function studies; uneven pulmonary ventilation in normal subjects and in patients with pulmonary disease." *Journal ofApplied Physiology*, vol. XXXIV, no. 6, pp. 399–403, 1949.

[60] S. Gonem, A. Scadding, M. Soares, A. Singapuri, P. Gustafsson, C. Ohri, S. Range, C. E. Brightling, I. Pavord, A. Horsley, and S. Siddiqui, "Lung

clearance index in adults with non-cystic fibrosis bronchiectasis," *Respiratory Research*, vol. 15, no. 1, pp. 1–9, 2014.

[61] C. M. Owens, P. Aurora, S. Stanojevic, A. Bush, A. Wade, C. Oliver, A. Calder, J. Price, S. B. Carr, A. Shankar, and J. Stocks, "Lung clearance index and HRCT are complementary markers of lung abnormalities in young children with CF," *Thorax*, vol. 66, no. 6, pp. 481–488, 2011.

[62] S. Lum, P. Gustafsson, H. Ljungberg, G. Hülskamp, A. Bush, S. B. Carr, R. Castle, A. F. Hoo, J. Price, S. Ranganathan, J. Stroobant, A. Wade, C. Wallis, H. Wyatt, and J. Stocks, "Early detection of cystic fibrosis lung disease: Multiple-breath washout versus raised volume tests," *Thorax*, vol. 62, no. 4, pp. 341–347, 2007.

[63] A. Larsson, D. Linnarsson, C. Jonmarker, B. Jonson, H. Larsson, and O. Werner, "Measurement of lung volume by sulfur hexafluoride washout during spontaneous and controlled ventilation: Further development of a method," *Anesthesiology*, vol. 67, no. 4, pp. 543–550, 1987.

[64] A. L. Coates, R. Peslin, D. Rodenstein, and J. Stocks, "Measurement of lung volumes by plethysmography," *European Respiratory Journal*, vol. 10, no. 6, pp. 1415–1427, 1997.

[65] P. A. Phan, C. E. Hahn, and A. D. Farmery, "A modification of the Bohr method to determine airways deadspace for non-uniform inspired gas tensions," *Physiological Measurement*, vol. 38, no. 7, pp. 107–117, 2017.

[66] C. R. O'Donnell, A. A. Bankier, L. Stiebellehner, J. J. Reilly, R. Brown, and S. H. Loring, "Comparison of plethysmographic and helium dilution lung volumes: Which is best for COPD?" *Chest*, vol. 137, no. 5, pp. 1108–1115, 2010.

[67] A. Zwart, R. C. Seagrave, and A. Van Dieren, "Ventilation-perfusion ratio obtained by a noninvasive frequency response technique," *Journal of applied physiology*, vol. 41, no. 3, pp. 419 –424, 1976.

[68] C. E. Hahn, A. M. Black, S. A. Barton, and I. Scott, "Gas exchange in a three-compartment lung model analyzed by forcing sinusoids of N2O." *Journal of applied physiology*, vol. 75, no. 4, pp. 1863–1876, 1993.

[69] C. E. W. Hahn, "Oxygen respiratory gas analysis by sine-wave measurement: a theoretical model." *Journal of applied physiology*, vol. 81, no. 2, pp. 985–997, 1996.

[70] A. D. Farmery, "Interrogation of the Cardiopulmonary System with Inspired Gas Tension Sinusoids," Ph.D. dissertation, 2008.

[71] J. P. Whiteley, M. J. Turner, A. B. Baker, D. J. Gavaghan, and C. E. W. Hahn, "The effects of ventilation pattern on carbon dioxide transfer in three computer models of the airways," *Respiratory Physiology and Neurobiology*, vol. 131, no. 3, pp. 269–284, 2002.

[72] A. R. Lambert, P. T. O'Shaughnessy, M. H. Tawhai, E. A. Hoffman, and C. L. Lin, "Regional deposition of particles in an image-based airway model: Large-

eddy simulation and left-right lung ventilation asymmetry," *Aerosol Science and Technology*, vol. 45, no. 1, pp. 11–25, 2011.

[73] S. M. Lewis, J. W. Evans, and A. A. Jalowayski, "Continuous distributions of specific ventilation recovered from inert gas washout," *Journal of Applied Physiology Respiratory Environmental and Exercise Physiology*, vol. 44, no. 3, pp. 416–423, 1978.

[74] S. A. Verbanck, M. Polfliet, D. Schuermans, B. Ilsen, J. de Mey, E. Vanderhelst, and J. Vandemeulebroucke, "Ventilation heterogeneity in smokers: Role of unequal lung expansion and peripheral lung structure," *Journal of Applied Physiology*, vol. 129, no. 3, pp. 583–590, 2020.

[75] P. R. Buchanan, S. J. Tavener, S. J. Withy, and E. A. Harris, "Recovery of ventilation distributions by gas wash-out of a mechanical pump," *Clinical Physics and Physiological Measurement*, vol. 7, no. 3, pp. 237–252, 1986.

[76] D. J. Gavaghan and C. E. W. Hahn, "A tidal breathing model of the forced inspired inert gas sine wave technique," *Respiration Physiology*, vol. 106, no. 2, pp. 209–221, 1996.

[77] E. M. Williams, L. B. Gale, P. A. Oakley, M. C. Sainsbury, and C. E. W. Hahn, "Development of a concentric water-displacement model lung," *Journal of Biomedical Engineering*, vol. 15, no. 5, pp. 420–424, 1993.

[78] J. P. Whiteley, D. J. Gavaghan, and C. E. W. Hahn, "A tidal breathing

model of the inert gas sinewave technique for inhomogeneous lungs," *Respiration Physiology*, vol. 124, no. 1, pp. 65–83, 2000.

[79] C. F. D. Committee, *Guide: Guide for the Verification and Validation of Computational Fluid Dynamics Simulations (AIAA G-077-1998(2002))*, 1998.

[80] G. Qian, A. Mahdi, and Q. M. Jan, "Sensitivity analysis methods in the biomedical sciences," *Mathematical Biosciences*, p. 108306, 2020.

[81] Z. Zi, "Sensitivity analysis approaches applied to systems biology models," *IET Systems Biology*, vol. 5, no. 6, pp. 336–346, 2011.

[82] S. Marino, I. B. Hogue, C. J. Ray, and D. E. Kirschner, *A Methodology for Performing Global Ucertainty and Sensitivity Analysis in Systems Biology*, 2009, vol. 254, no. 1.

[83] M. D. Morris, "Factorial plans for preliminary computational experiments," *Technometrics*, vol. 33, no. 2, pp. 161–174, 1991.

[84] D. Garcia Sanchez, B. Lacarrière, M. Musy, and B. Bourges, "Application of sensitivity analysis in building energy simulations: Combining first- and second-order elementary effects methods," *Energy and Buildings*, vol. 68, no. PART C, pp. 741–750, 2014.

[85] L. Pronzalo and E. Walter, *Identification of parametric models from experimental data*, 1997.

[86] D.-Z. Du, P. M. Pardalos, and W. Wu, *History of Optimization*, 2008.

[87] C. Cosentino and D. Bates, *Feedback Control in Systems Biology*, 2019.

[88] A. Charnes, E. L. Frome, and P. L. Yu, "The equivalence of generalized least squares and maximum likelihood estimates in the exponential family," *Journal of the American Statistical Association*, vol. 71, no. 353, pp. 169–171, 1976.

[89] S. Amaran, N. V. Sahinidis, B. Sharda, and S. J. Bury, "Simulation optimization: a review of algorithms and applications," *Annals of Operations Research*, vol. 240, no. 1, pp. 351–380, 2016.

[90] J. Snoek, H. Larochelle, and R. P. Adams, "Practical Bayesian optimization of machine learning algorithms," in *Advances in neural information processing systems*, 2012, pp. 2951–2959.

[91] B. Shahriari, K. Swersky, Z. Wang, R. P. Adams, and N. D. Freitas, "Taking the human out of the loop: A review of bayesian optimization," pp. 148–175, 1 2016.

[92] C. E. Rasmussen and C. K. I. Williams, *Gaussian processes for machine learning.*, 2004, vol. 14, no. 2.

[93] C. E. Rasmussen, "Gaussian processes for machine learning," 2006.

[94] D. R. Jones, M. Schonlau, and W. J. Welch, "Efficient global optimization of expensive black-box functions," *Journal of Global optimization*, vol. 13, no. 4, pp. 455–492, 1998.

[95] A. D. Bull, "Convergence rates of efficient global optimization algorithms," *The Journal of Machine Learning Research*, vol. 12, pp. 2879–2904, 2011.

[96] V. Nguyen, S. Gupta, S. Rana, C. Li, and S. Venkatesh, "Regret for Expected Improvement over the Best-Observed Value and Stopping Condition," in *Proceedings of The 9th Asian Conference on Machine Learning (ACML)*, 2017, pp. 279–294.

[97] C. D. Harrison, "Methods for Determining Lung Function from Tracer Gas Concentrations," Ph.D. dissertation, University of Oxford, 2016.

[98] J. Mountain, "The Lognormal Lung : Quantifying Inhomogeneity of Ventilation," Ph.D. dissertation, University of Oxford, 2016.

[99] B. Lachmann, B. Robertson, and J. Vogel, "In Vivo Lung Lavage as an Experimental Model of the Respiratory Distress Syndrome," *Acta Anaesthesiologica Scandinavica*, vol. 24, no. 3, pp. 231–236, 1980.

[100] C. Kilkenny, W. J. Browne, I. C. Cuthill, M. Emerson, and D. G. Altman, "Improving bioscience research reporting: The arrive guidelines for reporting animal research," *Animals*, vol. 4, no. 1, pp. 35–44, 2013.

[101] D. C. Crockett, M. C. Tran, F. Formenti, J. N. J. J. Cronin, G. Hedenstierna, A. Larsson, P. A. P. Phan, and A. D. Farmery, "Validating the inspired sinewave technique to measure the volume of the 'baby lung' in a porcine lung-injury model," *British Journal of Anaesthesia*, vol. 124, no. September, pp. 1–9, 2020.

[102] W. Ganz and H. J. Swan, "Measurement of blood flow by thermodilution," *The American Journal of Cardiology*, vol. 29, no. 2, pp. 241–246, 1972.

[103] C. P. Criée, S. Sorichter, H. J. Smith, P. Kardos, R. Merget, D. Heise, D. Berdel, D. Köhler, H. Magnussen, W. Marek, H. Mitfessel, K. Rasche, M. Rolke, H. Worth, and R. A. Jörres, "Body plethysmography - Its principles and clinical use," *Respiratory Medicine*, vol. 105, no. 7, pp. 959–971, 2011.

[104] P. R. Burgel, J. L. Paillasseur, D. Caillaud, I. Tillie-Leblond, P. Chanez, R. Escamilla, I. Court-Fortune, T. Perez, P. Carré, and N. Roche, "Clinical COPD phenotypes: A novel approach using principal component and cluster analyses," *European Respiratory Journal*, vol. 36, no. 3, pp. 531–539, 2010.

[105] P. W. Jones, G. Harding, P. Berry, I. Wiklund, W. H. Chen, and N. Kline Leidy, "Development and first validation of the COPD Assessment Test," *European Respiratory Journal*, vol. 34, no. 3, pp. 648–654, 2009.

[106] C. F. Vogelmeier, G. J. Criner, F. J. Martinez, A. Anzueto, P. J. Barnes, J. Bourbeau, B. R. Celli, R. Chen, M. Decramer, L. M. Fabbri, P. Frith, D. M. Halpin, M. V. L. Varela, M. Nishimura, N. Roche, R. Rodriguez-Roisin, D. D. Sin, D. Singh, R. Stockley, J. Vestbo, J. A. Wedzicha, and A. Agustí, "Global strategy for the diagnosis, management, and prevention of chronic obstructive lung disease 2017 report," *American Journal of Respiratory and Critical Care Medicine*, vol. 195, no. 5, pp. 557–582, 2017.

[107] A. B. Baker and A. D. Farmery, "Inert gas transport in blood and tissues," *Comprehensive Physiology*, vol. 1, no. 2, pp. 569–592, 2011.

[108] A. D. Farmery, "Simulating hypoxia and modelling the airway," *Anaesthesia*, vol. 66, no. SUPPL. 2, pp. 11–18, 2011.

[109] A. Fedorov, R. Beichel, J. Kalpathy-Cramer, J. Finet, J. C. Fillion-Robin, S. Pujol, C. Bauer, D. Jennings, F. Fennessy, M. Sonka, J. Buatti, S. Aylward, J. V. Miller, S. Pieper, and R. Kikinis, "3D Slicer as an image computing platform for the Quantitative Imaging Network," *Magnetic Resonance Imaging*, vol. 30, no. 9, pp. 1323–1341, 2012.

[110] R. Konieczny and R. Idczak, "Mössbauer study of Fe-Re alloys prepared by mechanical alloying," *Hyperfine Interactions*, vol. 237, no. 1, pp. 1–8, 2016.

[111] T. Fawcett, "An introduction to ROC analysis," *Pattern Recognition Letters*, vol. 27, no. 8, pp. 861–874, 2006.

[112] J. M. Bland and D. G. Altman, "Agreement between methods of measurement with multiple observations per individual," *Journal of Biopharmaceutical Statistics*, vol. 17, no. 4, pp. 571–582, 2007.

[113] J. Wanger, J. L. Clausen, A. Coates, O. F. Pedersen, V. Brusasco, F. Burgos, R. Casaburi, R. Crapo, P. Enright, C. P. M. van der Grinten, P. Gustafsson, J. Hankinson, R. Jensen, D. C. Johnson, N. MacIntyre, R. McKay, M. R. Miller, D. Navajas, R. Pellegrino, and G. Veigi, "Standardisation of the measurement

of lung volumes," *European Respiratory Journal*, vol. 26, no. 3, pp. 511–522, 2005.

[114] R. H. Kallet, H. Zhuo, K. Ho, M. S. Lipnick, A. Gomez, and M. A. Matthay, "Lung injury etiology and other factors influencing the relationship between dead-space fraction and mortality in ARDS," *Respiratory Care*, vol. 62, no. 10, pp. 1241–1248, 2017.

[115] V. Nguyen, S. Gupta, S. Rana, C. Li, and S. Venkatesh, "Filtering Bayesian optimization approach in weakly specified search space," in *Knowledge and Information Systems*, vol. 60, no. 1, 2019, pp. 385–413.

[116] C. E. Rasmussen and H. Nickisch, "Gaussian processes for machine learning (GPML) toolbox," *The Journal of Machine Learning Research*, vol. 11, pp. 3011–3015, 2010.

[117] M. B. Christopher and C. M. Bishop, *Pattern Recognition and Machine Learning*. Springer-Verlag New York, 2016.

[118] D. R. Cox, "The regression analysis of binary sequences," *Journal of the Royal Statistical Society: Series B (Methodological)*, vol. 20, no. 2, pp. 215–232, 1958.

[119] V. Nguyen, T. D. Nguyen, T. Le, S. Venkatesh, and D. Phung, "One-Pass Logistic Regression for Label-Drift and Large-Scale Classification on Distributed Systems," *2016 IEEE 16th International Conference on Data Mining (ICDM)*, pp. 1113–1118, 2017.

[120] N. Breslow, "A generalized Kruskal-Wallis test for comparing k samples subject to unequal patterns of censorship," *Biometrika*, vol. 57, no. 3, pp. 579–594, 1970.

[121] S. R. Downie, C. M. Salome, S. Verbanck, B. Thompson, N. Berend, and G. G. King, "Ventilation heterogeneity is a major determinant of airway hyperresponsiveness in asthma, independent of airway inflammation," *Thorax*, vol. 62, no. 8, pp. 684–689, 2007.

[122] D. M. Mannino and A. S. Buist, "Global burden of COPD: risk factors, prevalence, and future trends," *Lancet*, vol. 370, no. 9589, pp. 765–773, 2007.

Appendix A: Published papers

Physiological Measurement

IPEM
Institute of Physics and Engineering in Medicine

PAPER • OPEN ACCESS

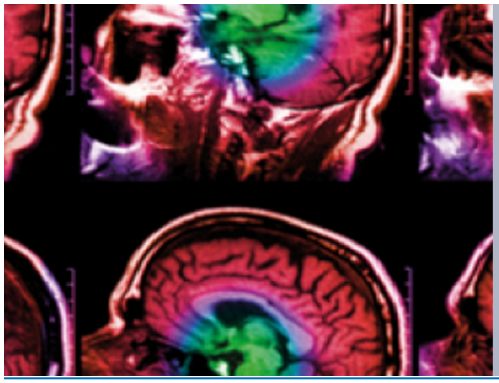
Lung heterogeneity and deadspace volume in animals with acute respiratory distress syndrome using the inspired sinewave test

To cite this article: Minh C Tran *et al* 2020 *Physiol. Meas.* **41** 115009

View the article online for updates and enhancements.

You may also like

- The Induced Surface Tension Contribution for the Equation of State of Neutron Stars
Violetta V. Sagun, Ilídio Lopes and Aleksei I. Ivanytskyi
- Neutron Stars: A Novel Equation of State with Induced Surface Tension
Violetta V. Sagun and Ilídio Lopes
- The IST spectral portraits of the first order doubly periodic solutions of the nonlinear Schrödinger equation
N Akhmediev and J M Soto-Crespo



IPEM | IOP
Series in Physics and Engineering in Medicine and Biology

Your publishing choice in medical physics, biomedical engineering and related subjects.

Start exploring the collection–download the first chapter of every title for free.

This content was downloaded from IP address 192.76.28.49 on 26/10/2021 at 22:50

IOP Publishing Physiol. Meas. 41 (2020) 115009 https://doi.org/10.1088/1361-6579/abc0b5

Physiological Measurement

IPEM Institute of Physics and Engineering in Medicine

CrossMark

OPEN ACCESS

RECEIVED
7 July 2020

REVISED
29 September 2020

ACCEPTED FOR PUBLICATION
13 October 2020

PUBLISHED
9 December 2020

Original Content from this work may be used under the terms of the Creative Commons Attribution 4.0 licence.

Any further distribution of this work must maintain attribution to the author(s) and the title of the work, journal citation and DOI.

PAPER

Lung heterogeneity and deadspace volume in animals with acute respiratory distress syndrome using the inspired sinewave test

Minh C Tran[1,2], Douglas C Crockett[1], Federico Formenti[3], Phi A Phan[1], Göran Hedenstierna[4], Anders Larsson[4], Stephen J Payne[2] and Andrew D Farmery[1]

[1] Nuffield Division of Anaesthetics, University of Oxford, Oxford, United Kingdom
[2] The Institute of Biomedical Engineering, University of Oxford, Oxford, United Kingdom
[3] Centre for Human and Applied Physiological Sciences, King' s College London, London, United Kingdom
[4] Hedenstierna Laboratory, Department of Medical Sciences, Uppsala University, Uppsala, Sweden

E-mail: minh.tran@chch.ox.ac.uk

Keywords: acute respiratory distress syndrome, ARDS, IST, lung simulation, lung heterogeneity

Abstract

Acute respiratory distress syndrome (ARDS) is associated with a high rate of morbidity and mortality, as patients undergoing mechanical ventilation are at risk of ventilator-induced lung injuries. *Objective*: To measure the lung heterogeneity and deadspace volume to find safer ventilator strategies. The ventilator settings could then offer homogeneous ventilation and theoretically equalize and reduce tidal strain/stress in the lung parenchyma. *Approach*: The inspired sinewave test (IST) is a non-invasive lung measurement tool which does not require cooperation from the patient. The IST can measure the effective lung volume, pulmonary blood flow and deadspace volume. We developed a computational simulation of the cardiopulmonary system to allow lung heterogeneity to be quantified using data solely derived from the IST. Then, the method to quantify lung heterogeneity using two IST tracer gas frequencies (180 and 60 s) was introduced and used in lung simulations and animal models. Thirteen anaesthetized pigs were studied with the IST both before and after experimental lung injury (saline-lavage ARDS model). The deadspace volume was compared between the IST and the SF_6 washout method. *Main results*: The IST could measure lung heterogeneity using two tracer gas frequencies. Furthermore, the value of IST ventilation heterogeneity in ARDS lungs was higher than in control lungs at a positive end-expiratory pressure of 10 cmH_2O (area under the curve $= 0.85$, $p < 0.001$). Values for the deadspace volume measured by the IST have a strong relationship with the measured values of SF_6 (9 ml bias and limits of agreement from −79 to 57 ml in control animals). *Significance*: The IST technique has the potential for use in the identification of ventilation and perfusion heterogeneity during ventilator support.

Abbreviations

ARDS	Acute respiratory distress syndrome
ELV	Effective lung volume measured by the IST (l)
$f_{p,i}$	Perfusion fraction to the lung compartment i
$f_{v,i}$	Ventilation fraction to the lung compartment i
Q_p	Blood flow measured by the IST (l min^{-1})
VT	Tidal volume (ml)
V_A	Alveolar lung volume (l)
VD_{IST}	Deadspace volume measured by the IST (ml)
VD_{SF_6}	Deadspace volume measured by the SF_6 (ml)
PEEP	Positive end-expiratory pressure
$\dot{V}$	Ventilation (l min^{-1})
$\dot{Q}$	Perfusion (l min^{-1})

© 2020 Institute of Physics and Engineering in Medicine

1. Introduction

Acute respiratory distress syndrome (ARDS) is characterized by pulmonary inflammation and carries significant morbidity and mortality (Summers *et al* 2016). The prognosis of ARDS has improved within the past decades, with in-hospital mortality rates decreasing from 90% in the 1970s to approximately 30% in a recent study (de Prost *et al* 2011). Guidelines for mechanical ventilation have probably contributed to this result by reducing ventilator-induced lung injury. The mainstay of ventilator treatment is a reduction in tidal volume (V_T) and inspiratory and driving pressures, thereby reducing the stress and strain applied to the lungs. But there is currently no conclusive way to determine optimal ventilation for an individual patient at the bedside.

In ARDS the lung is mechanically very heterogeneous, causing heterogeneous and harmful ventilation. However, if lung mechanics could be homogenized [such as by positive end-expiratory pressure (PEEP) titration and lung recruitment], the result could be more homogeneous, and thus less harmful, lung ventilation. Lung heterogeneity is the unequal distribution of airflow (ventilation) relative to the size of the lung regions to which it is distributed or to gas exchange to the bloodstream (perfusion) (West 2012). There are no simple methods that can be used at the bedside to evaluate lung heterogeneity or to quantify the effect of different manoeuvres and ventilator settings on lung homogeneity (Stahr *et al* 2016, Mountain *et al* 2018). The measurement of lung homogeneity could potentially benefit ventilated patients.

The inspired sinewave test (IST) was introduced as a non-invasive test which requires no cooperation from patients being tested and does not involve ionizing radiation. The IST applies a forced oscillation of a low dose of N_2O tracer gas with a sinusoidal period which can be determined by the user. The results of the IST provide lung function parameters including deadspace volume (VD), effective lung volume (ELV) and pulmonary blood flow (Q_p) (Phan *et al* 2017b, Crockett *et al* 2019, Bruce *et al* 2018, Hahn and Farmery 2003, Clifton *et al* 2013). The IST results, including VD and ELV, provide suggestions for optimizing the ventilator setting. Furthermore, it is proposed that by using two tracer gas frequencies, the IST can quantify the ventilatory heterogeneity of the lung. In a previous study, the IST in combination with data from another lung function test (plethysmography) was able to detect changes in ventilatory heterogeneity which occur normally with age in healthy participants (Bruce *et al* 2018). In other research in simulated patients, the IST showed the potential to identify that simulated patients had emphysema (ventilation heterogeneity) and pulmonary embolism (perfusion heterogeneity) (Tran *et al* 2020). There is thus the possibility of developing the IST such that lung heterogeneity could be determined solely from the IST data without recourse to other techniques.

We therefore developed a model to quantify the degree of lung heterogeneity using the IST. We then performed experiments in anaesthetized piglets using only the heterogeneity obtained using the IST. The experiments included measurements before and after the lung was damaged by following the saline lavage protocol (ARDS model). We also compared the absolute VD measured by the IST with that obtained by SF_6 washout.

2. Materials and methods

2.1. Measurement protocol

We developed a two-compartment lung simulation to provide a theoretical framework for understanding the ventilation and perfusion heterogeneity values measured by the IST. Then the IST was performed in animal models before (control) and after lung injury (ARDS). After that, the IST heterogeneity indices were calculated and compared with the PaO_2:FiO_2 ratio (or PFR; the ratio of partial pressure of oxygen in arterial blood and the fraction of inspired oxygena clinical indicator showing hypoxaemia). Additionally, VD measured by the IST was compared with the values measured by SF_6 washout.

Animals were anaesthetized and instrumented; table 1 summarizes baseline data. Thirteen pigs were mechanically ventilated (volume-control ventilation) at 20–25 breaths min^{-1}, with a V_T of 10 ml kg^{-1} and an inspiratory/expiratory ratio of 1:2 (Servo-I, Maquet, Rastatt, Germany). The right internal jugular vein was cannulated and a pulmonary artery catheter was inserted and used to measure pulmonary artery pressure continuously and cardiac output via thermodilution intermittently.

During the IST, N_2O tracer gas, added to the inspired air, was oscillated with periods of 60 and 180 s. PEEP levels were incrementally changed from 5 through 10, 15 and 20 cmH_2O. The PaO_2:FiO_2 ratio and paired measurements of VD by the IST and SF_6 washout test (VD_{IST} and VD_{SF6}) were recorded at each PEEP level. The SF_6 washout test is a technique for measuring lung volume and VD using SF_6 tracer gas (Larsson *et al* 1987). After measurements in the control group, lung injury was induced as described below, and the same measurements were repeated in the injured state.

Table 1. Animal baseline characteristics for $n = 13$ animals.

Parameters	Control	Injured	p
Weight (kg)	29 (2)	–	–
Heart rate (bpm)	86 (12)	85 (11)	0.42
CO (l min^{-1})	3.4 (0.8)	3.2 (0.4)	0.26
pH	7.38 (0.07)	7.25 (0.08)	0.0004
PaO_2 (mmHg)	144 (119–161)	96 (85–195)	0.39
FiO_2	0.4 (0.3–0.4)	0.8 (0.7–0.9)	0.0002
PFR	377 (304–513)	128 (101–248)	0.0002

Mean (SD) or median (95% confidence interval) for non-parametric data are shown. CO, cardiac output calculated by thermodilution; PaO_2, arterial O_2 partial pressure; FiO_2, fraction of inspired O_2; PFR, PaO_2:FiO_2 ratio.

2.2. Inspired sinewave test heterogeneity indices

In the IST analysis the VD inside the lung, VD_{IST}, was first measured using the modified Bohr method (Phan *et al* 2017a). Secondly, ELV and Q_p were calculated from a model assuming one well-mixed lung compartment (Bruce *et al* 2018).

Theory dictates that in a completely homogeneously ventilated and perfused lung, the values of ELV and Q_p recovered from the IST are independent of the tracer gas period used. The IST accuracies of ELV and Q_p values are published elsewhere (Bruce *et al* 2019, Crockett *et al* 2020). However, as the degree of heterogeneity increases, the ELV and Q_p values (based on the assumption of perfect homogeneity) begin to diverge from true values; moreover, those values recovered from periods of 60 s and 180 s also diverge from each other. Consequently, the ratio of these latter values provides an index of the degree of heterogeneity. The IST ventilatory and perfusion heterogeneity ratio of the lung are given by the following expressions:

$$\mathrm{IST}_{\text{Vent-Heterogeneity}} = \frac{\mathrm{ELV}_{180\ \mathrm{s}}}{\mathrm{ELV}_{60\ \mathrm{s}}} \tag{1}$$

$$\mathrm{IST}_{\text{Perf-Heterogeneity}} = \frac{Q_{p60\ \mathrm{s}}}{Q_{p180\ \mathrm{s}}} \tag{2}$$

where $\mathrm{ELV}_{180\ \mathrm{s}}/\mathrm{ELV}_{60\ \mathrm{s}}$ are the effective lung volumes measured by IST with tracer gas periods of 180 s or 60 s, and similarly for Q_p.

2.3. Lung heterogeneity simulation model

A heterogeneous lung was simulated by compartments, including three serial deadspace compartments (Harrison *et al* 2017), two alveolar compartments (tidal compartments) (Hahn and Farmery 2003, Whiteley *et al* 2003, Whiteley *et al* 2001) and five compartments to present the whole body (lung, viscera fast, viscera liver, lean and fat) (Baker and Farmery 2011). All compartments were linked together by conservation of mass equations. The significance of this simulation was as a suitable test for the IST and it also had clear settings in two tidal lung compartments to quantify lung heterogeneity. The simulated patient weighs 70 kg, with a lung volume of 2.5 l and pulmonary blood flow of 5.0 l min^{-1}.

The volume fractions of the two tidal lung compartments were fixed at 0.1 and 0.9. Ventilation and perfusion fractions to the first lung compartment (0.1 fraction of volume) were changed to f_v and f_p. The ventilation and perfusion fractions to the second compartment (0.9 fraction of volume) were calculated by $1 - f_v$ and $1 - f_p$.

Due to the model setting, the lung was homogeneous when $f_{v1} = 0.1$ and $f_{p1} = 0.1$. An increase in value of f_{v1} caused the mismatch of the ventilation and higher lung ventilation heterogeneity. Similarly, when f_{p1} increased, the lung perfusion heterogeneity also increased. A schematic diagram of the lung simulation is presented in figure 1. The full process of model development and the modelling parameters are described in Appendix A.

2.4. Ethical approval

This study adhered to the *in vivo* experiments (ARRIVE) guidelines (Kilkenny *et al* 2013). In the Hedenstierna Laboratory, Uppsala University, Sweden, 13 pigs were studied under the auspices of the regional animal welfare and ethics committee (ref. C98/16).

2.5. Lung injury

Lung injury replicated the ARDS conditions in the animal model. Lachmann' s method was applied to induce lung injury (Lachmann *et al* 1980). The ventilator was disconnected and 0.9% saline solution (at

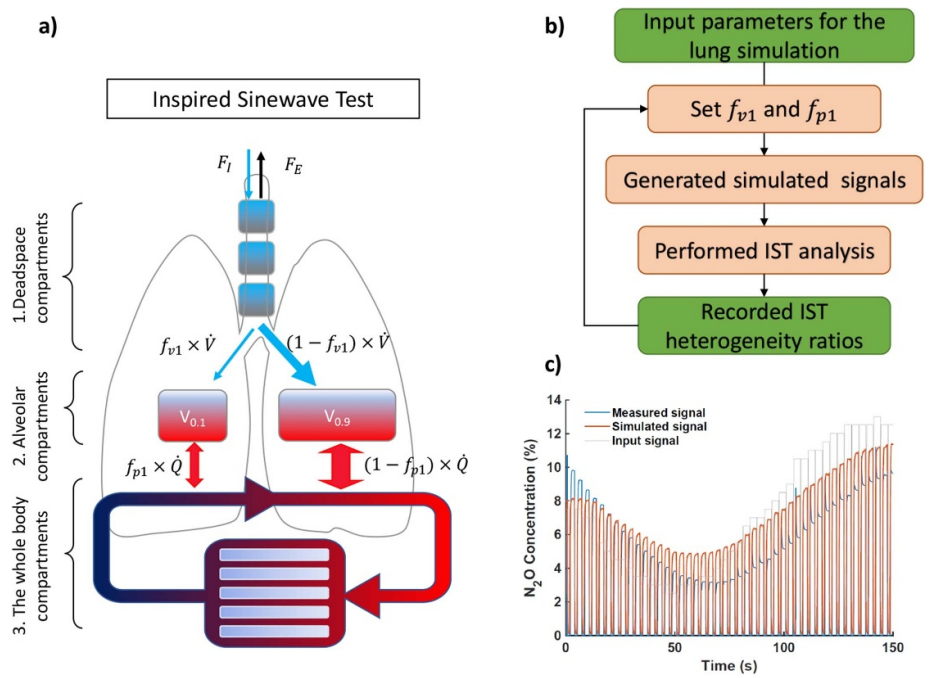


Figure 1. Panel (a) shows a schematic diagram of the two-compartment tidal lung simulation. The fraction of lung volume is set at 0.1 and 0.9. The ventilation heterogeneity is controlled by parameter f_{v1} and the perfusion heterogeneity is f_{p1}. Panel (b) shows a flow diagram for the experiment on IST heterogeneity ratios using the lung simulation. Panel (c) shows the example of the IST-measured and simulated exhaled (F_E) signals in response to the 180 s period input tracer gas (F_I) at a PEEP of 10 cmH_2O.

37 °C) was instilled into the lungs via the endotracheal tube. The saline was drained out of the lungs after 30 s. The protocol was repeated until PaO_2:FiO_2 was less than 300 mmHg.

2.6. Statistical analysis

We used the Student's *t*-test to compare two parametric data groups and the Wilcoxon signed-rank test for non-parametric data. We then analysed the area under the receiver operating characteristic (ROC) curve (AuC) to show the degree or measure of separability between control and injured animals (Fawcett 2006). The linear regression and Bland–Altman plots were used to analyse the relationship between paired measurements from the IST versus the SF_6 results (Bland and Altman 2007). Lung simulations were developed and validated in Matlab (MathWorks, USA; www.mathworks.com). Statistical tests were performed in Graphpad Prism v.8.1.2 (GraphPad Software, USA; www.graphpad.com).

3. Results

The ability to measure lung heterogeneity in the IST was assessed using the simulated heterogeneous lungs (figure 2). The difference between control and ARDS lungs in the IST ventilation and perfusion heterogeneity ratios was analysed by statistical tests (figure 4). Six of the 13 animals had measurements at PEEP 15 and 20 cmH_2O. Additionally, a total of $n = 72$ paired VD measurements in 13 pigs at four different PEEP levels were analysed. Statistical analyses revealed that VD_{IST} and VD_{SF6} was not different in both control and ARDS lungs.

3.1. IST lung heterogeneity values in simulated data

Figure 2 shows the IST results in the simulated heterogeneous lungs. Theoretically, in a homogeneous or healthy lung the IST results do not depend on any sinewave period. As the heterogeneity value increases, the ELV and Q_p values for the 60 s and 180 s sinewave periods start to diverge (figure 2(a)). Tracking the degree of divergence could provide the index of lung heterogeneity in panel (b).

When the ventilatory fraction assigned to compartment 1 (which comprises 10% of the lung volume) is 0.1 ($f_{v1} = 0.1$), the lung is assumed to be entirely homogeneous. Thus, ELV values at both 60 s and 180 s were recorded at approximately 2.46 l (98% similar to the set value of 2.5 l) in figure 2(a). When f_{v1} increased from 0.1 to 0.9, the heterogeneity of the lung was progressively increased. As a result, ELV values declined in both frequencies (panel a) and, moreover, the decrease in ELV at 60 s was greater than at 180 s. This divergence, represented as a ratio of $IST_{Vent\text{-}Heterogeneity}$, is shown in panel (b).

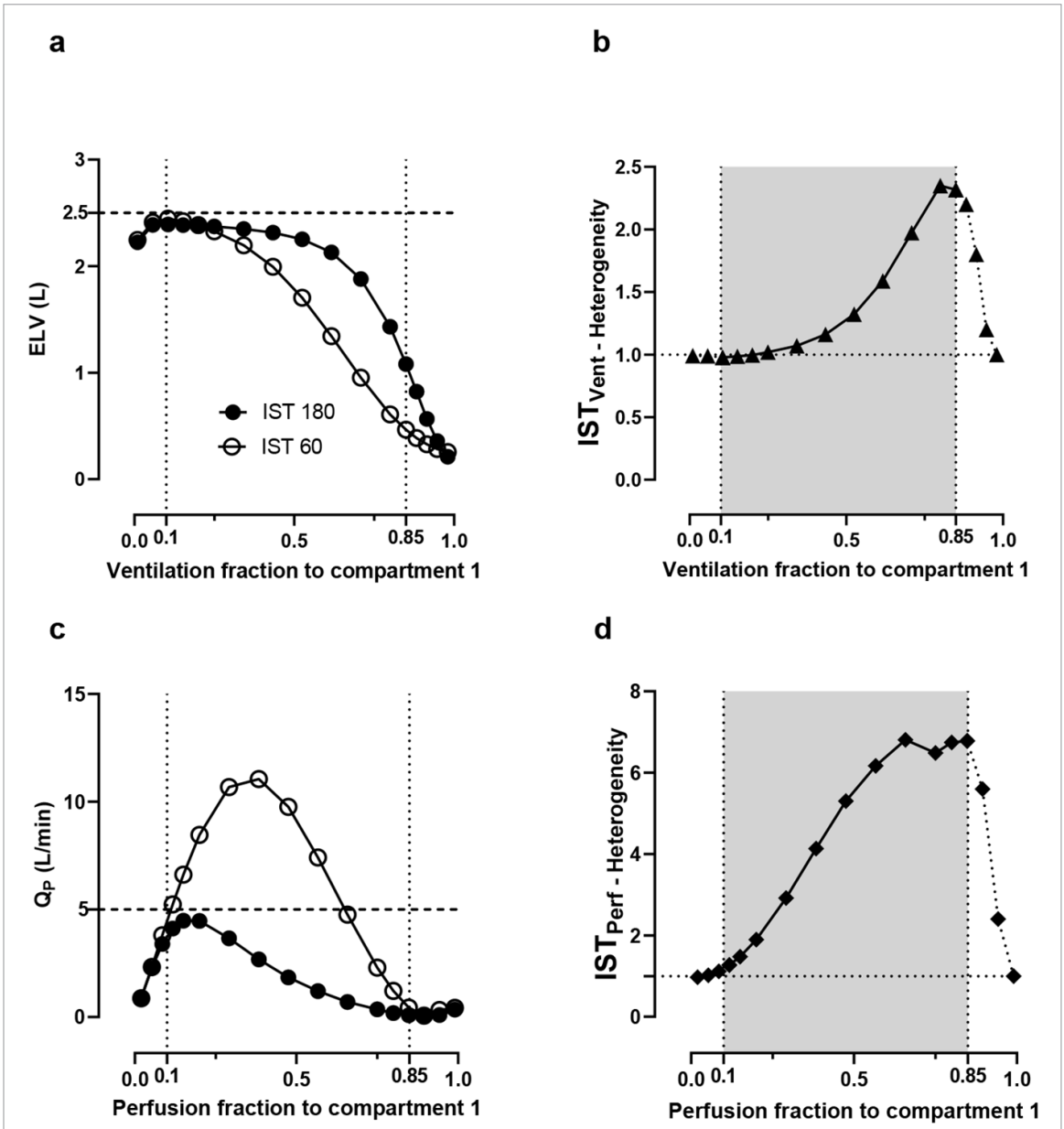


Figure 2. The divergences of the IST recovered values and IST heterogeneity indices in simulated heterogeneous lungs. Panels (a) and (b) show the IST values for different variations in ventilation heterogeneity and panels (c) and (d) show the changes in perfusion heterogeneity. The lung is assumed to be homogeneous when the ventilation fraction to compartment 1 (x-axis) is 0.1 ($f_{v1} = 0.1$, the first vertical dotted lines). Each point on the x-axis presents one lung condition with the heterogeneity increased from 0 to 1. In panels (b) and (d), the simulation would break down beyond the grey regions.

Values outside the grey region (0.1–0.85) introduce more complexity to the model so were not included. When ventilation heterogeneity increases to such a level that 100% of ventilation is delivered to compartment 1, then ventilation would by definition return to being fully homogeneous, albeit very maldistributed (the lung just becomes a single, small compartment). Similar to the ventilation, when the perfusion fraction to compartment 1 is 0.1 ($f_{p1} = 0.1$, perfect perfusion homogeneity), the ratio of these values predicts the degree of perfusion heterogeneity ($IST_{Perf\text{-}Heterogeneity}$ in panel (d)). A healthy lung should have heterogeneity ratios of about 1. The homogeneity of the lung will become worse the further away the ratios are from 1.

3.2. IST heterogeneity indices: a comparison between control and injured animals

Figure 3 shows the relationship between the IST heterogeneity indices and the PaO_2:FiO_2 ratio. This ratio is used clinically as a broad indicator of dysfunction of gas exchange (Rice *et al* 2007, Ferguson *et al* 2012). PaO_2:FiO_2 <300 mmHg indicates significant impairment of gas exchange (Rice *et al* 2007). Figures 3(a) and (b) compare the IST heterogeneity values between animals with PaO_2:FiO_2 <300 mmHg and >300 mmHg. The PEEP values used are not specifically controlled in this comparison. In panel (a) there is a significant

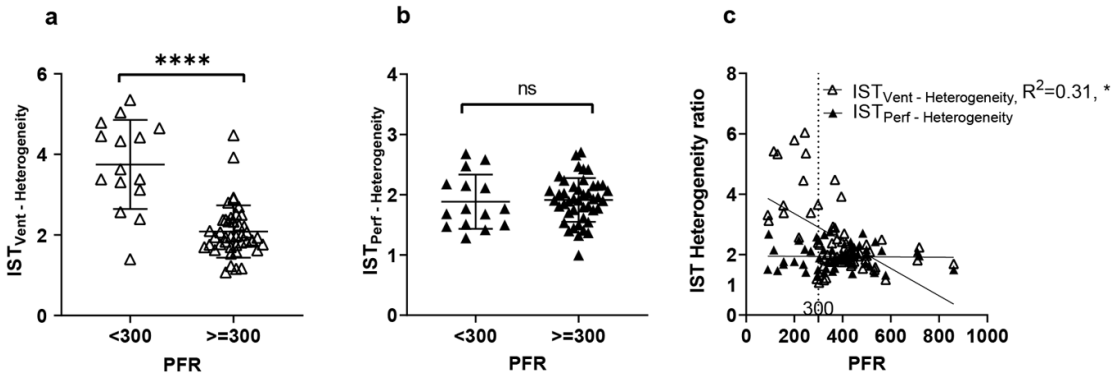


Figure 3. Validation of the IST heterogeneity ratios. Panels (a) and (b) show comparisons of IST heterogeneity indices with the PaO_2:FiO_2 ratio (PFR). A Student's *t*-test comparison of the IST heterogeneity indices between two groups (PFR <300 mmHg and PFR >300 mmHg) was performed. Panel (c) shows the linear relationship between IST heterogeneity indices and PFR. **** $p < 0.0001$; ns, non-significant.

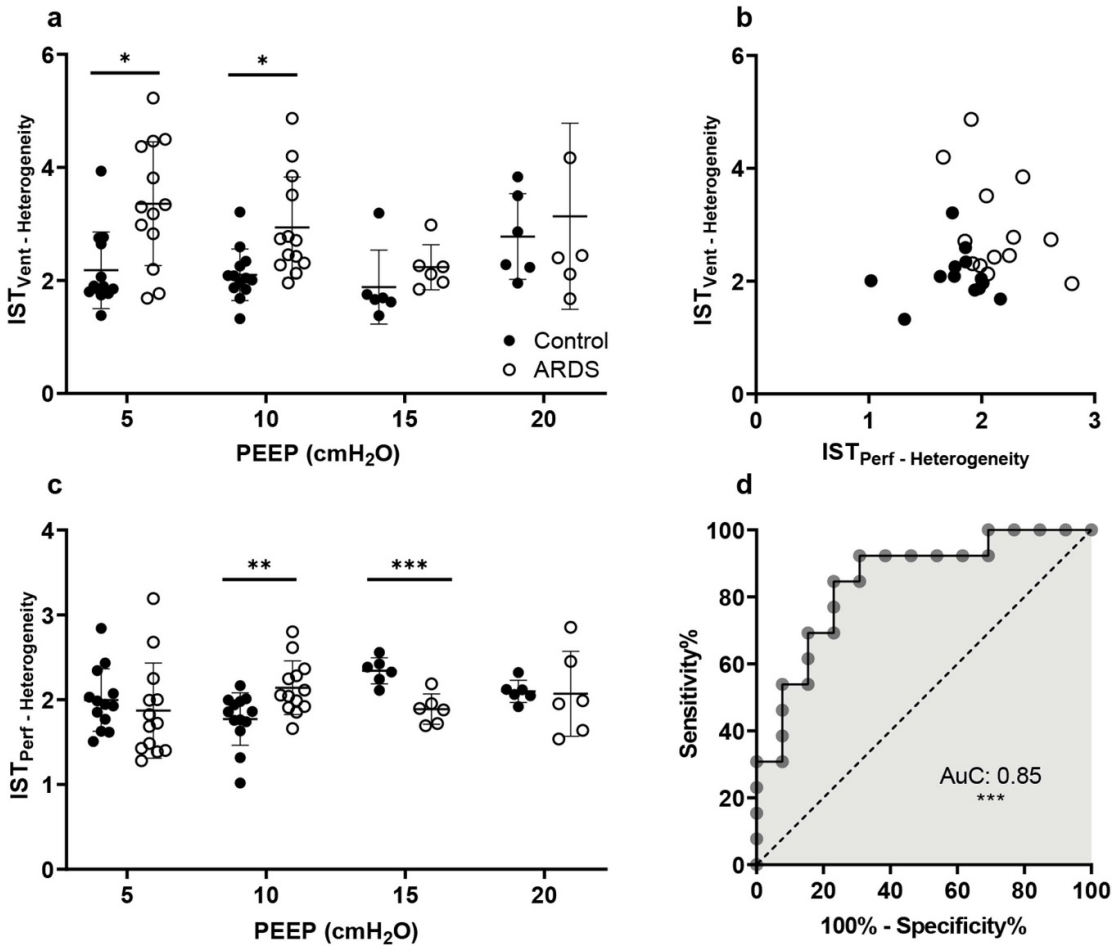


Figure 4. IST heterogeneity ratios in control and ARDS animals at different PEEP levels. Panel (a) shows IST ventilatory heterogeneity and panel (c) shows perfusion heterogeneity. A scatter plot in panel (b) shows the IST ventilation against perfusion heterogeneity indices at a PEEP of 10 cmH_2O. Panel (d) is the receiver operating characteristic curve between ARDS and control at a PEEP level of 10 cmH_2O (AuC, area under the curve). Student's *t*-tests were performed. *** $p < 0.001$, ** $p < 0.01$ and * $p < 0.05$.

difference in the IST ventilatory heterogeneity value between PFR <300 mmHg and PFR ≥300 mmHg (mean value of 3.9 versus 2.1, $p < 0.0001$). Panel (c) shows a linear regression analysis of the IST heterogeneity ratios versus the PFR. There is a linear relationship of the PFR with the IST ventilation heterogeneity ratio ($R^2 = 0.31, p < 0.05$) but not with the IST perfusion ratio.

The IST heterogeneity indices in control and injured groups at different levels of applied PEEP are shown in figures 4(a) and (c). At low PEEP levels (5 and 10 cmH_2O) the mean heterogeneity indices in the injured

lungs were higher than in controls (3.4 versus 2.2 at a PEEP of 5 cmH_2O, and 2.9 versus 2.1 at a PEEP of 10 cmH_2O, $p < 0.05$ for both). The injured group at low PEEP also shows a greater scatter of IST heterogeneity values. The application of PEEP from 5 through 15 cmH_2O reduced mean heterogeneity within the injured group and also reduced data scatter, indicating a stabilizing effect of PEEP. In figure 4(c), the IST perfusion heterogeneity ratio shows significant differences at PEEP = 10 cmH_2O ($p < 0.05$) and 15 cmH_2O ($p < 0.001$). In panel (b), a clear scatter plot shows the significant difference between control and injured animals at PEEP =
10 cmH_2O. Control animals have IST heterogeneity values of less than 2.1 and the values for the injured animals are higher.

Additionally, the ROC curve was used to classify control versus ARDS animals at a PEEP of 10 cmH_2O. The AuC was 0.85 ($p < 0.001$) with a 95% confidence interval from 0.69 to 0.99.

3.3. Deadspace volume: a comparison of IST with SF_6

Figure 5 shows the relationship and correlation between VD measured by the IST and the SF_6 test. In general, VD increased when the PEEP was raised, and the ARDS group had larger VDs than controls (panels (a) and (b)). SF_6 measurements showed smaller variations than IST ones. There was a robust relationship between VD_{IST} and VD_{SF6}: the linear regression slope was 0.87 with $R^2 = 0.5$ in the control group (panel (c)). The volume bias was 9 ml (limits of agreement −79 to 57 ml) in controls and similarly 10 ml (limits of agreement −51 to 32 ml) in ARDS lungs (figures 5(e) and (f)).

4. Discussion

This research shows the ability of the IST to measure lung heterogeneity and absolute VD in uninjured lungs and the ARDS model of lung injury compared with the 'gold standard' SF_6 washout technique. The IST heterogeneity indices have the potential to identify ARDS from control subjects with reasonable diagnostic accuracy; the AuC being 0.85 ($p < 0.001$) at a PEEP of 10 cmH_2O. Additionally, VD measured by the IST had a small bias (10 ml) compared with values measured by the SF_6 technique.

A previous study of lung heterogeneity in human patients measured by the IST did not achieve any significant results because of the wide variability in the severity of conditions in the study population. Our research in animals, in which we were able to standardize and control the degree of lung injury more reliably, proved more insightful. Bruce *et al* showed that ventilation heterogeneity could be determined using the IST values in combination with plethysmography results (Bruce *et al* 2018). However, in this study, for the first time, we used only the IST to measure the heterogeneity of the lung without the need for plethysmography. We implemented a simulation model and used it to understand the IST heterogeneity indices and their boundaries. Healthy simulated lung should have an IST heterogeneity ratio of 1, although healthy human subjects would not quite achieve this.

The IST has shown potential strengths, including working as a bedside monitor and diagnostic tool. Firstly, it can be used with spontaneously ventilating subjects. In this research, mechanically ventilated animals were investigated. Further study in ventilated patients could improve development of the IST. The IST also can measure the size of a 'baby lung' (equivalent to a small well-ventilated compartment) and results compare well with SF_6 and CT scan data in ventilated animals (Crockett *et al* 2020). We show that the heterogeneity of the lung changes with applied PEEP; this is of potential interest to the bedside clinician seeking to optimize ventilator settings. Secondly, at the appropriate ventilator setting significant differences between control and ARDS conditions were distinguishable (AuC = 0.85). The results of this study could pave the way for study of disease classification at the bedside using lung heterogeneity. Patients could benefit as a result of better-informed ventilation settings and the reduction of ventilator-induced lung injury (Nieman *et al* 2017, Brochard *et al* 2017).

In addition, this study reveals the ability of the IST to measure the absolute VD; it compares well with the SF_6 wash-in–washout method. The correlation between the two methods had a slope of 0.87 ($R^2 = 0.5$) and the limits of agreements were from −51 ml to 32 ml in control lungs. Clinically, deadspace volume has a strong association with mortality risk in patients with ARDS, wherein the risk of death increased by 22% for every 0.05 increase in VD:V_T (Kallet *et al* 2017).

We implemented a lung simulation to show how lung heterogeneity can be captured by the IST. However, the simulation and our work contain limitations. A lung simulation with two alveolar compartments may not be enough to represent the complexity of real-life lung heterogeneity. In figure 2, the heterogeneity index is only valid between certain limits of ventilatory misdistribution (within the grey zone) Outside this region, the simulations break down as described above (in the results, section 3). Of note, whereas in the simulation perfect homogeneity gives a heterogeneity index of 1, healthy subjects do not achieve this value (it being closer to 2). This is not surprising given that even in healthy people ventilation is not perfectly uniformly

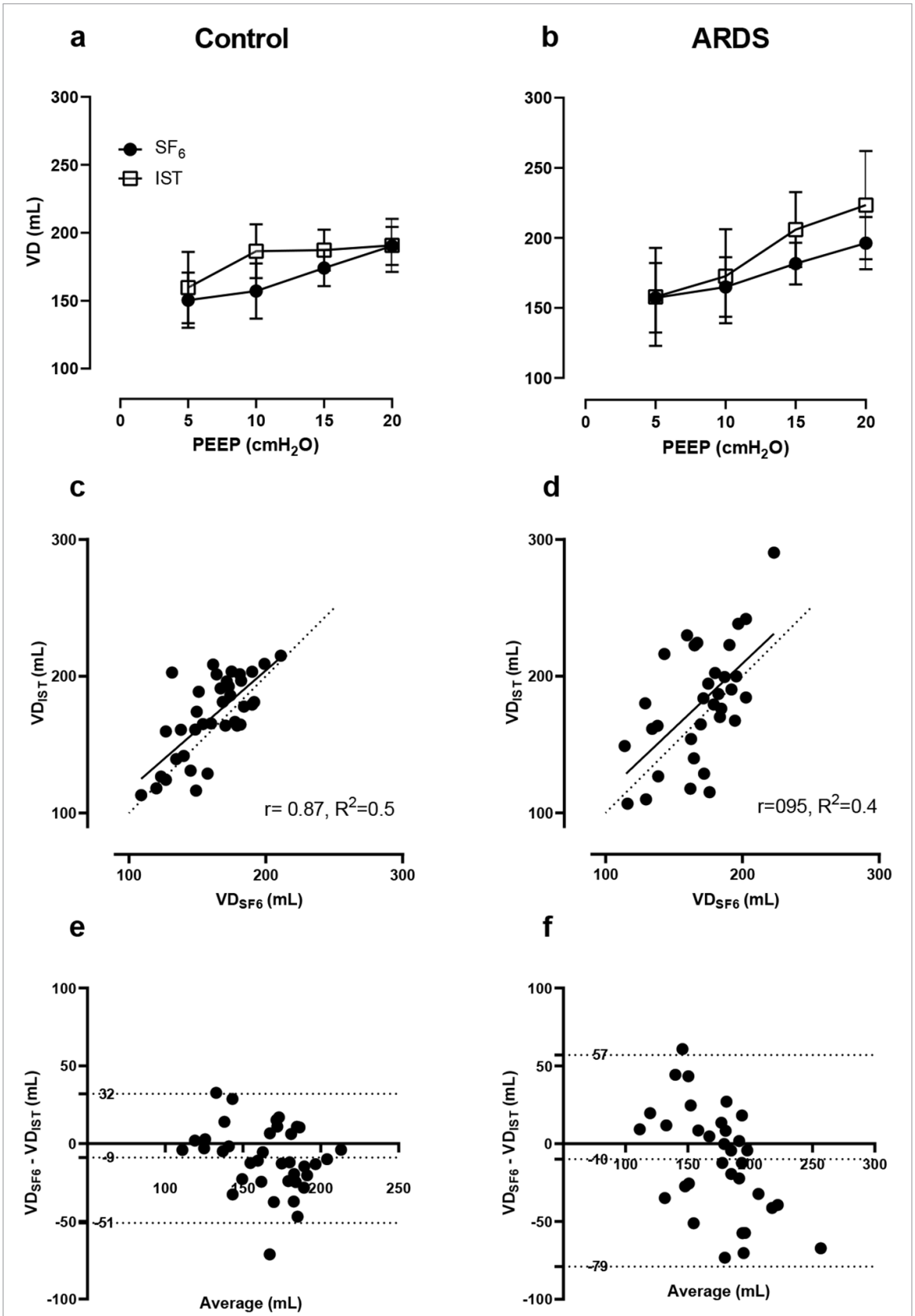


Figure 5. Comparison of VD between the IST and the SF_6 washout test. Panels (a) and (b) show paired VD_{IST} and VD_{SF6} measurements in control (pre-injury) and ARDS lungs (post-injury). Panels (c) and (d) show linear regressions of absolute VD measured by the IST and SF_6 test. The continuous lines are regression lines and dashed lines are the reference lines. Panels (e) and (f) show Bland–Altman plots: the bias lines are the central horizontal dotted lines and the top and bottom dotted lines are the limits of agreement.

distributed. A better simulation including the effects of hypoxic pulmonary vasoconstriction could be developed in the future (Whiteley *et al* 2003, Alford *et al* 2010). Furthermore, only six animals were studied at PEEP 15 and 20 cmH_2O because, in two cases, the pigs were too unstable to tolerate such high levels of PEEP and these experiments were undertaken in parallel with the collection of data for other studies. Further research could explore IST heterogeneity indices at higher PEEP levels.

The IST is a potentially translatable research tool. This research examined the utility of the IST in measuring lung heterogeneity and VD in ventilated lungs at the bedside. Accurate measurement of VD could help in the prognostication of acute lung injury/ARDS. Furthermore, measurement of the heterogeneity of the lung might be used to quantify the extent of lung injury and inform ventilatory therapy. Our results support further development of these IST heterogeneity indices and their translation to classify lung diseases.

5. Conclusion

A quantitative method for measuring lung heterogeneity was introduced and explored in animal models. The IST ventilation and perfusion heterogeneity ratios have the potential to inform and optimize mechanical ventilation strategy at the bedside in real time. This work provides a fundamental foundation for the study of lung heterogeneity in clinical trials. The IST can also measure VD with small bias compared with the values measured by the SF_6 technique. Further research is required to determine how the IST could be used to inform mechanical ventilation.

Acknowledgment

The authors are grateful for the important contribution from veterinary anaesthetists Christian Dancker and William McFadzean, and for the technical assistance by Hanne McPeak and Kristina Britchford.

Funding

This project was funded by the National Institute for Health Research, grant number II-LA-0214-20 005.

Appendix A

The lung simulation consisted of three space compartments, two tidal lung compartments and five body compartments with a shunt block. In the two tidal lung compartments, the fraction of lung volume was fixed at 0.1 and 0.9. Parameters for the lung simulation are summarized in table A1. This lung simulation has been described and validated elsewhere (Tran *et al* 2020).

The ode45 solver and Simulink Matlab were chosen for simulation. Ten mixing compartments of deadspace are included in this model. The equation for each deadspace compartment during inspiration is

$$V_{M,i}\frac{dF_{M,i}}{dt} = \dot{V}_A(t)(F_{M,i-1}(t) - F_{M,i}(t)) \tag{A1}$$

where i is the number of deadspace compartments (from 1 to 10) and $F_{(M,1)}(t) = F_I(t)$ and $F_{M,10}(t) = F_{IA}(t)$. $V_{M,i}$ is the VD of compartment i and $\dot{V}_A(t)$ is the ventilation at time t. The equivalent equation during expiration is

$$V_{M,i}\frac{dF_{M,i}}{dt} = \dot{V}_A(t)(F_{M,i}(t) - F_{M,i+1}(t)) \tag{A2}$$

where i is from 1 to 10 and $F_{M,1}(t) = F_E(t)$ and $F_{M,10}(t) = F_A(t)$. F_I, F_{IA} and F_E are the fractional concentrations of the tracer gas coming into the deadspace compartment, coming out from the deadspace compartment to the lung compartment and exhaled from the deadspace to the environment, respectively.

The deadspace compartments are serially connected with two parallel lung blocks. These lung blocks are generated from physiological equations of the tidal lung (Hahn and Farmery 2003) as follows. Inspiration:

$$V_A(t) = f_{\text{Volume}} \times \bar{V}_A + \frac{V_T \times t}{t_i}. \tag{A3}$$

Table A1. Simulation parameters for the tidal lung simulation. f_v is the ventilation fraction to the first lung compartment and f_q is the perfusion fraction to the first compartment.

Parameter	Value
Deadspace volume (VD) (ml)	150
Alveolar volume (l)	2.5
Pulmonary blood flow (l min^{-1})	5
Shunt (l min^{-1})	0
Tidal volume (l)	0.5
Ventilation fraction	$[f_v, 1-f_v]$
Alveolar volume fraction	[0.1, 0.9]
Perfusion fraction	$[f_q, 1-f_q]$
IST forced time period (s)	180 s and 60 s
Respiration rate (breaths min^{-1})	12
Inspiration time (s)	1.5

Expiration:

$$V_A(t) = f_{\text{Volume}} \times \bar{V}_A + V_T \times \exp(-\gamma(t - t_i)) \tag{A4}$$

where γ is the rate constant of expiratory flow, $V_A(t)$ is the alveolar volume, V_T is the tidal volume and t_i is the inspiration starting time. $\bar{V}_A$ is end-expired alveolar volume. In the first compartment $f_{\text{Volume}} = 0.1$ and in the second compartment $f_{\text{Volume}} = 0.9$.

All the compartments are linked together by governing equations which represent the equilibrium of the mass concentration of the tracer gas. $C_{\bar{v}}$ and C_a are the mixed venous and pulmonary end-capillary gas concentrations, respectively. In the first lung compartment inspiration is

$$\frac{d}{dt}(V_A(t)F_A(t)) = f_v \dot{V}_{A,i}(t)F_{IA}(t) + f_p \dot{Q}_{p,i}(C_{\bar{v}} - C_a) \tag{A5}$$

and expiration

$$\frac{d}{dt}(V_A(t)F_A(t)) = f_v \dot{V}_{A,i}(t)F_A(t) + f_p \dot{Q}_{p,i}(C_{\bar{v}} - C_a). \tag{A6}$$

Each compartment has its own fraction of ventilation f_v and fraction of perfusion f_p (table A1). The body compartments of a standard human consist of five different tissues inside the human body with different tissue gas coefficients (Hahn *et al* 1993, Baker and Farmery 2011):

$$V_i^* \frac{dC_i(t)}{dt} = \dot{Q}_i(C_{\bar{a}}(t) - C_i(t)) \tag{A7}$$

where V_i^*, C_i and $\dot{Q}_i$ are the equivalent blood volume, concentration of the tracer gas and blood flow rate of i compartment. V_i is given by the following equation, where $V_{(b,i)}$ and $V_{(t,i)}$ are the blood and tissue volumes of each body compartments and $\lambda_{(t,i)}$ is the Ostwald tissue gas coefficient of each compartment (these values are given in Farmery (2008)):

$$V_i^* = V_{b,i} + \frac{\lambda_{t,i}}{\lambda} V_{t,i}. \tag{A8}$$

The Ostwald coefficient is the relation between the concentrations of the tracer gas in the blood to the fractional concentration in the lung. λ is the blood-gas partition coefficient. The body temperature is assumed to be constant (37° C), so the Ostwald coefficient is stable:

$$C_a = \lambda \times F_A. \tag{A9}$$

Since, $\dot{Q}_T = \dot{Q}_S + \dot{Q}_P$. The mixed arterial concentration $C_{\bar{a}}$ is given below with $\dot{Q}_S$ being the shunt flow rate, $\dot{Q}_P$ the pulmonary blood flow rate and $\dot{Q}_T$ the total blood flow:

$$C_{\bar{a}}(t) = \frac{\dot{Q}_S}{\dot{Q}_T} C_{\bar{v}}(t) + \frac{\dot{Q}_p}{\dot{Q}_T} C_a(t). \tag{A10}$$

ORCID iDs

Minh C Tran https://orcid.org/0000-0003-2622-1365
Douglas C Crockett https://orcid.org/0000-0003-0330-3026
Phi A Phan https://orcid.org/0000-0003-4831-2743

References

Alford S K, Van Beek E J R, McLennan G and Hoffman E A 2010 Heterogeneity of pulmonary perfusion as a mechanistic image-based phenotype in emphysema susceptible smokers *Proc. Natl Acad. Sci. USA* **107** 7485–90
Baker A B and Farmery A D 2011 Inert gas transport in blood and tissues *Compr. Physiol.* **1** 569–92
Bland J M and Altman D G 2007 Agreement between methods of measurement with multiple observations per individual *J. Biopharm. Stat.* **17** 571–82
Brochard L, Slutsky A and Pesenti A 2017 Mechanical ventilation to minimize progression of lung injury in acute respiratory failure *Am. J. Respir. Crit. Care Med.* **195** 438–42
Bruce R M, Crockett D C, Morgan A, Tran M C, Formenti F, Phan P A and Farmery A D 2019 Noninvasive cardiac output monitoring in a porcine model using the inspired sinewave technique: a proof-of-concept study *Br. J. Anaesth.* **123** 126–34
Bruce R M, Phan P A, Pacpaco E, Rahman N M and Farmery A D 2018 The inspired sine-wave technique: a novel method to measure lung volume and ventilatory heterogeneity *Exp. Physiol.* **103** 738–47
Clifton L, Clifton D A, Hahn C E W and Farmery A D 2013 Assessment of lung function using a non-invasive oscillating gas-forcing technique *Respir. Physiol. Neurobiol.* **189** 174–82
Crockett D C, Cronin J N, Bommakanti N, Chen R, Hahn C E W, Hedenstierna G, Larsson A, Farmery A D and Formenti F 2019 Tidal changes in PaO2 and their relationship to cyclical lung recruitment/derecruitment in a porcine lung injury model *Br. J. Anaesth.* **122** 277–85
Crockett D C, Tran M C, Formenti F, Cronin J N, Hedenstierna G, Larsson A, Phan P A and Farmery A D 2020 Validating the inspired sinewave technique to measure the volume of the 'baby lung' in a porcine lung-injury model *Br. J. Anaesth.* **124** 345–53
de Prost N, Ricard J-D, Saumon G and Dreyfuss D 2011 Ventilator-induced lung injury: historical perspectives and clinical implications *Ann. Intensive Care* **1** 28
Farmery A D 2008 Interrogation of the cardiopulmonary system with inspired gas tension sinusoids *PhD Thesis* King's College London. Guy's and St Thomas's School of Medicine
Fawcett T 2006 An introduction to ROC analysis *Pattern Recognit. Lett.* **27** 861–74
Ferguson N D *et al* 2012 The Berlin definition of ARDS: an expanded rationale, justification and supplementary material *Intensive Care Med.* **38** 1573–82
Hahn C E W and Farmery A D 2003 Gas exchange modelling: no more gills, please *Br. J. Anaesth.* **91** 2–15
Hahn C E, Black A M, Barton S A and Scott I 1993 Gas exchange in a three-compartment lung model analyzed by forcing sinusoids of N_2O *J. Appl. Physiol.* **75** 1863–76
Harrison C D, Phan P A, Zhang C, Geer D, Farmery A D and Payne S J 2017 Modelling mixing within the dead space of the lung improves predictions of functional residual capacity *Respir. Physiol. Neurobiol.* **242** 12–18
Kallet R H, Zhuo H, Kelly H, Lipnick M S, Gomez A and Matthay M A 2017 Lung injury etiology and other factors influencing the relationship between dead-space fraction and mortality in ARDS *Respir. Care* **62** 1241–8
Kilkenny C, Browne W J, Cuthill I C, Emerson M and Altman D G 2013 Improving bioscience research reporting: the arrive guidelines for reporting animal research *Animals* **4** 35–44
Lachmann B, Robertson B and Vogel J 1980 In vivo lung lavage as an experimental model of the respiratory distress syndrome *Acta Anaesthesiol. Scand.* **24** 231–6
Larsson A, Linnarsson D, Jonmarker C, Jonson B, Larsson H and Werner O 1987 Measurement of lung volume by sulfur hexafluoride washout during spontaneous and controlled ventilation: further development of a method *Anesthesiology* **67** 543–50
Mountain J E *et al* 2018 Potential for non-invasive assessment of lung inhomogeneity using highly precise, highly time-resolved, measurements of gas exchange *J. Appl. Physiol.* **124** 615–31
Nieman G F, Satalin J, Andrews P, Aiash H, Habashi N M and Gatto L A 2017 Personalizing mechanical ventilation according to physiologic parameters to stabilize alveoli and minimize ventilator induced lung injury (VILI) *Intensive Care Med. Exp.* **5** 1–21
Phan P A, Hahn C E W and Farmery A D 2017a A modification of the Bohr method to determine airways deadspace for non-uniform inspired gas tensions *Physiol. Meas.* **38** 107–17
Phan P A, Zhang C, Geer D, Formenti F, Hahn C and Farmery A 2017b The inspired sinewave technique: a comparison study with body plethysmography in healthy volunteers *IEEE J. Transl. Eng. Health Med.* **5** 1–9
Rice T W, Wheeler A P, Bernard G R, Hayden D L, Schoenfeld D A and Ware L B 2007 Comparison of the SpO2/FIO2 ratio and the PaO2/FIO2 ratio in patients with acute lung injury or ARDS *Chest* **132** 410–17
Stahr C S *et al* 2016 Quantification of heterogeneity in lung disease with image-based pulmonary function testing *Sci. Rep.* **6** 1–10
Summers C, Singh N R, Worpole L, Simmonds R, Babar J, Condliffe A M, Gunning K E, Johnston A J and Chilvers E R 2016 Incidence and recognition of acute respiratory distress syndrome in a UK intensive care unit *Thorax* **71** 1050–1
Tran M C, Crockett D C, Phan P A, Payne S J and Farmery A D 2020 A tidal lung simulation to quantify lung heterogeneity with the inspired sinewave test *42nd Annual Int. Conf. of the IEEE Engineering in Medicine and Biology Society (EMBC 2020)* pp 13–16
West J B 2012 *Respiratory Physiology–the Essentials* 9th edn (London: Lippincott Williams and Wilkins)
Whiteley J P, Farmery A D, Gavaghan D J and Hahn C E W 2003 A tidal ventilation model for oxygenation in respiratory failure *Respir. Physiol. Neurobiol.* **136** 77–88
Whiteley J P, Gavaghan D J and Hahn C E W 2001 Modelling inert gas exchange in tissue and mixed-venous blood return to the lungs *J. Theor. Biol.* **209** 431–43

scientific reports

Check for updates

OPEN

Simulation-based optimisation to quantify heterogeneity of specific ventilation and perfusion in the lung by the Inspired Sinewave Test

M. C. Tran[1,2]✉, V. Nguyen[3], R. Bruce[4], D. C. Crockett[2], F. Formenti[2,4,5], P. A. Phan[2], S. J. Payne[1] & A. D. Farmery[2]

The degree of specific ventilatory heterogeneity (spatial unevenness of ventilation) of the lung is a useful marker of early structural lung changes which has the potential to detect early-onset disease. The Inspired Sinewave Test (IST) is an established noninvasive 'gas-distribution' type of respiratory test capable of measuring the cardiopulmonary parameters. We developed a simulation-based optimisation for the IST, with a simulation of a realistic heterogeneous lung, namely a lognormal distribution of spatial ventilation and perfusion. We tested this method in datasets from 13 anaesthetised pigs (pre and post-lung injury) and 104 human subjects (32 healthy and 72 COPD subjects). The 72 COPD subjects were classified into four COPD phenotypes based on 'GOLD' classification. This method allowed IST to identify and quantify heterogeneity of both ventilation and perfusion, permitting diagnostic distinction between health and disease states. In healthy volunteers, we show a linear relationship between the ventilatory heterogeneity versus age ($R^2 = 0.42$). In a mechanically ventilated pig, IST ventilatory heterogeneity in noninjured and injured lungs was significantly different ($p < 0.0001$). Additionally, measured indices could accurately identify patients with COPD (area under the receiver operating characteristic curve is 0.76, $p < 0.0001$). The IST also could distinguish different phenotypes of COPD with 73% agreement with spirometry.

COPD is the third most frequent cause of death globally[1–3]. In COPD, cellular and structural lung changes develop early in the disease, decades before observable gross airflow obstruction is detected by spirometry[4]. Abnormalities of ventilatory heterogeneity accompany these early structural changes before airflow limitation as measured by spirometry, becomes evident[5]. Considerable benefits can be achieved by early diagnosis and treatment since the most rapid decline in lung function occurs in the early stages[2,6]. Acute lung injury and (ARDS) are typically seen in critically ill patients being treated with mechanical ventilation in Intensive Care Units (ICU). Coronavirus disease 2019 (COVID-19) is an emerging infectious disease that caused a global pandemic[7,8]. In a study of 201 COVID-19 patients, 41.8% of patients developed ARDS and 52.4% of those died[8]. One characteristic of ARDS is significant ventilatory heterogeneity.

Consequently, there is renewed interest in simple bedside/clinic-based measures of ventilatory heterogeneity as a new maker of early lung abnormality and guide for treatment[9,10]. Ventilatory heterogeneity is the unequal distribution of the airflow (ventilation) relative to the size of the lung regions to which it is distributed. This is related to, but distinct from, heterogeneity in regional balances of ventilation relative to perfusion (V/Q heterogeneity)[5]. Several lung tests have been claimed to accurately measure ventilatory heterogeneity[9,11]. These are not yet amenable to widespread use at the bedside or clinic. Of the simple available noninvasive lung function tests, the Multiple Breath Nitrogen Washout technique has been used in the past to investigate the ventilation–volume distribution[11–14].

[1]Institute of Biomedical Engineering, Department of Engineering Science, University of Oxford, Oxford OX3 7DQ, UK. [2]Nuffield Department of Clinical Neurosciences, John Radcliffe Hospital, Oxford OX3 9DU, UK. [3]Department of Materials and Oxford-Man Institute of Quantitative Finance, University of Oxford, Oxford OX2 6ED, UK. [4]Centre for Human and Applied Physiological Sciences, King's College London, London SE1 9RT, UK. [5]Department of Biomechanics, University of Nebraska, Omaha, NE, USA. ✉email: minh.tran@chch.ox.ac.uk

Characteristic	Animal			Human		
	Noninjured	Injured	*p*	Healthy	COPD	*p*
ELV(L)	1.23 (0.54)	0.86 (0.47)	< 0.01	2.3 (0.4)	2.0 (0.5)	< 0.05
Q_P(L/min)	2.9 (0.9)	3.2 (1.0)	ns	4.9 (1.8)	4.8 (2.0)	ns
μ_V	1.08 (0.23)	1.14 (0.34)	ns	1.14 (0.32)	1.11 (0.36)	ns
σ_V	0.20 (0.04)	0.31 (0.10)	< 0.0001	0.71 (0.16)	0.89 (0.33)	< 0.01
μ_P	1.02 (0.33)	1.15 (0.41)	ns	1.21 (0.44)	1.22 (0.31)	ns
σ_P	0.28 (0.11)	0.27 (0.19)	ns	1.01 (0.28)	1.2 (0.28)	< 0.001

Table 1. Results of the simulation-based optimisation in three datasets. Mean and standard deviation are shown. *ELV*: Effective lung volume; Q_P: pulmonary blood flow; μ_V and σ_V: mean and standard deviation of the ventilation lognormal distribution;μ_P and σ_P: mean and standard deviation of the perfusion lognormal distribution. Student's *t* test was applied with ns = non-significant.

The Inspired Sinewave Test (IST) is a non-invasive method to continuously monitor cardiopulmonary indices by using forced oscillations of nitrous oxide (N_2O) tracer gas signals[15–18]. The IST can measure several lung parameters (E_{LV}—effective lung volume, V_D—deadspace volume and Q_p—pulmonary blood flow) based on a single, well-mixed compartment model. The ability of IST to detect ventilatory heterogeneity has been assessed in healthy volunteers[19]. This study showed that with increasing heterogeneity, the recovered effective lung volume is reduced with reference to a standard measure (plethysmography). There is potential for further developing the IST to be able to characterise heterogeneity intrinsically, and independently of a second standard measure by using a simulation-based optimisation.

Simulation-based optimisation is a technique used in engineering, science and business research to take advantage of the ability of simulations to model phenomena and systems[20,21]. A simulation could be described as a 'black-box' that depends on input–output data from the simulation in its search for optimal input settings. Bayesian optimisation (BO) can speed up the experimental process by using machine learning to guide the search[22,23].

Therefore, we developed a simulation-based optimisation for the IST to estimate heterogeneity of specific ventilation and perfusion. The method combines the advantages of using a multicompartment lung simulation and Bayesian optimisation to improve performance. We implemented the optimisation in two IST data sets, including human COPD data and experimental animal ARDS data. This is the first study to use IST to evaluate changes in lung heterogeneity in different lung conditions.

Results

The mean and standard deviation of the model outputs in animal and human data sets are presented in Table 1. There were no significant differences in the *mean* values of the lognormal distributions of either ventilation or perfusion between the normal and abnormal lung in both animal and human studies, i.e. there was no left–right shift in the position of the distributions. However, the standard deviations of the lognormal distributions (σ_V and σ_P) differ significantly between the normal and the diseased lung, i.e. the distributions widen with disease. Noticeably, the values of σ_V (standard deviation of the ventilation lognormal distribution) shows significant differences in both data sets ($p < 0.0001$ in animal set and $p < 0.01$ in COPD).

Verification of the model in simulated patients. The lung simulation has been previously developed and verified and was then applied here to complete the simulation-based optimisation model. Firstly, this simulation is developed for the IST. The verification results are included in the appendix. Repeated calculations in the same data were undertaken. Repeated results had a variation of less than 5%. A demonstration of the simulated lognormal lung of emphysema and pulmonary embolism are shown in Fig. 1c, d. In Fig. 1c, the emphysema patient has a wider distribution of ventilation (greater heterogeneity) than the healthy one ($\sigma_V = 1.2$ compared with $\sigma_V = 0.3$ in healthy). In Fig. 1d, the patient with pulmonary embolism has a wider distribution of both ventilation and perfusion than the healthy case ($\sigma_V = 0.8$ and $\sigma_P = 1.3$).

IST heterogeneity indices in animal data. Figure 2 shows the IST heterogeneity results in noninjured versus injured animal data. The measurements were performed at different levels of positive end-expiratory pressure (PEEP). In panel a, the IST ventilation heterogeneity was not significantly influenced by the PEEP level in noninjured animals. Figure 2b shows pooled data separated into noninjured and injured data in all PEEP levels. A significant difference was observed in the IST ventilation heterogeneity (σ_V), $p < 0.0001$, however, no significance was seen in the IST perfusion heterogeneity (σ_P) in panel d. However, as shown in panel a and c, although there is no overall significant influence of the PEEP level on lung heterogeneity, at PEEP 15 cmH_2O, there was a wide separation between noninjured and injured data.

IST heterogeneity indices in human subjects. In the human data set, Fig. 3, the IST heterogeneity indices show the potential to classify healthy versus COPD groups. In panel a and b, results of unpaired t-test illustrate the ability to identify healthy versus COPD subjects. However, the classification was not entirely robust, with an area under the receiver operating characteristic curve of 0.76 ($p < 0.0001$), panel 3d. Interestingly, in

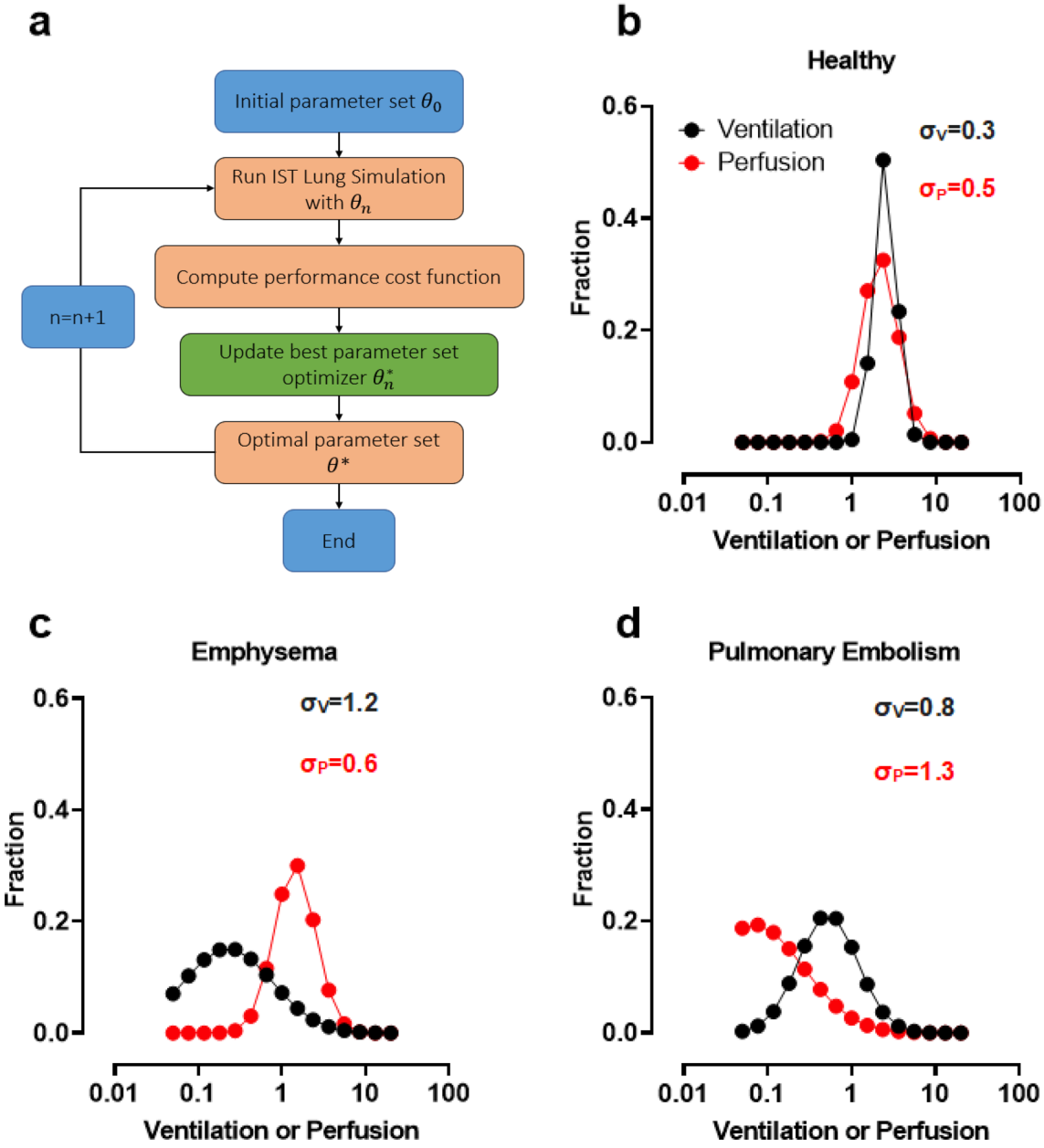


Figure 1. A schematic diagram of the lung simulation-based optimisation and examples of the simulated lognormal distributions. The model incorporated ventilatory and perfusion distributions which were taken from the literature, to represent the healthy individual and patients with emphysema and pulmonary embolism[33]. Panels **b**, **c** and **d** show the recovery of these distributions when a simulated IST is applied to the model.

Fig. 3a, two distinct sub-populations of COPD phenotype can be observed in the distribution graph of σ_V, indicating the wide range of disease severities within the diagnostic label of COPD.

Furthermore, in healthy subjects, Fig. 3c shows the relationship between IST heterogeneity indices and age, which was found to be a linear $\left(R^2 = 0.42, p < 0.0001\right)$. Based on this relationship, we normalised IST heterogeneity to account for the influences of normal ageing in further analysis. The equations are reported below (age in years):

$$\sigma_V = 0.0043 * age + 0.46 \quad (1)$$

$$\sigma_P = 0.0045 * age + 0.75 \quad (2)$$

In Fig. 4, further understanding of the IST lung heterogeneity in different COPD phenotype is revealed. In this figure, % of predicted values for age were calculated according to Eqs. (1) and (2), thereby eliminating the influence of normal ageing. The IST heterogeneity indices (both ventilation and perfusion) of healthy versus COPD patients ($p < 0.05$) are now clearly distinct. However, there was no clear distinction among the COPD groups.

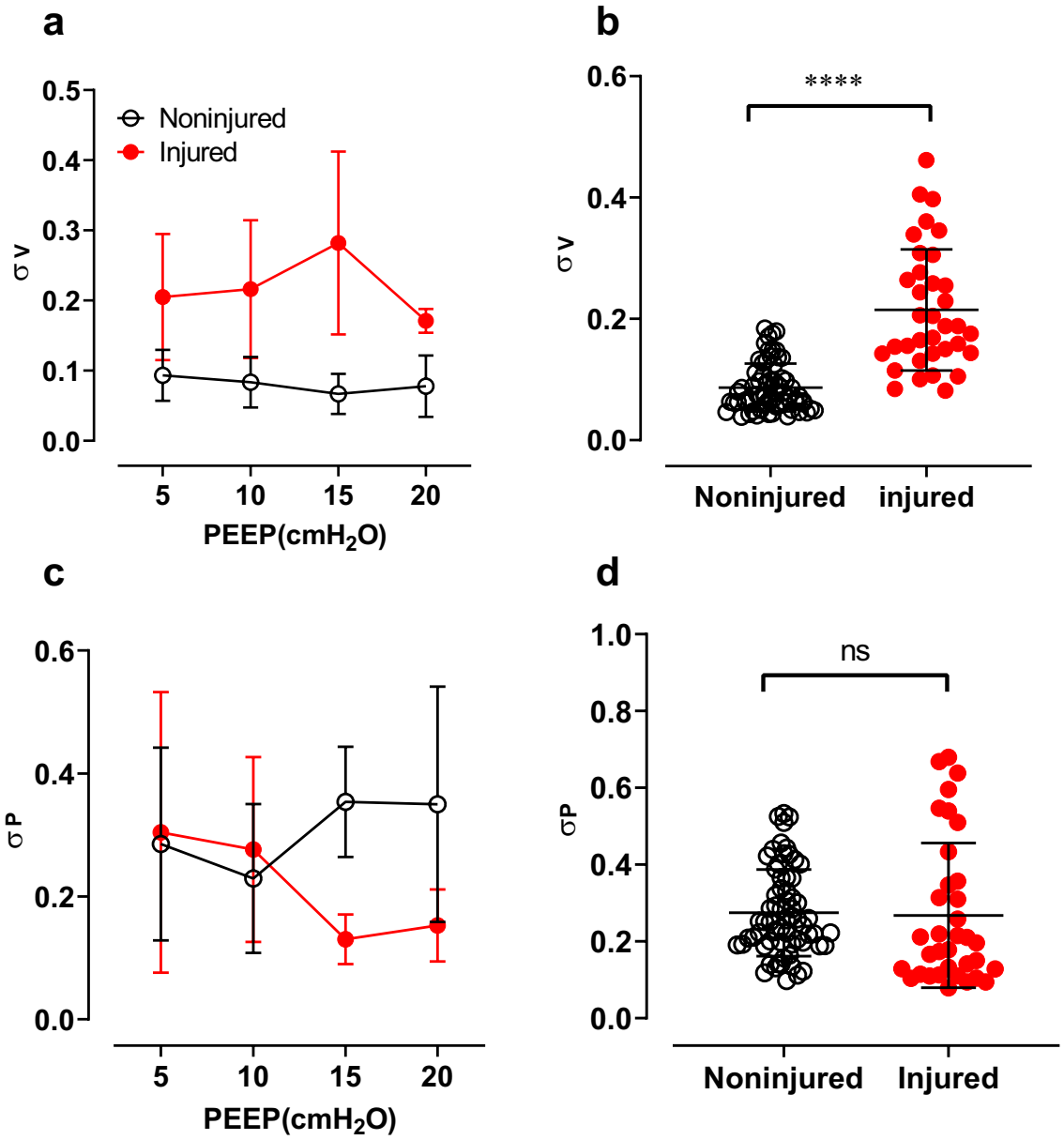


Figure 2. The IST heterogeneity indices in animal data. Panels (**a**) and (**b**) show the distribution of the IST ventilation heterogeneity index (σ_V) in noninjured and injured lungs. Similarly, panels **c** and **d** show the IST perfusion heterogeneity index (σ_P). Panels (**a**) and (**c**) present the mean and standard deviation of the IST heterogeneity indices versus PEEP levels. Panels (**b**) and (**d**) present the unpaired Student's *t* test comparisons in all PEEP levels. ns: non-significant and ****$p < 0.0001$.

Additionally, panel c shows a confusion matrix of patient classification results using only IST heterogeneity indices. The 'GOLD' classification was assumed to present the ground truth. This classification results achieved an accuracy of 73% similarity compared to GOLD classification. The highest predicted accuracy was the healthy group (100% accuracy) and the lowest was COPD phenotype 1 and 4 (57%).

Bayesian optimisation performance. Figure 5 compares the efficiency and time consumption among optimisation methods (Bayesian optimisation, Neider–Mead and random search). Panel a shows one example of the loss function versus iterations in one example data set. The Bayesian optimisation can provide more accurate approximations in less than 15 min compared to others. In panel c, the success rate is the percentage of the meaningful results in total. This rate was higher in Bayesian optimisation when compared to other methods (95% in animal data and 82% in human set).

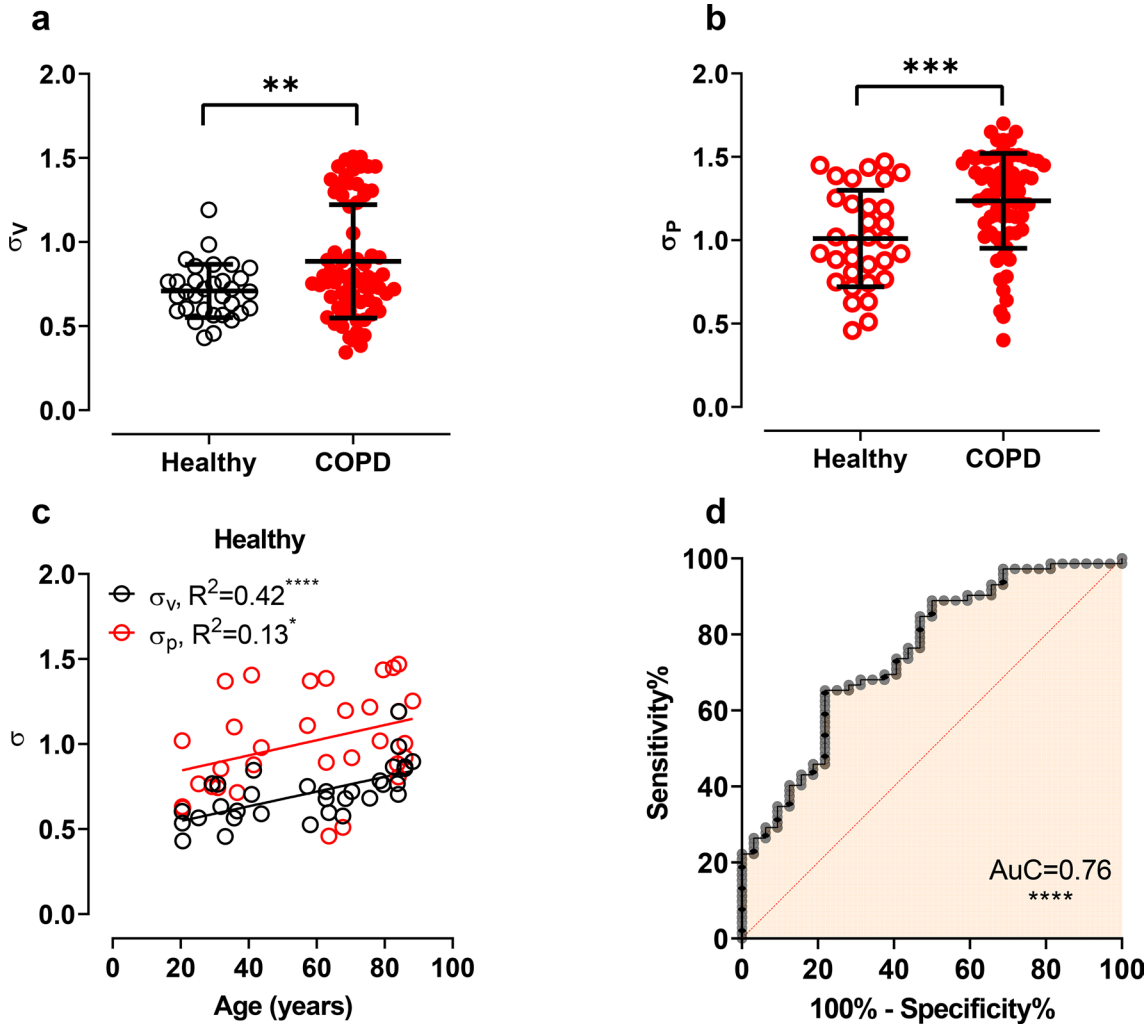


Figure 3. The IST heterogeneity indices in human data. Panels (**a**) and (**b**) show unpaired Student's *t* test of the IST ventilation (σ_V) and perfusion heterogeneity (σ_P) indices. Panel (**c**) shows the linear regression of the IST heterogeneity indices versus ages in healthy people. Panel (**d**) shows the receiver operating characteristic curve of the COPD classification using only IST heterogeneity indices. $^{*}p<0.05$; $^{**}p<0.01$; $^{***}p<0.001$; $^{****}p<0.0001$.

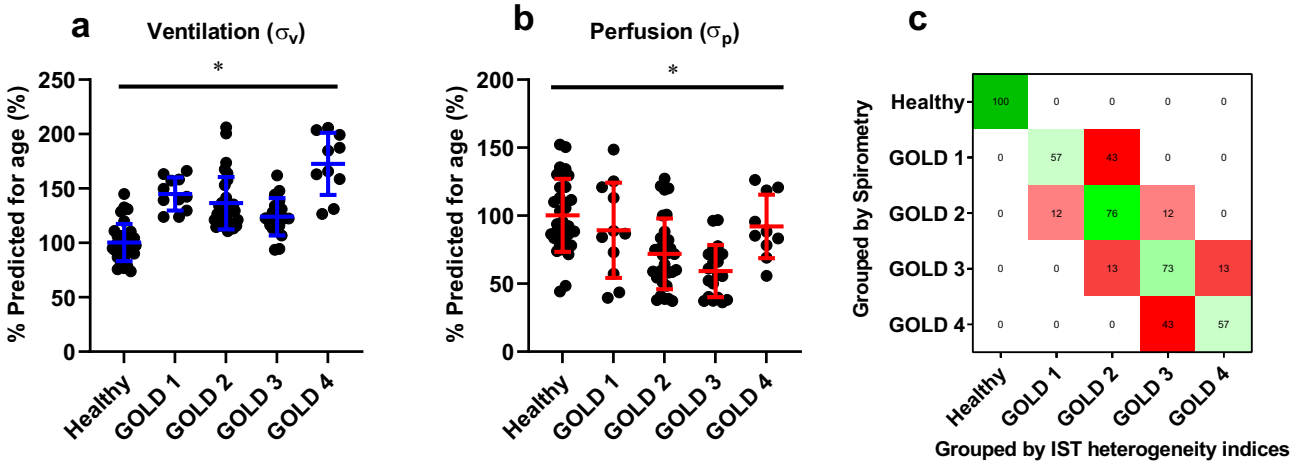


Figure 4. The IST heterogeneity results in the human data set, including healthy and COPD phenotypes (GOLD 1–4). Panels (**a**) and (**b**) show % of measured values over the predicted values for age in different lung conditions. Kruskal–Wallis test was applied for multiple groups comparison with abnormal distribution. Panel (**c**) shows the confusion matrix result of the logistic regression analysis in percentage. This analysis grouped patients by the IST heterogeneity indices and compared them with the classification results using Spirometry (standard method). $^{*}p<0.05$.

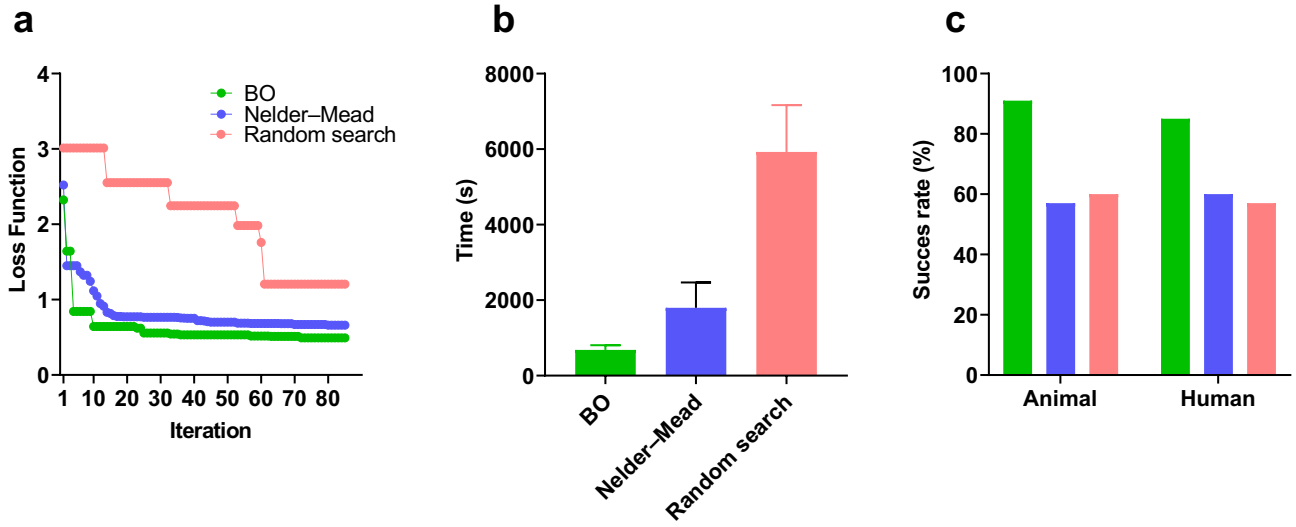


Figure 5. Performance comparison in three optimisation methods: Bayesian optimisation (BO), Nelder–Mead and random search. Panel (**a**) shows the loss function of three methods analysed in one data set. Panel (**b**) shows the mean and variance of the time consumptions of three techniques in three random data. Panel (**c**) shows the success rate (the percentage of optimisation solutions in total) of each method in three data sets.

Discussion

Overall, this study has quantified lung heterogeneity using a non-invasive lung function test, the Inspired Sinewave Test, combined with advanced computational methods. Heterogeneity values were captured and demonstrated in both animal and human studies, in both health and disease. In this section, we discuss in detail the method to calculate the lung heterogeneity noninvasively, and consider the use of these indices as a tool to classify lung conditions.

Ventilatory heterogeneity is the mismatch in distribution of the ventilation relative to compartment size. The latter is sometimes referred to as 'specific ventilation' and represents the reciprocal of the time-constant of a compartment. Perfusion heterogeneity is mismatch of perfusion relative to compartment size. Both of these forms of heterogeneity are related to, but distinct from, V/Q heterogeneity which is the non-uniform distribution of V/Q ratios (with respect to perfusion or ventilation), which is not the subject of this paper. In this work, the standard deviation of the lognormal distributions of ventilation and perfusion (σ_V and σ_P) was shown to adequately represent and usefully quantify heterogeneity of both ventilation and perfusion (both relative to compartment size). Such heterogeneity has previously been shown to be represented by a lognormal distribution. An example of this is the Multiple breath Nitrogen Washout technique; a relatively technically complex technique which assumes this distribution[11,24]. Ventilatory heterogeneity could be usefully presented to clinicians in both numerical format (standard deviation) and visually, in the form of a lognormal plot. The lognormal distribution is straightforward to understand and easily recognised by clinicians. Thirdly, this distribution could be upgraded easily in the future to allow for bi-modal or multimodal distributions.

Our results for the ventilation and perfusion lognormal distributions agreed with previous studies. Other research using different lung measurement technique has shown similar standard deviations of ventilation and perfusion of 0.53 and 0.55 in healthy people, albeit in a much smaller sample ($n = 6$)[9]. In our study, in Fig. 3, healthy people had mean values of $\sigma_v = 0.71$ and $\sigma_p = 1.0$. Because age is an important factor in COPD, in Fig. 3c, we were able to compensate for this effect in future analyses. The outlying results in the confusion matrix for the GOLD phenotypes were never greater than ± 1, indicating generally good agreement. Heterogeneity indices (expressed as % predicted for age) were significantly different between healthy and COPD cohorts. Overall, % predicted $\sigma_v = 100 \pm 17$ (healthy) versus $\sigma_v = 140 \pm 26$ (pooled COPD).

In the human data set (classified according to 'GOLD'), the result was not accurately classified by the IST heterogeneity indices. This is likely because COPD represents a wide variety of pathology and severity, and further still, the GOLD classification is based on spirometry and reported symptoms which themselves have an unknown relationship to pathological severity. Age is known to be an essential factor in COPD disease prediction[19]. Our research shows similar results. We have also demonstrated a correlation between specific ventilatory heterogeneity and perfusion heterogeneity versus age in healthy participants. Thus, although we normalised the lung heterogeneity indices to account for the effect of age, genetic factors, tobacco smoke and outdoor air pollutants play essential roles in the patients' lung heterogeneity[25], which could not be controlled for. In contrast, however, there was greater uniformity in experimental conditions both before and after lung injury, which would have allowed the specific effects of injury to be more evident in the animal experiments.

Although the optimisation process was time-consuming, Bayesian optimisation boosted the performance of the lung simulation-based optimisation model. A similar optimisation problem has been tackled before, but the time and computing power required were prohibitive[9]. However, we have demonstrated that Bayesian optimisation could calculate results in ten minutes using a standard office computer. In addition, our approach was more effective in dealing with the potentially non-convex optimisation problem than the Nelder-Mead.

Our advanced optimisation method not only improves the diagnostic ability of the IST but also its translation to human medicine.

In this work, we demonstrated the ability of the IST, a relatively simple to implement lung function test, as a diagnostic tool. The IST results are reliable and clinically meaningful[17,18]. Previous studies indicated that, in ventilated subjects, the IST could measure the effective lung volume ("baby lung") and capture the pulmonary blood flow trend[17,18]. The IST does not require special, forced manoeuvres, which patients often find challenging and uncomfortable. In an assessment of comfort (n = 18), 78% of participants selected the IST as their preferred test comparing to spirometry and body plethysmography[26]. The ability of IST to measure ventilatory heterogeneity could improve the impact of the IST when used as a diagnostic tool. For example, in Fig. 4c, a simple multi-class logistic classification was implemented. If we assumed that the GOLD classification (based on the spirometry values) was a ground truth[6], the classification result using the IST heterogeneity values could predict accurately 100% of healthy patients and 73% overall.

Furthermore, the IST also could classify ARDS lungs (injured) versus control (noninjured), the $AuC = 0.76$ ($p < 0.0001$) of the ROC curve (in Fig. 3d). Application of IST could benefit patients undergoing mechanical ventilation. Clinicians could use IST measured values to optimise ventilator settings to match the individual patient's lung conditions.

This study has several strengths. We included a large number of data sets from IST (13 animals and 104 participants). This work is the first study to provide detailed lung heterogeneity data in ARDS and COPD patients using the IST. However, we acknowledge several limitations. The included data were collected during experiments designed for other purposes. Moreover, because the IST is a gas exchange technique, and N_2O has only modest blood solubility, the influence of perfusion is weaker than that of ventilation. This is likely to yield less reliable parameter recovery values than ventilation data (results presented in Fig. 2b, d). Additionally, our model results contained two sets of parameters: the parameters to control the shape of the lognormal distributions and the absolute physiological lung parameters. Because this paper aims to report the heterogeneity of the lung, the volumetric lung parameters will be reported in another study. Furthermore, our lung simulation and its lognormal assumptions might not perfectly fit the measured data. This lognormal distribution was assumed to be an accurate representation of the lung heterogeneity[27,28]. But, in several patients, the distribution of lung heterogeneity was recorded in the bimodal log-distribution. Therefore, future work will aim to loosen the prior assumptions of the distribution and to accommodate alternative possibilities. Future comparison of IST ventilation heterogeneity and perfusion heterogeneity indices with those measured by CT scanning will be performed[29,30]. Sophisticated lung simulations or advanced optimisation methods could also be introduced in the future. However, the required time and computer power consumption might then be considerable.

We have presented a new approach to quantify ventilatory heterogeneity using Bayesian optimisation combined with a non-invasive lung function test (the Inspired Sinewave Technique). We have shown that the IST can measure heterogeneity indices and we applied this model to further explore lung heterogeneity in health and disease. Our results support further development of this technique and its translation to human medicine. The need to measure the lung volume of mechanically ventilated patients and to personalise ventilation, may aid in reducing driving pressure and therefore mortality in patients with COPD and acute respiratory distress syndrome (ARDS) in the future.

Methods

A lung simulation was developed to work with the Inspired Sinewave Technique. The IST compares the tracer gas (N_2O) inhaled and exhaled signals and applies an analytical model to calculate cardiopulmonary parameters[18,31,32]. In theory, the analytical model should be invertible, and we should be able to recalculate the lung parameters from this model. However, in practice, the complexity of signal processing, the signal to noise ratio and the non-convexity of the optimisation means that inversion of the model is not practicable. Therefore, we developed a simulation-based optimisation and applied Bayesian optimisation to quantify the ventilation and perfusion heterogeneity using the IST results.

The Bayesian optimisation was then applied to match simulated to measured data so creating a simulation-based optimisation model. The model was then verified by simulated patient data from the literature (emphysema and pulmonary embolism). A simulated emphysema patient's lung displayed abnormal ventilation heterogeneity, and similarly, a simulated pulmonary embolism patient revealed abnormal perfusion heterogeneity[33]. A schematic diagram of the model and results of simulated heterogeneous lungs are shown in Fig. 1.

When the model was completed and verified, we applied this to calculate lung heterogeneity indices from our IST patient and animal studies data. The characteristic summary of the animal and human data is presented in Table 2. We executed the IST measurements at two tracer gas oscillation frequencies (periods 180s and 60s). All IST measurements and analysis were carried out in accordance with relevant guidelines and regulations in the study.

Animal data were obtained from 13 anaesthetised pigs which were studied by the IST both before lung injury (noninjured) and after lung injury (injured). Experiments were performed at the Hedenstierna Laboratory, Uppsala University, Uppsala, Sweden. It was approved by the regional animal welfare and ethics committee (Ref: C98/16). Lachmann's method was applied to induce lung injury to model the ARDS[34]. Details of the animal preparation can be found in[18]. PEEP was applied at 5, 10, 15 and 20 cmH_2O incrementally. The fraction of inspired oxygen (FiO_2) was kept unchanged at 0.4 before injury and 0.8 after injury to maintain oxygenation. Reporting in this paper adheres to the Animal Research: Reporting of In Vivo Experiments guidelines[35].

The human clinical data used here comprised two datasets taken from another research study[19,36]. Informed consent was obtained from all subjects. We analysed data from 104 participants (32 Healthy and 72 COPD). COPD patients met the inclusion criteria if they were aged > 40 years, had a 10-pack year smoking history, and

Parameter	Noninjured	Injured
Animal		
Number	13	13
Weight (kg)	29 (2)	–
Heart rate (bpm)	86 (12)	85 (11)
pH	7.42 (0.03)	7.28 (0.09)
F_IO_2	0.4 (0.1)	0.8 (0.1)
Cardiac output (L/min)	3.4 (0.8)	3.2 (0.4)
	Healthy	**COPD**
Human		
Number	32	72
Age	53 (22)	67 (10)
Height (m)	1.7 (0.1)	1.7 (0.1)
Weight (kg)	72 (12)	79 (18)
BMI	25 (4)	28 (5)

Table 2. Characteristic summary of the animal and human data measured by the IST. Mean (SD) are shown. F_IO_2 is the fraction of inspired oxygen.

a $FEV_1/FVC < 0.7$. Patients were classified into the four "GOLD" categories (1–4) based upon FEV1%[2,6,37]. The protocol for the study was approved by an NHS ethical committee (16/SC/0057, South Central—Hampshire B Research Ethics Committee) and conformed to the Declaration of Helsinki, 2013. All procedures for each participant were performed on the same day within the Respiratory Medicine Department of the Churchill Hospital, Oxford University Hospitals.

Finally, to compare the optimisation performance, three optimisation methods (Bayesian optimisation, Nelder-Mead and random search) were performed using the same desktop computer (Intel core I7, 32 GB of RAM).

The lung simulation-based optimisation model. Figure 1a presents a schematic diagram of the lung simulation-based optimisation model. This model contains two parts, which are the lung simulation and the optimisation. The lung was simulated by ten dead-space compartments, 125 alveolar compartments (tidally ventilated) and five body compartments. A simple version of this lung simulation was implemented and validated previously in[31,38]. In this work, we increased the number of alveolar compartments to 125 and applied the fraction of ventilation and perfusion to each individual compartment to represent the heterogeneity of the lung. These fractions were described and generated by a lognormal distribution[9].

Some of the parameters of this lung simulation were taken directly from the patient's record, such as tidal volume, respiration rate, inspiration-expiration ratio and deadspace volume (measured by the IST). The unknown parameters are alveolar volume, pulmonary blood flow and the width (i.e. the log Standard Deviation) of the ventilation and perfusion heterogeneity lognormal distribution, which were the focus in the optimisation.

The concept of the lognormal lung has been presented elsewhere[9]. In this paper, we introduce a simple lognormal distribution of the lung to show lung heterogeneity. For example, in Fig. 1b, in a healthy patient, the log standard deviation of the specific ventilation heterogeneity (σ_V) was found to be 0.3 and the log standard deviation of the perfusion heterogeneity (σ_P) was found to be 0.5[9]. In this lognormal distribution, the more damaged the lung, the wider the distribution (larger σ_V or μ being further away from 1). The shape of the distribution depends on σ and μ.

We used Bayesian optimisation to match the data from the simulated lung to that of the measured data to calculate these unknown parameters[39,40]. A loss function showed the difference between the simulated and measured values. Thus, the Bayesian optimisation can statistically suggest parameters for the simulation to minimise the loss function. Minimising the loss function $f(\theta)$ can estimate the input parameters θ, including $(V_A, Q_P, \sigma_V, \mu_V, \sigma_P, \mu_P)$, where V_A is alveolar volume and Q_P is pulmonary blood flow,

$$arg\left(\left|\frac{ELV_{180}^{Sim}(\theta) - ELV_{180}^{M}}{ELV_{180}^{M}}\right| + \left|\frac{ELV_{60}^{Sim}(\theta) - ELV_{60}^{M}}{ELV_{60}^{M}}\right| + \left|\frac{Qp_{180}^{Sim}(\theta) - Qp_{180}^{M}}{Qp_{180}^{M}}\right| + \left|\frac{Qp_{60}^{Sim}(\theta) - Qp_{60}^{M}}{Qp_{60}^{M}}\right|\right) \tag{3}$$

where $ELV_{180}^{Sim}(\theta)$ is the simulated effective lung volume value based on the set parameter θ and ELV_{180}^{M} is the measured effective lung volume from the patient. The $ELV_{180}^{Sim}(\theta)$ is the result of the IST running on a simulation lung with known conditions (parameter θ). Similarly, with $Q_{P,180}^{Sim}(\theta)$ and $Q_{P,180}^{M}$. 180s and 60s were the periods of the IST tracer gas oscillation. Further details of the lung model development and the Bayesian optimisation are included in the appendix.

Statistical analysis. Statistical analyses were conducted using GraphPad Prism (GraphPad Software inc.) and Matlab v2018b (Mathworks, Natick, MA, USA). To compare differences between healthy participants and patients in the 1–4 GOLD classifications, Kruskal–Wallis test was used[41]. To compare two groups, we used an

unpaired *t* test. The Area under The Curve (AuC) of the Receiver Operating Characteristics (ROC) curve was used to measure the ability of our test to distinguish between healthy and COPD[42]. Furthermore, we also applied a maximum likelihood estimation of the logistic regression model using only our IST outputs to classify participants as healthy or into the 1–4 GOLD categories[43,44].

Data availability

Data available upon request.

Received: 25 October 2020; Accepted: 24 May 2021
Published online: 16 June 2021

References

1. Hussain, M., Madl, P. & Khan, A. Lung deposition predictions of airborne particles and the emergence of contemporary diseases, Part-I. *Health (Irvine, CA)* **2**, 51–59 (2011).
2. Pauwels, R. A., Buist, A. S., Calverley, P. M., Jenkins, C. R. & Hurd, S. S. Global strategy for the diagnosis, management, and prevention of chronic obstructive pulmonary disease: NHLBI/WHO Global Initiative for Chronic Obstructive Lung Disease (GOLD) Workshop summary. *Am. J. Respir. Crit. Care Med.* **163**(5), 1256–1276 (2001).
3. Kent, B. D., Mitchell, P. D. & Mcnicholas, W. T. Hypoxemia in patients with COPD: Cause, effects, and disease progression. *Int. J. COPD* **6**, 199–208 (2011).
4. Csikesz, N. G. & Gartman, E. J. New developments in the assessment of COPD: Early diagnosis is key. *Int. J. COPD* **9**, 277–286 (2014).
5. West, J. B. *Respiratory physiology: the essentials. Lippincott, Williams & Wilkins* (2012).
6. Vogelmeier, C. F. *et al.* Global strategy for the diagnosis, management, and prevention of chronic obstructive lung disease 2017 report. *Am. J. Respir. Crit. Care Med.* **195**, 557–582 (2017).
7. Phua, J. *et al.* Intensive care management of coronavirus disease 2019 (COVID-19): Challenges and recommendations. *Lancet Respir. Med.* **2019**, 1–12 (2020).
8. Wu, C. *et al.* Risk factors associated with acute respiratory distress syndrome and death in Patients with coronavirus disease 2019 pneumonia in Wuhan, China. *JAMA Intern. Med.* **180**, 934–943 (2020).
9. Mountain, J. E. *et al.* Potential for noninvasive assessment of lung inhomogeneity using highly precise, highly time-resolved measurements of gas exchange. *J. Appl. Physiol.* **124**, 615–631 (2018).
10. Lui, J. K. & Lutchen, K. R. The role of heterogeneity in asthma: a structure-to-function perspective. *Clin. Transl. Med.* **6**, 29 (2017).
11. Verbanck, S. A. B. *et al.* Ventilation heterogeneity in smokers: Role of unequal lung expansion and peripheral lung structure. *J. Appl. Physiol.* **129**, 583–590 (2020).
12. Lewis, S. M., Evans, J. W. & Jalowayski, A. A. Continuous distributions of specific ventilation recovered from inert gas washout. *J. Appl. Physiol. Respir. Environ. Exerc. Physiol.* **44**, 416–423 (1978).
13. Buchanan, P. R., Tavener, S. J., Withy, S. J. & Harris, E. A. Recovery of ventilation distributions by gas wash-out of a mechanical pump. *Clin. Phys. Physiol. Meas.* **7**, 237–252 (1986).
14. Sá, R. C. *et al.* Validating the distribution of specific ventilation in healthy humans measured using proton MR imaging. *J. Appl. Physiol.* **116**, 1048–1056 (2014).
15. Harrison, C. *et al.* Modelling mixing within the dead space of the lung improves predictions of functional residual capacity. *Respir. Physiol. Neurobiol.* **242**, 12–18 (2017).
16. Hahn, C. E. W. & Farmery, A. D. Gas exchange modelling: No more gills, please. *Br. J. Anaesth.* **91**, 2–15 (2003).
17. Bruce, R. M. *et al.* Noninvasive cardiac output monitoring in a porcine model using the inspired sinewave technique: A proof-of-concept study. *Br. J. Anaesth.* **123**, 126–134 (2019).
18. Crockett, D. C. *et al.* Validating the inspired sinewave technique to measure the volume of the 'baby lung' in a porcine lung-injury model. *Br. J. Anaesth.* **124**, 345–353 (2020).
19. Bruce, R. M., Phan, P. A., Pacpaco, E., Rahman, N. M. & Farmery, A. D. The inspired sine-wave technique: A novel method to measure lung volume and ventilatory heterogeneity. *Exp. Physiol.* **103**, 738–747 (2018).
20. Amaran, S., Sahinidis, N. V., Sharda, B. & Bury, S. J. Simulation optimization: a review of algorithms and applications. *Ann. Oper. Res.* **240**, 351–380 (2016).
21. Wolpert, D. H. & Macready, W. G. No free lunch theorems for optimization. *IEEE Trans. Evol. Comput.* **1**, 67–82 (1997).
22. Snoek, J., Larochelle, H. & Adams, R. P. Practical Bayesian optimization of machine learning algorithms. in *Advances in Neural Information Processing Systems* 2951–2959 (2012).
23. Le, T., Nguyen, K., Nguyen, V., Nguyen, T. D. & Phung, D. GoGP: Fast online regression with Gaussian processes. in *IEEE International Conference on Data Mining (ICDM)* (2017).
24. Downie, S. R. *et al.* Ventilation heterogeneity is a major determinant of airway hyperresponsiveness in asthma, independent of airway inflammation. *Thorax* **62**, 684–689 (2007).
25. Mannino, D. M. & Buist, A. S. Global burden of COPD: Risk factors, prevalence, and future trends. *Lancet* **370**, 765–773 (2007).
26. Phan, P. A. *et al.* The inspired sinewave technique: A comparison study with body plethysmography in healthy volunteers. *IEEE J. Transl. Eng. Heal. Med.* **5**, 1–9 (2017).
27. Motta-Ribeiro, G. C., Jandre, F. C., Wrigge, H. & Giannella-Neto, A. Generalized estimation of the ventilatory distribution from the multiple-breath nitrogen washout. *Biomed. Eng. Online* **15**, 1–18 (2016).
28. Whiteley, J. P., Gavaghan, D. J. & Hahn, C. E. W. The effect of the width of the ventilation-perfusion distribution on arterial blood oxygen content. *J. Theor. Biol.* **201**, 271–279 (1999).
29. Cressoni, M. *et al.* Lung inhomogeneity in patients with acute respiratory distress syndrome. *Am. J. Respir. Crit. Care Med.* **189**, 149–158 (2014).
30. Cronin, J. N. *et al.* Dynamic single-slice CT estimates whole-lung dual-energy CT variables in pigs with and without experimental lung injury. *Intensive Care Med. Exp.* **7**, 1–14 (2019).
31. Tran, M. C. *et al.* Lung heterogeneity and deadspace volume in animals with acute respiratory distress syndrome using the Inspired Sinewave Test. *Physiol. Meas.* **41**, 1–10 (2020).
32. Tran, M. C. *et al.* Validating the inspired sinewave technique to measure lung heterogeneity compared to atelectasis & over-distended volume in computed tomography images. *ICASSP 2021–2021 IEEE Int. Conf. Acoust. Speech Signal Process.* **1**, 1010–1014 (2021).
33. Yem, J. S., Turner, M. J., Baker, A. B., Young, I. H. & Crawford, A. B. H. H. A tidally breathing model of ventilation, perfusion and volume in normal and diseased lungs. *Br. J. Anaesth.* **97**, 718–731 (2006).
34. Lachmann, B., Robertson, B. & Vogel, J. In vivo lung lavage as an experimental model of the respiratory distress syndrome. *Acta Anaesthesiol. Scand.* **24**, 231–236 (1980).

35. Kilkenny, C., Browne, W. J., Cuthill, I. C., Emerson, M. & Altman, D. G. Improving bioscience research reporting: The arrive guidelines for reporting animal research. *Animals* **4**, 35–44 (2013).
36. Bruce, R. M. *et al.* Assessment of ventilatory heterogeneity in chronic obstructive pulmonary disease using the Inspired Sinewave Test. *Int. J. COPD* **16**, 401–413 (2021).
37. Jones, P. W. *et al.* Development and first validation of the COPD Assessment Test. *Eur. Respir. J.* **34**, 648–654 (2009).
38. Tran, M. C., Crockett, D. C., Phan, P. A., Payne, S. J. & Farmery, A. D. A tidal lung simulation to quantify lung heterogeneity with the Inspired Sinewave Test. in *2020 42nd Annual International Conference of the IEEE Engineering in Medicine & Biology Society (EMBC)* 2438–2441 (2020).
39. Nguyen, V., Gupta, S., Rana, S., Li, C. & Venkatesh, S. Regret for expected improvement over the best-observed value and stopping condition. in *Proceedings of The 9th Asian Conference on Machine Learning (ACML)* 279–294 (2017).
40. Nguyen, V., Gupta, S., Rana, S., Li, C. & Venkatesh, S. Filtering Bayesian optimization approach in weakly specified search space. *Knowl. Inf. Syst.* **60**, 385–413 (2019).
41. Breslow, N. A generalized Kruskal–Wallis test for comparing k samples subject to unequal patterns of censorship. *Biometrika* **57**, 579–594 (1970).
42. Fawcett, T. An introduction to ROC analysis. *Pattern Recognit. Lett.* **27**, 861–874 (2006).
43. Bishop, C. M. *Pattern recognition and machine learning*. (Springer, New York, 2006).
44. Nguyen, V., Nguyen, T. D., Le, T., Venkatesh, S. & Phung, D. One-pass logistic regression for label-drift and large-scale classification on distributed systems. *2016 IEEE 16th Int. Conf. Data Min.* 1113–1118 (2017).

Acknowledgements

The authors are grateful to Hedenstierna Laboratory, Uppsala, Sweden, for their technical support in the animal study. The authors also appreciate the time given up by all the participants and the critical technical assistance from Clinical Scientists at Oxford University Hospitals NHS Foundation Trust.

Author contributions

Study design: A.F., D.C., P.P., R.B. Study conduct: D.C., R.B., F.F. Data analysis: M.T., R.B., V.N. Writing of paper: M.T., A.F., S.P. Critical revision: all authors. Financial support: A.F., P.P., F.F., R.B.

Funding

NIHR the National Institute for Health Research II-LA-0214- 20005 and NIHR200029 funded the IST development to PP and AD. Royal Academy of Engineering Enterprise Fellowship funded the animal experiments to PP. Medical Research Council (MC_PC_17164) and The Physiological Society (Formenti 2018) supported FF.

Competing interests

The authors declare no competing interests.

Additional information

Supplementary Information The online version contains supplementary material available at https://doi.org/10.1038/s41598-021-92062-w.

Correspondence and requests for materials should be addressed to M.C.T.

Reprints and permissions information is available at www.nature.com/reprints.

Publisher's note Springer Nature remains neutral with regard to jurisdictional claims in published maps and institutional affiliations.

Open Access This article is licensed under a Creative Commons Attribution 4.0 International License, which permits use, sharing, adaptation, distribution and reproduction in any medium or format, as long as you give appropriate credit to the original author(s) and the source, provide a link to the Creative Commons licence, and indicate if changes were made. The images or other third party material in this article are included in the article's Creative Commons licence, unless indicated otherwise in a credit line to the material. If material is not included in the article's Creative Commons licence and your intended use is not permitted by statutory regulation or exceeds the permitted use, you will need to obtain permission directly from the copyright holder. To view a copy of this licence, visit http://creativecommons.org/licenses/by/4.0/.

© The Author(s) 2021

A tidal lung simulation to quantify lung heterogeneity with the Inspired Sinewave Test

Minh C. Tran[1,2], Douglas C. Crockett[1], Phi A. Phan[1], Stephen J. Payne[2], Andrew D. Farmery[1]

***Abstract*— We have created a lung simulation to quantify lung heterogeneity from the results of the inspired sinewave test (IST). The IST is a lung function test that is non-invasive, non-ionising and does not require patients' cooperation. A tidal lung simulation is developed to assess this test and also a method is proposed to calculate lung heterogeneity from IST results. A sensitivity analysis based on the Morris method and linear regression were applied to verify and to validate the simulation. Additionally, simulated emphysema and pulmonary embolism conditions were created using the simulation to assess the ability of the IST to identify these conditions. Experimental data from five pigs (pre-injured vs injured) were used for validation. This paper contributes to the development of the IST. Firstly, our sensitivity analysis reveals that the IST is highly accurate with an underestimation of about 5% of the simulated values. Sensitivity analysis suggested that both instability in tidal volume and extreme expiratory flow coefficients during the test cause random errors in the IST results. Secondly, the ratios of IST results obtained at two tracer gas oscillation frequencies can identify lung heterogeneity (ELV_{60}/ELV_{180} and Qp_{60}/Qp_{180}). There was dissimilarity between simulated emphysema and pulmonary embolism ($p < 0.0001$). In the animal model, the control group had $ELV_{60}/ELV_{180} = 0.58$ compared with 0.39 in injured animals ($p < 0.0001$).**

***Keywords*— inspired sinewave test, lung simulation, lung heterogeneity.**

I. INTRODUCTION

Respiratory diseases, including chronic obstructive pulmonary disease (COPD) and acute respiratory distress syndrome (ARDS) account for considerable mortality worldwide [1]. Lung heterogeneity is proposed as a sensitive index of lung disease [2], [3], [4]. The lung heterogeneity index is a number describing the mismatch between ventilation, alveolar volume and pulmonary blood flow throughout the lung. [5]. This index has been mainly measured by invasive methods or medical imaging with ionising tracer gases [6].

The inspired sinewave test (IST) is a non-invasive, non-ionising method, using an inert tracer gas (N_2O) which is forced to oscillate at a given frequency to measure various cardio-pulmonary indices [7], [8], [9]. The IST has been described elsewhere [10]. The IST can measure deadspace volume (V_D), alveolar lung volume (V_A) in the form of effective lung volume (ELV) and pulmonary blood flow (Qp). The IST has the potential to detect lung disease at the early states based on lung heterogeneity indices.

[1]M. Tran, D. Crockett, P. Phan and A. Farmery are with Nuffield Division of Anaesthetics, University of Oxford, UK.

[2]M. Tran and S. Payne are with the Institute of Biomedical Engineering, University of Oxford, UK.

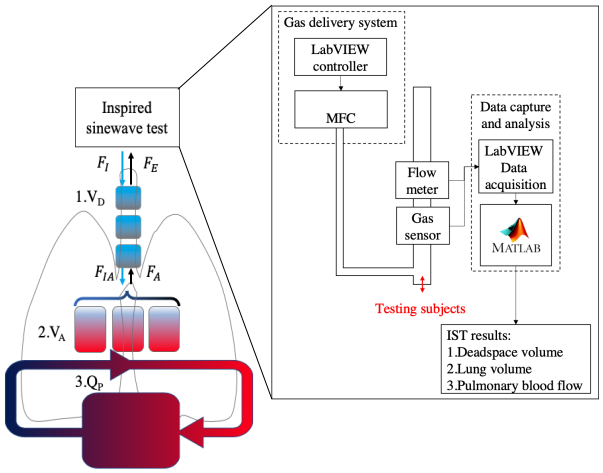


Fig. 1. Schematic diagram of the tidal lung simulation and representation of the inspired sinewave test.

We have therefore developed a lung simulation to investigate the ability of IST to determine lung heterogeneity. We propose a method to quantify lung heterogeneity by using two different forcing periods of the tracer gas for the IST. This method is validated by using both simulated data(three virtual patients - healthy, emphysema and pulmonary embolism) and ARDS animal data (pre - injured and post - injured).

II. METHOD

A. Computational model

The lung simulation consisted of ten deadspace compartments [11], three tidal lung compartments, a shunt and five body compartments [12]. Compartments were governed by conservation of mass equations. The *ode45* solver and *Simulink* from Matlab were adopted for simulation. The simulation was then combined directly with the IST analysis to create a forward-backward model [10]. The model details are included in Appendix A and the schematic diagram of the model is shown in Fig 1.

For sensitivity analysis, the three lung compartments were assumed to be homogeneous and to behave as one well-mixed compartment. The setting parameters and testing ranges for the simulation are presented in Table 1.

The Morris method for sensitivity analysis was applied to verify and to validate the model [13]. This method calculates the elementary effect values of each input parameter which were then used to identify the main input parameters and

their relationship between the input and output [13], [14]. A thousand samples were simulated for each parameter. Gaussian white noise was added to the simulated signal to justify the robustness of the IST results to noise.

B. Method to quantify IST lung heterogeneity indices

To assess the ability of the IST to calculate lung heterogeneity, heterogeneous lungs were firstly simulated according to the parameters in Yem et al. [15]. These parameters were calculated from patients. Three conditions with different degrees of heterogeneity were simulated: normal lung, emphysema (ventilatory heterogeneous distributed), and pulmonary embolism (perfusion heterogeneous distributed). The IST was repeated twice with tracer gas oscillating at time periods of $180s$ and $60s$. The IST Ventilation heterogeneity of the lung was calculated by:

$$ELV_{60}/ELV_{180} \tag{1}$$

and the IST perfusion heterogeneity was calculated by:

$$Qp_{60}/Qp_{180} \tag{2}$$

Afterward, experimental data collected from five porcine models were analysed. The animals were under mechanical ventilation (control), before the lung was damaged by saline lavage to simulate the ARDS (injured) [16]. The $180s$ and $60s$ IST were measured and compared during both states: pre-injured (control) and injured. The animal details, protocol and regulation are included elsewhere [8].

III. RESULTS

According to the Morris method, the input parameters of the simulation were linearly linked to the IST outputs, as shown in Table 2. So, the lung simulation model is compatible with the IST. Unsurprisingly, alveolar volume input was the first rank in the most influential parameter to the V_A output. Tidal volume and expiratory flow coefficients had high ranks, but they caused random error to the IST outputs because of their non-monotonic relationship to the output. In Table 2, when the input changed, recovered values were compared with the true values and recorded in the error (%) column. Overall, IST errors were less than 5%.

Fig. 2 shows the results of linear regression of three output parameters. A strong correlation between the simulation inputs and the IST outputs ($R^2 = 1$) could be seen from the figures. The IST results also suggested that V_D could be calculated correctly even with added noise. However, under noisy conditions, the V_A regression slope shifted from 0.96 to 0.87 and the Qp slope shifted from 0.70 to 0.74.

Diseased and healthy simulated patients could be distinguished easily using the different IST ratios, Fig. 3, panel a and b ($p < 0.0001$). In emphysema, the ratio of ELV_{60}/ELV_{180} could identify the heterogeneity of the lung (about 0.58). However, the opposite was observed in the embolism. The ratio of Qp_{60}/Qp_{180} was approximately 5.8, higher than the values in the healthy and emphysema conditions.

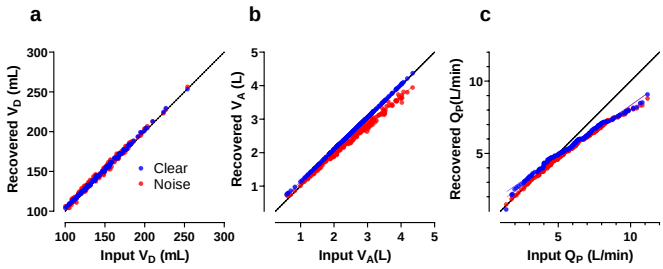


Fig. 2. Linear regression analysis of the IST input and recovered values of V_D, V_A and Qp. Gaussian white noise was applied.

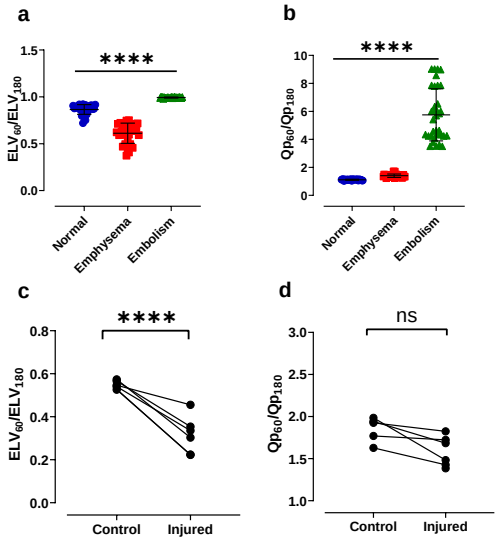


Fig. 3. IST ratios of ELV and Qp with different lung conditions. In panel a and b are simulated data and analysed with the ordinary one-way ANOVA test. Panel c and d are IST ratios between pre-injured (control group) and post-injured in five anesthetised pigs ($5cmH_2O$ PEEP, tidal volume of $10mL/Kg$). Student's t-test was implemented. ****= $p < 0.0001$, ns = non-significant.

Additionally, from the experiments in five animals (weight of $28 \pm 2kg$), the IST could classify the pre-injured (control) and the post-injured animals (ARDS model) reliably using the IST ventilation heterogeneity ratio ($p < 0.0001$)(Fig. 3c). However, the classification with the IST perfusion heterogeneity ratio was not significant (cf. Fig. 3d).

IV. DISCUSSION

Lung simulations can be used to validate lung measurement techniques such as the IST and provide information to improve performance. This work has combined a validated lung simulation using parameters taken from the literature to undertake error analysis and evaluation of the accuracy and precision of the IST. We empirically demonstrated that the IST ratio of two frequencies is an impactful method to quantify the lung heterogeneity using only IST results.

The results of sensitivity analysis and linear regression also suggested that the IST analysis offered a high accuracy (error of 3% to 5%) and a high precision (6% variation) in a healthy lung condition.

TABLE I

LUNG SIMULATION PARAMETERS IN NORMAL LUNG, EMPHYSEMA AND EMBOLISM CONDITIONS [15]. MEAN + SD PARAMETERS IN HEALTHY CONDITIONS ARE RANGES FOR THE SENSITIVITY ANALYSIS TEST.

Variable	Normal	Emphysema	Embolism
Deadspace volume (L)	0.15 ± 0.025	0.33	0.157
Alveolar volume (L)	2.5 ± 0.75	4.5	2.813
Tidal volume (L)	0.7 ± 0.3	0.54	0.46
Inhaled time (s)	2 ± 0.5	1	0.75
Respiration rate (Breath/min)	12 ± 5	22	29
Expiratory flow coefficient (1/s)	1 ± 0.3	1	1
Shunt (L/min)	0	0.015	0.74
Blood flow (L/min)	5 ± 1.5	5	3.7
IST forced periods (s)	60 & 180	60 & 180	60 & 180
Tidal fraction	[1]	[0.102 0.065 0.833]	[0.334 0.666]
Lung volume fraction	[1]	[0.196 0.577 0.227]	[0.333 0.667]
Blood flow fraction	[1]	[0.889 0.072 0.039]	[0.507 0.493]

The results of this work are consistent with previous comparison studies and provide further understanding of the IST. Previous work comparing the IST measurement of Qp and Qp measured from the thermodilution showed good agreement, although the IST was seen to marginally underestimate true Qp [7]. A similar result has been shown using our simulation, where IST Qp was seen to underestimate the true value by $0.52L/min$. Furthermore, our simulations show that the error will increase by up to 25% of the real value as Qp exceeds $7L/min$, suggesting that in its current embodiment, the IST is best suited to normal or low cardiac output states.

Secondly, previous clinical and animal studies comparing IST estimates of V_A to those measured by plethysmography found that the IST underestimated lung volume by an amount ranging from 0.88 to $1.09L$ compared to CT and plethysmography [3], [8]. In our simulation however, IST ELV underestimated V_A by only $0.2L$. One explanation for this is that plethysmography and CT measures estimate the total volume of lung gas, including trapped gas, whereas the IST measure the volume involved in gas exchange. Our simulation did not include any such trapped gas compartment. Further underestimation of V_A was discovered by our sensitivity analysis which showed that a changing tidal volume during IST (as wold occur during real breathing) caused errors which contributed to the underestimation of V_A.

This is the first study of the lung heterogeneity measured entirely by the IST and to evaluate its values in simulated and experimental data. Bruce et al. [3] showed that ventilation heterogeneity can be captured by the IST and the plethysmography. Our work only implemented IST results at 60s and 180s signals and required no additional measurement technique. It could be a potential parameter to identify lung disease at early stages. Although, there are limitations of the IST ratios, further research could be done in the future.

Modelling saves time, money and effort. In this work, thousands of simulated patients with different lung conditions were created and tested by the IST. We provided a simple and effective lung simulation that combines the advantages of previous simulations and works directly with a clinical measurement (IST).

The IST is suitable for bedside monitoring. It is non-invasive, easy to perform and does not require patient effort. Furthermore, our analysis has shown that when keeping the tidal volume unchanged, the IST error was minimised. Thus, it may be ideally suited to patients undergoing mechanical ventilation.

V. CONCLUSION

In this paper, we have used a mathematical model to create a lung simulation which is compatible with the IST. The results suggested that stable tidal volume can reduce error when performing the IST. We also have demonstrated how the IST can be used to classify lung heterogeneity. The method was applied in animal data (control vs ARDS injured). We proposed two new indices of heterogeneity; one describing the mismatch between regional ventilation and regional volume, the other describing the mismatch between regional ventilation and perfusion. These are alternative parameters to those measured by sophisticated invasive methods or medical imaging with ionising radiation and/or tracers.

VI. APPENDIX A

The equation for the deadspace compartment during inspiration is:

$$V_{M,i}\frac{dF_{M,i}}{dt} = \dot{V}_A(t)(F_{M,i-1}(t) - F_{M,i}(t)) \tag{3}$$

where i is the number of deadspace compartments (from 1 to 10); and $F_{(M,1)}(t) = F_I(t)$ and $F_{M,10}(t) = F_{IA}(t)$. $V_{M,i}$ is the deadspace volume of a compartment i and $\dot{V}_A(t)$ is the flow at time t. The equivalent equation during expiration is:

$$V_{M,i}\frac{dF_{M,i}}{dt} = \dot{V}_A(t)(F_{M,i}(t) - F_{M,i+1}(t)) \tag{4}$$

where i is from 1 to 10 and $F_{M,1}(t) = F_E(t)$ and $F_{M,10}(t) = F_A(t)$. F_I, F_{IA} and F_E are the fractional concentrations of the tracer gas coming into the deadspace compartment, coming out from the deadspace compartment to the lung compartment and exhaling from the deadspace to the environment, respectively.

For the tidal compartment during inspiration and expiration:

$$V_A(t) = \bar{V}_A + \frac{V_T \times t}{t_i} \tag{5}$$

$$V_A(t) = \bar{V}_A + V_T \exp(-\gamma(t - t_i)) \tag{6}$$

where γ is the rate-constant of expiratory flow [11], $V_A(t)$ is the alveolar volume, V_T is the tidal volume and t_i is the inspiration starting time. $\bar{V}_A$ is end-expired alveolar volume. All compartments are linked together by governed equations: during inspiration is (*7*) and expiration is (*8*):

$$\frac{d}{dt}(V_A(t) \times F_A(t)) = \dot{V}_A(t) \times F_{IA}(t) + \dot{Q}_p(C_{\bar{v}} - C_a) \tag{7}$$

$$\frac{d}{dt}(V_A(t) \times F_A(t)) = \dot{V}_A(t) \times F_A(t) + \dot{Q}_p(C_{\bar{v}} - C_a) \tag{8}$$

TABLE II

MORRIS METHOD RESULTS OF THE RELATIONSHIP BETWEEN SIMULATION PARAMETERS AND IST RESULTS (V_D, V_A AND Qp).

	VD			**VA**			**Qp**		
	Rank	**Relationship**	**Error (%)**	**Rank**	**Relationship**	**Error (%)**	**Rank**	**Relationship**	**Error (%)**
Deadspace volume (L)	**2**	**L**	**3**	7	AM	-	9	M	-
Alveolar volume (L)	3	M	-2	**1**	**L**	**-7**	4	M	4
Tidal volume (L)	1	NM	-3	2	NM	-5	1	AM	-4
Inhaled time (s)	5	NM	-	9	NM	-	7	NM	-
RR (Breath/min)	8	NM	-	6	M	-	8	AM	-
Expiratory flow (1/s)	4	NM	-4	3	NM	-2	3	NM	1
Shunt (L/min)	6	NM	-	4	M	-4	5	AM	4
Bloodflow (L/min)	5	NM	3	5	M	-3	**2**	**L**	**4**
IST forced period (s)	7	AM	-	8	L	-	6	AM	-

L: linear, M: monotonic, AM: almost monotonic, NM: non monotonic. Percentage error of some input of some parameter were negligible. Error (%) was calculated by percentage difference between simulation input and the recovered values

To create lung heterogeneity, the fraction of ventilation ($\dot{V}_A(t)$), lung volume ($\bar{V}_A$) and perfusion ($\dot{Q}_p$) changed according to Table 1. $C_{\bar{v}}$ and C_a are the mixed venous and pulmonary end-capillary gas concentrations. The body compartments of a standard human consist of five different tissues inside the human body with different tissue-gas coefficient [17], [18].

$$V_i^* \frac{dC_i(t)}{dt} = \dot{Q}_i(C_{\bar{a}}(t) - C_i(t)) \tag{9}$$

where V_i^*, C_i and $\dot{Q}_i$ are the equivalent blood volume, concentration of the tracer gas and blood flow rate of i compartment. V_i is given by the following equation where $V_{(b,i)}$ and $V_{(t,i)}$ are the blood and tissue volumes of each body compartments and $\lambda_{(t,i)}$ is the Ostwald tissue-gas coefficient of each compartment. The values of $V_{(b,i)}$, $V_{(t,i)}$ and $\lambda_{(t,i)}$ are given in data of a $70kg$ standard man [18].

$$V_i^* = V_{b,i} + \frac{\lambda_{t,i}}{\lambda} V_{t,i} \tag{10}$$

Furthermore, the Ostwald coefficient is the blood-gas partition coefficient (λ). In the IST, the Ostwald coefficient of the N_2O is 0.47. The body temperature is assumed to be constant (37^oC), so the Ostwald coefficient is stable.

$$C_a = \lambda \times F_A \tag{11}$$

Finally, the shunt equation is:

$$\frac{\dot{Q}_S}{\dot{Q}_T} = \frac{C_a(t) - C_{\bar{a}}(t)}{C_a(t) - C_{\bar{v}}(t)} \tag{12}$$

REFERENCES

[1] World Health Organization, "The global impact of respiratory diseases (second edition)," .

[2] Massimo Cressoni, Paolo Cadringher, Chiara Chiurazzi, Martina Amini, Elisabetta Gallazzi, Antonella Marino, Matteo Brioni, Eleonora Carlesso, Davide Chiumello, Michael Quintel, Guillermo Bugedo, and Luciano Gattinoni, "Lung inhomogeneity in patients with acute respiratory distress syndrome," *American Journal of Respiratory and Critical Care Medicine*, vol. 189, no. 2, pp. 149–158, 2014.

[3] Richard M. Bruce, Phi Anh Phan, Edmund Pacpaco, Najib M. Rahman, and Andrew D. Farmery, "The inspired sine-wave technique: A novel method to measure lung volume and ventilatory heterogeneity," *Experimental Physiology*, vol. 103, no. 5, pp. 738–747, 2018.

[4] James E. Mountain, Peter Santer, David Patrick O'Neill, Nicholas M. J. Smith, Luca Ciaffoni, John H. Couper, Grant A.D. Ritchie, Gus Hancock, Jonathan P. Whiteley, and Peter A. Robbins, "Potential for non-invasive assessment of lung inhomogeneity using highly precise, highly time-resolved, measurements of gas exchange," *Journal of Applied Physiology*, p. jap.00745.2017, 2017.

[5] John B. West, *Respiratory Physiology-The Essentials*, vol. Ninth Edit, 2012.

[6] Peter D. Wagner, "The multiple inert gas elimination technique (MIGET)," *Applied Physiology in Intensive Care Medicine 1: Physiological Notes - Technical Notes - Seminal Studies in Intensive Care, Third Edition*, pp. 35–42, 2012.

[7] Richard M. Bruce, Douglas C. Crockett, Anna Morgan, Minh Cong Tran, Federico Formenti, Phi Anh Phan, and Andrew D. Farmery, "Noninvasive cardiac output monitoring in a porcine model using the inspired sinewave technique: a proof-of-concept study," *British Journal of Anaesthesia*, vol. 123, no. 2, pp. 126–134, 2019.

[8] Douglas C Crockett, Minh C Tran, Federico Formenti, John N Cronin, Göran Hedenstierna, Anders Larsson, Phi A Phan, and Andrew D Farmery, "Validating the inspired sinewave technique to measure the volume of the "baby lung" in a porcine lung-injury model.," *British Journal of Anaesthesia*, 2020.

[9] Phi Anh Phan, Cathy Zhang, Daniel Geer, Federico Formenti, Clive Hahn, and Andrew Farmery, "The Inspired Sinewave Technique: A Comparison Study With Body Plethysmography In Healthy Volunteers," *IEEE Journal of Translational Engineering in Health and Medicine*, vol. 5, no. April, 2017.

[10] Phi Anh Phan, Andrew Farmery, and Clive Hahn, "Method and apparatus for measurement of cardiopulmonary function," apr 2015.

[11] Chris D Harrison, Phi Anh Phan, Cathy Zhang, Daniel Geer, Andrew D Farmery, and Stephen J Payne, "Modelling mixing within the dead space of the lung improves predictions of functional residual capacity," *Respiratory Physiology & Neurobiology*, vol. 242, pp. 12–18, 2017.

[12] Clive E.W. Hahn and A. D. Farmery, "Gas exchange modelling: No more gills, please," *British Journal of Anaesthesia*, vol. 91, no. 1, pp. 2–15, 2003.

[13] M D Morris, "Factorial plans for preliminary computational experiments," *Technometrics*, vol. 33, no. 2, pp. 161–174, 1991.

[14] Kathrin Menberg, Yeonsook Heo, Godfried Augenbroe, and Ruchi Choudhary, "New extension of Morris method for sensitivity analysis of building energy models," *Building Simulation & Optimization 2016*, , no. September 2016, 2016.

[15] J. S. Yem, M. J. Turner, A. B. Baker, I. H. Young, and A. B.H. Crawford, "A tidally breathing model of ventilation, perfusion and volume in normal and diseased lungs," *British Journal of Anaesthesia*, vol. 97, no. 5, pp. 718–731, 2006.

[16] B. Lachmann, B. Robertson, and J. Vogel, "In Vivo Lung Lavage as an Experimental Model of the Respiratory Distress Syndrome," *Acta Anaesthesiologica Scandinavica*, vol. 24, no. 3, pp. 231–236, 1980.

[17] CE Hahn, AM Black, SA Barton, and I Scott, "Gas exchange in a three-compartment lung model analyzed by forcing sinusoids of N2O.," *Journal of applied physiology (Bethesda, Md. : 1985)*, vol. 75, no. 4, pp. 1863–1876, 1993.

[18] A D Farmery, *Interrogation of the Cardiopulmonary System with Inspired Gas Tension Sinusoids*, Ph.D. thesis, Guy's, King's and St. Thomas's School of Medicine, 2008.

ICASSP 2021 - 2021 IEEE International Conference on Acoustics, Speech and Signal Processing (ICASSP) | 978-1-7281-7605-5/20/$31.00 ©2021 IEEE | DOI: 10.1109/ICASSP39728.2021.9413942

VALIDATING THE INSPIRED SINEWAVE TECHNIQUE TO MEASURE LUNG HETEROGENEITY COMPARED TO ATELECTASIS & OVER-DISTENDED VOLUME IN COMPUTED TOMOGRAPHY IMAGES

Minh C. Tran[1], Phi-Anh Phan[1], Douglas C. Crockett[1], Federico Formenti[2], John N. Cronin[2], Stephen J. Payne[1] & Andrew D. Farmery[1]

[1]University of Oxford, Oxford, UK.
[2]Kings's College London, London, UK.

ABSTRACT

The inspired sinewave technique (IST) is a non-invasive non-ionising method which can measure accurately lung parameters. Six anaesthetised pigs were studied after surfactant depletion by saline-lavage. Paired measurements of lung heterogeneity were taken with the IST and computed tomography (CT). Lung heterogeneity measured by the IST was calculated by the ratio of tracer gas outputs measured at 180s and 60s. In CT images, lungs were manually segmented and divided into different regions according to voxel density. The IST and CT show strong agreement on lung heterogeneity measurements. In the IST ventilation heterogeneity value, the linear correlation in total of six pigs are weaker than individual animal (R^2=0.33 vs R^2=0.67 on average). The IST perfusion heterogeneity agreements are lower than IST ventilation values due to the IST technical setup. IST has the potential to measure the lung heterogeneity in ARDS animals.

Index Terms— Lung heterogeneity, IST, ARDS, Lung simulation, CT images.

1. INTRODUCTION

The acute respiratory distress syndrome (ARDS) affects 10% of critical care patients and has an associated mortality of 40% [1]. ARDS has a high mortality rate, brings higher hospital costs and survivors have a low health-related quality of life [2]. During the 2019-2020 coronavirus pandemic (COVID-19) [3], [4] a study of 201 COVID-19 patients showed 41.8% of patients developed ARDS and 52.4% died [4]. Having the ability to measure lung heterogeneity at the bedside and provide optimal ventilator setup could help survival in ARDS patients.

Heterogeneity of the lung is the mismatch between ventilation (air coming into the lung), alveolar volume and perfusion (pulmonary blood flow) [5]. Lung heterogeneity has been considered as a critical tool or to support respiratory diseases classification [6], [7]. Therefore, measuring lung heterogeneity at the bedside could provide the clinician with valuable information with which to optimise the ventilator-settings for patients with lung conditions. Recently, CT imaging has been shown to be able to quantify lung heterogeneity [8], [9]. However, CT puts patients at risk by necessitating transfer to a scanner and exposure to ionising radiation. On the other hand, lung monitoring using the IST has shown potential to capture lung parameters at the bedside [10].

IST has the potential to provide bedside measurement of deadspace volume, effective lung volume (ELV), pulmonary blood flow (Qp) and lung heterogeneity. Measurements of the first three parameters have been validated elsewhere [6], [10]–[12]. IST uses available components commonly used in anaesthetic/intensive care practice and has proven efficacy in spontaneously ventilating healthy volunteers [13]. Lung heterogeneity measured by the IST was first introduced and conceptualised by Tran et al. [14]. To date IST's measurements of lung heterogeneity have not been compared against any established method.

We aimed to compare measurements of lung heterogeneity made by the IST with those made by CT in animals with ARDS. This is the first study to validate IST (a signal processing-based technique in respiratory monitoring) to measure lung heterogeneity.

2. METHOD

2.1. Protocol & animal preparation

Experiments in six anesthetised pigs were studied at the Hedenstierna Laboratory, Uppsala University, Sweden and approved by the regional animal welfare and ethics committee (Ref: C98/16). The summary of animals' baseline characteristics is shown in TABLE 1. Mechanical ventilation with a Servo-I, Maquet, (Rastatt, Germany) was in volume-

Authorized licensed use limited to: University of Oxford Libraries. Downloaded on May 21,2021 at 14:35:41 UTC from IEEE Xplore. Restrictions apply.

control mode at 20-25 breaths per minute. Tidal volume was 10mL/kg and the inspiration: expiration (I:E) ratio was 1:2.

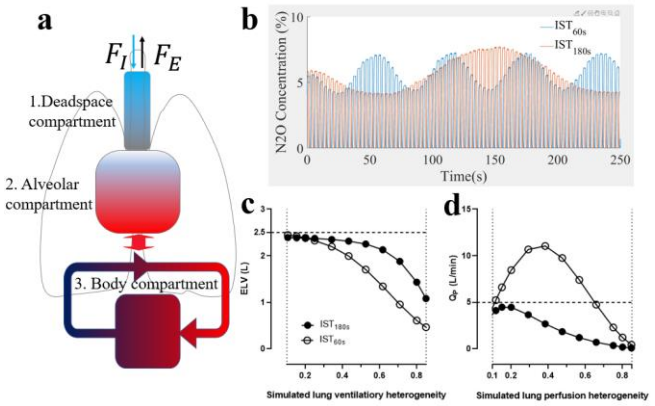


Fig. 1: Summary of the IST. Panel a is a schematic diagram of the IST lung model. Panel b shows examples of the measured output of IST 180s and 60s period tracer gases. Panel c shows the changes of ELV values measured by the IST when the lung ventilation heterogeneity varies. Similarly, panel d shows the changes of Qp measured by the IST when perfusion heterogeneity changed.

The ARDS model in animals was induced by injuring the lung using Lachmann's method [15]. Mechanical ventilation was disconnected. The installation of 0.9% saline solution (37°C) was transferred to the lung passing through the endotracheal tube. After 30s, we drained the saline out of the lungs and connected the ventilator. This process was repeated until the PaO_2:FIO_2 ratio (PFR) <300 mmHg (40 kPa) condition was achieved at a PEEP of 5 cmH_2O and FIO_2 of 0.7.

During the experiments, the PEEP level was incrementally changed from 5 through 10, 15 and 20 cmH_2O and decreased back to 15, 10 and 5 cmH_2O. At each PEEP, paired measurements of the lung volume by the IST and CT were performed.

2.2. Inspired Sinewave Test

2.2.1. Device and analysis

The IST applies a forced oscillation of a low dose of N_2O tracer gas with a sinusoidal period which can be determined by the user. A mainstream infrared N_2O and CO_2 sensor and an ultrasonic flowmeter are placed in the breathing circuit between a patient-end heat-moisture exchange filter and the ventilator tubing. At the beginning of each inspiration, a set volume of N_2O is injected into the inspired gas by a mass flow controller. The volume of IST tracer gas is oscillated at periods of 60s and 180s, in Fig. 1.

Input and output of the IST are analysed by the IST analysis (breath-by-breath analysis) to compute the lung parameters [16]. IST analysis is shown in Fig. 2. The IST quantifies the deadspace volume by using modified Bohr method [11] and subsequently the ELV and Qp are calculated according to this one well-mixed lung compartment (Fig. 1a). This simulation of the lung consisted of one deadspace and one alveolar compartment.

However, this simple one compartment might not present fully the heterogeneity of the lung. Therefore, IST requires two different period tracer gas to measure the lung heterogeneity.

TABLE 1

BASELINE CHARACTERISTICS OF N=6 PIGS. MEAN AND STANDARD DEVIATION ARE SHOWN.

Parameter	Mean (SD)
Weight (Kg)	30.3(1.64)
Heart rate (bpm)	99.5(20.5)
Cardiac output (L/min)	3.35(0.38)
Hb (g/L)	88.5(12.0)
FIO_2	0.78(0.02)
SaO_2 (%)	98.3(0.85)

FIO_2: fraction of inspired O_2, Hb: haemoglobin, SaO_2: oxygen saturation.

2.2.2. Lung heterogeneity measured by the IST

Theory dictates that in a completely homogeneously ventilated and perfused lung, the values of ELV and Qp recovered from the IST are independent of the tracer gas period used. However, as the degree of heterogeneity increases, the ELV and Qp values (based on the assumption of perfect homogeneity) begin to diverge from true values, and moreover, those values recovered from periods of 60 and 180s also diverge from each other. Consequently, the ratio of these latter values provides an index of the degree of heterogeneity. Example of ELV and Qp changes with simulated lung heterogeneity were presented in Fig. 1c and d.

The IST's ventilatory and perfusion heterogeneity ratios of the lung are given by the following:

$$IST_{Vent-Heterogeneity} = \frac{ELV_{180s}}{ELV_{60s}} \quad (1)$$

$$IST_{Perf-Heterogeneity} = \frac{Qp_{60s}}{Qp_{180s}} \quad (2)$$

where ELV_{180s} and ELV_{60s} the effective lung volume measured by IST 180s and 60s tracer gas periods; and similarly, for pulmonary blood flow (Qp).

2.2. CT image analysis

A Somatom Definition Flash (Siemens, Munich, Germany) was used to acquire images as a series of transverse sections.

Authorized licensed use limited to: University of Oxford Libraries. Downloaded on May 21,2021 at 14:35:41 UTC from IEEE Xplore. Restrictions apply.

with a reconstituted voxel size of 0.5x0.5x5 mm. We conducted a 20s end-expiratory paused without ventilator disconnection to scan the whole-lung volume.

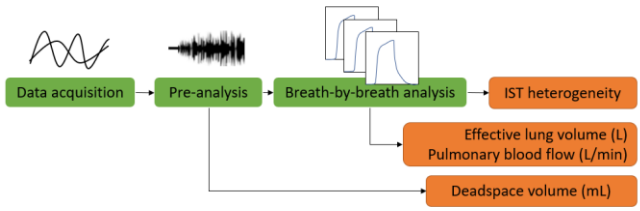


Fig. 2: Signal processing block diagram of the in the inspired sinewave technique.

The scans were segmented by 3D Slicer (https://www.slicer.org). Exclusion of intrapulmonary vessels within regions of increased voxel density was not possible as they were not distinguishable from lung tissue, and these, along with the conducting airways up to the level of the clavicles, were included in the analysis. The Hounsfield unit (HU) boundaries were water with a density of 1 g cm^{-3} (0 HU) and air with a density of 0 g cm^{-3} (-1000 HU) [17]. Lung CT images were divided into three different regions [18] (Fig. 3):

- Atelectasis (including collapse and poor aeration): -500 to +100 HU
- Normally aerated volume: -900 to -501 HU
- Over-distended volume: -1000 to -901 HU

The mass of each lung fraction (e.g. atelectasis) was then calculated using the mean density and volume of each fraction assuming the lung is composed solely of air and water. To quantify the lung heterogeneity using CT images, we assumed that the ratios of atelectasis and over-distended over normally aeriated could present the lung heterogeneity.

Statistical analysis was implemented in GraphPad Prism (https://www.graphpad.com). IST analysis were performed in Matlab (https://uk.mathworks.com/). Linear regression was used to access the agreement and correlation between two measurement techniques.

3. RESULTS

A total number of 83 measurements of the lung at four different incremental and decremental PEEP levels were analysed. Fig. 4 shows the agreement between IST heterogeneity values and the CT image values in six animals.

In Fig. 4, panels a and b, the overall relationship of the IST ventilation heterogeneity vs CT values were recorded (R^2=0.33 in Atelectasis ratio and R^2=0.18 in Over-distended ratio). However, there was no linear relationship between CT heterogeneity values and the IST perfusion heterogeneity (panels c and d). Interestingly, the linear relationship in the individual animal is strong than overall linear relationship. The R^2 values were summarised in TABLE 2. In the comparison of IST ventilation heterogeneity in both CT heterogeneity values, five pigs had strong agreements (R^2>0.68) except pig number 4. Similarly, in the comparison of IST perfusion heterogeneity vs CT values, the strongest agreements were observed in pig number 2 and 4.

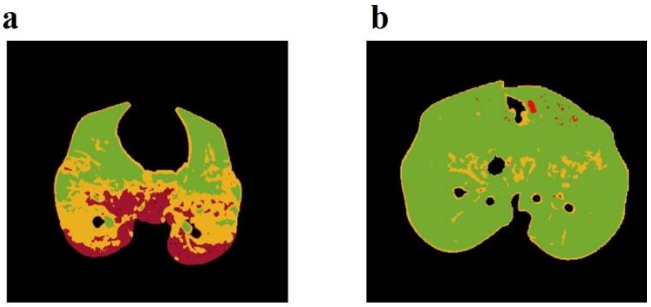


Fig. 3: Lung heterogeneity measured by the CT images. Panels a and b show the animal lung in PEEP 5 (panel a) and PEEP 20 cmH_2O (panel b). Green: normally aerated mass; yellow: poorly aerated, dark red: atelectasis, red: over-distended.

Additionally, repeated lung heterogeneity measurements using the IST at the same PEEP level during both incremental and decremental changes had variation less than 10%.

4. DISCUSSION

This work fitted into a bigger picture of measuring the lung heterogeneity using a non-invasive technique. The IST has been developed and validated to be used as a clinical tool for lung monitoring at the bedside [6], [19]. In this paper, the IST analysis used a simple one, well-mixed, lung compartment and the heterogeneity of the lung was calculated according to the degree of breakdown of this model. It is a simple technique with no requirement to compute time and power. However, the accuracy of the model might be a concern. In this study, we compared the IST heterogeneity vs values calculated from CT images. Although each technique has its own assumptions and working principles, agreement was observed in individual testing subjects.

We experimented a similar protocol through six animals, but the degree of the damaged lung was different in different pigs. The results were well presented in Fig. 4. In individual animal, CT and IST had a strong correlation.

CT has been used as a standard measurement to quantify the lung and also lung heterogeneity [8], [10]. In this study, we presented a validation of the IST heterogeneity results in CT images. However, CT measured voxel density, so radio dense

Authorized licensed use limited to: University of Oxford Libraries. Downloaded on May 21,2021 at 14:35:41 UTC from IEEE Xplore. Restrictions apply.

material, such as fluid (alveolar flooding) or blood may influence the true atelectasis volume. Manual segmentation also contains limitations.

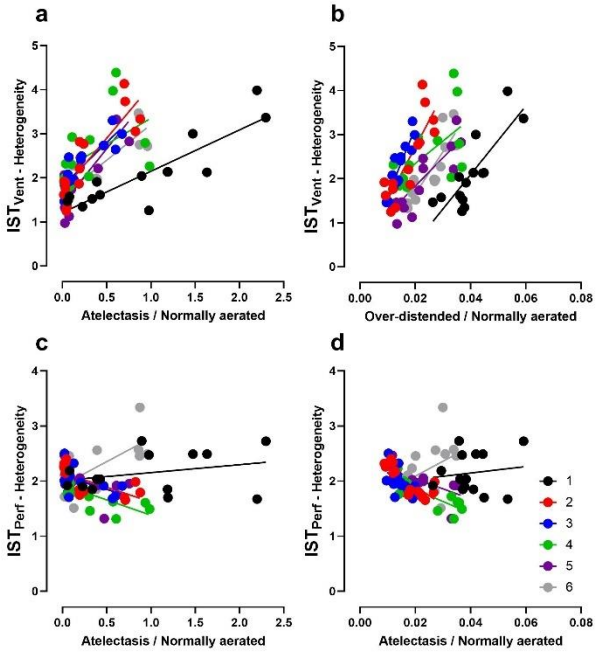


Fig. 2: Color-coded individual pigs. Comparison of the IST heterogeneity (ventilation and perfusion) vs the heterogeneity indices measured by the CT images (Atelectasis/normally aerated and over-distended/normally aerated ratios) in six animals. Panels a and b show an agreement between the IST ventilation heterogeneity vs CT indices. Besides, panels c and d show the correlation of the IST perfusion heterogeneity. Linear regression analysis was performed.

The mechanical ventilator is a method to save ARDS patients, but it also induces lung injury in case of wrong setup. Therefore, bedside lung monitor could benefit both healthy patients and patients with lung diseases. It also is the final aim of the IST to monitor and suggest the optimal setting for the ventilator.

The IST is suitable for bedside monitoring. IST can measure accurately the effective lung volume and deadspace volume, which are key parameters to personalise mechanical ventilator [20]. The changes in lung volume due to increased PEEP were reported correctly by the IST [10]. Besides, IST shown its advantages to measure accurate value when the patient breathes stably. A sensitivity analysis has pointed out stable breathes and unchanged tidal volume during IST could minimise its technical error [6].

In previous studies, the heterogeneity index measured by the IST has shown its potential to identify COPD patients in comparison with other lung function test [19]. In research, heterogeneity has been used to detect and track patients with lung conditions [7], [21], [22]. However, there was no standard in measuring lung heterogeneity. For example, the lognormal distribution is used to present the lung heterogeneity with ventilation and perfusion mismatch [7], [21].

TABLE 2

R^2 VALUES OF THE LINEAR REGRESSION ON INDIVIDUAL ANIMAL

Pig	1	2	3	4	5	6
IST_{Vent} vs A/N	0.75	0.75	0.75	0.25	0.73	0.78
IST_{Vent} vs OE/N	0.68	0.71	0.83	0.38	0.69	0.73
IST_{Perf} vs A/N	0.09	0.43	0.28	0.56	0.26	0.46
IST_{Perf} vs OE/N	0.02	0.68	0.30	0.69	0.39	0.12

IST_{Vent} : IST ventilation heterogeneity ratio, IST_{Perf} : IST perfusion heterogeneity ratio, A/N : Atelectasis/Normal aerated ratio, OE/N : Over-Extended/Normal aerated ratio.

Limitations of this study were mainly using the porcine model to describe ARDS in human. It only can present mild and moderate lung injury [17]. Additionally, there was no comparison with healthy lung. Due to the experimental setup, the animal's lung was damaged before moving into the CT scanner. Furthermore, IST contains its own limitations. IST requires two period-tracer gas tests in series.

Future analysis of the lung heterogeneity can be performed by the IST advance lung simulation. This is an advanced computational technique that uses Bayesian optimisation to match simulated data to measured IST data. Additionally, other research can be carried out in the future based on CT images. Cressoni et al. introduced a filter which can quantify lung inhomogeneity in CT images. This was tested in 148 human data [8]. Additionally, a dynamic single-slice CT scan could provide better images and counter the effect of inspiration-related lung movement [23].

5. CONCLUSION

In this paper, we have validated the use of a non-invasive lung function test (Inspired sinewave technique) to quantify lung heterogeneity in comparison with the CT technique. We demonstrated a potential application for the use of IST as a bedside monitor of lung heterogeneity. Our study warrants further investigation into the use of IST in human clinical medicine.

6. ACKNOWLEDGEMENTS

The authors would like to thank the team in Hedenstierna Laboratory, Sweden for their technical supports, especially Professor Göran Hedenstierna and Professor Anders Larsson. I am grateful to Mr. Thang C. Tran for assistance with data analysis.

Authorized licensed use limited to: University of Oxford Libraries. Downloaded on May 21,2021 at 14:35:41 UTC from IEEE Xplore. Restrictions apply.

7. REFERENCES

[1] G. Bellani *et al.*, "Epidemiology, patterns of care, and mortality for patients with acute respiratory distress syndrome in intensive care units in 50 countries," *JAMA - J. Am. Med. Assoc.*, vol. 315, no. 8, pp. 788–800, 2016.

[2] J. Marti *et al.*, "One-year resource utilisation, costs and quality of life in patients with acute respiratory distress syndrome (ARDS): Secondary analysis of a randomised controlled trial," *J. Intensive Care*, vol. 4, no. 1, pp. 1–11, 2016.

[3] J. Phua *et al.*, "Intensive care management of coronavirus disease 2019 (COVID-19): challenges and recommendations," *Lancet Respir. Med.*, vol. 2019, no. 20, pp. 1–12, 2020.

[4] C. Wu *et al.*, "Risk Factors Associated with Acute Respiratory Distress Syndrome and Death in Patients with Coronavirus Disease 2019 Pneumonia in Wuhan, China," *JAMA Intern. Med.*, pp. 1–10, 2020.

[5] J. B. West, *Respiratory Physiology-The Essentials*, vol. Ninth Edit. 2012.

[6] M. C. Tran, D. C. Crockett, P. A. Phan, S. J. Payne, and A. D. Farmery, "A tidal lung simulation to quantify lung heterogeneity with the Inspired Sinewave Test," in *42nd Annual International Conference of the IEEE Engineering in Medicine and Biology Society (EMBC 2020)*, 2020, pp. 13–16.

[7] J. E. Mountain *et al.*, "Potential for non-invasive assessment of lung inhomogeneity using highly precise, highly time-resolved, measurements of gas exchange," *J. Appl. Physiol.*, p. jap.00745.2017, 2017.

[8] M. Cressoni *et al.*, "Lung inhomogeneity in patients with acute respiratory distress syndrome," *Am. J. Respir. Crit. Care Med.*, vol. 189, no. 2, pp. 149–158, 2014.

[9] M. Cressoni *et al.*, "Lung inhomogeneities, inflation and [18F]2-fluoro-2-deoxy-D-glucose uptake rate in acute respiratory distress syndrome," *Eur. Respir. J.*, vol. 47, no. 1, pp. 233–242, 2016.

[10] D. C. Crockett *et al.*, "Validating the inspired sinewave technique to measure the volume of the 'baby lung' in a porcine lung-injury model. Authors:," *Br. J. Anaesthesiao*, pp. 0–30, 2019.

[11] P. A. Phan, C. E. W. Hahn, and A. D. Farmery, "A modification of the Bohr method to determine airways deadspace for non-uniform inspired gas tensions," *Physiol. Meas.*, vol. 38, no. 7, pp. 107–117, 2017.

[12] R. M. Bruce *et al.*, "Noninvasive cardiac output monitoring in a porcine model using the inspired sinewave technique: a proof-of-concept study," *Br. J. Anaesth.*, vol. 123, no. 2, 2019.

[13] P. A. Phan, C. Zhang, D. Geer, F. Formenti, C. Hahn, and A. Farmery, "The Inspired Sinewave Technique: A Comparison Study With Body Plethysmography In Healthy Volunteers," *IEEE J. Transl. Eng. Heal. Med.*, vol. 5, no. April, 2017.

[14] M. C. Tran *et al.*, "Lung heterogeneity and deadspace volume in acute respiratory distress syndrome animals using the inspired sinewave test," *J. Physiol. Meas.*, vol. 0, no. 0, pp. 1–10, 2020.

[15] B. Lachmann, B. Robertson, and J. Vogel, "In Vivo Lung Lavage as an Experimental Model of the Respiratory Distress Syndrome," *Acta Anaesthesiol. Scand.*, vol. 24, no. 3, pp. 231–236, 1980.

[16] A. D. Farmery, "Interrogation of the Cardiopulmonary System with Inspired Gas Tension Sinusoids," Guy's, King's and St. Thomas's School of Medicine, 2008.

[17] D. C. Crockett *et al.*, "Tidal changes in PaO 2 and their relationship to cyclical lung recruitment/derecruitment in a porcine lung injury model," *Br. J. Anaesth.*, vol. 122, no. 2, pp. 277–285, 2019.

[18] L. Gattinoni *et al.*, "Relationships between lung computed tomographic density, gas exchange, and PEEP in acute respiratory failure," *Anesthesiology*, vol. 69, no. 6, pp. 824–832, 1988.

[19] R. M. Bruce, P. A. Phan, E. Pacpaco, N. M. Rahman, and A. D. Farmery, "The inspired sine-wave technique: A novel method to measure lung volume and ventilatory heterogeneity," *Exp. Physiol.*, vol. 103, no. 5, pp. 738–747, 2018.

[20] J. M. Constantin *et al.*, "Personalised mechanical ventilation tailored to lung morphology versus low positive end-expiratory pressure for patients with acute respiratory distress syndrome in France (the LIVE study): a multicentre, single-blind, randomised controlled trial," *Lancet Respir. Med.*, vol. 7, no. 10, pp. 870–880, 2019.

[21] R. Rodríguez-Roisin, M. Drakulovic, D. A. Rodríguez, J. Roca, J. A. Barberà, and P. D. Wagner, "Ventilation-perfusion imbalance and chronic obstructive pulmonary disease staging severity," *J. Appl. Physiol.*, vol. 106, no. 6, pp. 1902–1908, 2009.

[22] W. Wang *et al.*, "Can computer simulators accurately represent the pathophysiology of individual COPD patients?," *Intensive Care Med. Exp.*, vol. 2, no. 1, pp. 1–14, 2014.

[23] J. N. Cronin *et al.*, "Dynamic single-slice CT estimates whole-lung dual-energy CT variables in pigs with and without experimental lung injury," *Intensive Care Med. Exp.*, Dec. 2019.

Authorized licensed use limited to: University of Oxford Libraries. Downloaded on May 21,2021 at 14:35:41 UTC from IEEE Xplore. Restrictions apply.